Developments in Geotechnical Engineering

G.L. Sivakumar Babu
Krishna R. Reddy
Anirban De
Manoj Datta *Editors*

Geoenvironmental Practices and Sustainability

Linkages and Directions

Springer

Developments in Geotechnical Engineering

More information about this series at http://www.springer.com/series/13410

G.L. Sivakumar Babu • Krishna R. Reddy
Anirban De • Manoj Datta
Editors

Geoenvironmental Practices and Sustainability

Linkages and Directions

Springer

Editors
G.L. Sivakumar Babu
Department of Civil Engineering
Indian Institute of Science
Bengaluru, Karnataka, India

Anirban De
Civil and Environmental Engineering Department
Manhattan College
Bronx, NY, USA

Krishna R. Reddy
Department of Civil and Materials Engineering
University of Illinois at Chicago
Chicago, IL, USA

Manoj Datta
Civil Engineering Department
IIT Delhi
New Delhi, India

ISSN 2364-5156 ISSN 2364-5164 (electronic)
Developments in Geotechnical Engineering
ISBN 978-981-10-4076-4 ISBN 978-981-10-4077-1 (eBook)
DOI 10.1007/978-981-10-4077-1

Library of Congress Control Number: 2017941622

Printed on acid-free paper

This Springer imprint is published by Springer Nature
The registered company is Springer Nature Singapore Pte Ltd.
The registered company address is: 152 Beach Road, #21-01/04 Gateway East, Singapore 189721, Singapore

Preface

Geoenvironmental challenges such as waste management and landfills, polluted soils and groundwater, beneficial reuse of waste and recycled materials, and sustainable development are of growing concern worldwide to protect public health and the environment as well as economic growth. Many advances have been made in geotechnical practices such as landfill engineering, polluted site remediation, and beneficial reuse of industrial byproducts in the USA. Similar advancements are being made in India with unique initiatives such as smart cities. The broader geographic, economic, and sociological differences between the USA and India play a vital role in determining the priorities and approaches for sustainable development. Many geoenvironmental challenges have a global effect. For example, improper waste disposal practices in developing countries result in huge quantities of greenhouse gas emissions. The resulting effects on climate change can be felt worldwide. There are significant opportunities to develop, transfer, and combine technologies and practices of the USA and India so that the geoenvironment is protected while making sustainable progress.

Geoenvironmental sustainability will be the key concern in the next century, and it is imperative for researchers and professionals in both India and the USA to collaborate and develop an understanding of the issues and needs of the developing world. By combining the respective geoenvironmental expertise and resources in India and the USA, researchers and professionals will have an increased ability to meet these challenges and mitigate the global effects of these challenges. Efforts are being made to establish such international collaborations in sustainability issues and geoenvironmental practices through a series of workshops.

The first US-India Workshop on Global Geoenvironmental Engineering Challenges was held in conjunction with the 6th International Congress on Environmental Geotechnics (6ICEG) in November 2010, New Delhi, India. Following the success of this workshop, the second "US-India Workshop on Geoenvironmental Practices and Sustainability – Linkages and Directions" was held in conjunction with "Geo-Chicago 2016: Sustainability, Energy, and the Geoenvironment" in August 2016, Chicago, USA. These workshops aim (1) to facilitate exchange of information on the current state of the art and the state of the

practice of geoenvironmental engineering and identify the emerging global geoenvironmental engineering challenges; (2) to prioritize research opportunities that will be of mutual interest to US and Indian researchers; (3) to identify the individuals and organizations in the USA and India that can make intellectual contributions, maintain useful facilities, and form collaborative partnerships to address specific projects in a strategic and complementing fashion; (4) to prepare and submit higher-quality and higher-impact collaborative research proposals to the funding agencies in the USA and India, including the US National Science Foundation and India's Department of Science & Technology; and (5) to facilitate and reaffirm a research agenda and foster continued collaboration among US and Indian researchers through periodic workshops and conferences.

Both workshops have identified several broad technical areas of interest that include sustainable waste management, green and sustainable remediation, renewable and alternative energy, global climate change impacts, mitigation of greenhouse gases, and sustainable geo-infrastructure development, among others. Specifically, the technical issues discussed included thermo–bio–hydro–chemical–mechanical processes, embodied energy and green materials, field and laboratory characterization, landfill design and construction and bioreactor landfills, contaminant transport, methane emissions and oxidation in landfills, new and recycled materials, performance monitoring of geosynthetic reinforced pavements, physical properties and behavior of geosynthetic clay liners and covers, reuse of residual materials, sustainable geo-infrastructures, sustainable remediation of contaminated sites and waste dumps, and reliability and resilience.

This book titled *Geoenvironmental Practices and Sustainability: Linkages and Directions* is the outcome of the deliberations made at the second US-India workshop. Over 40 researchers and practitioners contributed white papers reflecting the current state of the art and the current state of the practice as well as future research directions. The book is organized into 32 chapters covering a wide range of topics ranging from wastes to landfills to sustainability.

Characterization and management of municipal solid waste (MSW) as well as addressing various issues related to waste dumps and engineered landfill continue to be challenges in both the USA and India. These issues include geophysical imaging of landfill interiors (Chap. 1), evolution of MSW shear strength parameters with biodegradation (Chap. 2), seismic design of MSW landfill considering stability (Chap. 4), dynamic properties of MSW and amplification of landfill site (Chap. 5), load resistance factor design (LRFD) of MSW landfill slopes (Chap. 6), rehabilitation and expansion of operational MSW dumps (Chap. 7), site characterization of landfills through in situ testing (Chap. 10), effective management of aged stockpiled solid wastes in India (Chap. 11), performance evaluation of coal ash-based barrier landfill covers subjected to flexural distress (Chap. 20), sustainable waste management using MSE berms at disposal sites (Chap. 28), and coupled hydro–bio–mechanical modeling of bioreactor landfills (Chap. 31).

Besides MSW, characterization and management of other waste streams such as dredged sediments, red mud waste, mine tailings, coal ash, etc. have received relatively less attention from geoenvironmental professionals, and many opportunities

exist to address these wastes. Some specific issues include surface charge properties and particle size analysis of red mud waste from zeta potential measurements (Chap. 8) and sustainable management of dredged sediments and waste using geotextile tube dewatering system (Chap. 9).

Waste containment systems in terms of landfill liners and vertical barriers have been developed, but challenges still exist to ensure their integrity during and after construction and their effectiveness to contain toxic pollutants. An active research agenda is needed to address challenges such as sustainability of vertical barriers based on energy and carbon footprint (Chap. 21), organo-clay-enhanced bentonite mixtures for use in sustainable barriers (Chap. 22), observations of field condition of exposed geosynthetic liner systems (Chap. 23), and advanced bentonite-based containment barriers (Chap. 24).

Natural resources are limited and are being depleted at an alarming rate. It is essential to explore the beneficial reuse of waste and recycled materials in civil and environmental engineering applications. Geoenvironmental engineers have been actively seeking innovative and practical uses of waste materials such as the use of sand–tire chip mixtures as backfill material in retaining walls (Chap. 25), shredded waste tires as a geomaterial (Chap. 26), and geopolymer–fly ash-stabilized reclaimed asphalt pavement as base courses (Chap. 27).

Contamination of soils and groundwater is a pervasive problem and poses great risk to public health and the environment. New technologies are much warranted to characterize and remediate the polluted sites. Challenges and research opportunities in this field are broad, such as advances in Raman spectroscopy for the geoenvironment (Chap. 12), heavy metal removal by aquatic plants and its disposal by using as a concrete ingredient (Chap. 29), and human health risk-based sustainable management of contaminated sites (Chap. 30)

Extreme events and natural hazards have continued to cause enormous loss of life and damage to infrastructure and the environment. Questions on the validity of current analysis and design methods are being raised, and resiliency and resilient design concepts are slowly emerging. Geoenvironmental professionals are actively engaged in such challenges such as environmental benign electrokinetics for landslide mitigation (Chap. 3), non-stationarity in sustainability and resilience of geoinfrastructure (Chap. 15), and risk management practice for dam and levee safety (Chap. 18).

Fossil fuel contribution to carbon footprint is enormous; thus, alternative and renewable energy sources are being sought. Geoenvironmental professionals have embarked on wind energy, geothermal energy, and energy foundation. New advancements are rapidly being made under the theme of energy geotechnics toward a sustainable energy future (Chap. 19), a sustainable design of offshore wind turbine (Chap. 13), and geothermal energy piles (Chap. 14).

Sustainability concepts and the necessity for designing sustainable geoinfrastructure have gained momentum among the researchers and practitioners. These concepts and projects address carbon footprint, natural resource conservation, minimizing wastes, etc. through the lifecycle of a project. Sustainability can be incorporated on any scale and at any stage or component of a project. Such examples

include quality control and quality assurance for large infrastructure projects (Chap. 17), reliability-based sustainable design of piled raft supported structure (Chap. 16), and electromagnetic enhancement of microbially induced calcite precipitation (Chap. 32).

We hope that this book will serve as a catalyst to highlight the challenges of geoenvironmental sustainability and create collaborations among the geoenvironmental researchers worldwide to develop and implement methods and means for sustainable development without endangering our planet and future generations.

The authors thank the authors who presented papers for the India- USA workshop, Indo-US Science Technology Forum (IUSSTF), New Delhi and the Geo Institute of American Society of Civil Engineers (GI-ASCE).

Bangalore, India — G.L. Sivakumar Babu
Chicago, IL, USA — Krishna R. Reddy
Bronx, NY, USA — Anirban De
New Delhi, India — Manoj Datta

Contents

About the Editors

G.L. Sivakumar Babu completed his Ph.D. (geotechnical engineering) in 1991 from the Indian Institute of Science, Bangalore, India, after earning his master's degree (soil mechanics and foundation engineering) in 1987 from Anna University, Madras, and B.Tech. (civil engineering) in 1983 from Sri Venkateswara University, Tirupati. He worked in Central Road Research Institute and the International Airports Authority of India, New Delhi. He joined the Indian Institute of Science in 1997, and his teaching and research activities include courses on geomechanics, soil investigations, risk and reliability applications in civil engineering, pavement engineering, geosynthetics, and ground improvement. He is editor in chief of the *Indian Geotechnical Journal* and is editorial board member of the (1) *Journal of Hazardous, Toxic, and Radioactive Waste*, ASCE; (2) *International Journal of Geomechanics*, ASCE; (3) *Georisk: Assessment and Management of Risk for Engineered Systems and Geohazards*, Taylor & Francis Group; (4) *International Journal of System Assurance Engineering and Management*, Springer Publications; and (5) *International Journal of Geosynthetics and Ground Engineering* and *Ground Improvement, Proceedings of the Institution of Civil Engineers*, UK (during 2006–2013). He is the governor of Region 10, ASCE, the ex-president of ASCE (India Section), and a member of the Sectoral Innovation Council, Ministry of Road Transport and Highways, and Highway Research Board (Identification, Monitoring and Research Application Committee), Indian Roads Congress, New Delhi. He worked as a Humboldt Fellow and visiting scientist in Germany during June 1999 to July 2000 and as a visiting scholar of Purdue University, Lafayette, USA, during February 1995 to February 1996. He is presently the chairman of the International Technical Committee (TC-302) on Forensic Geotechnical Engineering (FGE) of the International Society for Soil Mechanics and Geotechnical Engineering (ISSMGE) and served as its secretary during 2005–2009 and 2009–2013. He was a member of the International Technical Committee (TC-32) on Risk Assessment in Geotechnical Engineering during 1997–2001 and 2001–2005. He is a Fellow of ASCE, life member of the Indian Roads Congress, Fellow of the Institution of Engineers India, Fellow of the Indian Geotechnical Society, and Fellow of the Association of Consulting Engineers (ACCE). He has guided a number of students for research

degrees [Ph.D. and M.Sc. (engineering)]. He wrote a book on soil reinforcement and geosynthetics, edited six books and proceedings, and has over 200 publications to his credit in journals and conferences of international repute. He has received several awards for his work such as the Best Ph.D. Thesis in Geotechnical Engineering in India from the Indian Geotechnical Society; a Humboldt Fellowship from Germany; a DST Boyscast Fellowship; the Young Engineer Award from the Central Board of Irrigation and Power, New Delhi; and a few awards for best papers from ASCE and the Indian Geotechnical Society.

Dr. Krishna R. Reddy is a professor of civil and environmental engineering, the director of the Sustainable Engineering Research Laboratory (SERL), and also the director of the Geotechnical and Geoenvironmental Engineering Laboratory (GAGEL) in the Department of Civil and Materials Engineering at the University of Illinois at Chicago (UIC). He has over 25 years of research, teaching, and consulting experience within the broad fields of civil, geotechnical, materials, and environmental engineering, addressing the nexus among sustainability, resiliency, infrastructure, water, energy, and the environment in urban setting. His research expertise includes (1) environmental remediation of soils, sediments, groundwater, and stormwater; (2) solid and hazardous waste management and landfill engineering; (3) engineering applications of waste/recycled materials; (4) life cycle assessment and sustainable engineering; and (5) geotechnical engineering. His research is funded by the US National Science Foundation, the United States Environmental Protection Agency, and several prominent state and local government agencies and industries. His research includes laboratory studies, field experiments, and computer modeling, ultimately leading to practical solutions to real-world problems. He is the author of three books: (1) *Geoenvironmental Engineering: Site Remediation, Waste Containment, and Emerging Waste Management Technologies*, (2) *Electrochemical Remediation Technologies for Polluted Soils, Sediments and Groundwater*, and (3) *Sustainable Remediation of Contaminated Sites*. He is also author of 182 journal papers (with an h-index of 43 and number of citations 6500), 15 edited books and conference proceedings, 10 book chapters, and 170 full conference papers. Dr. Reddy has given 160 invited presentations in the USA and 15 other countries (Canada, UK, Germany, France, Spain, Italy, India, Sri Lanka, China, Hong Kong, Thailand, South Korea, Japan, Brazil, and Colombia). He has served or currently serves as an associate editor or editorial board member of over 10 different journals, including the ASCE *Journal of Geotechnical and Geoenvironmental Engineering*, the ASTM *Geotechnical Testing Journal*, the ASCE *Journal of Hazardous, Toxic, and Radioactive Waste*, and the *Journal of Hazardous Materials*, among others. He has also served on various professional committees, including the Geoenvironmental Engineering Committee and Technical Coordinating Council of the Geo-Institute (GI) of the American Society of Civil Engineers (ASCE) and the Environmental Geotechnics Committee of the International Society for Soil Mechanics and Geotechnical Engineering (ISSMGE). He has received several awards for excellence in research and teaching, including the ASTM Hogentogler Award, the UIC Distinguished Researcher Award, the University of Illinois Scholar Award, and the University of Illinois Award for Excellence in Teaching.

He is a fellow of the American Society of Civil Engineers (FASCE), a Diplomate of Geotechnical Engineering (DGE), and a Board Certified Environmental Engineer (BCEE). He is also a registered Professional Civil Engineer (PE) and an Envision™ Sustainability Professional (ENV SP).

Dr. Anirban De is an associate professor and chairman of the Civil and Environmental Engineering Department at Manhattan College, located in New York City. Prior to joining his current position, Dr. De served as a project engineer in a major geoenvironmental engineering firm, where he was responsible for tasks ranging from site characterization and design to construction and post-closure monitoring of municipal solid waste and hazardous waste landfills. He has over 25 years of experience performing analyses and design in the field of geotechnical and geoenvironmental engineering. His current research interests include the design of geosynthetic systems, site characterization, geotechnical centrifuge modeling, and settlement of landfills. Additional areas of research include physical and numerical modeling of high strain rate loading, such as effects of blasts and penetrations. His professional specialty is the design of geotechnical and geosynthetic components for a variety of geotechnical and geoenvironmental applications, as well as behavior of geotechnical systems under seismic, blast, and other types of dynamic loading. He has authored one book *Geotechnical Site Characterization* and numerous papers published in peer-reviewed journals and conference proceedings. He has served as a principal investigator (PI) or co-principal investigator (co-PI) on multiple projects sponsored by the National Science Foundation (NSF), in geotechnical engineering, as well as in engineering education. He has served on various professional committees, including the Geotechnical Committee of the ASCE Metropolitan New York Section and the Geoenvironmental Engineering Committee of the Geo-Institute (GI) of the American Society of Civil Engineers (ASCE). Dr. De is a fellow of the American Society of Civil Engineers (FASCE) and a registered Professional Civil Engineer (PE) in the states of California and New York.

Dr. Manoj Datta is currently professor and head of the Civil Engineering Department at IIT Delhi where he has been teaching and conducting research since 1980. He has also held the office of director of PEC University of Technology at Chandigarh and of dean (Alumni Affairs and International Programmes) at IIT Delhi. His current areas of interest include environmental geotechnics, landfills, ash and tailings impoundments, embankments and dams, ground improvement, energy geotechnics, foundation engineering, education, accreditation, and rankings. He has edited four books in the area of geoenvironmental engineering and coauthored a textbook titled *Geotechnical Engineering* with Prof. S. K. Gulhati. He has been associated with the Central Pollution Control Board, Ministry of Environment and Forests, as well as Ministry of Urban Development in framing guidelines and design manuals for municipal solid waste landfills and hazardous waste landfills. He has received five best paper awards of the Indian Geotechnical Society. He was awarded the IGS (Delhi Chapter) Leadership Award in July 2008. He delivered the prestigious IGS Annual Lecture in 2011 at Kochi.

Chapter 1
Geophysical Imaging of Landfill Interiors: Examples from Northern Illinois, USA

Philip J. Carpenter and Krishna R. Reddy

Abstract Geophysical methods used to image landfill interiors in Northern Illinois have evolved from the relatively simple one-dimensional (1D) resistivity soundings, used in the 1970s and 1980s, to more sophisticated two-dimensional (2D) resistivity and seismic refraction tomography profiles, augmented by ground-penetrating radar (GPR) and geophysical well logging. To illustrate this evolution of methods, geophysical imaging is described at two sites: the Mallard North landfill in Hanover Park, IL, and the Orchard Hills landfill, near Davis Junction, IL.

Resistivity soundings from Mallard North were inverted for true resistivity. The resistivity of municipal solid waste (MSW), mixed with clay soil, was between 9 and 19 Ω-m (unsaturated) and between 2 and 7 Ω-m (leachate saturated). Refuse thickness and leachate levels were also accurately predicted.

Orchard Hills 2D resistivity surveys showed most MSW had resistivities between 20 and 130 Ω-m (unsaturated). MSW resistivity near the leachate recirculation lines fell by as much as 3% after leachate injection started. Elastic properties of the waste were assessed using seismic wave velocities from seismic refraction tomography. The final tomographic model consisted of hundreds of cells ranging in P-wave velocity from 350 to 643 m/s, with an average value of 484 m/s. Two separate regions were identified: an upper zone consisting of a lower velocity (380–460 m/s), 3–6 m thick, and a deeper region of higher velocity (505–560 m/s). Poisson's ratio ranged from 0.38 to 0.44 with the deeper waste exhibiting higher Poisson's ratios, suggesting less rigidity.

Keywords Landfill • Geophysics • Illinois • Leachate • Tomography

P.J. Carpenter (✉)
Department of Geology and Environmental Geosciences, Northern Illinois University, DeKalb, IL 60115-2854, USA
e-mail: pjcarpenter@niu.edu

K.R. Reddy
Department of Civil and Materials Engineering, University of Illinois at Chicago, Chicago, IL 60607-7023, USA
e-mail: kreddy@uic.edu

G.L. Sivakumar Babu et al. (eds.), *Geoenvironmental Practices and Sustainability*, Developments in Geotechnical Engineering,
DOI 10.1007/978-981-10-4077-1_1

1.1 Introduction

Geophysical methods are proving useful for noninvasive imaging of landfill interiors. Once calibrated with existing borings or landfill construction records, they may be used to map subsurface features, such as waste thickness, leachate depth, and different types of waste, and to characterize waste, leachate, and elastic or strength properties of the waste.

1.2 Resistivity Surveys at a Suburban Chicago Landfill

The first study site illustrates the utility of resistivity soundings at a closed municipal landfill. This is a very simple geophysical method which may be executed with inexpensive equipment. The study site is the Mallard North 16 hectare landfill in Hanover Park, Illinois, 48 km northwest of Chicago (Fig. 1.1). Municipal solid waste (MSW) was buried there between 1970 and 1974. The West Branch of the DuPage River flows around this landfill on the east, south, and west, and a housing subdivision borders it on the north. About 40 m of unconsolidated sediments underlie Mallard North consisting of the Wisconsinan Wadsworth Till, outwash and lacustrine deposits, above an important Silurian dolomite aquifer.

The compacted and fractured final clay cover averages 1.7 m thick, overlying 2–20 m of MSW consisting primarily of paper, wood, cloth, plastic, glass, organic materials, and disseminated metal. The refuse occurs in 7.6 m thick lifts with occasional compacted clay units 0.15–0.3 m thick between the lifts, as determined from bucket-auger borings (Price 1990). A substantial thickness of the refuse is leachate-saturated and rests directly on the clayey Wadsworth Till or alluvium from the West Branch of the DuPage River.

Generally north-trending fractures and fracture zones cut the landfill cover. Fractures up to 15 cm wide allow landfill gas to escape as well as surface water to infiltrate into the waste (Booth and Price 1989). As a result this landfill is largely saturated with leachate, which produces artesian leachate springs adjacent to the West Branch DuPage River on the landfill's south flank.

Resistivity Soundings Sixteen resistivity soundings were collected across the landfill to help map leachate levels and refuse thicknesses. In resistivity sounding electrodes are inserted with increasing separations around a center-point and apparent resistivity values inverted to provide a layered model of the landfill. Both Wenner and Schlumberger electrode arrays were employed, sometimes along the same lines and other times at different locations. Lines were as long as 180 m in some cases. The maximum "*a*" spacing for Wenner arrays ranged between 45 and 60 m, and the maximum *AB*/2 spacing for Schlumberger arrays was 60 m. Four stainless steel stakes inserted into the cover were used as electrodes with an ABEM SAS 300B resistivity meter to collect the resistivity sounding data. Soundings were made over relatively flat areas of the landfill with no or little vegetation (Fig. 1.1).

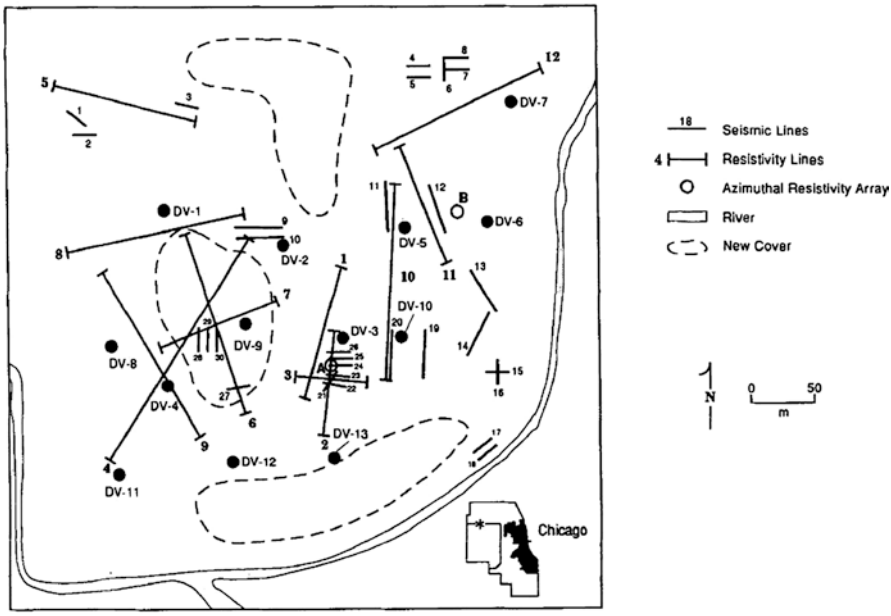

Fig. 1.1 The Mallard North landfill with locations of resistivity, seismic refraction lines and gas vents (used for obtaining leachate samples and leachate depths) (After Carpenter et al. 1991). The location of the landfill northwest of Chicago is shown at the *lower right*. New cover indicates areas of intense fracturing undergoing remediation during the surveys

ResixPlus™ (Interpex 1988) was used to invert the apparent resistivity sounding data into layered resistivity models. Four-layer models fit the sounding curves the best. These layers were correlated with final landfill cover, unsaturated MSW, leachate-saturated MSW, and underlying alluvium and/or glacial till. Sounding 10 (Fig. 1.2) illustrates the basic sounding curve shape and resistivity model, compared to a boring log from a nearby deep gas vent.

These resistivity surveys are discussed in more detail in Carpenter et al. (1990, 1991, 1994, 2009). In general, the leachate levels predicted by resistivity modeling show good agreement with the measured leachate levels from deep vents. Accurate imaging of the leachate depth is probably the result of a large resistivity contrast between the unsaturated MSW and leachate-saturated MSW. At Mallard North unsaturated MSW exhibits resistivities ranging from 9 to 19 Ω-m, whereas saturated MSW has resistivities of 2–7 Ω-m. Accurate estimation of the refuse thickness in these resistivity models is dependent on a strong resistivity contrast between the leachate-saturated refuse, which averages about 3 Ω-m, and the resistivity of the underlying till and alluvium (12–50 Ω-m).

Thirty seismic refraction profiles were also made over Mallard North, as shown in Fig. 1.1. These could only be used to evaluate the velocity of cover materials since critically refracted waves from the top of the refuse (or deeper interfaces) were

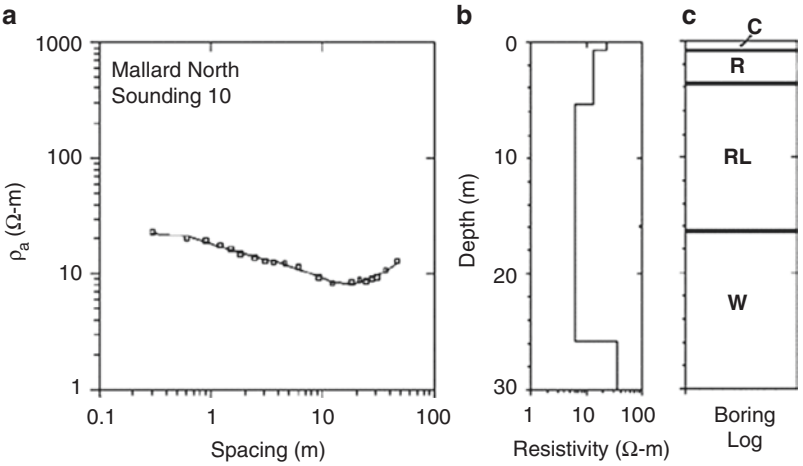

Fig. 1.2 (**a**) Wenner array resistivity sounding 10 obtained over the Mallard North landfill (After Carpenter et al. 2009). The resistivity inversion model shown in (**b**) and (**c**) shows a boring log from a deep gas vent. *C* cover material, *R* unsaturated refuse, *RL* leachate-saturated refuse, *W* Wadsworth Till and/or alluvium

not evident on any of the refraction lines. This is probably due to a reduced velocity in the upper MSW, as compared with the cover materials. This is discussed further in Carpenter et al. (1991).

1.3 Surveys at the Orchard Hills Landfill

More sophisticated geophysical methods were employed to characterize the Orchard Hills landfill about 15 km south of Rockford, IL (Fig. 1.3). This is a leachate recirculation landfill. Injecting leachate at shallow levels in the landfill, and allowing it to infiltrate and percolate through the MSW, should produce faster anaerobic degradation of the MSW. However, monitoring moisture distribution after leachate injection is a huge challenge. Rapid degradation of the waste also leads to changes in geotechnical parameters, such as stiffness (bulk, shear moduli, Poisson's ratio), angle of internal friction, and cohesion of the MSW, which can affect the stability of the landfill. Nonuniform moisture distribution is a particular concern since it might lead to a reduction in strength in only a localized area of a landfill, leading to failure of this area, either through subsidence or slope failure.

Directly monitoring leachate percolation within a leachate recirculation landfill usually includes installation of sensors within the MSW (e.g., time-domain reflectance (TDR) cables). This type of in-situ monitoring is expensive and only provides data at a few locations and depths. Likewise, the monitoring of various elastic parameters requires drilling and sampling and/or in-situ testing (blow counts, shear

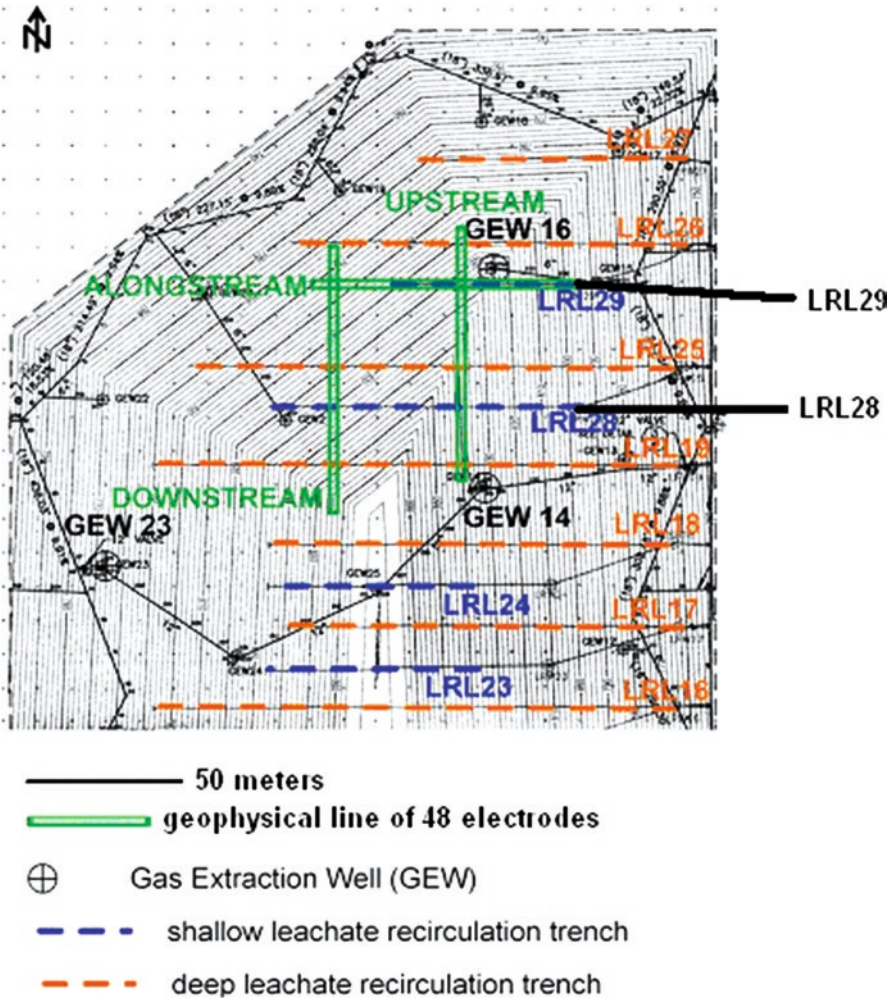

Fig. 1.3 The recirculation cell at the Orchard Hills landfill (After Carpenter et al. 2013). Leachate recirculation trenches contain the leachate recirculation lines

vane testing, cone penetrometer tip resistance, etc.). Such testing is expensive and, depending on the density of sampling, may provide only limited information about spatial variations in the elastic and geotechnical properties of the MSW. It also requires penetration of the final cover's geomembrane.

Geophysical techniques offer a number of advantages in their ability to noninvasively monitor moisture distribution and changes in geotechnical parameters within a leachate recirculation landfill. Two-dimensional (2D) resistivity imaging, frequency-domain electromagnetic (EM) and ground-penetrating radar (GPR) profiling, and well logging have all been used to noninvasively monitor conditions within this landfill (Carpenter et al. 2008b). The results are summarized below.

Electrical Resistivity Tomography (ERT) Leachate recirculation at the Orchard Hills landfill was monitored using 2D electrical resistivity imaging during, and after, leachate injection. A Syscal Pro resistivity meter was used in a pole-dipole array with electrodes planted beneath the final cover geomembrane. Seven surveys were achieved. All apparent resistivity values were inverted for true resistivity using the program RES2DINV (Loke 1996; Loke and Barker 1996) and then contoured as a 2D cross section of the recirculation cell. For each survey, the apparent resistivity was measured prior to recirculation and inverted for true resistivity (the reference). After recirculation started apparent resistivities were regularly measured and inverted for true resistivity. The reference was then subtracted from these values. Thus a negative variation indicates a decrease in resistivity, as might be expected from leachate percolating through the waste. In at least one case, the inverted ERT values showed a decrease in resistivity along segments of an injection line that may correlate with leachate permeating the waste (Fig. 1.4). This resistivity decrease is very localized. However, in most cases the volume of recirculated leachate was too small to show a resistivity change (Grellier et al. 2007).

Electromagnetic Conductivity (EM) A Geonics EM34 EM conductivity meter recorded conductivity increases associated with leachate injection along the same leachate recirculation line as shown in Fig. 1.4. Transmitter-receiver coil separations of 10 and 20 m were used. The EM conductivity distributions suggest nonuniform injection and percolation of leachate, which is consistent with the 2D resistivity images.

Ground-Penetrating Radar (GPR) Subsurface features were imaged to a depth of 8 m within the landfill using a Sensors and Software PulseEKKO IV system, with 50 and 25 MHz antennas. The leachate recirculation line (or its gravel-filled trench) shows up as a diffraction on GPR sections made with the 50 MHz antennas. Accumulations of leachate in the vicinity of leachate recirculation lines may also have been imaged (Carpenter et al. 2008a; Carpenter and Reddy 2016).

Geophysical Well Logging Natural gamma and EM conductivity logging was performed with a Mt. Sopris MGX logging system. MSW exhibited natural gamma values of 25–32 counts per second. In some cases logging showed conductivity values similar to those recorded at the surface. In other cases conductivity logs were disturbed by metal objects near the boreholes.

Seismic Refraction and Surface Waves Data were collected over both the leachate recirculation cell and an area without leachate recirculation using a Geometrics Geode seismograph with 24 geophones and a sledgehammer hitting a steel plate source. Fig. 1.5 shows the approximate raypaths for the “through-pile” fan shots conducted on the leachate recirculation cell, and Figs. 1.6, 1.7, and 1.8 the tomographic images obtained from this experiment after inversion of travel times. Both P- and SH-waves were successfully recorded and utilized. The topography of the bioreactor cell was exploited to obtain the best possible solution. Carpenter et al. (2013) discuss this experiment in more detail, including conventional refraction

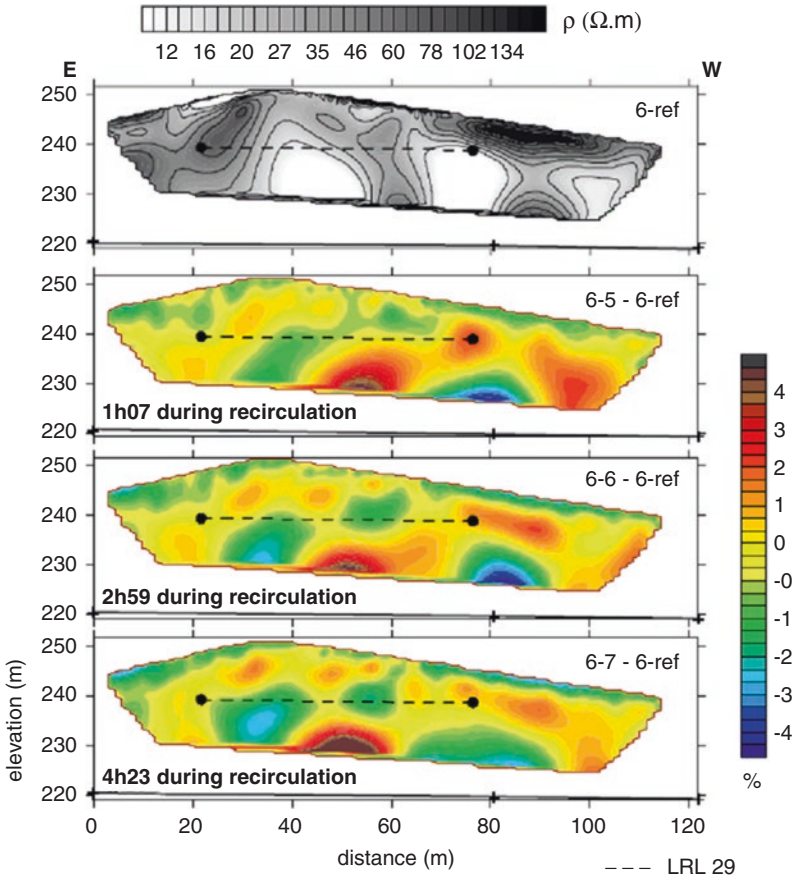

Fig. 1.4 Decrease in resistivity (in %) below the leachate recirculation line LRL29 (*dashed*) at the Orchard Hills landfill between positions 20 and 40 m. The *top figure* depicts true resistivity before leachate injection began (After Grellier et al. 2007)

surveys, application of the multichannel analysis of surface wave (MASW) method to this site, and comparison with surveys conducted over the non-circulation landfill cells.

The contoured tomographic P-wave velocity model is shown in Fig. 1.6. This was obtained through inversion of P-wave arrival times using the program GeoTomGC (GeoTom 2008), based on an earlier algorithm by Tweeton et al. (1992). P-wave velocities range from 350 to 643 m/s, with an average of 484 m/s. Two separate regions are suggested: a lower-velocity (380–460 m/s) upper zone 3–6 m thick and a deeper higher-velocity region (505–560 m/s). The apparent eastward dip of the interface between these regions is possibly a model artifact due to the limited and one-sided shot-receiver coverage. Figures 1.7 and 1.8 show SH-wave velocities and Poisson's ratio, respectively. Poisson's ratio varies from about 0.38 to 0.44, with

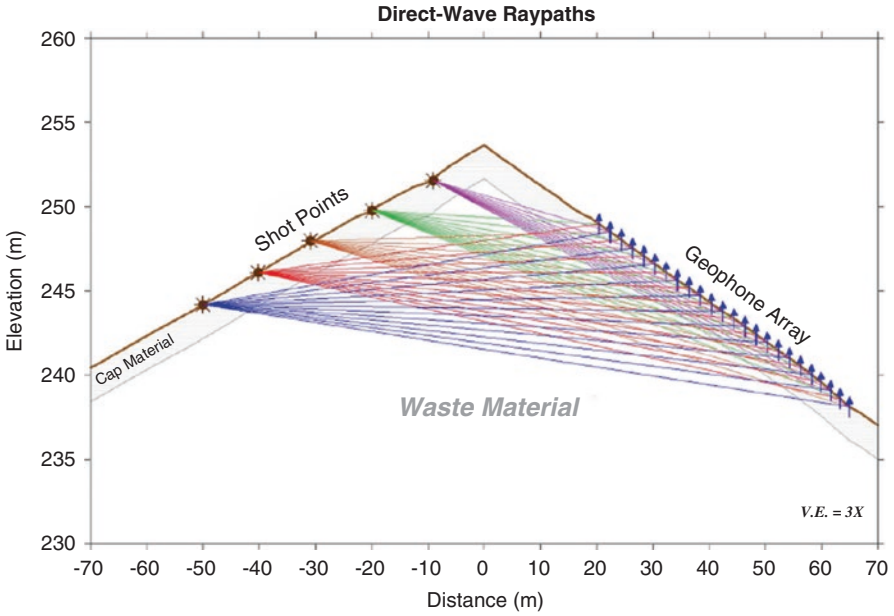

Fig. 1.5 Shot-receiver geometry and approximate raypaths for the "through-pile" seismic experiment across the leachate recirculation cell (After Carpenter et al. 2013). The geophone array consisted of both P- and S-wave geophones

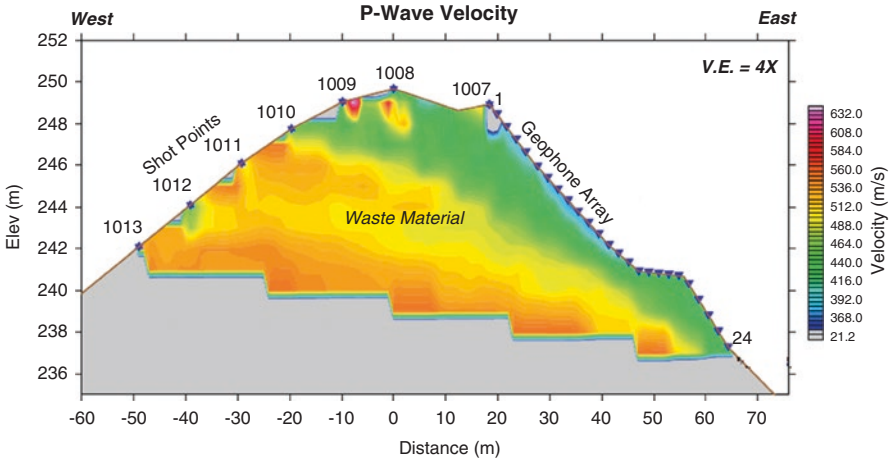

Fig. 1.6 P-wave velocity within the leachate recirculation cell (After Thompson 2008)

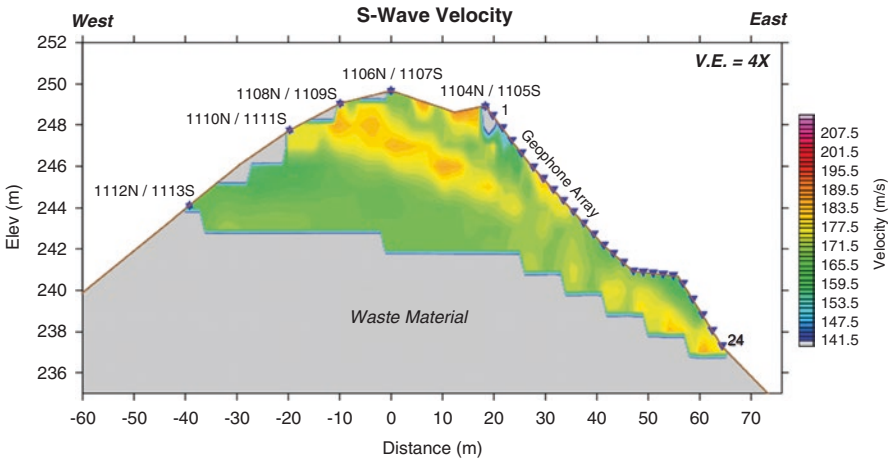

Fig. 1.7 SH-wave velocity within the leachate recirculation cell (After Thompson 2008)

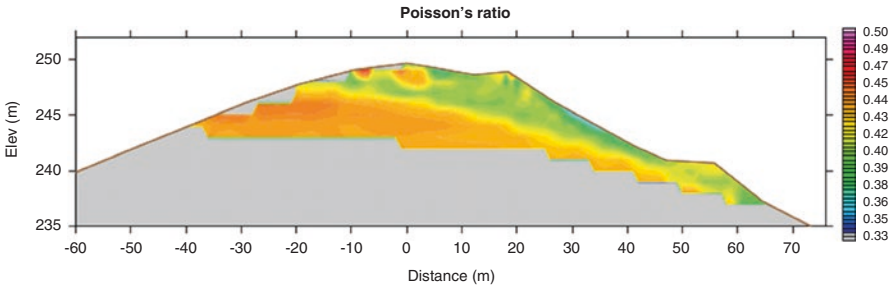

Fig. 1.8 Poisson's ratio, computed from the P- and SH-wave velocities (After Thompson 2008)

a distinctly lower Poisson's ratio in the lower part of the recirculation cell. This suggests less rigid materials at depth.

1.4 Conclusions

This paper illustrates the use of geophysical methods to investigate landfills in the Northern Illinois, USA. The first example, from the Mallard North landfill in Hanover Park, IL, showed how even simple resistivity soundings with simple equipment may provide much useful information about waste thickness, leachate levels, and geo-electrical properties of the waste. The second example, from the Orchard Hills landfill, utilized more sophisticated two-dimensional (2D) resistivity and seismic refraction tomography profiles, along with ground-penetrating radar (GPR) surveys and geophysical well logging.

Resistivity soundings from Mallard North, inverted for true resistivity, revealed municipal solid waste (MSW) resistivities of 9–19 Ω-m (unsaturated) and 2–7 Ω-m (leachate saturated). Refuse thickness and leachate levels were also accurately predicted in most cases. Leachate levels in this old landfill were shown to be alarmingly high.

At Orchard Hills 2D resistivity surveys showed most MSW resistivity between 20 and 130 Ω-m (unsaturated). MSW resistivity near the leachate recirculation lines fell by as much as 3% after leachate injection started, although in most cases amounts of injected leachate were too small to show a response.

Elastic properties of the waste were assessed using seismic wave velocities from seismic refraction tomography. P-wave velocity in the final tomographic model ranged from 350 to 643 m/s, with an average value of 484 m/s. Two separate regions may be present: a lower-velocity (380–460 m/s) upper zone, 3–6 m thick, and a deeper higher-velocity zone (505–560 m/s). Poisson's ratio ranges from 0.38 to 0.44 with the deeper waste exhibiting higher Poisson's ratios, suggesting less rigidity at depth.

References

Booth CJ, Price BC (1989) Infiltration, soil moisture, and related measurements at a landfill with a fractured cover, Illinois. J Hydrol 108:175–188

Carpenter PJ, Reddy KR (2016) Ground-penetrating radar (GPR) surveys and geophysical well logs at a leachate-recirculation landfill, Northern Illinois. Geo-Chicago 2016 Proceedings, ASCE, http://ascelibrary.org/doi/abs/10.1061/9780784480144.016, 12 p

Carpenter PJ, Kaufmann RS, Price B (1990) Use of resistivity soundings to determine landfill structure. Ground Water 28(4):569–575

Carpenter PJ, Calkin SF, Kaufmann RS (1991) Assessing a fractured landfill cover using electrical resistivity and seismic refraction techniques. Geophysics 56(11):1896–1904

Carpenter PJ, Keeley MC, Kaufmann RS (1994) Azimuthal resistivity surveys over a fractured landfill cover. Bull Assoc Eng Geol 31:123–131

Carpenter PJ, Grellier S, Reddy KR, Adib R, Peters C, Gangathulasi J (2008a) Investigating the interior of a landfill cell with leachate injection using electromagnetic conductivity and ground-penetrating radar surveys. SAGEEP2008: Symposium on the Application of Geophysics to Engineering and Environmental Problems, Environmental and Engineering Geophysical Society, Wheat Ridge, CO, 212–222 (published on CD-ROM)

Carpenter PJ, Grellier S, Reddy KR, Bogner JE, Janardhanan G Gangathulasi (2008b) Leachate distribution and geotechnical stability of bioreactor landfills: Part 2: Geophysical methods for bioreactor landfill performance. Report, August, 2005–January, 2007. University of Illinois at Chicago, Department of Civil and Materials Engineering, Chicago, IL, submitted to Veolia Environmental, November, 2008, 78 p

Carpenter PJ, Ding A, Cheng L, Liu P, Chu F (2009) Apparent formation factor for leachate-saturated waste and sediments: examples from the USA and China. J Earth Sci 20:606–617. doi:10.1007/s12583-9-0050-z

Carpenter PJ, Reddy KR, Thompson MD (2013) Seismic imaging of a bioreactor cell. J Hazar Toxic Radioact Waste ASCE 17(4):331–341

GeoTom LLC (2008) GeoTomCG: three-dimensional seismic-tomography program and manual, published by GeoTom, LLC, Apple Valley, MN, p 71. www.geotom.net

Grellier S, Reddy KR, Carpenter PJ, Bogner JE, J Gangathulasi (2007) Leachate distribution and geotechnical stability of bioreactor landfills. Progress Report, August, 2005 – January, 2007. University of Illinois at Chicago, Department of Civil and Materials Engineering, Chicago, 272 p

Interpex (1988) ResixPlusTM user's manual (including disks). Interpex, Ltd., Golden, CO. 120 p

Loke MH (1996) RES2DINV ver. 2.1: Rapid 2D resistivity inversion using the least-squares method. Users manual and software, Penang, Malaysia

Loke MH, Barker RD (1996) Rapid least-squares inversion of apparent resistivity pseudosections by a quasi-Newton method. Geophys Prospect 44:131–152

Price BC, 1990 Infiltration at a Northeastern Illinois Landfill. Unpublished M.S. thesis, Deparment of Geology and Environmental Geosciences, Northern Illinois University, DeKalb, IL, 233 p

Thompson MD (2008) Seismic investigations at the Orchard Hills landfill, Davis Junction, IL. Report RPT-1001-061508, MDT-Associates, Bolingbrook, IL, 36 p

Tweeton DR, Jackson MJ, Roessler KS (1992) BOMCRATR – a curved ray tomographic computer program for geophysical applications. U.S. Bureau of Mines Report of Investigations (RI) 9411, 39 p

Chapter 2
Large-Scale Experimental Assessment of the Effect of Degradation on Shear Strength of Municipal Solid Waste from a Texas Landfill

S. Datta, X. Fei, and D. Zekkos

Abstract The degradation process of a municipal solid waste (MSW) sample from a landfill in Texas (TX), USA, was monitored in a large-scale laboratory landfill simulator for 1136 days. Simple shear testing was performed on reconstituted fresh and degraded waste specimens and an "undisturbed" degraded specimen. Shear resistance at 10% shear strain was defined as the shear strength in this study. The shear strength of the degraded waste was found to be 17–35% lower than the shear strength of the fresh waste. The effective friction angles of the fresh and degraded waste were 17–21° and 12–17°, respectively. The relatively low friction angles are due to the low compaction effort and density of the specimens. The shear strength of a specimen removed from the simulator in an "undisturbed" manner was found to be nearly identical to the shear strength of a reconstituted degraded specimen.

Keywords Landfill • Municipal solid waste • Large scale • Degradation • Shear strength

2.1 Introduction

Municipal solid waste (MSW) landfills are annually increasing in size to accommodate the large quantities of waste produced. Landfill design requires appropriate characterization of the mechanical properties of waste involved. Shear strength estimates are usually based on large-size laboratory testing with direct shear testing being the most common (Bareither et al. 2012; Bray et al. 2009). In this study, a 300 mm in diameter landfill simulator and a 300 mm in diameter simple shear device were used to study the effect of MSW degradation on its shear strength.

S. Datta (✉) • X. Fei • D. Zekkos
Department of Civil and Environmental Engineering, University of Michigan, Ann Arbor, MI, USA
e-mail: sampurna@umich.edu; xcfei@umich.edu; zekkos@geoengineer.org

G.L. Sivakumar Babu et al. (eds.), *Geoenvironmental Practices and Sustainability*, Developments in Geotechnical Engineering,
DOI 10.1007/978-981-10-4077-1_2

2.2 Methodology

2.2.1 Waste Characterization

The MSW used in this study was collected from Austin Community landfill in Texas (TX-ACL) and was transported in sealed drums to the laboratory. Field composition was characterized according to the procedure described by Zekkos et al. (2010). Waste was segregated into a finer and coarser fraction using a 20 mm sieve. The <20 mm material is silty sand (SM) with 33% fines of high plasticity (liquid limit = 65%, plastic limit = 46%, plasticity index = 19%). The initial total mass, waste composition (percentage of a constituent on a wet mass basis), moisture content, and volatile solids were assessed and are provided in Table 2.1.

2.2.2 Degradation Testing of MSW

A specimen was reconstituted based on the field waste composition and used for degradation testing. A 42-L simulator accompanied by a system to recirculate and store leachate and a system to monitor the long-term waste degradation process was constructed and is described in detail by Fei et al. 2014 (Fig. 2.1). The material was generally placed at a loose state, i.e., without significant compaction. Besides the vertical load from a plastic leachate distribution plate and a stainless steel rod for settlement measurement that impose <1 kPa vertical stress, no additional vertical stress was applied to the specimens. The temperature of the simulator was raised from laboratory temperature to 40 ± 3 °C using heating blankets. Liquids were recirculated through the waste mass three times per week.

Leachate samples were analyzed for total and soluble chemical oxygen demand (COD), respectively. The specimen unit weight at field capacity ($\gamma_{t,fc}$) and at saturation ($\gamma_{t,s}$) and the settlement were also measured with time. Biogas composition and volume were also measured to assess the progress of waste degradation. The experiment was stopped after 1136 days of operation and the simulator was disassembled.

Table 2.1 Composition, moisture content, and volatile solids of MSW specimen

<20 mm particles (%)	Paper (%)	Soft plastic (%)	Wood (%)	$W_{t,0}$ (kg)	$w_{c,ave.}$ (%)	VS in <20 mm fraction (g/g)	VS in paper (g/g)
79.1	10.6	6.0	4.3	30.02	34.6	0.070	0.610

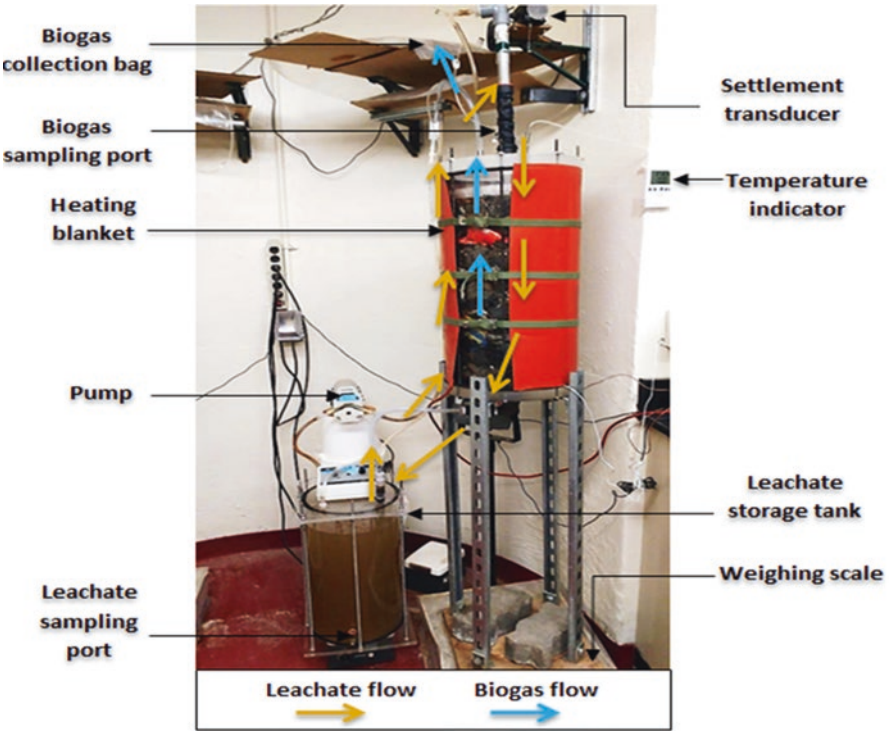

Fig. 2.1 Schematic of the simulator setup for MSW degradation

2.2.3 Simple Shear Testing of MSW

A 300 mm-diameter simple shear device, shown in Fig. 2.2, was used to test the shear resistance of MSW specimens at fresh and degraded state. Upon completion of the degradation experiment, the degraded specimen was removed from the simulator in an undisturbed manner and was placed in the simple shear device for testing. Additional specimens using the degraded material were reconstituted to perform additional simple shear testing at the degraded state.

Each specimen was consolidated for 24 ± 2 h and sheared at a strain rate of 0.35 ± 0.02%/min under constant load (CL) conditions, which are equivalent to consolidated drained condition. Tests were conducted at vertical effective stresses varying from 50 to 500 kPa. In this study, the shear resistance at 10% shear strain is defined as the shear strength of the specimen. Assuming that the horizontal plane is the failure plane, the friction angle is calculated by the following equation as discussed in DeGroot et al. (1992):

$$\varphi_{\tan} = \tan^{-1} \frac{\tau_{hf}}{\sigma_{vf'}} \tag{2.1}$$

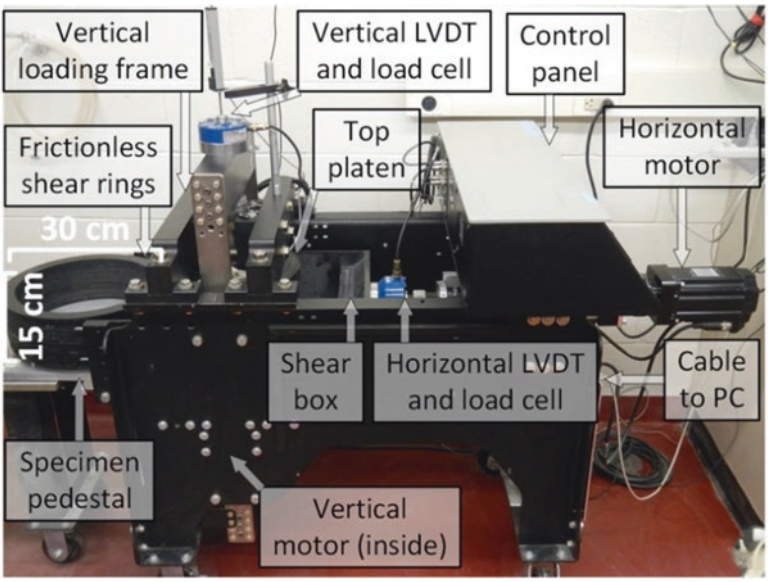

Fig. 2.2 Schematic of the large-size simple shear testing device (Fei 2015)

where τ_{hf} is the measured horizontal shear stress at failure, and σ_{vf}' is the measured vertical effective stress at failure.

2.3 Results and Discussion

2.3.1 Degradation Experiment

Long-term settlement of the waste specimen was found to follow three phases, as discussed in Fei and Zekkos (2013). Immediate compression associated with the first few leachate recirculations through the waste mass was observed between days 1 and 10. Active biodegradation took place from day 10 to day 800, and the remaining was residual compression (Fig. 2.3a). The initial total unit weight of the specimen was 7.9 kN/m^3 which increased to 10 kN/m^3 by day 10 and then to 11 kN/m^3 by day 720 before the specimen started becoming submerged due to clogging at its base (Fig. 2.3b). The biogas generated primarily consisted of CH_4 and CO_2 (Fig. 2.3c). Gas generation was completed at day 308 (Fig. 2.3e and 2.3f), and the total volume of biogas generated was 800 L (Fig. 2.3f). The changes of total COD (tCOD) and soluble COD (sCOD) in the leachate with time were typical of waste degradation under favorable conditions for microbial activity (Fig. 2.3d). The degradation experiment was stopped after 1136 days of operation, and the simulator was disassembled.

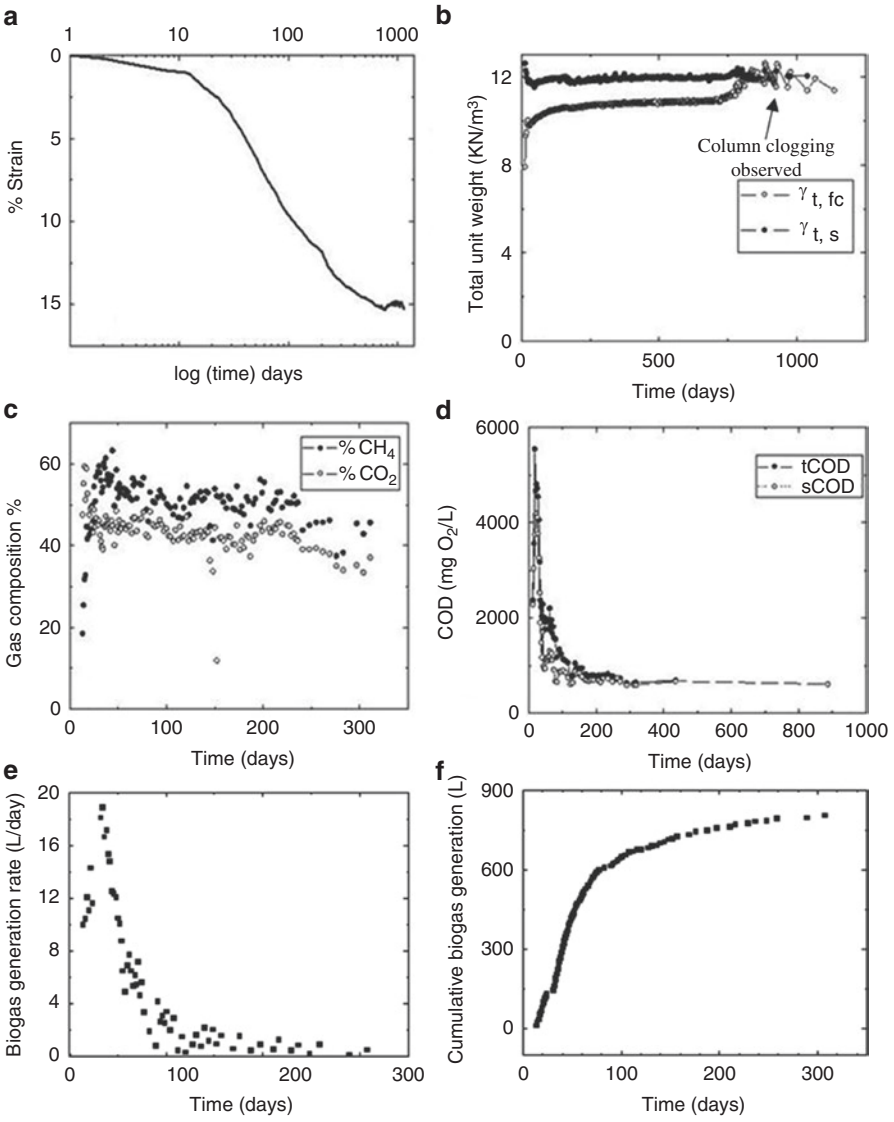

Fig. 2.3 Evolution of parameters during waste degradation: (**a**) strain, (**b**) saturated ($\gamma_{t,s}$) and field capacity ($\gamma_{t,fc}$) total unit weight, (**c**) biogas composition, (**d**) total COD (tCOD) and soluble COD (sCOD) in the leachate, (**e**) biogas generation rate, and (**f**) cumulative biogas generation

2.3.2 Simple Shear Testing

The MSW from Texas was tested at fresh and degraded state. All fresh and degraded waste specimens showed similar stress-strain response with a peak shear resistance reached at large shear strains (as shown in Fig. 2.4a). The fresh and degraded

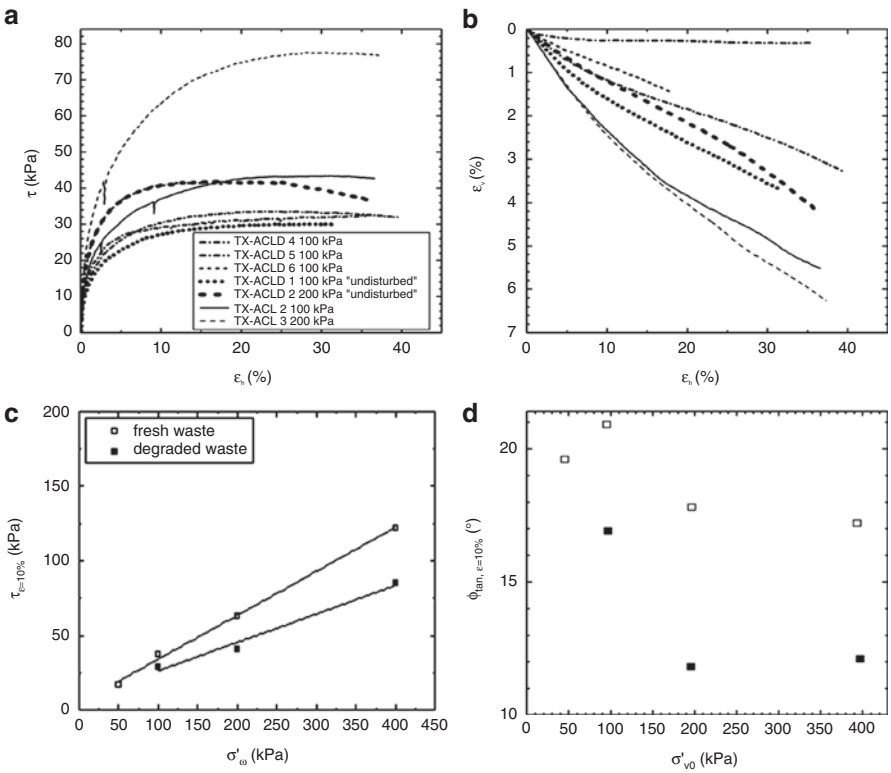

Fig. 2.4 Shear strength characteristics of fresh and degraded TX waste showing relationships between (**a**) stress-strain, (**b**) vertical strain(ε_v) and shear strain(ε_h), (**c**) shear strength($\tau_{\varepsilon=10\%}$) and vertical stress(σ'_{v0}) and (**d**) tangent friction angle($\varphi_{\varepsilon=10\%}$) and vertical stress($\sigma'_{v0}$)

specimens were tested at 35% and 47% moisture contents, respectively. The volumetric strain of the fresh specimen during shearing was higher than that of the degraded ones (Fig. 2.4b). The average as-prepared total density for the fresh waste was 7.65 kN/m^3. The consolidated total density of fresh waste before shearing ranged from 11 to 16.5 kN/m^3 for effective vertical stresses ranging from 50 to 400 kPa, and that of degraded waste ranged from 15 to 17 kN/m^3 for effective vertical stresses ranging from 100 to 400 kPa.

The shear strength of the "undisturbed" degraded specimen was approximately equal to that of the reconstituted degraded specimen indicating that reconstitution of specimen using the degraded waste resulted in similar material as the "undisturbed" degraded waste. The effective friction angle is 17°–21° for the fresh waste and 12°–17° for the degraded waste (Fig. 2.4d). The shear strength was generally low due to the minimal compaction effort used during specimen preparation. As shown in Fig. 2.4c, the cohesion and friction angle for fresh waste are 5.9 kPa and 16.4, and that of degraded waste are 7.8 kPa and 10.8°, respectively. Thus, for this waste the data indicates that cohesion was least affected post-degradation, but there was a

34% decrease in friction angle. More importantly, the reduction in shear strength was between 17 and 35%.

2.4 Conclusion

A waste degradation experiment was conducted and monitored in a large-scale laboratory simulator for 1136 days. Simple shear testing was performed on reconstituted fresh and degraded waste specimens as well as an "undisturbed" degraded specimen. In terms of strength parameters, cohesion was least affected by degradation, but the friction angle decreased by 34%. Overall, for this waste sample composition, the reduction in shear strength due to biodegradation ranged between 17% and 35%. Note, however, that although the initial states of fresh and degraded specimens were identical, the comparison is made between the waste at fresh state and their state after degradation. Thus, the fresh and degraded specimens have different moisture content and total density. The effective friction angles of the fresh and degraded waste were 17°–21° and 12°–17°, respectively. An "undisturbed" degraded specimen had practically the same shear strength as that of a reconstituted degraded specimen. The waste degradation process altered the composition and unit weight, and each of the factors influenced the shear strength of waste.

Acknowledgment This research was supported by the National Science Foundation (NSF) Division of Computer and Communication Foundations under Grant no. 1442773. ConeTec Investigations Ltd. and the ConeTec Education Foundation are acknowledged for their support to the Geotechnical Engineering Laboratories at the University of Michigan. Any opinions, findings, conclusions, and recommendations expressed in this paper are those of the authors and do not necessarily reflect the views of the NSF.

References

Bareither CA, Benson CH, Edil TB (2012) Effects of waste composition and decomposition on the shear strength of municipal solid waste. J Geotech Geoenviron 138:1161–1174

Bray JD, Zekkos D, Kavazanjian E Jr, Athanasopoulos GA, Riemer MF (2009) Shear strength of municipal solid waste. J Geotech Geoenviron 135:709–722

DeGroot DJ, Ladd CC, Germaine JT (1992) Direct simple shear testing of cohesive soils. Research, Massachusetts Institute of Technology, Department of Civil Engineering

Fei X (2015) Experimental assessment of coupled physical, biochemical-mechanical-hydraulic processes of municipal solid waste undergoing biodegradation. Doctoral thesis, University of Michigan, Ann Arbor

Fei X, Zekkos D (2013) Factors influencing long-term settlement of municipal solid waste in laboratory bioreactor landfill simulators. J Hazard Toxic RadioactWaste 17:25–271

Fei X, Zekkos D, Raskin L (2014) An experimental setup for simultaneous physical, geotechnical and biochemical characterization of municipal solid waste undergoing biodegradation in the laboratory. ASTM Geotech Test J 37(1):1–12

Zekkos D, Kavazanjian E, Bray JD, Matasovic N, Riemer MF (2010) Physical characterization of municipal solid waste for geotechnical purposes. J Geotech Geoenviron 136:1231–1241

Chapter 3
Environmental Benign Electrokinetics for Landslide Mitigation

Jiale Li and Xiong (Bill) Yu

Abstract Landslide is one of the major geological disasters that pose serious threat to the communities. The use of electrochemical stabilization techniques can provide effective remediation for shallow and intermediate depth landslide failures through cohesive weak soils. It is a promising alternative to conventional remediation measures under situations where regular construction loads might trigger catastrophic landslide failure. Electrokinetic treatment, however, requires a large amount of electricity that is typically produced with a mobile fuel-based generator. The high fuel consumption and carbon dioxide emission lead to undesirable economic and environmental consequences. Renewable energy such as the wind and solar energy provides a promising electricity supply for electrochemical treatment. This paper provides a conceptual analysis on the electrochemical treatment with renewable wind energy. The results show that electrokinetic soil improvements using a renewable generator can be more economical than the traditional generator. It is an environmental friendly option for electrokinetic stabilization of landslide.

Keywords Electrokinetics • Landslides • Wind energy • Sustainability • Soil improvements

3.1 Introduction

Landslides are prevalent natural disasters worldwide. As a snapshot on their impacts, there are nearly 18,000 landslides in the highway system of the State of Ohio, USA. The Ohio Department of Transportation (Ohio DOT) spends over $40 M each

J. Li
Department of Civil Engineering, Case Western Reserve University, 2104 Adelbert Road, Bingham 257, Cleveland, OH 44106-7201, USA
e-mail: jxl780@case.edu

X. Yu (✉)
Department of Civil Engineering, Case Western Reserve University, 2104 Adelbert Road, Bingham 206, Cleveland, OH 44106-7201, USA
e-mail: xxy21@case.edu

G.L. Sivakumar Babu et al. (eds.), *Geoenvironmental Practices and Sustainability*, Developments in Geotechnical Engineering,
DOI 10.1007/978-981-10-4077-1_3

year to remediate problems caused by landslides. Many of these landslides occur as a result of low-strength soils and the occurrence of groundwater. Several weathered bedrock units (e.g., "redbed" units of the Conemaugh Formation) and problematic soils (e.g., Minford Clays) yield very low strength (phi angles). Mass movement of these soils generally occurs following saturation during the spring rainfall. Current remediation measures (e.g., removal, removal and reconstruction, drilled shafts) do not offer a cost-effective solution to landslides involving low-strength soils. As a promising alternative, the use of electrochemical stabilization techniques is expected to provide an effective means of remediation for shallow and intermediate depth landslide failures. Research (within the USA) into the use of electrochemical stabilization of soils dates back to the 1940s. European application of this technology started even earlier.

The concept involves strategic placement of suitable anions and cations in trenches to facilitate the migration of these chemical constituents, as dissolved species, through groundwater transport. A DC current is introduced to aid in the transport of the chemical species and to catalyze the electrochemical processes used to form cementations or other mineral precipitates within the soil horizon. Typical anions and cations to be considered include, but are not limited to, oxide, hydroxide, sulfate, phosphate, carbonate and calcium, magnesium, iron, and aluminum, respectively. The application will involve the placement of anionic species in trenches near the cathodes and cationic species in trenches near the anodes, followed by the electromigration of dissolved constituents toward opposite charged fields.

Renewable energy such as wind or solar energy is promising to provide power supply for landslide mitigation purpose. This research comes up with the idea of using renewable energy such as wind turbine and solar panel producing electricity to stabilize slope using electrochemical method (Fig. 3.1), for the reason that continuous usage of gasoline-powered portable generator that produces power on site could be costly and it has become a major issue that restricts the utilization of electrochemical stabilization. Renewable energy like wind turbine and photovoltaic power generation could be installed near the site of slides which will greatly reduce the transfer cost, and also they can be destructive and move to wherever they needed easily.

3.2 Background

The application of DC electrical current for electroosmotic consolidation and stabilization of fine-grained soils is referred to as electrokinetic soil treatment and was pioneered by Casagrande in the 1950s (Casagrande 1953). The electrochemical process has since then been used globally for slope stabilization, chemical alteration of clay soils, remediation of contaminated soils, soil consolidation and dewatering, reducing the negative skin frictions of piles, and increasing the bearing capacity of

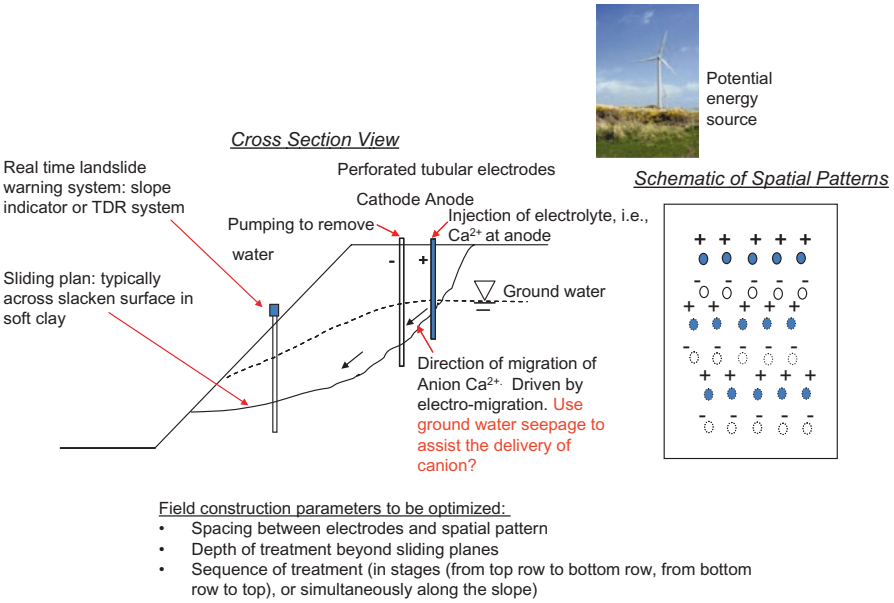

Fig. 3.1 Conceptual field implementation of electrochemical stabilization for slope treatment using wind energy

frictional piles for a variety of geotechnical and geo-environmental applications (Alshawabkeh et al. 2004). Examples include the work by Casagrande (1953, 1983), Gladwell (1965), Mise (1961), Esrig (1968), Wan and Mitchell (1976), Gray and Somogyi (1977), Johnston and Butterfield (1977), and Banerjee and Mitchell (1980), among many others.

A number of phenomena take place simultaneously when DC current is applied across soil, which is typically described with the term "*electrokinetics*" (Jennings and Mansharamani 1999). Figure 3.2 illustrates the most significant ones from the engineering perspectives (Coletta et al. 1997; Jennings and Mansharamani 1999).

There are several advantages of electrochemical treatment. Existing laboratory and field study indicates the electrochemical treatment is effective in improving the strength of weak soils, especially clay or silty clay. The improvements appear to be permanent, i.e., the soil strength will not be reduced by soaking underwater. The electrochemical technique can be less expensive than the other remedial alternatives for soft slopes. Especially, it does not disturb the site activities (Acar et al. 1995; Azzam and Oey 2001), which is desirable for slope stabilization purpose. Table 3.1 provides a list of laboratory and field case studies of using electrokinetics for soil improvements, particularly the amount of energy consumption associated with electrokinetic soil treatment.

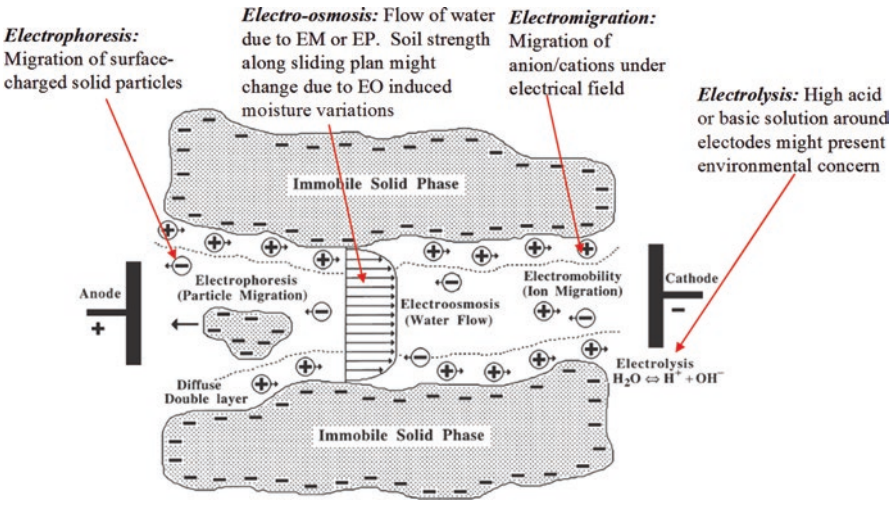

Fig. 3.2 Major electrokinetic phenomena and relationship to slope stabilization (Coletta et al. 1997; Jennings and Mansharamani 1999)

3.3 Renewable Energy

3.3.1 Wind Turbine

The wind turbine used as the prototype wind energy generator in this study is a 100 kW utility scale wind turbine (Northern Power® 100) located on the campus of CWRU (Fig. 3.3). The wind turbine which has 36 m hub height and 21 m rotor diameter was installed in November 2010 with financial support from the Ohio Third Frontier Program. The primary role of the turbine is to serve as a research test-bed for electrical and mechanical research. A Campbell Scientific data acquisition system (DAQ) is installed in the wind turbine to collect its operation data continuously (Li and Yu 2015).

3.3.2 Solar Panel

In 2008, Case Western Reserve University became one of the "anchor institutions" in the Ohio Solar Cooperative (OCS). OCS is one of several cooperatives being seeded by the Cleveland Foundation and provides employment opportunities in the renewable energy market. In July 2010 the OCS and the University collaborated on the installation of the 67.5 KW photovoltaic arrays on campus. This PV array is hosted on the roof of the Adelbert Gymnasium as shown in Fig. 3.4.

The meters installed in both wind turbine and the PV array monitors the power output. Energy production data from January 2013 to January 2014 are obtained at 15 min' intervals from facility management office. The annual average daily production behavior is shown in Fig. 3.5 which is used as the benchmark for the characteristics of wind

Table 3.1 Summary of representative research involving electrochemical soil improvement

	Soil type	Electrode	Chemical	Improvements	Energy
Adamson et al. (1967a)	Sand with various amount of clay (1.5 ~ 3.5%)	Anode: solid aluminum bar	$CaCl_2$	Increase of cohesion by 100 ~ 200 lb./ft^2	20 ~ 40 kWh/m^3
		Cathode: perforated iron tubes	$Al_2(SO_4)_3$		
Adamson et al. (1967b)	Highly expansive soils	Anode: solid aluminum bar		Reduce volume change associated with moisture	60kWh/m^3
		Cathode: perforated iron tubes			
Harton et al. (1967)	Clayey silt	Iron pipe for both anode and cathode	$CaCl_2$	Increase cohesion by 150–500 lb./ft^2	479 kWh/m3 (due to over treatment)
			$Al_2(SO_4)_3$	Increase of PL and LL	
Zhinkin (1952)		18 perforated iron anodes (28–35 mm diameter) equally spaced at 12.5 m distance	4% CaCl2	Cohesion increased from 0.04 kg/cm^2 to 0.12–0.15 kg/m^2	20 ~ 30 kWh/m^3 for drying 40–45 kWh/m^3 for soil improvement
		Treat depth 1.6 m			
Gray and Schlocker (1969)	Bentonite	Solid aluminum electrodes	Anolyte 1% $AlCl_3$	LL of bentonite greatly reduced	20–30 kWh/yd^3
	Illite		Catholyte 5% NaCl	LL of illite soil unaffected	
	Buckshot			LL of buckshot soil slightly changed	
Ou et al. (2009)	Silty clay	Tubular perforated stainless steel pipes	NaCl	400% increase in the undrained shear strength	Electrical gradient: 40–60 V/m
			KCl		
			$CaCl_2$		

Fig. 3.3 Wind turbine on CWRU campus

Fig. 3.4 Solar panel on CWRU campus

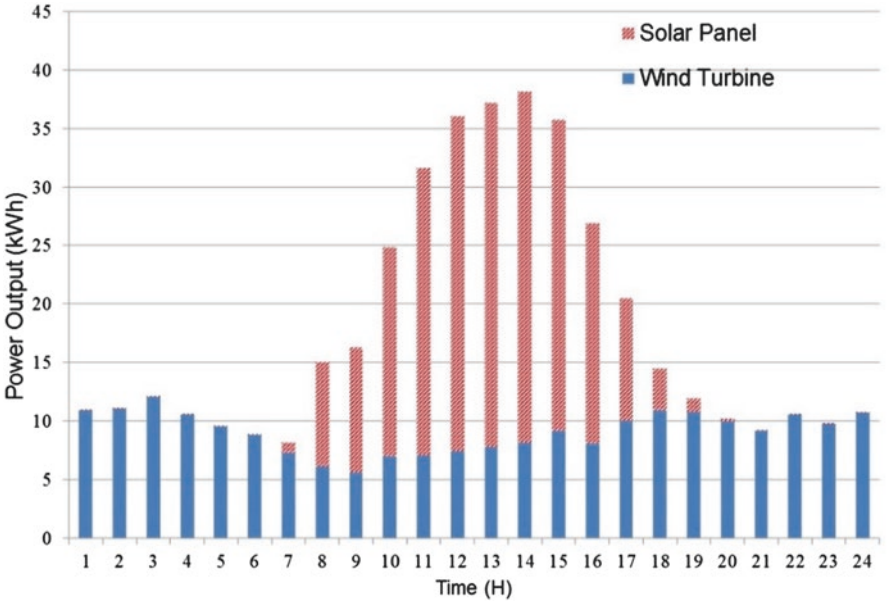

Fig. 3.5 Daily power output of wind turbine and solar panel of 2013

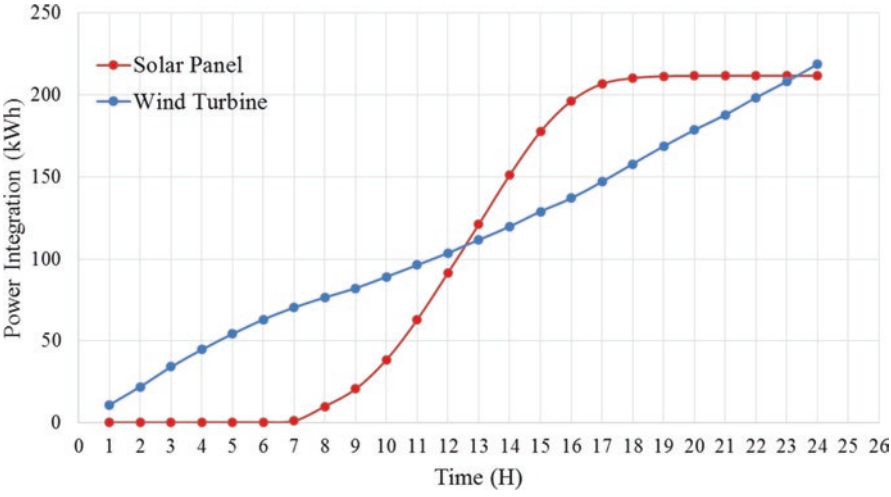

Fig. 3.6 Daily power output integration of wind turbine and solar panel from 2013 data

and solar energy production in this study. From this figure, it can be seen that the solar panel power output, which depends highly on the solar radiation, produces electricity primarily between 8:00 AM and 17:00 PM over a day. The wind turbine produces electricity all day but produces slightly higher amount of energy from 18:00 PM to 5:00 AM.

Figure 3.6 shows the power integration over 1-day time period. In which the solar panel produces approximately 212kWh per day and wind turbine output 219 kWh per day based on 1-year data.

3.4 Results and Analysis

Adamson et al. (1967a) stated that amounts of energy on the order of 20–40 kWh/m^3 of ground would be sufficient to effect substantial consolidation and strengthening. In the study, we chose electrochemical soil improvement method take 30kWh/m^3 for comparison. In Brunetti's work (Brunetti et al. 2009), probability distributions of landslide volumes range over 10^{-4} m^3 to 10^{13} m^3. In this study, we assume to stabilize $10^4 m^3$ soil.

A typical commercial gasoline-powered portable generator model # STGP-9500 EB is chosen as conventional on-site electrochemical soil improvement power source. This type of generator consumes 6.5 gallon of gasoline working 10 h at 50% load. For a $10^4 m^3$ landslides, the traditional portable generator will take almost 52,000 gallon of gasoline to complete the work. According to the US Energy Information Administration (EIA), the price of gasoline of 2014 was $3.36/gal, so the total cost to stabilize the assumed landslides will be $174,720.

For a 100 kW wind turbine, the cost could vary from $100,000 to $200,000 per turbine based on different commercial wind turbine suppliers. We chose the cost of wind turbine to be $100,000 for base type. So each installation or the removal of the wind turbine would cost approximately $23,500. And the design life of a wind turbine is 20 years. The total cost that includes the installation and depreciation over the duration of treatment will be $42,265. This corresponds to about 75.8% cost saving compared to the use of conventional fuel-burning generator.

According to industry average cost, to install 67.5 kW solar panel would cost $200,000, and the design life of solar panel is 25 years. The installation cost of the solar panel is around 15% of its total cost, which is about $30,000. The total cost of using solar panel to generate electricity to stabilize $10^4 m^3$ landslides will be $61,015 (including the installation cost and depreciation cost over the period of operation for soil treatment). This leads to 65% saving compared to conventional method. The results for the above analysis are shown in Table 3.2.

With the cost saving in treatment of landslide, it takes about 4 years to break even the cost of initial investment for the $100,000 wind turbine or $200,000 solar farm.

Table 3.2 Cost comparison for treatment of a landslide of 10^5 m^3 with alternative electricity supply

Electricity production method	Cost to stabilize the volume	Cost-saving to fuel-burning generator	Breakeven
Fuel-burning generator	$174,720 (fuel consumption)	–	
Solar panel	$61,015 (installation + depreciation)	65.1%	Treatment of 2 landslides (for $100,000 mobile turbine) or in about 4 year
Wind turbine	$42,265 (installation + depreciation)	75.8%	Treatment of 5 landslides (for $200,000 mobile solar farm) or in about 4 year

3.5 Conclusion

Electrokinetic treatment is effective for remediation of landslides over soft soils. It improves the compressive strength of soils with no impacts on its structural stability. While developed several decades ago, the high cost and environmental consequence are major barriers for its wide applications. This study intends to analyze the possibility of a novel idea that utilizes renewable wind or solar energy for landslide mitigation. These renewable energy generators can be moved to new locations once the landslide treatment is over. Therefore, it has the potential to be more cost effective and environmental friendly for landslide mitigation via electrochemical soil improvement compared with traditional gasoline-powered generator. The paper compared with cost benefits of the proposed concept versus conventional electrochemical treatment for on-site electrochemical stabilization on soft soils. The results show that renewable energy, both wind turbine and PV, are more economical for on-site electrochemical stabilization of landslides than gasoline generator. For treatment of a typical medium- to large-scale landslide, solar panel saves 65.1% of the cost, while wind turbine could save 75.8% cost compared to the use of conventional fuel-burning generator. The major issue with renewable is the high initial cost, which however can be quickly recouped over its designed operation life. The use of mobile renewable energy generator therefore provides a potential environmental friendly method for electrochemical stabilization of landslides.

References

Acar YB, Gale RJ, Alshawabkeh AN, Marks RE, Puppala S, Bricka M, Parker R (1995) Electrokinetic remediation: basics and technology status. J Hazard Mater 40(2):117–137

Adamson LG, Quigley WG, Ainsworth HR, Chilingar GV (1967a) Electrochemical strengthening of clayey sandy soils. Eng Geol 1(6):451–459

Adamson LG, Chilinger GV, Beeson CM, Armstron RA (1967b) Electrokinetic dewatering, consolidation and stabilization of soils. Eng Geol 1(4):291–304

Alshawabkeh AN, Sheahan TC, Wu X (2004) Coupling of electrochemical and mechanical processes in soils under DC fields. Mech Mater 36(5):453–465

Azzam R, Oey W (2001) The utilization of electrokinetics in geotechnical and environmental engineering. Transp Porous Media 42(3):293–314

Banerjee S, Mitchell JK (1980) In-situ volume-change properties by electro-osmosis--theory. J Geotech Geoenviron Eng. 106(ASCE15370)

Brunetti M, Guzzetti F, Rossi M (2009) Probability distributions of landslide volumes. Nonlinear Process Geophys 16(2):179–188

Casagrande L (1953) Review of past and currentwork on Electro-osmotic stabilization of soils-report to the Bureau of Yards and Docks. Contract No. Noy-76303- December

Casagrande L (1983) Stabilization of soils by means of electro-osmosis: state of the art. J Boston Soc Civil Eng 69(2):255–302

Coletta TF, Bruell CJ, Ryan DK, Inyang HI (1997) Cation-enhanced removal of lead from kaolinite by electrokinetics. J Environ Eng 123(12):1227–1233

Esrig MI (1968) Pore pressures, consolidation, and electrokinetics. Am Soc Civil Engr J Soil Mech 94(4):899–921

Gladwell J (1965) Practical applications of electro-osmosis. N Z Eng 20(2):66
Gray DH, Schlocker J (1969) Electrochemical alteration of clay soils. Clay Clay Miner 17:309–322
Gray DH, Somogyi F (1977) Electro-osmotic dewatering with polarity reversals. J Geotech Eng Div 103(1):51–54
Harton JH, Hamid S, Abi-Chedid E, Chilingar GV (1967) Effects of electrochemical treatment on selected physical properties of a clayey Silt. Eng Geol 2(3):191–196
Jennings AA, Mansharamani P (1999) Modeling electrokinetically-enhanced aggregate remediation. Environ Model Softw 14(6):625–634
Johnston I, Butterfield R (1977) A laboratory investigation of soil consolidation by electro-osmosis. Aust Geomech J 7(1):21–32
Li J, Yu X (2015) Model and procedures for reliable near term wind energy production forecast. Wind Eng 39(6):595–608
Mise T (1961) Electro-osmotic dewatering of soil and distribution of the pore water pressure. In: Proceedings of the 15th international conference on soil mechanics and foundation engineering, pp 247–255
Ou C-Y, Chien S-C, Chang H-H (2009) Soil improvement using electroosmosis with the injection of chemical solutions: field tests. Can Geotech J 46(6):727–733
Wan T.-Y, Mitchell JK (1976) Electro-osmotic consolidation of soils. J Geotech Geoenviron Eng 102(ASCE# 12156 Proceeding)
Zhinkin GN (1952) Experiment of utilizing electrochemical induration of grounds for stabilization of railway beds. Sb Tr Leningr Inst Inzh Zheleznodor Transp 144:64–78

Chapter 4
Recent Advances in Seismic Design of MSW Landfill Considering Stability

Deepankar Choudhury, B. Giridhar Rajesh, and Purnanand Savoikar

Abstract Pseudo-dynamic limit equilibrium-based analytical solutions to predict the sliding failure of MSW landfill under seismic conditions have been proposed. The proposed methodology incorporates the influences of time period and phase in the analyses. Various MSW landfills with sidehill configurations founded on (a) horizontal and partly sloping base, (b) sloping base and (c) stepped base are analysed. Results are presented in terms of yield acceleration coefficient. Neglecting seismic vertical acceleration brings about 14–28% increase in yield acceleration coefficient for the case of stepped base. The influence of landfill length to height (*L/H*) ratio is more prominent for the landfill founded on sloping base. Coefficient of yield acceleration is increased by 36%, with increase in *L/H* ratio from 2 to 10. These results with proposed methodology can be used for seismic design of MSW landfill considering sliding stability.

Keywords MSW landfill • Seismic design • Stability • Dynamic properties • Pseudo-dynamic

D. Choudhury (✉)
Department of Civil Engineering, Indian Institute of Technology Bombay, Mumbai 400076, India

Academy of Scientific and Innovative Research (AcSIR), New Delhi, India
e-mail: dc@civil.iitb.ac.in

B.G. Rajesh
Department of Civil Engineering, Indian Institute of Technology Bombay, Mumbai 400076, India
e-mail: bgrajesh@iitb.ac.in

P. Savoikar
Department of Civil Engineering, Goa College of Engineering, Ponda, Goa 403401, India
e-mail: psavoikar@gmail.com

G.L. Sivakumar Babu et al. (eds.), *Geoenvironmental Practices and Sustainability*, Developments in Geotechnical Engineering,
DOI 10.1007/978-981-10-4077-1_4

4.1 Introduction

Safe design of municipal solid waste (MSW) landfill systems in earthquake-prone areas is crucial as collapse of landfills can result in groundwater contamination with leachate and can induce associated geoenvironmental risks. Failures of landfill components due to seismic forces were described by Augello et al. (1995), Orr and Finch (1990) and a few others. Seismic stability is normally estimated using the limit equilibrium slope stability analysis or by analysis of permanent deformations caused by earthquake using conventional pseudo-static approach. Sarma (1975) studied the seismic slope stability and concluded that the seismic sliding displacements are not affected by the direction of inertia force, which results in least yield acceleration. Matasovic (1991) proposed solutions for computing yield accelerations of slopes. Shewbridge (1996) presented simplified method of limit equilibrium for estimation of yield acceleration of lined landfills which are subjected to horizontal seismic acceleration for the case of sidehill landfills. Ling and Leshchinsky (1997) suggested two-part failure wedges for the stability analysis of landfill considering both seismic horizontal and vertical accelerations. The authors also presented the equations for determination of yield acceleration for infinite cover slopes. Qian et al. (2001) studied the translational stability of cover soils both in static and seismic cases. The authors have presented a two-part wedge method using average seismic coefficient. Kim and Sitar (2004) developed an equation for yield acceleration incorporating only seismic horizontal acceleration. But this study is valid only for particular configuration of landfill. Qian and Koerner (2004) refined the two-part wedge method for translational stability of landfill by incorporating the influence of cohesion. They have proposed the equations and design charts for estimation of factor of safety against translational mode of failure by considering the effect of apparent cohesion of the waste. But this study did not consider the earthquake forces in the analysis. The majority of the literature on seismic analyses of MSW landfills neglected the influence of seismic vertical acceleration. Also, the seismic inertia forces are assumed as pseudo-static in nature as was also done by Choudhury and Savoikar (2011a). But in pseudo-static analysis, the influence of earthquake on landfills is characterized by constant, time-independent seismic inertia forces, and the effect of phase difference and time is neglected. Ground response analyses for MSW landfill and different soil profiles show significant variation in seismic acceleration and amplification (Choudhury and Savoikar 2009a; Phanikanth et al. 2011; Shukla and Choudhury 2012) which pseudo-static method cannot consider. The recent pseudo-dynamic method overcomes these limitations and considers the influence of time and phase difference (Choudhury et al. 2007; Choudhury and Nimbalkar 2008; Ahmad and Choudhury 2010; Ghosh and Choudhury 2011) on the seismic stability of the landfills (Choudhury and Savoikar 2010, 2011b); Savoikar and Choudhury 2010a, 2012). The current study summarizes the seismic stability analyses of different MSW landfill configurations using pseudo-dynamic method (Savoikar 2009).

4.2 Pseudo-dynamic Limit Equilibrium Analysis of MSW Landfills

4.2.1 Different Cases of Landfill Stability Considered

Failure of MSW landfills can be characterized as sliding, translational and rotational mode or a combination of these modes. In the present study, sliding failure mode of landfill is analysed by considering different landfill configurations. Various cases of sidehill landfill configurations considered in present study are listed below (Savoikar and Choudhury 2010b):

Case (a): Founded on horizontal and partly sloping base

A generalized model of landfill founded over a slope α and horizontal base is presented in Fig. 4.1a. The height, length, backfill slope and face slope of the landfill are H, L, S_1 and S_2, respectively.

Case (b): Founded on sloping base

A generalized model of landfill founded over a slope α is demonstrated in Fig. 4.1b. The dimensions of the landfill are height H, length L, face slope S_1 and backfill slope S_2 at an angle θ_2 with horizontal.

Case (c): Landfill with stepped base

A generalized model landfill with stepped base considered in the analysis is presented in Fig. 4.1c. The total height of the landfill is H. The height and length of upper block are H_1 and L, respectively. The slopes of backfill are S_1, S_2 and face slope is S_3.

4.2.2 Methodology

For sinusoidal shaking with frequency ω ($=2\pi/T$, where T is time period) at the base of landfill with the amplitude of horizontal seismic acceleration, $\ddot{x}_h$ ($=k_h g$), and the amplitude of vertical seismic acceleration, $\ddot{x}_v$ ($=k_v g$), the expressions of accelerations in terms of depth z and time t are

$$\ddot{x}_h(t,z) = \ddot{x}_h \sin\left(\frac{2\pi}{T}\right)\left(t - \frac{H-z}{V_s}\right) \tag{4.1}$$

$$\ddot{x}_v(t,z) = \ddot{x}_v \sin\left(\frac{2\pi}{T}\right)\left(t - \frac{H-z}{V_p}\right) \tag{4.2}$$

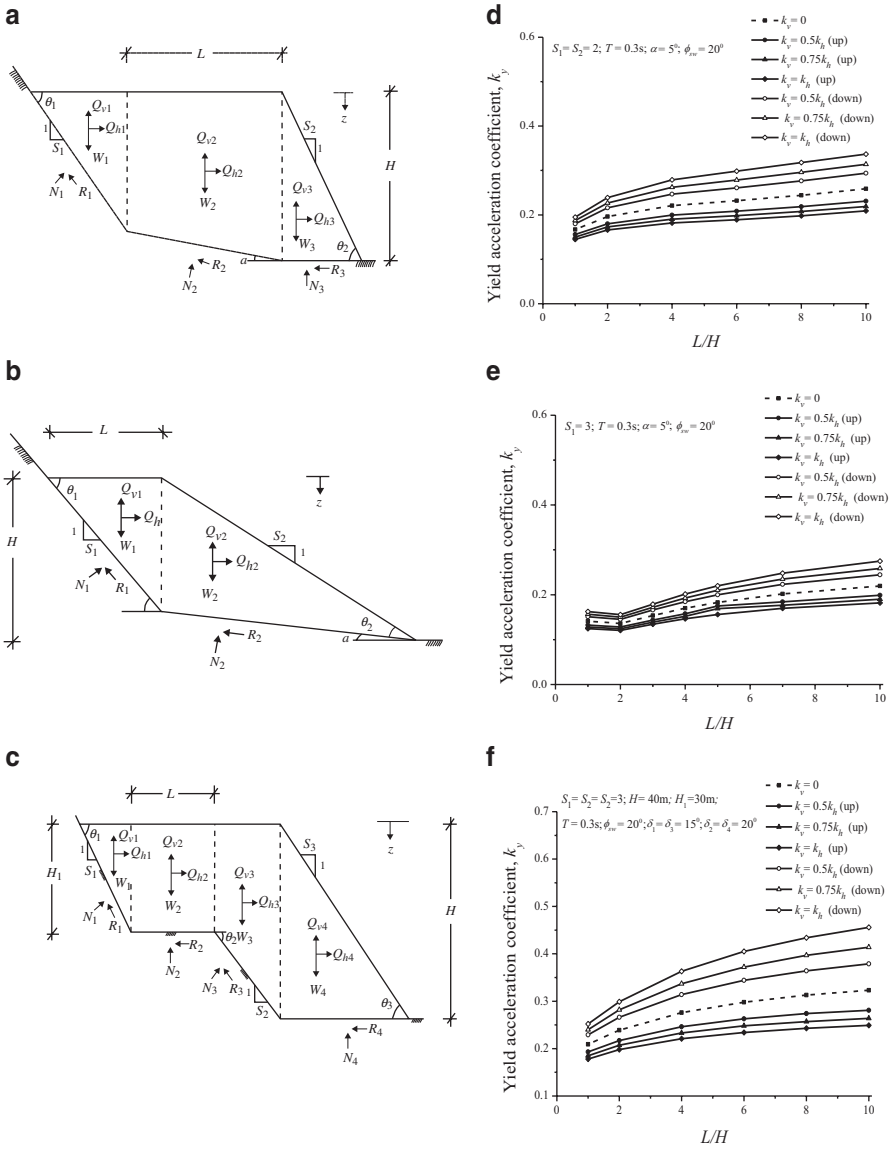

Fig. 4.1 Typical landfill configurations considered. (**a**) Founded on horizontal and partly sloping base. (**b**) Founded on sloping base. (**c**) With stepped base. (**d**) Yield acceleration coefficient for Case (**a**). (**e**) Yield acceleration coefficient for Case (**b**). (**f**) Yield acceleration coefficients for Case (**c**) [Savoikar and Choudhury 2010b]

where V_s is the shear wave velocity (= $(G/\rho)^{0.5}$), V_p is the primary wave velocity (= $G(2-2\nu)/\ \rho(1-2\nu))^{1/2}$, G is the maximum shear modulus, ρ is the density of the landfill material and ν is the Poisson's ratio for landfill material which needs to be characterized properly as shown by Choudhury and Savoikar (2009b). Three types of MSW landfill configurations are divided into segments as shown in Fig. 4.1a–c. A horizontal thin slice at depth z in every segment is considered, and the mass, $m(z)$, is computed. Total horizontal and vertical inertial forces of individual block can be written as

$$Q_h(t) = \int_0^H m(z)\ddot{x}_h \sin\left(\frac{2\pi}{T}\right)\left(t - \frac{H-z}{V_s}\right)dz \tag{4.3}$$

$$Q_v(t) = \int_0^H m(z)\ddot{x}_v \sin\left(\frac{2\pi}{T}\right)\left(t - \frac{H-z}{V_p}\right)dz \tag{4.4}$$

The forces acting on the various sections of landfill configurations considered are shown in Fig. 4.1a–c. Using the limit equilibrium approach, the horizontal and vertical equilibrium of forces is considered, and the factor of safety against sliding failure is obtained. The seismic acceleration coefficient corresponding to the factor of safety value of unity is defined as yield acceleration coefficient.

4.3 Results with Discussions

The seismic vertical acceleration has significant effect on yield acceleration coefficient (k_y). Compared to the downward vertical seismic acceleration, upward-seismic vertical acceleration is found to be critical. It can be seen from Fig. 4.1d–f that the yield acceleration coefficient (k_y) values corresponding to the upward vertical seismic acceleration are smaller than the yield acceleration coefficient values corresponding to downward vertical seismic acceleration. The negligence of seismic vertical acceleration generates intermediate values of yield acceleration coefficient. Among all the three configurations considered in the current study, neglecting seismic vertical acceleration in the analysis resulted greater overestimation for the Case (c). For example, for L/H = 6, the yield acceleration is decreased by about 14%, when k_v increases from 0 to 0.5 k_h, whereas if k_v increases to k_h, this overestimation is about 28%. For sidehill-type landfills resting partly on sloping and horizontal base, this overestimation is to the tune of 13% (at k_v = 0.5 k_h) to 24% (at k_v = k_h). When compared to the other configurations, the effect of seismic vertical acceleration is minimal for the Case (b). For L/H = 6, the overestimation due to the negligence of seismic vertical acceleration is about 4% when k_v = 0.5 k_h and 15% when

$k_v = k_h$. This overestimation of yield acceleration is expected, because seismic vertical acceleration induces seismic vertical inertia force which leads to the reduction of stability of landfills even at the small magnitudes of seismic shaking.

The coefficient of yield acceleration is also dependent on *L/H* ratio of the landfill. As the *L/H* ratio for landfill increases, yield acceleration coefficient also increases (Fig. 4.1d–f). The effect of *L/H* ratio is more prominent for the case of sidehill-type landfill with sloping base. For illustration, for $k_v = 0.5\ k_h$ the coefficient of yield acceleration is increased by 36%, when *L/H* increases from 2 to 10. In Case (a), for $k_v = 0.5\ k_h$, as the value of *L/H* increases from 2 to 10, the coefficient of yield acceleration is increased by about 28%. In all the considered landfill configurations, the influence of *L/H* ratio is lowest for Case (c). For this case, the coefficient of yield acceleration increases by about 23%, when the value of *L/H* ratio increased from 2 to 10. The reason for this increase in coefficient of yield acceleration with increase in *L/H* ratio can be attributed to the fact that the greater the *L/H* ratio, the greater the resisting forces acting in the landfill.

4.4 Conclusions

The pseudo-dynamic sliding stability analyses of different configurations of MSW landfills with sidehill configurations founded on (a) horizontal and partly sloping base, (b) sloping base and (c) stepped base are carried out. The proposed pseudo-dynamic stability analyses include the influence of time component and influence of time period and phase. Yield acceleration coefficients have been obtained by considering sliding failure mode of landfills. Neglecting the seismic vertical acceleration leads to an overestimation of yield acceleration coefficient by about 14–28% in case of sidehill-type landfill with stepped base. Among all the landfill configurations considered in the present study, the influence of seismic vertical acceleration is minimal for the case of sidehill-type landfill with sloping base. As the value of *L/H* ratio of landfill increases, yield acceleration coefficient for sliding failure also increases. For the sidehill-type landfill resting partly on sloping and horizontal base, there is a 28% increase in coefficient of yield acceleration when the value of *L/H* changes from 2 to 10.

References

Ahmad SM, Choudhury D (2010) Seismic rotational stability of waterfront retaining wall using pseudodynamic method. Int J Geosci 10(1):45–52

Augello AJ, Matasovic N, Bray JD, Kavazanjian E Jr, Seed RB (1995) Evaluation of solid waste landfill performance during the Northridge earthquake, GSP No. 54. ASCE, Reston, pp 17–50

Choudhury D, Nimbalkar SS (2008) Seismic rotational displacement of gravity walls by pseudo-dynamic method. Int J Geosci 8(3):169–175

Choudhury D, Savoikar P (2009a) Equivalent-linear seismic analyses of MSW landfills using DEEPSOIL. Eng Geol 107(3–4):98–108
Choudhury D, Savoikar P (2009b) Simplified method to characterize municipal solid waste properties under seismic conditions. Waste Manag 29(2):924–933
Choudhury D, Savoikar P (2010) Seismic translational failure analysis of MSW landfills using pseudo-static approach, GeoFlorida 2010, Geotechnical Special Publication GSP No. 199. ASCE, Reston, pp 2830–2839
Choudhury D, Savoikar P (2011a) Seismic stability analysis of expanded MSW landfills using pseudo-static limit equilibrium method. Waste Manag Res 29(2):135–145
Choudhury D, Savoikar P (2011b) Seismic yield accelerations of MSW landfills by pseudo-dynamic approach. Nat Hazards 56(1):275–297
Choudhury D, Nimbalkar SS, Mandal JN (2007) External stability of reinforced soil walls under seismic conditions. Geosynth Int 14(4):211–218
Ghosh P, Choudhury D (2011) Seismic bearing capacity factors for shallow strip footings by pseudo-dynamic approach. Disaster Adv 4(3):34–42
Kim J, Sitar N (2004) Direct estimation of yield acceleration in slope stability analysis. J Geotech Geoenviron 130(1):111–115
Ling HI, Leshchinsky D (1997) Seismic stability and permanent displacement of landfill cover system. J Geotech Geoenviron Eng 123(2):113–122
Matasovic N (1991) Selection of method for seismic slope stability analysis. In: Proceedings of the 2nd international conference on recent advances in geotechnical earthquake engineering and soil dynamics. University of Missouri-Rolla, Missouri, pp 1057–1062
Orr WR, Finch MA (1990) Solid waste landfill performance during the Loma Prieta earthquake. ASTM STP 1070, Geotechnics of waste fills – theory and practice, American Society for Testing of Materials, pp 22–30
Phanikanth VS, Choudhury D, Reddy GR (2011) Equivalent-linear seismic ground response analysis of some typical sites in Mumbai. Geotech Geol Eng 29(6):1109–1126
Qian X, Koerner RM (2004) Influence of apparent cohesion on translational failure analyses of landfills. J Geotech Geoenviron 130(1):71–80
Qian X, Koerner RM, Gray DH (2001) Geotechnical aspects of landfill design and construction. Prentice Hall, Upper Saddle River
Sarma SK (1975) Seismic stability of earth dams and embankments. Geotechnique 25(4):743–761
Savoikar P (2009) Seismic behavior of municipal sloid waste landfills. Ph.D thesis, Department of Civil Engineering IIT, Bombay
Savoikar P, Choudhury D (2010a) Effect of cohesion and fill amplification on seismic stability of MSW landfills using limit equilibrium method. Waste Manag Res 28(12):1096–1113
Savoikar P, Choudhury D (2010b) Computation of pseudo-static yield accelerations of landfills. Int J Geotech Eng 4(3):305–317
Savoikar P, Choudhury D (2012) Translational seismic failure analysis of MSW landfills using pseudo-dynamic approach. Int J Geosci 12(2):136–146
Shewbridge SE (1996) Yield acceleration of lined landfills. J Geotech Eng ASCE 122(2):156–158
Shukla J, Choudhury D (2012) Seismic hazard and site-specific ground motion for typical ports of Gujarat. Nat Hazards 60(2):541–565

Chapter 5
Dynamic Properties of Municipal Solid Waste and Amplification of Landfill Site

P. Anbazhagan, P. Lakshmikanthan, and G.L. Sivakumar Babu

Abstract Understanding of the dynamic properties of municipal solid waste (MSW) and the response of waste landfill for cyclic loads are important for safe seismic design and ensuring sustainability of landfills. This study presents estimation of the dynamic properties through field and laboratory tests of MSW landfill and dynamic response of Mavallipura landfill in Bangalore. Both field tests and laboratory tests are used to develop model to represent variation of shear modulus and damping ratio for different strain levels. Ten ground motions are selected based on regional seismicity of landfill site, and detailed site response analysis was carried out considering one-dimensional nonlinear analysis in DEEPSOIL programme. Surface response parameters have been estimated; the surface spectral response varied from 0.6 to 2 g and persisted only for a period of 1 s for most of the ground motions. The minimum and maximum amplifications are 1.35 and 4.05. This study shows that Indian MSW has less shear stiffness and loose filling, may be subject to more amplification for moderate earthquake ground motions, which need to be accounted for seismic design of landfills.

Keywords Shear modulus • Damping ratio • Cyclic triaxial tests • Municipal solid waste • Landfills

P. Anbazhagan • G.L. Sivakumar Babu
Department of Civil Engineering, Indian Institute of Science (IISc), Bangalore, Karnataka 560012, India
e-mail: anbazhagan@civil.iisc.ernet.in; gls@civil.iisc.ernet.in

P. Lakshmikanthan (✉)
Centre for Sustainable Technologies, Indian Institute of Science (IISc), Bangalore, Karnataka 560012, India
e-mail: lakshmikanth@astra.iisc.ernet.in

G.L. Sivakumar Babu et al. (eds.), *Geoenvironmental Practices and Sustainability*, Developments in Geotechnical Engineering,
DOI 10.1007/978-981-10-4077-1_5

5.1 Introduction

Landfills can be subjected to cyclic loads due to earthquakes, and the dynamic response under such loads depends on the cyclic stress-strain characteristics of the MSW. The evaluation of dynamic properties of municipal solid waste (MSW) is important for proper seismic response analysis, modelling and efficient design of landfills. It is essential to determine the dynamic parameters (small-strain shear modulus (Gmax), normalised shear modulus reduction (G/Gmax) and damping ratio (D)) in order to analyse the engineering response of MSW subjected to dynamic loadings. Shear stresses are related to shear strains by the shear modulus (G) of the material. The shear modulus is simply related to the velocity of shear waves; hence, measurements of shear wave velocity provide a convenient method for measuring stiffness. In this study shear modulus for low strain is obtained from field seismic test, and shear modulus and damping for high strain are measured by laboratory tests (cyclic triaxial tests). These values are further used to develop the normalised shear modulus reduction and damping relationships for MSW from India. These results are used as inputs along with recorded ground motions to perform nonlinear one-dimensional seismic response analysis of landfill site and site-specific amplification are estimated.

5.2 Site and Sample Description

The MSW used in this study is the compost reject collected from the Mavallipura Landfill site, Bangalore, India, and is referred to as MSW in this paper. The site is spread over 30 acres and is divided into cell 1 (6 acres) and cell 2 (2 acres). The height of the landfill is 10 m. Composting has been adopted as a potential pretreatment method. Hand sorting of recoverable waste was followed by aerobic windrow composting for a period of 2 months. The compost reject had particle sizes varying from 4 to 35 mm. The particles of size >20 mm, mostly consisting of large plastics, rubber shoes, leather bags and other inert materials, were hand sorted or removed by other mechanical procedures. As it was difficult to separate particles <20 mm, these were filled directly. Therefore, particles of size <20 mm were used in the laboratory for characterisation and testing. The compost reject contained 6.34% clothes, 28% plastics, 1.28% glass, 0.8% leather, 5.56% coconut, 1.96% stones, 0.88% rubber, 0.16% wood and 54.2% organic matter. The moisture content of the waste was calculated as the ratio of the weight loss of the weight that remained after heating at a temperature of 60°C until the specimen has dried to a constant mass. The natural water content of the sample was found to be 20%. The test for total volatile solids was performed according to the APHA 1965 (American Public Health Association) standard methods. The organic content of the compost reject <10 mm particle size was calculated as the ratio of the weight loss of the initial specimen weight after heating to a temperature of 550 °C in a muffle furnace. The

initial decomposable organic content of the waste was found to be 55% and the inerts constituted 45%.

5.3 Materials and Methods

5.3.1 Field Tests

In the present study, the multiple channel analysis of surface waves (MASW) method is used to measure shear wave velocity (*V*s) of in situ MSW. The MASW testing was done at the Mavallipura landfill site which is situated in the outskirts of Bangalore. More details about testing, data processing and results can be found in Anbazhagan et al. (2016). The G_{max} at low strain was calculated from the shear wave velocity measured at the site using the following Eq. (5.1):

$$G_{max} = \rho * V_s^2 \tag{5.1}$$

where *V*s is the shear wave velocity in m/s and ρ is the density in g/cc.

5.3.2 Laboratory Determination of Dynamic Properties

Cyclic triaxial compression method has been adopted as the test method in this study for the analysis of the dynamic properties of MSW in the laboratory. Shear strains in the range of 1%–10^{-3}% can be measured in the cyclic triaxial apparatus. Reconstituted MSW samples (50 mm × 100 mm) of particle size <20 mm and moisture content of 44% were used for testing in the laboratory. The loading was done in a sinusoidal pattern and the tests were stress controlled. More than 40 cyclic triaxial tests were conducted in laboratory, and the shear modulus and damping ratios were calculated according to ASTM D 3991-91 and ASTM D 5311-92. The G_{max} values from the field test and lab tests are combined to develop the G/G_{max} curves for MSW.

5.4 Results and Discussions

5.4.1 Field Tests

The MASW tests were conducted at selected locations at the landfill site, and the typical shear wave velocity profiles are presented in Fig. 5.1. Based on the total station survey and the previous available data, the depth of the landfill was arrived at

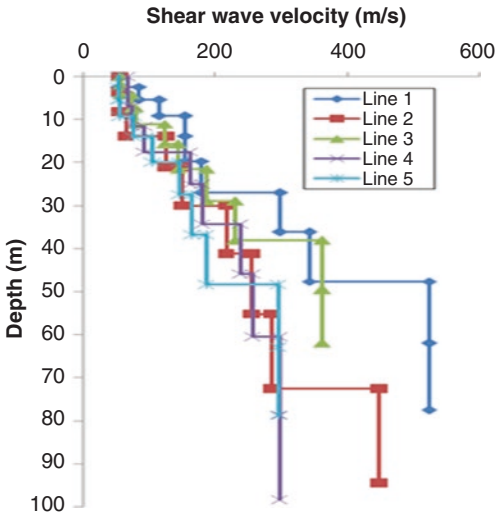

Fig. 5.1 Field measurements of shear wave velocities of municipal solid waste at Mavallipura landfill

9–10 m with *V*s values of 56 m/s. The waste below the depth of 10 m was composites of waste and soil with higher shear wave velocity.

5.4.2 Laboratory Tests

5.4.2.1 Normalised Shear Modulus Reduction and Damping Ratio Curves

Figure 5.2 shows the results of cyclic triaxial tests conducted on waste samples. The shear modulus increased from 4 to 6 MPa with the increase in frequency from 0.1 to 1 Hz. Similar increasing trends were found in the published literature for strains less than 0.05%.

The normalised shear modulus reduction values obtained from laboratory are presented in Fig. 5.3. Most of the values fall below the upper bound of the curves recommended by Matasovic and Kavazanjian (1998). The results closely match Zekkos et al. (2008). Idriss et al. (1995) and Augello et al. (1998) back-calculated the strain-dependent shear modulus reduction and material damping curves using the time histories recorded on top of OII landfill from earthquakes. MSW degrades with time, and therefore the shear modulus and damping ratio are likely to change which should be considered while developing modulus reduction curves. Though the results are obtained from limited laboratory and field tests in this study, a modulus reduction curve close to the lower bound can be recommended for MSW of Indian origin for seismic analysis. However, further studies including the effect of water content, particle size, sample size and composition of MSW on the modulus reduction curves can provide further details in understanding and developing the dynamic parameters.

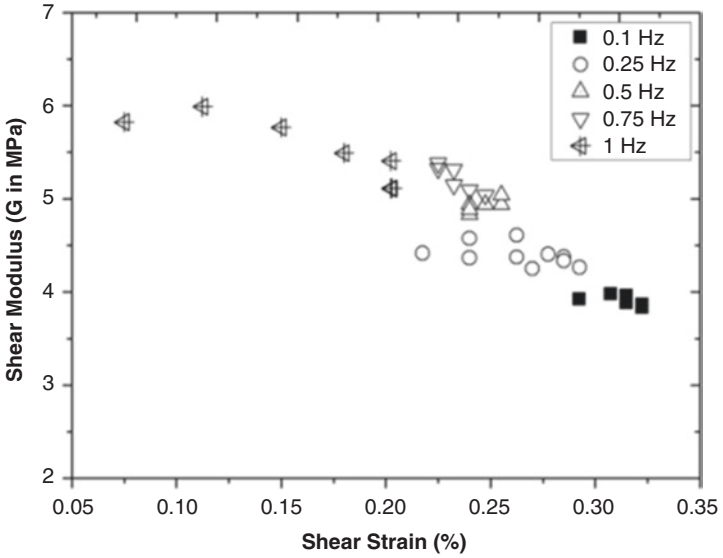

Fig. 5.2 Variation of shear modulus with shear strain

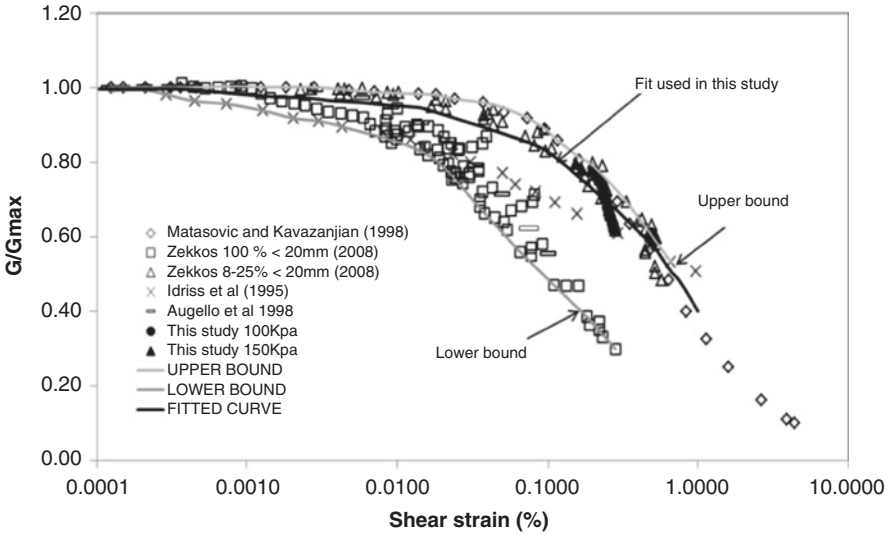

Fig. 5.3 Normalised shear modulus reduction curves from previous studies and the present study

Similarly the damping values of the MSW were calculated, and damping curve is developed for the MSW (Anbazghagan et al. 2016). The damping values varied from 10% to 17% in all the tests. Matasovic and Kavazanjian (1998) and Zekkos et al. (2008) observed high damping values in the range 20–30% compared to Augello et al. (1998) and Idriss et al. (1995) who reported values less than 15%.

5.4.3 Seismic Response Analysis of MSW

Site response analysis is used to predict the response of each subsurface layer subjected to an earthquake ground motion. MSW landfill site consists of MSW fill followed by filled soil layer and hard stratum. Site-specific data are modelled in DEEPSOIL to get one-dimensional (1-D) nonlinear response parameters. Fully nonlinear analyses are performed in the time domain, where shear modulus (G) and damping (ξ) vary throughout the duration of loading. The seismic response is studied by examining surface acceleration time history, response spectra and the maximum strain of the each location in the landfill. The input ground motion and estimated surface acceleration time history are used to predict amplification of MSW. Typical response spectrum for selected input motions is shown in Fig. 5.4. It can be observed that input motion has undergone considerable amplification and change in amplitude, frequency and duration are noticed. The peak spectral acceleration is noticed before 0.5 s in the input as well as in surface. A few input motions show multiple spectral peaks at the surface due to shallow hard stratum reverberation. This study shows that amplification and spectral signature of MSW fill is different from that of soils, which need to be accounted in seismic design of MSW landfill sites.

5.5 Conclusions

The cyclic characteristics of the MSW were established based upon field and laboratory testing. The shear wave velocity profile for the solid waste was measured using MASW survey. Cyclic triaxial test were carried out on MSW samples, and shear modulus and damping values were measured for strain values of 1%–10^{-3}%. The normalised shear modulus reduction and damping curves for waste were developed based on a combination of laboratory cyclic triaxial test results and literature. One-dimensional nonlinear site response study was carried out at five MSW columns at Mavallipura landfill. Ten input motions were selected considering seismicity of study and area of Bangalore and were used for site response analysis. This study shows that shallow MSW fill undergoes considerable seismic amplification for ground motion less than 0.2 g. The results indicate the potential of amplification of ground motions by the waste situated above a composite layer of soils and rock bed at the bottom. Hence, the site-specific amplifications need to be accounted for sustainable landfill design.

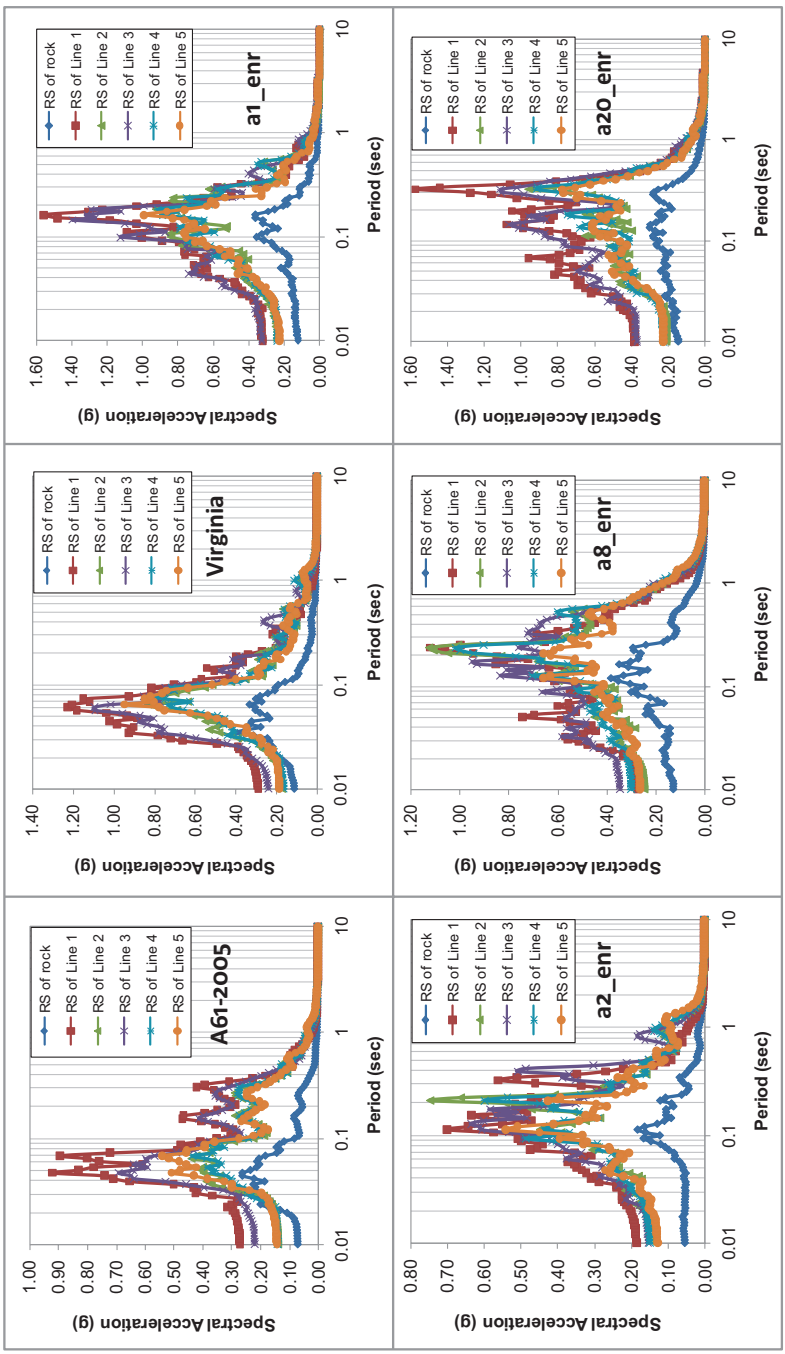

Fig. 5.4 Input and surface response spectrum for MSW sites

References

Anbazhagan P, Sivakumar Babu GL, Lakshmikanthan P, Vivek Anand KS (2016) Seismic characterization and dynamic site response of a municipal solid waste landfill in Bangalore, India. Waste Manag Res 34(3):205–213. doi:10.1177/0734242X15622814

Augello AJ, Bray JD, Abrahamson NA, Seed RB (1998) Dynamic properties of solid waste based on back-analysis of OII landfill. ASCE J Geotech Geoenviron Eng 124(3):211–222

Idriss IM, Fiegel G, Hudson MB, Mundy PK, Herzig R (1995) Seismic response of the operating industries landfill, earthquake design and performance of solid waste landfills, ASCE Geotech J Earthq Eng 8(4):545–566, Imperial College Press

Matasovic N, Kavazanjian E Jr (1998) Cyclic characterization of OII landfill solid waste. J Geotech Geoenviron 124(3):197–210

Zekkos D, Bray JD, Riemer MF (2008) Shear modulus and material damping of municipal solid waste based on large-scale cyclic triaxial testing. Can Geotech J 45(1):45–58

Chapter 6
Resistance Factor Calculations for Load Resistance Factor Design (LRFD) of MSW Landfill Slopes

B. Munwar Basha and K.V.N.S. Raviteja

Abstract It is obvious to note that there is a significant amount of variability connected with shear parameters of municipal solid waste (MSW) landfills. To ensure uniform safety and reliability, the design approaches in the US have progressively transformed to the load and resistance factor design (LRFD) format. It may be desirable to the successful development and adoption of reliability-based resistance factors for the design of landfill slopes taking into account the significant variability of shear strength parameters. The exhaustive studies reported on shear parameters of MSW are compiled and reviewed. The mean, standard deviation, and coefficient of variation (COV) associated with shear parameters are obtained using statistical analysis. The probability density functions (PDFs) are plotted for unit weight, cohesion, and friction angle. The PDFs show that high range of variability associated with shear parameters and should be given due consideration in the optimum designs. Therefore, the present work reports a procedure for determining the resistance factors for stability number (in terms of unit weight, cohesion) and friction angle of MSW in accordance with LRFD of MSW landfill slopes that target a specific reliability index. A simple first-order reliability method (FORM) is reported to compute the ranges for the resistance factors. Perhaps, this is the first study to propose resistance factors for the design of MSW slopes. The stability number (in terms of unit weight, cohesion) and friction angle of the MSW are treated as random variables. The Spencer method of slices has been employed to formulate the performance function against the sliding failure of finite slopes. It is illustrated that the uniform safety levels can be obtained by using the proposed resistance factors.

Keywords Load resistance factor design • Municipal solid waste • Slope • Landfills • Method of slices

B. Munwar Basha (✉) • K.V.N.S. Raviteja
Department of Civil Engineering, Indian Institute of Technology Hyderabad, Kandi, Sangareddy, 502285 Hyderabad, India
e-mail: basha@iith.ac.in; kvnsravi.teja@gmail.com

G.L. Sivakumar Babu et al. (eds.), *Geoenvironmental Practices and Sustainability*, Developments in Geotechnical Engineering,
DOI 10.1007/978-981-10-4077-1_6

6.1 Introduction

The stability of municipal solid waste (MSW) landfill slopes is the major concern in the landfill design. The stability of MSW landfill should include the stability of waste dump, final cover system, bottom liner, as well as the stability of foundation soil. The slope stability of MSW landfills is influenced by the various parameters. The design of landfill slopes should consider the geometry of the design section and the shear strength parameters of MSW. Probabilistic analysis is quite popular in dealing with uncertainties associated with MSW. In order to conduct the probabilistic stability analysis, it is important to know basic statistical data of uncertain parameters associated with MSW which are included in the analysis.

6.1.1 Studies on Probabilistic Analysis of Soil Slopes

Hassan et al. (1999) proposed an algorithm for the computation of critical reliability index for soil slopes. The surfaces of a minimum factor of safety and reliability index were examined. Malkawi et al. (2001) used the first-order second-moment (FOSM) method and Monte Carlo simulation (MCS) method of reliability analysis of the soil slopes. Low (2003) implemented Spencer's method of slices for a probabilistic approach to slope stability. Xue and Gavin (2007) reported a new approach to determine the minimum reliability index by taking into account the uncertainty associated with the soil properties. Bhattacharya and Dey (2010) coupled first-order reliability method (FORM) with the ordinary method of slices (OMS) for computation of factor of safety and reliability index. Basha and Babu (2013) and Basha and Babu (2014) reported the reliability-based LRFD for external seismic stability of reinforced soil walls. Review of literature clearly indicates that the LRFD approach for the design of MSW landfill slopes is not paid any attention.

6.1.2 Need for LRFD for MSW Landfill Slopes

The AASHTO has been progressively converted from allowable stress design (ASD) to LRFD methods. The major objective of LRFD is to achieve consistent levels of safety and reliability when the design parameters are random. However, the conventional factor of safety method using limit equilibrium approach cannot handle the variability. Moreover, the LRFD can improve the efficiency and accuracy of designs with small changes to existing design procedures. A considerable research work has been reported to develop LRFD methods, which include specific load and resistance factors to facilitate conversion from ASD to LRFD procedures. Adequate LRFD guidelines are available in the literature for the use by researchers. However, the

design of MSW landfill slopes considering the variability associated with MSW is severely lacking.

6.2 Objectives of the Present Study

The reliability-based studies reported in the literature mostly discussed on soil slopes. It is interesting to note that a few studies reported regarding the reliability analysis of MSW slopes. Consequently, there is a deficiency in understanding the mechanism behind the MSW slope failures. The present work is focused on LRFD approach for slope reliability analysis by taking into account the variability associated with the shear strength parameters. Spencer (1967) method is employed in the current study to perform MSW slope stability analysis. The effort made here is perhaps the pioneering study to propose a LRFD for the reliability assessment of MSW slopes.

6.3 Estimation of Variability Associated with MSW Properties

As discussed earlier, precise quantification of the variability of MSW shear strength properties is required for the probability-based design of landfill slopes. Stability of MSW slopes depends mainly on the properties of the waste materials including unit weight, friction angle, cohesion, and pore water pressure. The age of MSW, heterogeneous nature, degree of biodegradation, and degree of decomposition are the factors that affect the shear strength considerably. The uncertainty can be represented using probability distribution function (PDF) which is further characterized by mean and standard deviation of the design parameters (γ, c, and ϕ).

The ranges of MSW properties like unit weight and shear strength parameters (cohesion and friction angle) have been collected from review of literature published from 1984 to 2016. The data is divided into various bins and plotted as histograms to represent the variability precisely. The type of probability distribution is identified for unit weight, cohesion, and friction angle. Histograms are drawn by taking the lower bounds of parameters. It can be noted from Figs. 6.1, 6.2, and 6.3 that the normal distribution appears to be a sensible decent model for the observed magnitudes of unit weight (γ). Further, Weibull and Gumbel minimum distributions appear to be sensibly decent models for observed values of cohesion (c) and internal friction angle (ϕ), respectively. The optimized values mean and standard deviation of MSW properties are shown in Table 6.1. The basis for the optimization is the minimum error associated with quantile-quantile (ε_{QQ}), probability-probability (ε_{PP}), and cumulative distribution function (ε_{CDF}).

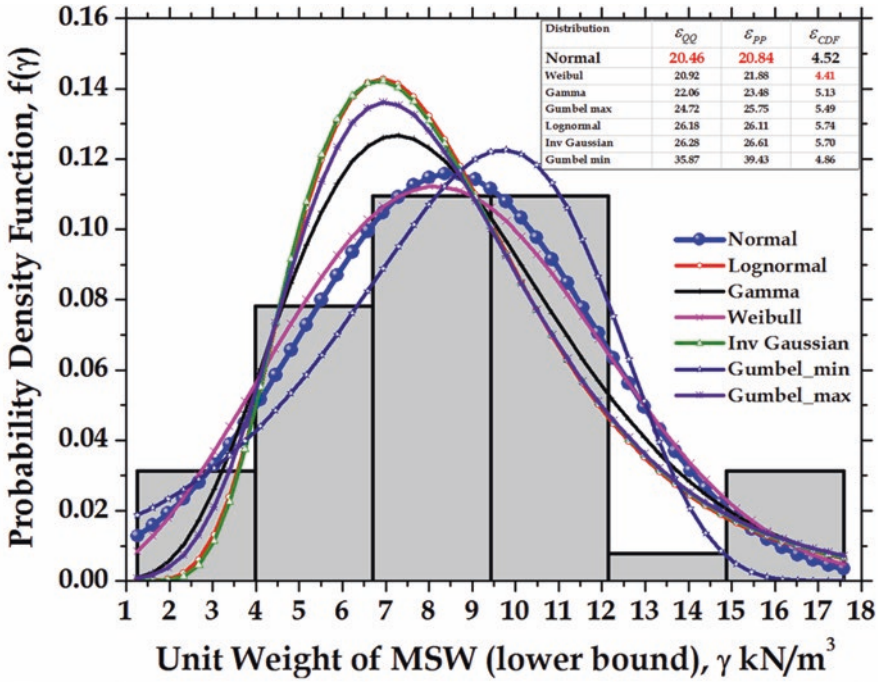

Fig. 6.1 Histogram with theatrical PDFs for unit weight (γ) of MSW

6.4 Spencer Method of Slices for MSW Slope Stability

This method considers both the interslice forces, assumes a constant interslice force function and satisfies both moment and force equilibrium simultaneously, and computes the factor of safety. The MSW slope geometry with the method of slices is shown in Fig. 6.4a. The slice considered to write force and moment equilibrium equations is shown in Fig. 6.4b. Considering the force equilibrium ($\sum F_h$) and moment equilibrium ($\sum F_m$) of the whole soil mass and solving for the factor of safety, the following two equations can be derived:

$$FS_{\text{Spencer\_f}} = \frac{\sum_{n}^{i=1} T_{i,\text{lim}}}{\sum_{n}^{i=1} T_i} = \frac{\sum_{n}^{i=1} (cdl_i + N_i \tan\phi) \times \cos\theta_i}{\sum_{n}^{i=1} N_i \sin\theta_i} \tag{6.1}$$

$$FS_{\text{Spencer\_m}} = \frac{\sum_{n}^{i=1} (cdl_i + N_i \tan\phi)\ R}{\sum_{n}^{i=1} w_i h_{off_i}} \tag{6.2}$$

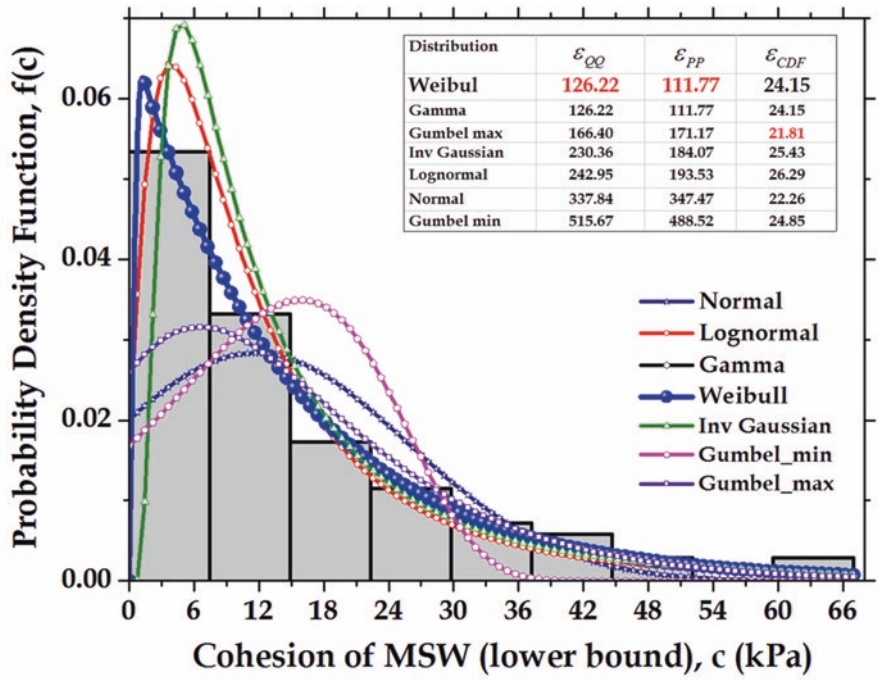

Fig. 6.2 Histogram with theoretical PDFs for cohesion (*c*) of MSW

where N_i = the total normal force on the base of a slice, T_i = the shear force mobilized on the base of each slice, c = cohesion, δ = internal frictional angle, E_i = the horizontal interslice normal forces, X_i = the vertical interslice shear forces, w_i = weight of a slice, h_{off} = the horizontal distance from the centroid of each slice to the center of rotation (=R sin θ_i), dl_i = length of slice along the base, θ_i = the angle between the tangent drawn at the center of the base of each slice and the horizontal, and R = radius of the slip circle.

Now considering the equilibrium of an individual slice, the magnitude of the shear force mobilized at the base of a slice, T_i, can be written in terms of the Mohr-Coulomb failure criterion as

$$T_i = \tau_i dl = \frac{\tau_{fi} dl_i}{FS_{\text{Spencer}}} = \frac{(c + \sigma \tan\phi) dl_i}{FS_{\text{Spencer}}} \tag{6.3}$$

where τ_i and τ_{fi} are the shear stress and shear stress at failure for the ith slice. Now, substituting $\sigma = N_i/dl$ in Eq. (6.3), we get

$$T_i = \frac{c dl_i + N_i dl_i \tan\phi}{FS_{\text{Spencer}}} \tag{6.4}$$

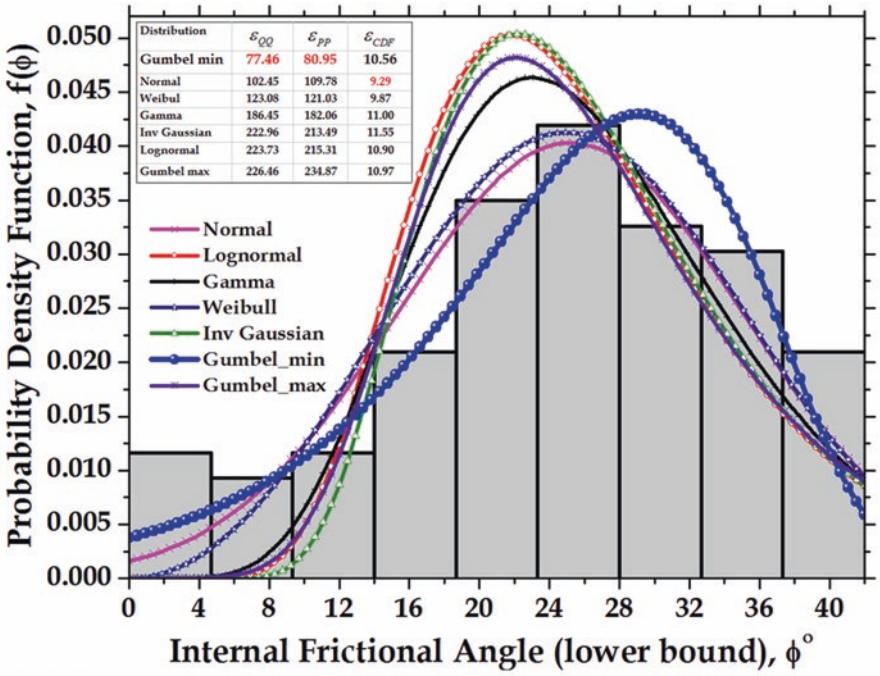

Fig. 6.3 Histogram with theoretical PDFs for friction angle (ϕ) of MSW

Table 6.1 Optimized values of mean (μ) and coefficient of variation (COV) of MSW properties

Variable	PDF	Mean (γ)	Coefficient of variation (COV) in %
γ (kN/m^3)	Normal	8.48	40.61
c (kN/m^2)	Weibull	14.62	100.00
ϕ (deg)	Gumbel min	34.10	32.22

Considering the force equilibrium in the vertical direction, we get

$$w_i + X_i - X_{i-1} - N_i \cos\theta_i - T_i \sin\theta_i = 0 \tag{6.5}$$

Substituting the value of T_i in the above equation and solving for N_i, we get

$$N_i = \frac{w_i + X_i - X_{i-1} - \dfrac{cdl_i \sin\theta_i}{FS_{\text{Spencer}}}}{\cos\theta_i + \dfrac{\tan\phi \sin\theta_i}{FS_{\text{Spencer}}}} \tag{6.6}$$

Now, considering the equilibrium of the slice in the horizontal direction, we get:

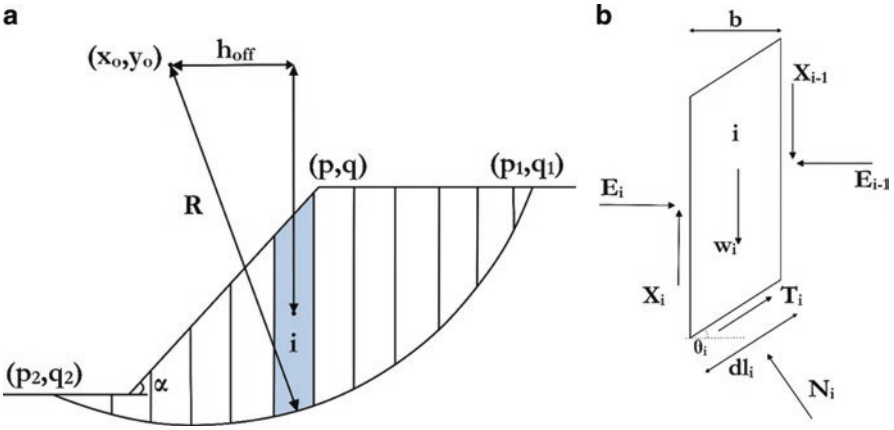

Fig. 6.4 (**a**) Geometry showing the parameters used and moment arms for circular slip surface (**b**) Forces acting on *i*th slice

$$E_{i-1} - E_i - N_i \sin\theta_i + T_i \cos\theta_i = 0 \tag{6.7}$$

$$E_i = E_{i-1} - N_i \sin\theta_i + T_i \cos\theta_i \tag{6.8}$$

The interslice forces within the sliding mass are defined through a function $f(x_i)$ and a scalar coefficient λ as

$$X_i / E_i = \lambda f(x_i) \tag{6.9}$$

In the above equation, x_i is the abscissa of the ith slice of the slope, $f(x_i) = \tan\delta$ describes the interslice variation of shear force (X_i) and normal force (E_i) across the slope, and "λ" is the coefficient which represents the percentage of $f(x_i)$ used in the solution. Spencer (1967) assumed $f(x_i)$ is equal to 1 and then λ is equal to tan δ, where δ = angle of the resultant interslice force with the horizontal. All the above equations are then collectively used to determine the factor of safety FS_{Spencer} that satisfies both the moment and force equilibrium simultaneously. In order to solve for Spencer method, we initially set $X_i - X_{i-1} = 0$. The equations of $FS_{\text{f\_Spencer}}$ and $FS_{\text{m\_Spencer}}$ are then calculated to obtain a first set. Also for the first slice, X_i is equal to 0. Then a trial value of "δ" is chosen to obtain new estimates for the values of X_i and E_i. Having these values in hand, $FS_{\text{f\_Spencer}}$ and $FS_{\text{m\_Spencer}}$ are recalculated to obtain the new estimates of the factors of safety. This computation is then repeated until the values of the interslice force function converge.

The values of $FS_{\text{f\_Spencer}}$ and $FS_{\text{m\_Spencer}}$ computed in the above step are not necessarily equal. $FS_{\text{f\_Spencer}} \neq FS_{\text{m\_Spencer}}$ means that the moment and force equilibrium are not satisfied simultaneously. Hence, the computation must be repeated with various trial values of "δ" until $FS_{\text{f\_Spencer}} \neq FS_{\text{m\_Spencer}}$. When the convergence is obtained, that value is then taken as the factor of safety $FS_{\text{Spencer}} = FS_{\text{f\_Spencer}} = FS_{\text{m\_Spencer}}$ for the

slope. The performance function of MSW slope against sliding failure can be expressed as

$$g(x) = FS_{\text{Spencer}} - 1 \tag{6.10}$$

The limit state function $g(x) \leq 0$ indicates the slope failure and $g(x) > 0$ indicates the stable slope. Now the design point in the standard normal space (u_k) can be expressed as

$$u_k = -\beta_t \frac{\sum_{n}^{i=1} \frac{\partial g}{\partial x_k} \sigma_i}{\sqrt{\sum_{n}^{j=1} \left\{ \sum_{n}^{i=1} \frac{\partial g}{\partial x_k} \sigma_i \right\}^2}}, \text{where} k = 1, 2, \ldots n \tag{6.11}$$

where σ_i is the standard deviation of a random variable x_i. Further, the random variable "x_i^*" can be found as follows:

$$x_i = \sigma_i u_i + \mu_i \tag{6.12}$$

where $i = 1, 2, \ldots n$ and μ_i is the mean of a random variable x_i. Once we obtain a design point (x_i^*), the resistance factors (Ψ_i) for a target reliability index (β_t) can be computed using the following equation:

$$\Psi_i = \frac{x_i^*}{\mu_i} \tag{6.13}$$

6.4.1 Resistance Factors for Stability Number ($\Psi_{c/\gamma H}$) and Friction Angle (Ψ_ϕ)

The results presented in Tables 6.2, 6.3, 6.4, and 6.5 show the effect of COV *of c* and ϕ on resistance factors for stability number, $\frac{c}{\gamma H}$ ($\Psi_{c/\gamma H}$), and friction angle, ϕ (Ψ_ϕ), against sliding failure mode for $\beta_t = 2$ to 4 and for COV of $c = 20\%$, COV of γ ranges from 10 to 30%, COV of ϕ ranges from 10 to 30%, and typical value of MSW landfill: $H = 10$ m, slope angle (α) = 26.56°, cohesion (c) = 14.62 kN/m^2, friction angle (ϕ) = 34.14°, and unit weight (γ) = 8.48 kN/m^3. The resistance factors for stability number, $\frac{c}{\gamma H}$ ($\Psi_{c/\gamma H}$), and friction angle, ϕ (Ψ_ϕ), for $\beta_t = 2$ to 4 are presented in Tables 6.2, 6.3, 6.4, and 6.5. It can be noted from Tables 6.2, 6.3, 6.4, and 6.5 that the resistance factors are reduced when the target value of reliability index (β_t) increases from 2 to 4. It may be observed from Table 6.2 that for a constant value of

Table 6.2 Influence of COV of c and ϕ on the resistance factors $\Psi_{c/\gamma H}$ and Ψ_{ϕ} for a target reliability (β_t) for COV of c = 20% and COV of γ = 10%

	COV of ϕ = 10%		COV of ϕ = 20%		COV of ϕ = 30%	
β_t	$\Psi_{c/\gamma H}$	Ψ_{ϕ}	$\Psi_{c/\gamma H}$	Ψ_{ϕ}	$\Psi_{c/\gamma H}$	Ψ_{ϕ}
2.0	0.78	0.84	0.83	0.68	0.85	0.55
2.5	0.71	0.81	0.77	0.62	0.79	0.49
3.0	0.63	0.78	0.70	0.58	0.72	0.43
3.5	0.55	0.75	0.63	0.53	–	–
4.0	0.47	0.72	0.54	0.50	–	–

Table 6.3 Influence of COV of c and ϕ on the resistance factors $\Psi_{c/\gamma H}$ and Ψ_{ϕ} for a target reliability (β_t) for COV of c = 20% and COV of γ = 20%

	COV of ϕ = 10%		COV of ϕ = 20%		COV of ϕ = 30%	
β_t	$\Psi_{c/\gamma H}$	Ψ_{ϕ}	$\Psi_{c/\gamma H}$	Ψ_{ϕ}	$\Psi_{c/\gamma H}$	Ψ_{ϕ}
2.0	0.67	0.85	0.75	0.69	0.77	0.56
2.5	0.57	0.82	0.66	0.64	0.68	0.50
3.0	0.47	0.79	0.56	0.59	0.58	0.45
3.5	0.36	0.76	0.46	0.55	–	–
4.0	0.25	0.74	0.34	0.52	–	–

Table 6.4 Influence of COV of c and ϕ on the resistance factors $\Psi_{c/\gamma H}$ and Ψ_{ϕ} for a target reliability (β_t) for COV of c = 20% and COV of γ = 30%

	COV of ϕ = 10%		COV of ϕ = 20%		COV of ϕ = 30%	
β_t	$\Psi_{c/\gamma H}$	Ψ_{ϕ}	$\Psi_{c/\gamma H}$	Ψ_{ϕ}	$\Psi_{c/\gamma H}$	Ψ_{ϕ}
2.0	0.52	0.86	0.62	0.70	0.66	0.57
2.5	0.38	0.83	0.49	0.65	0.53	0.51
3.0	0.23	0.81	0.36	0.61	0.38	0.47

Table 6.5 Influence of COV of c and ϕ on the resistance factors $\Psi_{c/\gamma H}$ and Ψ_{ϕ} for a target reliability (β_t) for COV of γ = 10% and COV of ϕ = 20%

	COV of c = 20%		COV of c = 40%	
β_t	$\Psi_{c/\gamma H}$	Ψ_{ϕ}	$\Psi_{c/\gamma H}$	Ψ_{ϕ}
2.0	0.83	0.68	0.53	0.71
2.5	0.77	0.62	0.38	0.66
3.0	0.70	0.58	0.21	0.62

COV of ϕ, resistance factor for stability number ($\Psi_{c/\gamma H}$) marginally increases with increase in COV of ϕ from 10 to 30%. Whereas, the resistance factor for friction angle (Ψ_{ϕ}) significantly reduces with increase in COV of ϕ from 10 to 30%. Moreover, an important observation can be made from Tables 6.2, 6.3, and 6.4 that for constant values of COV of c and COV of ϕ, COV of γ has a considerable effect on resistance factors for stability number, $\frac{c}{\gamma H}$ ($\Psi_{c/\gamma H}$), and friction angle, ϕ (Ψ_{ϕ}),

for a given reliability index. Another important observation can be made from Table 6.5 that for constant values of COV of $\phi$and COV of γ, a significant reduction in the magnitude of $\Psi_{c/\gamma H}$ from 0.83 to 0.21 can be observed with increase in COV of $\frac{c}{\gamma H}$ from 20 to 40%, whereas a marginal increase in the magnitude of Ψ_{ϕ} can be bserved with increase in COV of $\frac{c}{\gamma H}$ from 20 to 40%. Therefore, the influence of COV of c, COV of ϕ, and COV of γ for the stability of MSW slope may not be neglected as they are significant random variables.

6.5 Conclusions

Load resistance factor design (LRFD) procedure that considers variability associated with the design of MSW landfill slopes is illustrated in the paper. The resistance factors that are developed with the assumption of normal or lognormal distributions for unit weight (γ), cohesion (c), and internal friction angle (ϕ) may be either underestimated or overestimated. It is recommended from the present study that the normal Weibull and Gumbel minimum distributions are good models for the experimentally observed values of unit weight (γ), cohesion (c), and internal friction angle (ϕ), respectively. In addition, the optimized values of mean and standard deviation of MSW properties provided in the study are used to determine the resistance factor for stability number and friction angle. The effect of COV of c, COV of ϕ, and COV of γ on the resistance factors for stability number, $\frac{c}{\gamma \mathrm{H}}$ ($\Psi_{c/\gamma H}$), and friction angle, ϕ (Ψ_{ϕ}), is significant and should be given due consideration for the probabilistic and less conservative designs.

References

Basha BM, Babu GLS (2013) Reliability based LRFD approach for external stability of reinforced soil walls. Indian Geotech J 43(4):292–302

Basha BM, Babu GLS (2014) Reliability-based load and resistance factor design approach for external seismic stability of reinforced soil walls. Soil Dyn Earthq Eng 60:8–21

Bhattacharya G, Dey S (2010) Reliability evaluation of earth slopes by first order reliability method. In: Proceedings of Indian geotechnical conference, IGC-2010, Dec 16–18, Bombay, pp 1069–1072

Hassan F, Ahmed M, Wolff TF (1999) Search algorithm for minimum reliability index of earth slopes. J Geotech Geoenviron Eng 125(4):301–308

Low BK (2003) Practical probabilistic slope stability analysis, In: Proceedings of Soil and Rock America, vol 2, pp 2777–2784

Malkawi AI, Husein W, Hassan F, Sarma KS (2001) An efficient search method for finding the critical circular slip surface using the Monte Carlo technique. Can Geotech J 38(5):1081–1089

Spencer E (1967) A method of analysis of the stability of embankments assuming parallel interslice forces. Geotechnique 17(1):11–26

Xue J, Gavin K (2007) Simultaneous determination of critical slip surface and reliability index for slopes. J Geotech Geoenviron Eng 133:878–886

Chapter 7
Rehabilitation and Expansion of Operational Municipal Solid Waste (MSW) Dumps of India

Manoj Datta, Amit Kumar, and Riya Bhowmik

Abstract This paper presents a summary of the sizes and site characteristics of 30 operational MSW dumps of cities of India with population in excess of one million. The impact of these dumps (which have no liners and inadequate covers) on the environment is discussed. The study presents seven options for rehabilitation of old dumps and demonstrates the use of hazard rating systems to select the suitable option. Six alternatives for enhancing the capacities of existing MSW dumps are also highlighted.

Keywords Landfill • Waste dumps • Ranking system • Rehabilitation • Capacity enhancement

7.1 Introduction

Each major city of India has one or more MSW dumps. Some old dumps have been abandoned and covered with local soil, but at least one dump is operational in each city. These dumps have no liner at the base and nominal cover of local soil at the top. There is immense public pressure to close or rehabilitate existing waste dumps in a proper engineered manner to minimize their environmental impact. Further, the emphasis is on reducing the waste reaching landfills (through waste processing and resource recovery) and placing rejects/residue in well-designed landfills which will reduce environmental impact of the waste reaching the landfills.

Baseline conditions of operational MSW dumps were studied in cities having population above one million by sending a questionnaire to 53 cities. Data relating to 30 waste dumps from 20 cities was received. Table 7.1 presents the data relating

M. Datta (✉) • R. Bhowmik
Civil Engineering Department, IIT Delhi, New Delhi, India
e-mail: mdatta@iitd.ac.in; riyabhowmik89@gmail.com

A. Kumar
CTRANS, IIT Roorkee, Roorkee, India
e-mail: amitrathi.ucf@gmail.com

G.L. Sivakumar Babu et al. (eds.), *Geoenvironmental Practices and Sustainability*, Developments in Geotechnical Engineering,
DOI 10.1007/978-981-10-4077-1_7

Table 7.1 Base area, waste height and waste quantities of operational dumps

Area (ha)		Waste height (m)		Waste quantity (million tons)	
Range	% dumps	Range	% dumps	Range	% dumps
0–20	53	0–10	50	0–1	54
20–40	23	10–20	19	1–3	13
40–60	7	20–30	12	3–5	21
>60	17	>30	19	>5	13

Table 7.2 Proximity to groundwater, surface water and communities of the operational dumps

Depth to groundwater (m)		Distance to surface water body (m)		Distance to community (m)	
Range	Percent of dump sites	Range	Percent of dump sites	Range	Percent of dump sites
0–5	29	0–500	39	0–500	62
5–25	46	500–2000	23	500–2000	34
>25	25	>2000	38	>2000	4

to base area, waste height and waste quantity at these cities, and Table 7.2 presents the data relating to proximity to groundwater, surface water and community.

From these tables, it can be inferred that most of the operational waste dumps have base areas in the range of 0–40 ha and heights in the range of 0–20 m. The waste dump with largest base area of 120 ha is at Deonar in Mumbai, whereas the dump having maximum waste height of 60 m is at Okhla in New Delhi. More than 60% of the dumps are located within a community or up to 500 m from it, thus posing significant air pollution and odour-related problems. In addition, more than 70% of the waste dumps have groundwater within 25 m depth below their base, and amongst these, about 50% sit on alluvial deposits of sand and silt posing significant threat to groundwater resources. Thus, rehabilitation of these dumps is being accorded a high priority in the immediate future.

7.2 Objectives of Rehabilitation and Expansion

The objectives of rehabilitation and expansion of operational waste dumps are as follows:

(a) Minimize the impact of existing waste dumps on the environment.
(b) Reduce incoming waste through processing and resource recovery.
(c) Minimize the base area of the existing dump, and accommodate reduced incoming waste in new well-designed landfills.
(d) Stabilize the old dumps and allow limited access, wherever feasible.

Because of the large size of the MSW dumps, removal of waste followed by clean-up is not considered a feasible option. Containment of the waste to reduce contamination to an acceptable level is considered to be a remedy for rehabilitation at this stage (Sharma and Reddy 2004; Bonaparte et al. 2002). USEPA (1993) also prescribes containment as the presumptive remedy for MSW landfill sites.

Table 7.3 Impact of MSW on environment and the control measures

Environmental impact	Control measures
Groundwater contamination	Highly impervious cover; vertical cut-offs, pump and treat
Surface water contamination	Highly impervious cover; interceptor drains for surface water runoff and leachate runoff on ground surface
Air contamination (bad odour, GHG emissions)	Highly impervious cover; gas collection, treatment, utilization, methane oxidation
Litter, pests, rodents, birds	Daily soil cover with final cover of local soil
Landfill fire and smoke	Fencing and restricted access; daily soil cover and final cover of local soil
Slope instability	Regrading and flattening of waste slopes
Aesthetics	Vegetative cover

7.3 Impact on Environment and Control Measures

MSW dumps without liners and covers impact the neighbouring environment in a number of ways. Table 7.3 indicates the types of impacts and control measures which are usually adopted to mitigate each impact. The traditional practice of using daily soil cover to control adverse environmental impact at old landfills followed by a final capping of local soil plus vegetation helps reduce the problems of litter, pests, rodents, bird-hit, fire and aesthetics. It however has limited impact on groundwater pollution, surface water pollution and air pollution (bad odour and greenhouse gas emissions). For these, more stringent and expensive control measures are required as summarized in Table 7.3.

7.4 Variability in Site Conditions

The impact of a MSW dump on the adjacent environment is, to a large extent, governed by the site conditions at its location. A waste dump of the same size and with similar composition of waste would have much lower impact on the groundwater if it was located at a site with scanty rainfall, clayey subsoil and groundwater table at large depth in comparison to the same waste dump being located in a high rainfall area on sandy subsoil with groundwater table at shallow depth.

As another example, a large dump on sandy soil, far away from a water body but having water table at shallow depth, may harm the groundwater quality, but the same dump on clayey soil and adjacent to a lake with ground surface sloping towards the lake may have a significant adverse impact on the surface water quality.

The variability of site conditions in India becomes evident from Tables 7.1 and 7.2, as well as from the fact that annual rainfall in different locations may vary from less than 500 mm to more than 2500 mm. In addition, subsoil conditions vary from low permeability clays to high permeability sands or fractured rock. Table 7.4 provides values of different parameters for waste dumps of six cities and highlights

Table 7.4 Variability of site conditions for six waste dumps in India

Site condition	Dump A	Dump C	Dump H	Dump I	Dump L	Dump M
State	MP	RJ	WB	MH	NCR	MH
Area (ha), height (m)	8, 16	54, 5	21.4, 24	120, 15	28.3, 32	22.5, 20
Annual rain (mm)	950	633	1650	2400	721	885
Waste (ton/day)	[a]	400	3500	4000	2500	1000
Vadose zone thickness (m)	20 (M)	50 (H)	50 (H)	20 (M)	5 (L)	6 (L)
Soil type	Clay	Sand	Clay	Clay	Silty sand	Fractured rock
Distance to GW well (m)	1500	1500	2000	1500	500	750
GW uses	DW-SS	DW-SS	DW-SS	None	DW-MS	DW-MS
Nearest SW body type	Fresh river	Fresh river	Fresh wetland	Salt creek	Fresh river	River
Distance to SW body (m)	2000	3000	500	500	3000	>3000
SW uses	Irrigation	Irrigation	SENV	Fisheries	DW-MS	Irrigation
Percent built up area						
(up to 1500 m)	5–20%	Nil	Nil	20–50%	>50%	Nil
(1500–3000 m)	5–20%	5–20%	5–20%	20–50%	>50%	5–20%

MP Madhya Pradesh, *RJ* Rajasthan, *WB* West Bengal, *MH* Maharashtra, *NCR* National Capital Region, *DW-SS* drinking water-supplementary source, *DW-MS* drinking water-main source, *SENV* sensitive environment, *L* low, *M* medium, *H* high

[a]Unspecified rejects

the wide range over which parameters vary when one analyses the data received from various dumps of one million plus cities of India.

7.5 Relative Ranking Systems

To arrive at an appropriate set of control measures, one must be able to quantify the relative impact of the waste dumps on their neighbouring environment, i.e. groundwater, surface water and air. For this purpose, relative hazard rating systems are a useful tool. Relative hazard rating systems have been developed to quantify relative environmental impact of hazardous waste by several investigators. These systems, though simpler and quicker to use, suffer from subjectivity. Such systems evaluate

waste sites relative to a hypothetical base site; thus, the hazard values indicated by them are relative.

However, for the purpose of prioritization or ranking of waste disposal sites for remedial action, hazard rating systems are considered more suitable owing to their simpler and quicker methodology.

Some of these systems have been extended to municipal solid waste as well. Usually these rating systems give an overall index for all polluting pathways – groundwater, surface water and air. For rational decision-making regarding choice of control measures, it is more useful if rating systems indicate the relative impact of each pathway separately. Such rating systems have been developed for individual impact of MSW dumps on groundwater, surface water and air (Singh et al. 2009; Kumar et al. 2015, 2016).

The relative hazard rating values of 12 cities of India on a scale of 0–1000 for groundwater, surface water and air have been reported by Datta and Kumar (2015) and are depicted in Figs. 7.1, 7.2, and 7.3. A value from 0 to 250 indicates low relative

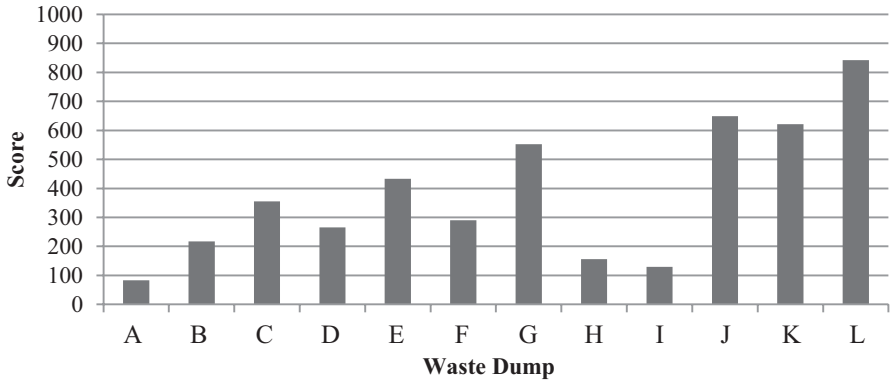

Fig. 7.1 Groundwater contamination hazard ratings for selected waste dumps

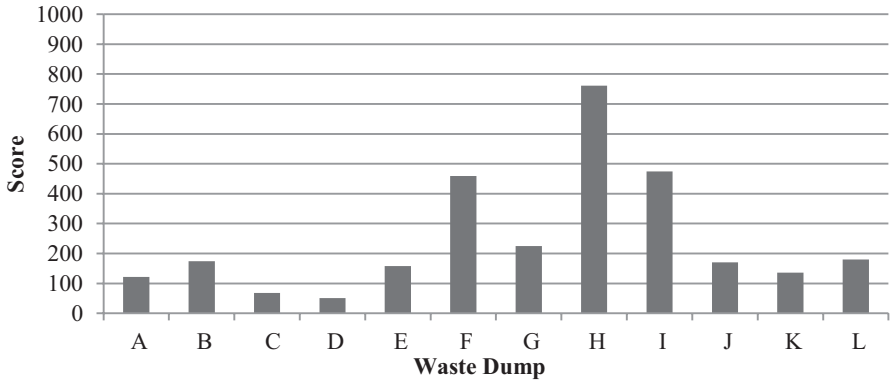

Fig. 7.2 Surface water contamination hazard ratings for selected waste dumps

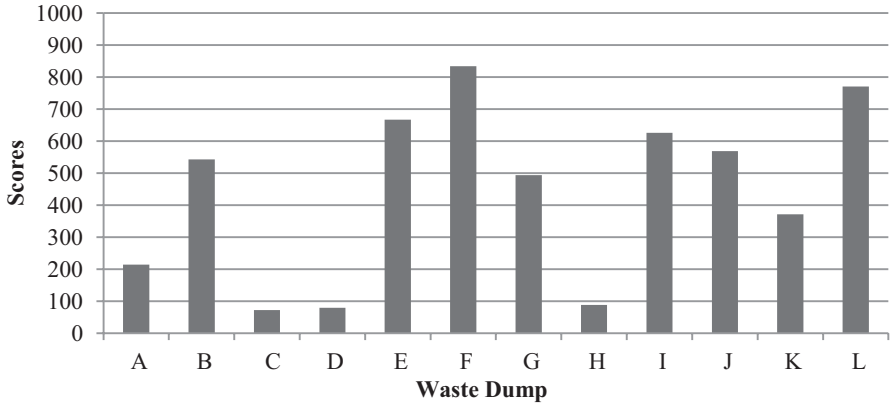

Fig. 7.3 Air contamination (odour) hazard ratings for selected waste dumps

hazard, from 250 to 500 as medium and from 500 to 1000 as high. One notes from these figures that the same dump may score high on one type of impact and low on the other two (e.g. Dump H) or vice versa (e.g. Dump L).

Using these results, one can choose the appropriate control measure as indicated in the next section.

7.6 Rehabilitation Options

Depending upon the type and level of impacts, different combinations of control measures listed in Table 7.3 can be undertaken for rehabilitation of a waste dump. Seven options are identified based on literature review and are listed below. Additional options are possible by various combinations of control measures, but these are beyond the scope of the present study.

Option I: Local soil cover – Regrade top of dump, nominally regrade slopes and provide local soil cover of 45 cm with surface water drain and leachate drain/pit.

Option II: MSW cover – Regrade top of dump, regrade slopes and provide cover as per MSW rules, compost window (for methane oxidation), passive gas vents, surface water drain and leachate drain/pit.

Option III: HW cover – Same as Option II but with cover as per hazardous waste rules by including geomembrane as additional barrier.

Option IV: HW cover with gas recovery – Same as Option III with gas collection wells and treatment/flaring/utilization of landfill gas.

Option V: HW cover with gas recovery and GW extraction – Same as Option IV with vertical cut-off walls and groundwater extraction wells for treatment and injection.

Option VI: Excavating the whole waste and putting it into a new engineered landfill.
Option VII: Mining and processing the whole waste and placing rejects/residue in a smaller new engineered landfill.

The minimum rehabilitation option is Option I. This would be applicable when all three hazard ratings for groundwater, surface water and air pollution are low such as in the case of a small MSW dump in a remote area, away from community and water body, having clayey subsoil. The local soil cover would take care of problems relating to fire, smoke, pests, rodents, litter and birds, and regrading would mitigate slope stability problems.

On the other hand, for a site having high rating for groundwater contamination, surface water contamination and air contamination, the option that would be suitable is V or VI.

Figure 7.4 shows the hazard rating scores of six waste dumps and the rehabilitation options suitable for them. One notes from the figure that for Dump A, (where all impacts are low) the suitable option is Option I.

The waste dump in Rajasthan, i.e. Dump C, has very low scores for surface water and air contamination ratings and a medium score in groundwater contamination hazard, and hence Option II is suitable, i.e. MSW cover (Fig. 7.4). For Dump H, the surface water contamination hazard rating is high, whereas the other scores for groundwater contamination and air contamination are low; thus, Option III, i.e. HW cover, is appropriate. The closure option for Dump I is Option IV (HW cover with gas recovery) as it has high rating for air contamination and a medium rating for surface water rating. Because of the high ratings for groundwater and odour, it becomes necessary to install Option V (HW cover with gas recovery and GW extraction) for Dump L. In contrast, for Dump M, one has to adopt Option VI as the MSW dump on fractured rock poses very high groundwater hazard.

7.7 Enhancement of Capacity

An important aspect of rehabilitation of MSW dumps is accommodating the fresh waste still reaching the site and placing it in a safe manner in well-designed landfills. The preferred option is to choose a new site for the incoming waste with adequate capacity for the next 25 years. However, because of non-availability of sites within or near a city, one often has to identify a site 50–100 km away which may be shared by different cities (regional landfill). Till then, one has to expand the capacity at the existing site.

The approach to expansion of capacity is based on utilizing the full area of the site and maximizing the height. From the perspective of acceptable visual aesthetics, a height of 15 m is usually considered acceptable on flat ground as the waste mound then does not become a dominant feature of the landscape. However, in

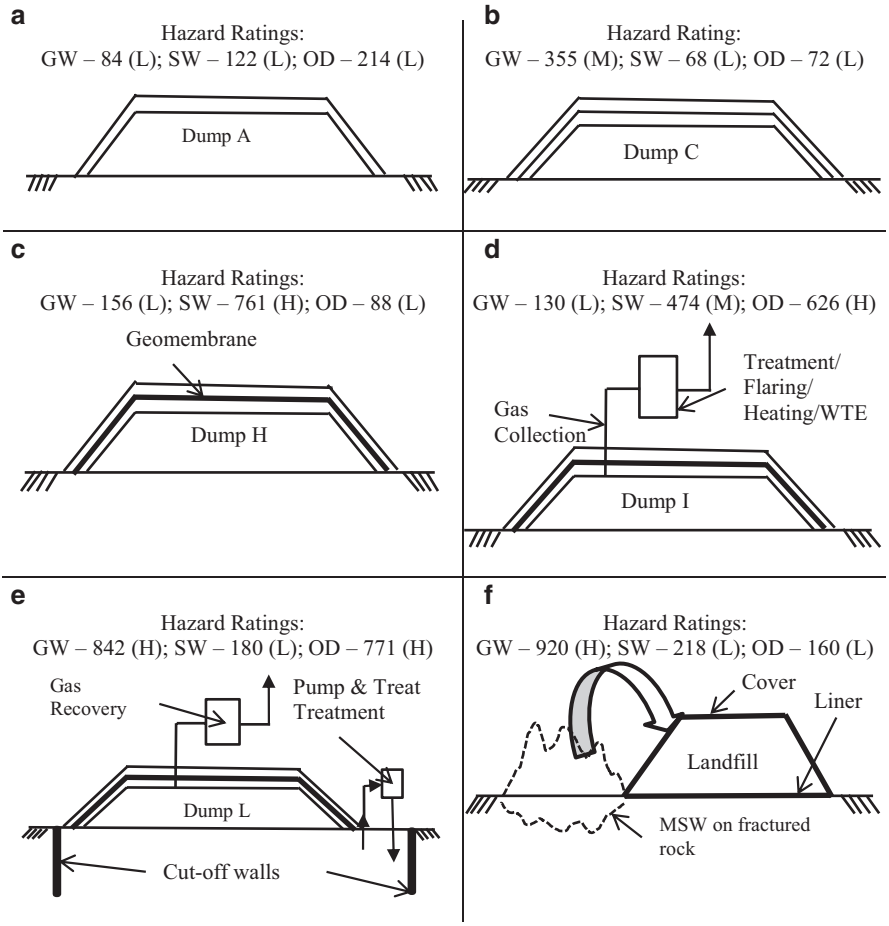

Fig. 7.4 Rehabilitation option for selected waste dumps (**a**) Local soil cover (Option I) (**b**) MSW cover (Option II) (**c**) HW cover (Option III) (**d**) HW cover with gas recovery (Option IV) (**e**) HW cover with gas recovery and GW extraction (Option V) (**f**) New landfill with liner and cover (Option VI) (*GW* groundwater, *SW* surface water, *OD* odour, *L* low, *M* medium, *H* high)

India, at many sites, the heights have reached 20 m or more. Figs. 7.5, 7.6, 7.7, 7.8, 7.9, and 7.10 show some alternatives for expansion of capacity at an existing site.

Figure 7.5 shows an existing waste dump as well as the outline of the maximum capacity of the waste dump if the full area and height is utilized.

Alternative A (Fig. 7.6) shows containment of the existing dump and lateral expansion of capacity by constructing a new landfill for future waste.

Alternative B (Fig. 7.7) shows lateral expansion after relocation of existing waste to its maximum height followed by containment measures and then construction of a new landfill. This allows a larger landfill to be constructed as the base area of the old dump is reduced. Alternative C (Fig. 7.8) is the same as alternative B with the

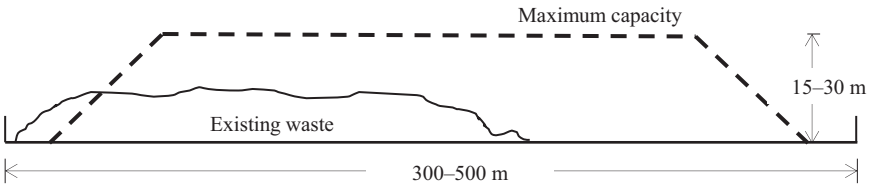

Fig. 7.5 Existing dump and maximum capacity of site

Fig. 7.6 Alternative A: Containment of existing waste; fresh waste in new landfill

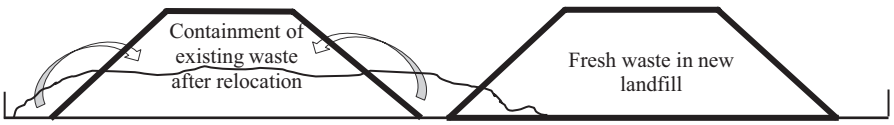

Fig. 7.7 Alternative B: Containment of existing waste after relocation to reduce base area; fresh waste in larger new landfill

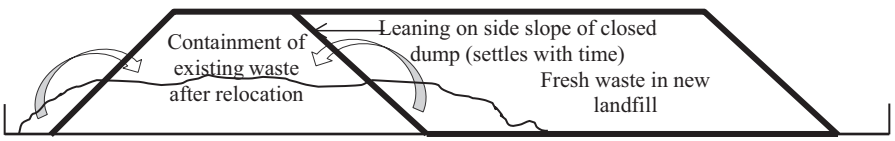

Fig. 7.8 Alternative C: Containment of existing waste after relocation; fresh waste in larger new landfill leaning on side slope of old dump

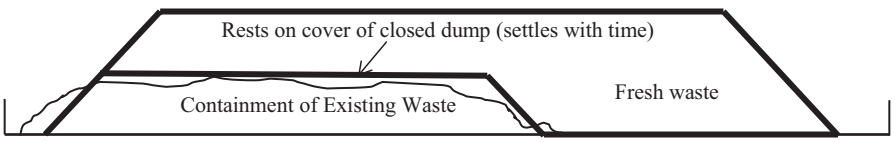

Fig. 7.9 Alternative D: Containment of existing waste after relocation; fresh waste in larger new landfill resting on top of cover of closed dump

modification that the new landfill rests partly on the side slope of the capped dump. The cover on the side slopes settles with time and needs special features in design.

Alternative D (Fig. 7.9) shows vertical expansion of capacity after containment of the old waste dump. The new landfill rests on the cover of the old waste dump. The cover settles with time and needs special features in its design to ensure that it

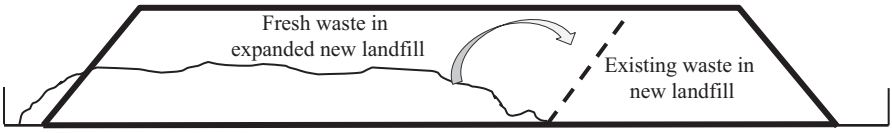

Fig. 7.10 Alternative E: Existing waste relocated to new landfill; fresh waste in expanded new landfill

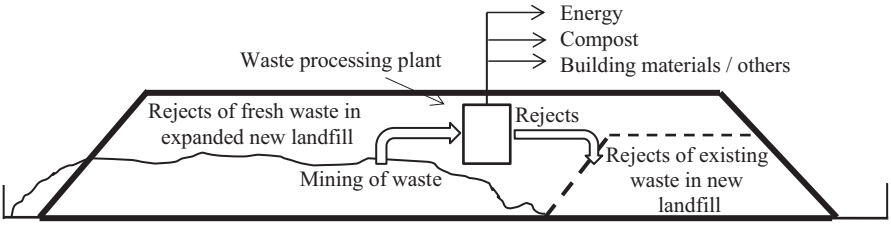

Fig. 7.11 Alternative F: Resource recovery from existing waste by mining and processing; rejects/residue of existing waste as well as of fresh waste in new landfill

functions satisfactorily as a liner for the new landfill even after significant settlement.

Alternative E (Fig. 7.10) depicts relocation of waste into a new landfill and then expanding it to its full capacity with fresh waste. The most desirable solution is shown as Alternative F in Fig. 7.11 which depicts mining the waste from the old dump, reducing its quantity by recovery of resources through processing and placing the reduced quantity of rejects/residue in a new landfill.

7.8 Concluding Remarks

The wide range of environmental impacts posed by MSW dumps of Indian cities having population more than one million is discussed. Seven options for rehabilitation of old sites are presented, and the use of hazard rating system to select the suitable options is demonstrated. Six alternatives for enhancing the capacity of existing MSW dumps are highlighted. The methods are likely to be adopted for rehabilitation and expansion of existing MSW dumps in the immediate future.

References

Bonaparte R, Daniel DE, Koerner RM (2002) Assessment and recommendations for improving the performance of waste containment systems, EPA/600/R-02/099. U.S. Environmental Protection Agency, Cincinnati

Datta M, Kumar A (2015) Hazard rating of MSW dumps and geo-environmental measures for closure. In: Proceedings of 50th Indian geotechnical conference (IGC – 2015), Pune, India

Kumar A, Datta M, Nema AK, Singh RK (2015) A new system for determining odour potential hazard of old MSW landfills (waste dumps). In: Proceedings of international conference on solid waste: knowledge transfer for sustainable resource management. Hong Kong SAR, P.R. China, pp 643–646

Kumar A, Datta M, Nema AK, Singh RK (2016) An improved rating system for assessing surface water contamination potential from MSW landfills. Environ Model Assess 21:489–505. doi:10.1007/s10666-015-9493-z

Sharma HD, Reddy KR (2004) Geoenvironmental engineering: site remediation, waste containment, and emerging waste management technologies. Wiley, Hoboken

Singh RK, Datta M, Nema AK (2009) A new system for groundwater contamination hazard rating of landfills. J Environ Manag 91(2):344–357, Elsevier Ltd.

USEPA (1993) Presumptive remedy for CERCLA municipal landfill sites, EPA 540-F-93-035. U.S. Environment Protection Agency, Washington, DC

Chapter 8
Zeta Potential and Particle Size Characteristics of Red Mud Waste

B. Hanumantha Rao and N. Gangadhara Reddy

Abstract Neutralization is essential for high alkaline wastes like red mud for its effective utilization. As such, the process of neutralization involves treating the red mud with either chemicals or other waste materials. Among several factors that affect the efficiency of the treatment, surface charge characteristics and particle diameter parameters predominantly influence the performance of the neutralization. The present study focuses on examining the surface charge properties which include flocculation and dispersion and determining the particle size characteristics which include mean particle diameter under variable pH conditions. Surface charge properties are interpreted from zeta potential, ζ, measurements made on suspensions prepared with red mud waste at different pH values. The average particle diameter is obtained from the grain size analysis established on the same suspensions using the zeta potential analyser. Results indicate that the zeta potential increases with pH up to a certain pH value of 4 and then begin to fall with the further increase in pH. The zeta potential turned into negative (up to a maximum value of −48 mV) at pH value of 6.6, which denotes the point of zero charge for the red mud, from the initial positive (from a maximum of +41.8 mV) value. However, the value becomes stabilized when the pH is 10 and above. An average particle diameter of (a) 65–150 nm at pH of 3.96 and above 9.00, indicating a complete dispersed state of the grains, and (b) 1660 nm, 2176 nm and 1080 nm at pH of 1.15, PZC (i.e. pH of 6.6) and pH of 7.48, respectively, indicating likely agglomeration of the grains, was recorded with the change in pH of the suspension. The study finds that the waste possesses surface charge characteristics, which appear to be greatly influenced by the pH.

Keywords Surface charge properties • Zeta potential • Particle size • Effect of pH • Red mud • Flocculation • Dispersion • Adsorption

B. Hanumantha Rao (✉) • N. Gangadhara Reddy
School of Infrastructure, IIT Bhubaneswar, Khurda, 752050 Bhubaneswar, Odisha, India
e-mail: bhrao@iitbbs.ac.in; gn11@iitbbs.ac.in

G.L. Sivakumar Babu et al. (eds.), *Geoenvironmental Practices and Sustainability*, Developments in Geotechnical Engineering,
DOI 10.1007/978-981-10-4077-1_8

8.1 Introduction

8.1.1 Red Mud Waste

Most of the developing countries are lacking in adequate technology for sustainable treatment and utilization of solid wastes/by-products generated in huge quantity annually. The physical presence of any waste poses a threat to land, water and environment as it can pollute them in the due course of time. Thus, utilization of the waste, instead of disposing of it, becomes inevitable. Several studies demonstrate that wastes or by-products can be employed for gainful utilization, especially in civil and environmental applications, which could be able to consume bulk quantity of waste materials.

Among many industrial by-products, red mud waste (RMW) is a solid waste residue formed after the caustic digestion of bauxite ores during the production of alumina (Parekh and Goldberger 1976). The high alkalinity (i.e. pH range from 10.5 to 13) is due to the presence of excessive caustic soda (NaOH) content that is added during the extraction of alumina from bauxite ore by Bayer's process. For every tonne of alumina produced, the process can leave 0.8–2.5 tonnes of red mud, depending on the origin and composition of raw material used. It is estimated that approximately 120 million tonnes of red mud is generated per annum from several numbers of aluminium refinery plants across the globe, and about 14 million tonnes of it is produced in India (Power et al. 2011). The waste usually is disposed in the form of slurry, which contains about 15–40% solids (Li 1998). In the last century, many countries (viz. France, Great Britain, Jamaica, Japan, Italy, USA) dumped red mud waste slurry simply into the sea. The disposal of red mud waste into the sea generally had a limited impact on the marine environment and marine organisms due to residual alkaline and fine particle suspension in the sea environment (Agrawal et al. 2004; Power et al. 2011). On the other hand, red mud waste produced by the alumina plants located in non-coastal areas have a practice of disposing the waste into the confined impoundments. The impoundments basically are divided into three types: (a) lagooning, (b) dry stacking and (c) dry cake disposal. The various types of disposal systems being in practice across India are shown in Table 8.1.

In the lagooning system, slurry form of red mud containing about 15 to 40% solids is pumped in. However, this kind of system requires lining at the bottom that acts as a sealant, minimizing the liquor leakage to the underlying ground and groundwater. The simplest is a single layer of compacted clay that separates the residue from the original soil of the storage area (Power et al. 2011). Additional security can be achieved by the use of multiple layers, featuring impermeable plastic or geomembrane materials to form a seal between the residue and the supporting clay or other layer beneath. Dry stacking system is a little different from lagooning system and is termed as thickened tailing disposal system (Power et al. 2011). In this sort of practice, slurry of waste containing approximately 48 to 55% solids is allowed. Initially, a thin layer of red mud waste slurry is disposed of, and the excess water is allowed to evaporate or is dewatered before placing of the next

Table 8.1 A summary on red mud waste generation and disposal practices adopted by alumina industry in India

Name of the plant	Present generation of red mud waste (million tonnes/annum)	Disposal or dumping practices
NALCO, Damanjodi	2.70	A modified close cycle disposal system is used for wet disposal. The bottom of the pond is covered with impervious and semi pervious clay with base filters
BALCO, Korba	1.30	Uses modified close cycle disposal system for wet disposal. The dykes of the currently used pond have stone masonry and well protected with clay layers
Hindalco, Renukoot, Belgaum and Muri	2.64	Dry cake disposal
		Dry cake disposal
		Wet slurry or lagooning disposal
Vedanta, Lanjigarh	1.82	Wet disposal
Utkal, Rayagada	1.93	Wet disposal
MALCO, Mettur	Closed (since November 2008)	Wet disposal

Prasad et al. (1996), Mohapatra et al. (2000), and Samal et al. (2013)

layer of slurry (Cooling 1989). The last type of disposal system is dry cake disposal, which refers to the removal of water as much as possible from the residue to produce a dry cake with a solid's content of more than 65% weight prior to disposal. The dry cake disposal is not an economical disposal method because the dry cake is not pumpable, so it is generally transported into the disposal area by conveyors or trucks (Shah and Gararia 1995) and increases particle suspended matter in the nearby environment (Rai et al. 2012).

In the lagooning disposal system, the chances for contamination of land and water are quite high. The contamination is essentially due to high alkalinity of the waste. This kind of system can pose a serious threat to environment. A catastrophic embankment failure of the red mud impoundment at Ajka, Hungary, on 4 October 2010, is a best example for this kind of disposal system. Around ten people died in this incidence, and life all along the river region vanished due to spillage of about one million cubic metres of highly alkaline red mud (Ruyters et al. 2011). Similarly, another such incident occurred at Luoyang, Henan Province of China, on 8 August 2016, releasing about two million cubic metres of red mud. A village with a population of more than 300 was severely affected by this incident, and many farms and domestic animals died. These examples of mine waste containment failures have led to major concerns regarding the storage practices of red mud. The high alkalinity is mainly impeding the large-scale utilization of red mud waste. In connection with this, many of the researchers suggested neutralization of the red mud employing either commercially available chemical solutions or industrial solid waste products (Reddy and Rao 2016; Gore et al. 2016).

Red mud waste is typically red in colour because of the presence of oxides of iron, which is a dominant compound in the total mass. The waste composes of a heterogeneous mixture of fine-grained particles, mainly consisting of iron, silicon, titanium oxides, hydroxides and other products (Liu et al. 2013). Typical particle compositions of red mud waste are shown in Figs. 8.1a and 8.1b.

The particle size was reported as 90% of the particles are finer than 75 μm in size and majority of the particles are in silt to clay size range, relatively with high specific surface area (13–50 m^2/g). The specific gravity of solids found to vary between the range from 2.7 to 3.3 (Parekh and Goldberger 1976; Kehagia 2010; Gräfe et al. 2011; Snars and Gilkes 2009). The combination of the heterogeneous particle size, chemical compositions, high specific gravity of solids and specific surface area makes the waste difficult to handle and utilize. Depending upon the origin, composition of the bauxite ore and type of alumina extraction method, the properties of the red mud vary widely from place to place and refinery to refinery (Parekh and Goldberger 1976; Bhatnagar et al. 2011). Clay-like minerals, which are quite common in conventional soils and responsible for inducing surface charge characteristics, however, are absent in the waste. Even then, the waste particles still exhibits surface charge characteristics similar to that of conventional clays. This behaviour may be due to constituent particle gradation, pore sizes and electrically charged properties of the hydroxysodalite, goethite and hematite minerals present in the red mud (Newson et al. 2006).

8.1.2 Zeta Potential

Zeta potential, ζ, is the electric potential in the interfacial double layer at the location of the slipping plane relative to a point in the bulk fluid away from the interface (refer to Fig. 8.2a). In other words, zeta potential is the potential difference between the dispersion medium and colloidal particle. Zeta potential is usually measured to know the behaviour of particle's surface charge characteristics which include flocculation and dispersion (refer to Fig. 8.2b).

Zeta potential is nothing but refers to strength of the interparticle repulsive force and is often used to define the state of slurry: flocculated or dispersed. Zeta potential is an intrinsic property of a material in liquid suspension, and the knowledge of it gives an insight into the strength of electrical double layer (EDL) and the stability of a colloidal system. Usually, stability of suspensions directly depends on the zeta potential of particles (Avadiar et al. 2014; Au and Leong 2015). The pH has a great influence on the zeta potential, and it can alter the sign of electric surface charge on the particle surfaces under extreme pH conditions. The colloidal behaviour of material suspension changes with the change in particle size due to change in their surface charge (Kosmulski et al. 1999). Colloidal particles like clay particles, in the aqueous medium, usually exhibit higher zeta potential at high pH, at which particles show good dispersibility as the electrostatic repulsion becomes stronger. However, as the zeta potential registers close to zero, the particles become unstable and are

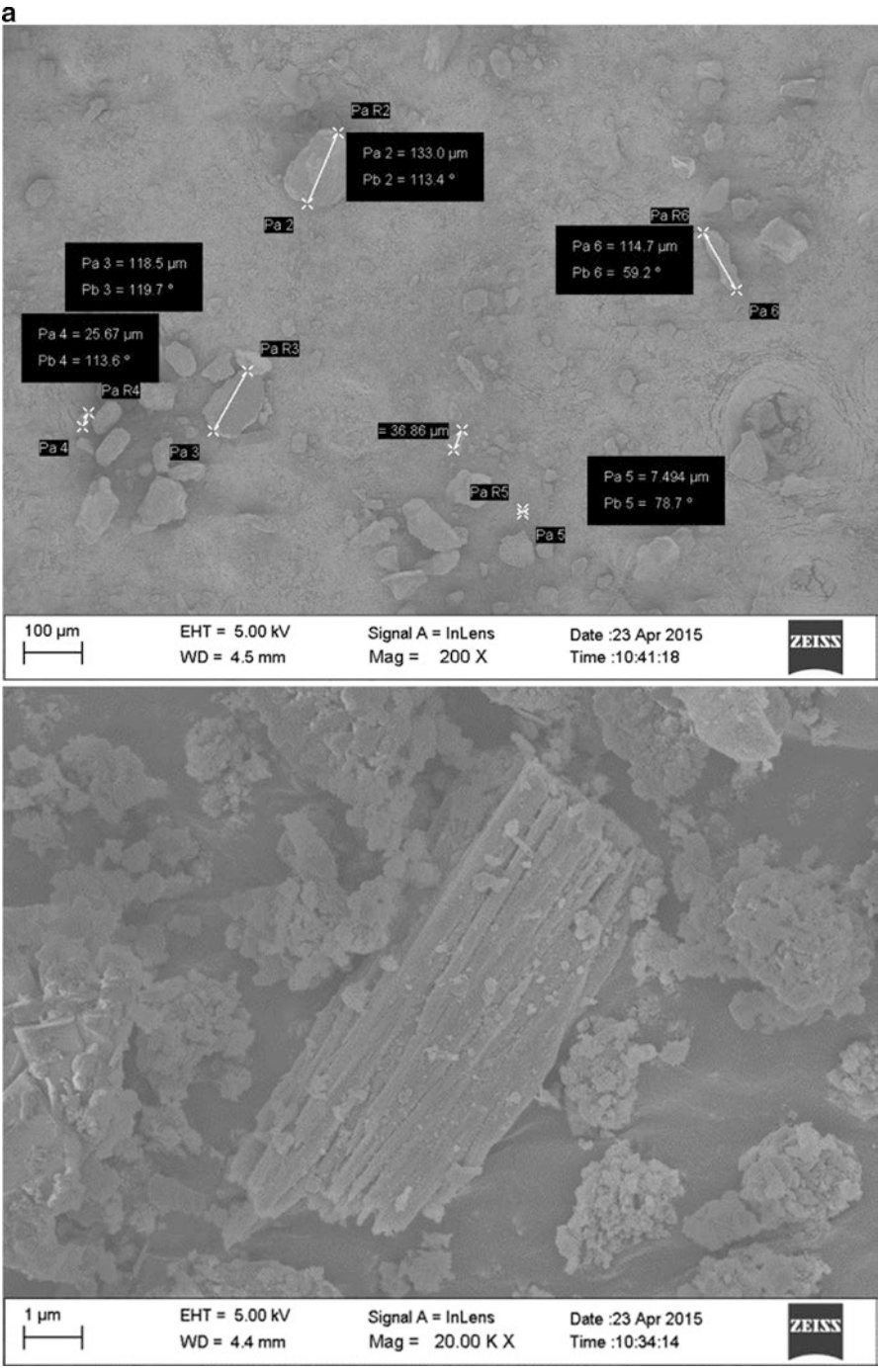

Fig. 8.1a SEM images of red mud waste depicting irregular shaped particles

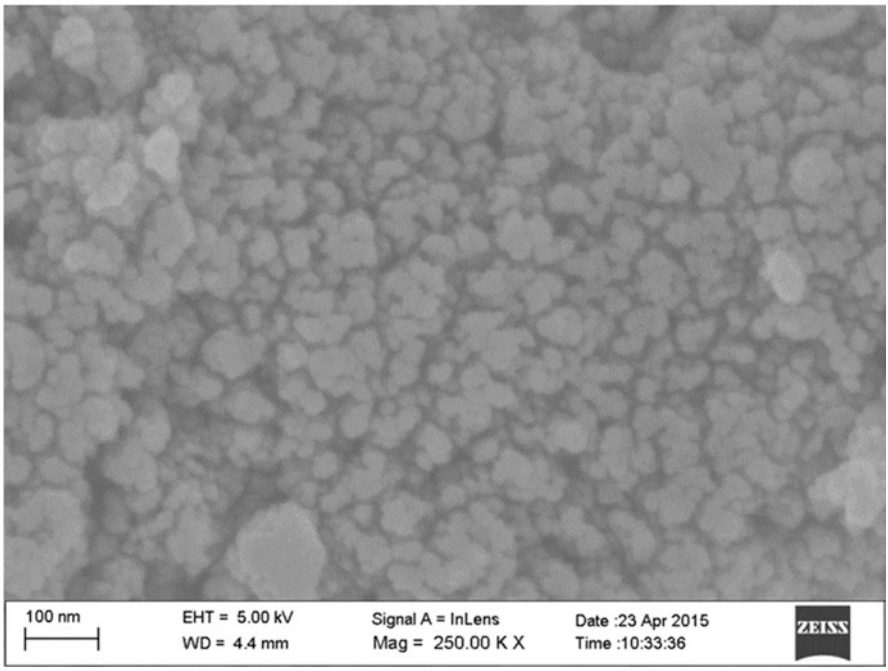

Fig. 8.1a (continued)

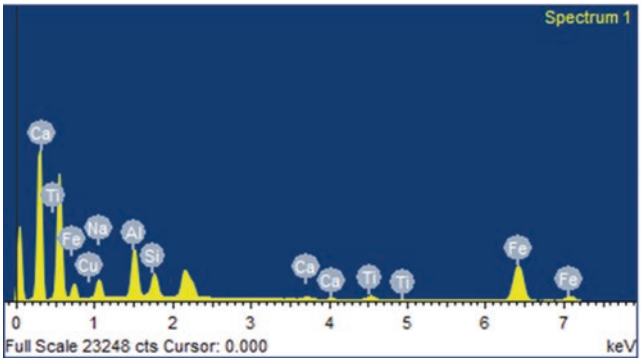

Element	Weight (%)
Na	13.53
Al	20.82
Si	10.65
Ca	1.32
Ti	2.80
Fe	49.36
Cu	1.53
Total	100.00

Fig. 8.1b Elemental analysis by EDS showing major elements of red mud waste

likely to aggregate as the pH of the aqueous medium decreases (i.e. more acidic). The relationship between suspension stability and zeta potential values is provided in Table 8.2.

Ionic bond, van der Waals forces and covalent bond kind of behaviour in the presence of water are critically dependent on the surface charge of the constituent particles. Similarly, other properties like rheology, ion exchange capacity, pH buffering capacity and adsorption capacity are also highly dependent upon the

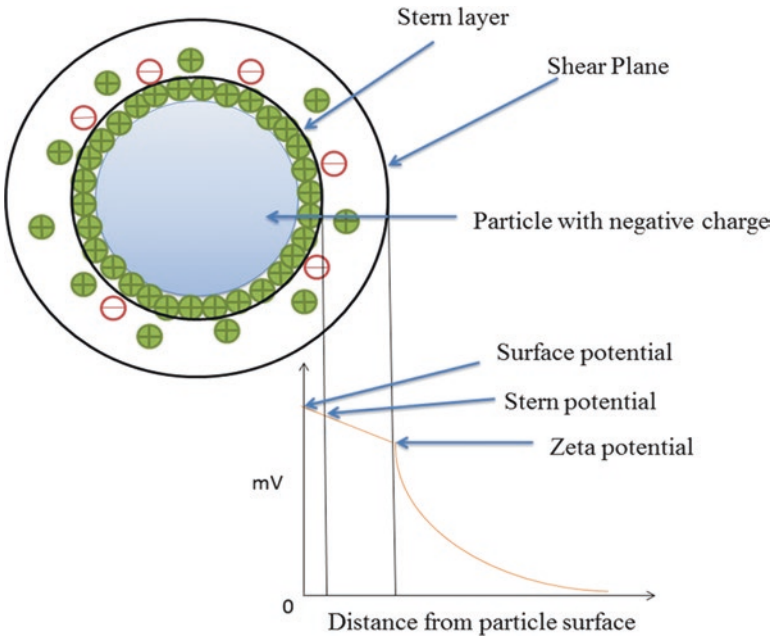

Fig. 8.2a Schematic view of zeta potential of a particle in suspension

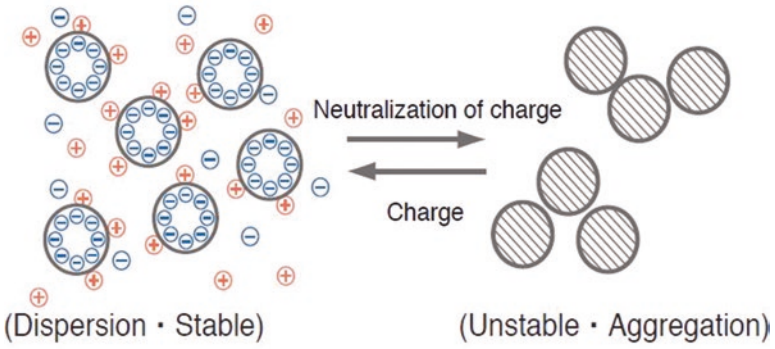

Fig. 8.2b Flocculation or dispersion mechanism of suspended particles

surface charge properties of individual particles (Gräfe et al. 2011). The complete understanding or characterization of any material, establishment of its surface charge properties, is very important (point of zero charge or isoelectric point).

Generally, these properties either in individual or in their combination largely control the mechanical behaviour or performance of neutralization or stabilization processes of the red mud waste. Thus, measurement and understanding about the surface charge properties help in to deal with the waste in field application perspective.

Table 8.2 Relationship between suspension stability and zeta potential value

Zeta potential (mV)	Stability behaviour of colloid
+3 to 0	Maximum agglomeration and precipitation
−1 to −4	Excellent agglomeration and precipitation
−5 to −10	Fair agglomeration and precipitation
−11 to −20	Threshold of agglomeration
−21 to −30	Plateau of slightly dispersion
−31 to −40	Moderate dispersion
−41 to −60	Good to very good dispersion
−60 to −80	Excellent to maximum dispersion

Riddick (1968)

In addition, the understanding of surface charge characteristics may obviously facilitate in identifying an appropriate additive, which would be effective in neutralizing and/or stabilizing the waste.

8.1.3 Theory on Measurement of Zeta Potential

8.1.3.1 Henry's Equation for Measuring Electrophoresis

When an electric field is applied across an electrolyte, charged particles suspended in the electrolyte are attracted towards the electrode of an opposite charge. However, viscous forces acting upon the particles tend to oppose this movement. When an equilibrium is reached between these two opposing forces, the particles move with a constant velocity. The velocity with which a particle under constant electric potential moves with a certain velocity is referred to as electrophoretic mobility. Knowing the electrophoretic mobility, zeta potential on the particle can be determined using Henry's equation, as expressed below:

$$U_{\mathrm{E}} = \frac{2\zeta f(Ka)}{3\eta} \tag{8.1}$$

where ζ is the zeta potential (mV), η is the viscosity of solution, ε is the dielectric constant, U_{E} is the electrophoretic mobility and f (Ka) is the Henry function.

Similarly, Smoluchowski's formula is a well-known one widely used to determine the zeta potential of particles. The mathematical form of the equation is shown in Eq. (8.2):

$$\zeta = \frac{4\pi\eta}{\varepsilon} \times U \times 300 \times 300 \times 1000 \tag{8.2}$$

where ζ is the zeta potential (mV), η is the viscosity of solution, ε is the dielectric constant and U is the electrophoretic mobility.

8.1.4 Objectives

The objective of this study is to understand the behaviour of the red mud waste of Indian origin from zeta potential measurements and interpret the surface charge behaviour such as flocculation or dispersion from these measurements. In addition, average particle diameter under varying pH conditions was measured to confirm the formation of flocculation or dispersion phenomenon in the particles. The study gains significant practical importance, particularly in the viewpoint of neutralization or stabilization of red mud waste using commercial chemicals or industrial solid wastes/by-products.

8.1.5 Zeta Potential Measurements

Zeta potential measurements were performed using Zetasizer Nano ZS90 (made in Malvern, UK). The device uses laser Doppler electrophoresis technique to measure the zeta potential, ζ, of a sample. While carrying out the measurements, an electric field is applied to suspension molecules, causing the particles move with a velocity related to their zeta potential. This velocity is commonly referred to as electrophoretic mobility, which is measured by a laser interferometric technique using laser Doppler velocimetry (LDV). With the knowledge of known electrophoretic mobility and the applied electric field, along with two more constants of the sample, that is, viscosity and dielectric constant, zeta potential of a sample is calculated using Henry's equation. Each measurement is the mean of 20 runs, each of which was averaged over three individual measurements performed automatically by the instrument. Measurements were conducted on suspensions of the red mud waste prepared with liquid to solid (L/S) ratio of 50 and 100, respectively, at time intervals of 0, 30, 60, 120 and 240 min by setting the refractive index and adsorption of the instrument as 2.55 and 1, respectively. All the measurements were performed on suspensions maintaining pH values ranging from 1 to 10. Volume of HCl/NaOH solutions required to attain the desired pH values of red mud suspension is prepared by mixing the corresponding aqueous solution with distilled water as per the calculated proportions. The suspensions were taken in a disposable polystyrene cuvette cell, which would then carefully be inserted into the cuvette holder during the measurement. Figs. 8.3a and 8.3b depicts the schematic view of the measurement of zeta potential of a sample.

The Zetasizer is also equipped with capability of measuring grain sizes within the range from 0.3 to 5000 nm. A typical dynamic light scattering (DLS) at a

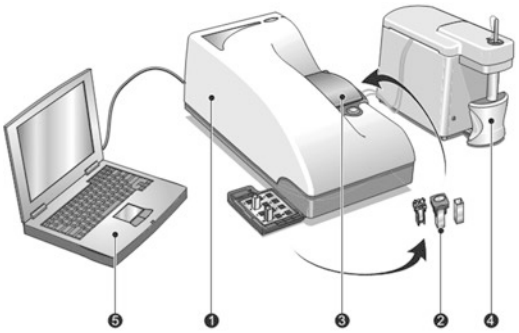

Fig. 8.3a Zeta potential instrument *1* Zetasizer Nano optical unit, *2* cells, *3* cell area, *4* MPT-2 titrator, *5* computer running the Zetasizer software

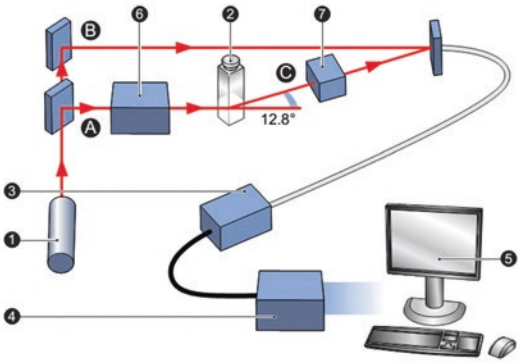

Fig. 8.3b Enumeration of steps in measurement of zeta potential of sample (Malvern 2009) *1* laser, *2* cell, *3* detector, *4* digital signal processor, *5* computer, *6* attenuator, *7* compensation optics

scattering angle of 90 is used to measure the particle diameter. This technique measures the diffusion of particles moving under Brownian motion in suspension, which would subsequently be converted into mean diameter using the Stokes-Einstein relationship. Each data value is the mean of 15 runs, each of which is an average of three measurements. Average particle diameter was measured for each L/S ratio corresponding to pH ranging from 1 to 10.

8.2 Materials

The red mud waste used in the present study belongs to NALCO's alumina refinery plant located in Damanjodi, Koraput, Odisha, India. The physical, chemical and mineralogical properties were established on the samples in accordance with the guidelines outlined in respective standards.

8.3 Results and Discussion

8.3.1 Properties of Red Mud

The summary of physical, chemical, mineralogical and geotechnical properties of the red mud waste is presented in Table 8.3. The physical and geotechnical properties are widely used in the identification and classification for any soil type in the field of geotechnical engineering. The specific gravity, G_s, one of the most important properties of the red mud, is measured as 3.05. The value is obviously considerably higher than the natural soils. The red mud waste mainly comprises of oxides/minerals of iron family (i.e. goethite and hematite) in a significant amount, leading to show high value of specific gravity. Figure 8.4 shows the gradational characteristics of the red mud waste. It can be seen from the graph that 95% constituent particles of the waste are falling under the fine-grained category (i.e. <75 μm), with a clay size fraction of 27% and silt size fraction of 68%. The majority of particles in the red mud waste are silt size range. Since the waste constitutes with silt to clay range particles, Atterberg's limits were established for this waste, as listed in Table 8.3. The liquid and plastic limits were determined as 41% and 36%, respectively, and plasticity index was calculated as 5%. Although the waste comprises of a reasonable amount of clay size particles, plasticity behaviour is confined to a very narrow range of water content. From the consistency limits and gradational characteristic properties, the red mud is classified as silt of low plasticity, ML, soil. The other properties show that the red mud waste has high pH ranging from 10.7 to 11.5, high specific surface area ranging from 41.6 to 47.2 m^2/g, low pore volume and high pore radius. Mineralogical analysis shows that Fe and Al group minerals are dominated in the red mud waste.

The various minerals identified in the red mud waste are listed in Table 8.3. It is worth noting that the waste does not compose of minerals, which are typically found in conventional soils like clays and sandy soils. Even in the absence of clay-like minerals, red mud waste still exhibited plasticity characteristics.

Table 8.3 Physical, chemical, geotechnical and mineralogical properties of RMW used in the study

S. no.	Property	Value
1.	Specific gravity	3.05
2.	Consistency limits (%)	
	Liquid limit	41
	Plastic limit	36
	Plasticity index	5
3.	% fractions	
	Sand	5
	Silt	68
	Clay	27
4.	pH	10.7–11.5
5.	USCS	ML type
6.	SSA (m^2/g)	41.57–47.20
7.	Pore volume (cc/g)	0.083–0.097
8.	Pore radius (Å)	17.47–20.99
9.	Chemical compositions	
	Fe_2O_3	48.90
	Al_2O_3	18.96
	SiO_2	18.35
	Na_2O	4.80
	TiO_2	3.69
	CaO	1.52
	K_2O	1.05
	P_2O_5	0.64
	SO_3	0.54
	MgO	0.50
	Cl	0.45
	Others	0.60
10.	Mineralogical compositions	Calcite, goethite, gibbsite, hematite, ilmenite, magnetite, perovskite, rutile, sodalite

8.3.2 Zeta Potential of RMW

Initial attempts are made to establish the stability time at which the value of ζ becomes constant for a given liquid to solid, L/S, ratio. Two L/S ratios (i.e. 50 and 100) are considered for the testing purpose. Figure 8.5 depicts measured zeta potential values with time at L/S ratios of 50 and 100, respectively, under variable pH conditions.

Trends in Fig. 8.5 show that ζ values become stabilized after approximately 120 min, corresponding to L/S ratio of 100, only, whereas the values found remain fluctuating corresponding to L/S ratio of 50. Thus, all zeta potential measurements are

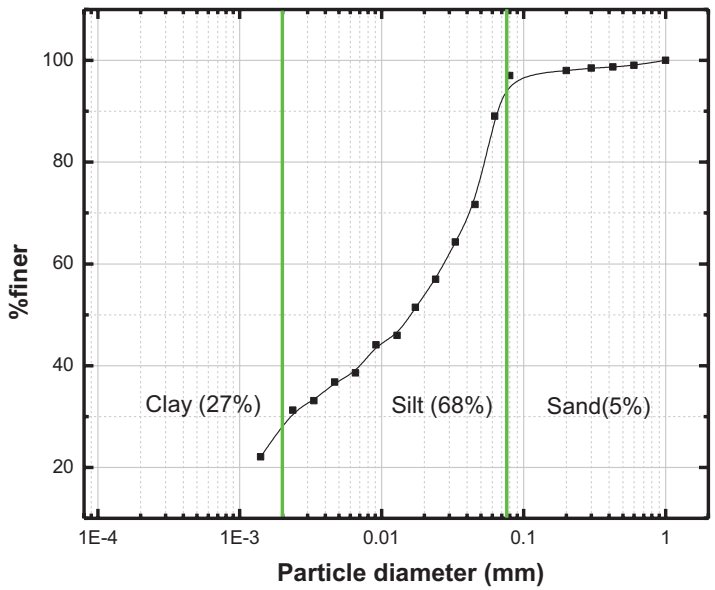

Fig. 8.4 Gradational characteristics of red mud waste used for the study

carried out considering L/S ratio of the suspension as 100. Further, results show that the value of ζ did not remain constant with change in pH. In fact, studies document that pH is an important and critical parameter that affects the zeta potential and, hence, the surface charge properties of a material. For a much better understanding, the variation of ζ with pH is plotted, as depicted in Fig. 8.6.

From the figure, it can be observed that ζ increased with pH up to a certain pH value of 4 and then decreased steadily beyond this pH value. It is obvious from the results that ζ becomes more negative when the pH of suspension exceeds 6.6 and becomes more positive when the pH of the suspension is below this value. Generally, the adsorption of H^+ and OH^- ions onto the surface of the particles is responsible to changes in the surface charge characteristics of a material (e.g. zeta potential value). The more positive or more negative values of ζ with variation in pH may be attributed to dominant adsorption of either H^+ or OH^- ions on the particle surface, depending upon the pH of the suspension.

In acidic condition, H^+ ion concentration is prominent, and hence, adsorption of these ions on the particle surfaces dominates, leading to positive values of zeta potential. Contrarily, in basic condition, the amount of OH^- ion availability becomes predominant, and therefore, the zeta potential decreases, leading to negative value. Ideally, this could have been occurring in the suspension with change in pH, leading to the red mud waste showing both positive and negative values of the zeta potential, as presented in Fig. 8.6.

From Fig. 8.6, it can also be seen that at pH equal to 6.6, ζ becomes zero. The point at which ζ becomes zero is called as point of zero charge, PZC, or isoelectric

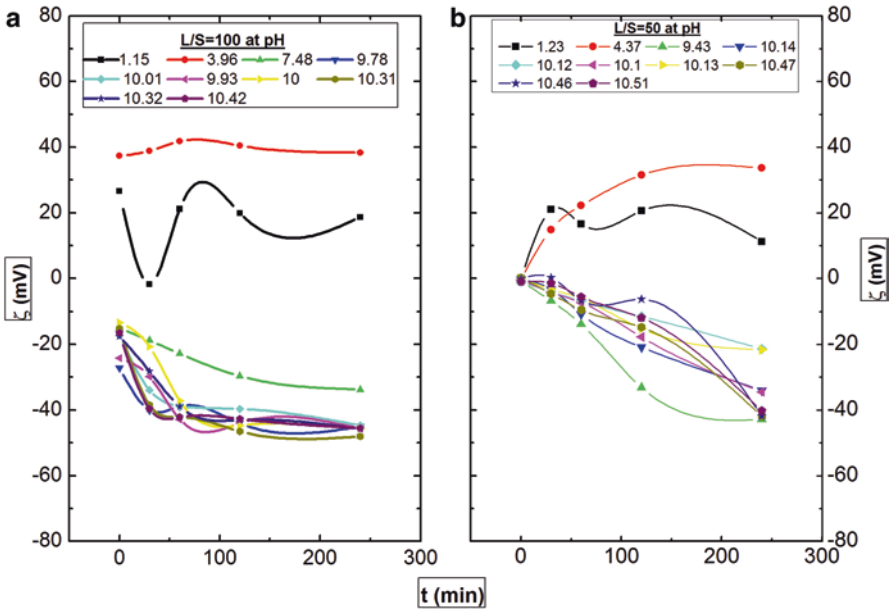

Fig. 8.5 Establishment of stability time for measurement of zeta potential (**a**) L/S = 100 and (**b**) L/S = 50

point, IEP. Generally, the PZC is the point where the colloidal system is least stable. At PZC/IEP, molecules carry no net charge on their surfaces. In other words, at this point the total positive charge becomes equal to the total negative charge. The significance of the PZC/IEP is that it can affect the solubility of a molecule at a given pH. Moreover, the tendency of particles to agglomerations becomes pronounced at PZC. A maximum ζ value of +41.8 mV and −48 mV is recorded at pH of approximately 4 and above 10, respectively, for red mud waste. This maximum positive and negative value of zeta potential is a clear indication for the red mud waste possessing the surface charge characteristics. A range of zeta potential values with a likely inference, which can help in identifying the behaviour of charged particles such as formation of flocculation or dispersion, is also depicted in the graph. It can be inferred from the constant ζ value of −48 mV that the particles of the red mud waste show 'good to very good dispersion' when the pH is above 8. This finding has a tremendous practical significance, as it advocates that pH of red mud during its neutralization or stabilization with a suitable additive needs to be maintained at least above 8, in order to obtain the benefit of particles interacting liberally with the added additive(s).

As such, studies report that the surface charge properties are strongly dependent upon the mineralogical composition of a material. For example, in the case of layer-silicate minerals (such as clays) due to the substitution of $A1^{3+}$ for Si^{4+} in the silica tetrahedral and Mg^{2+} for $A1^{3+}$ in the octahedral layer of the crystal lattice, resulting

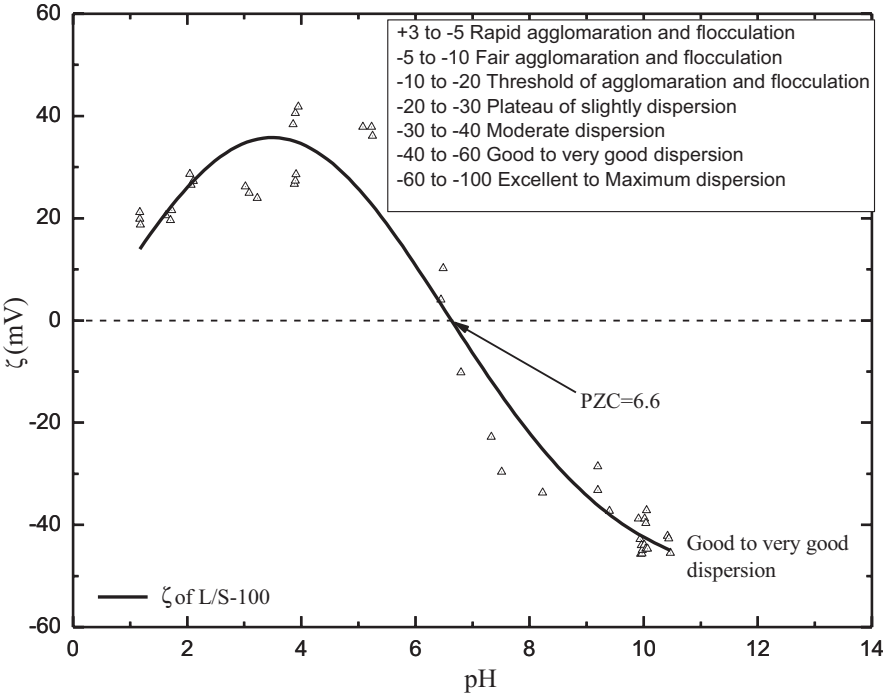

Fig. 8.6 Variation of zeta potential with pH

in surfaces of these crystal faces carries a constant negative charge that is independent of solution conditions (Fuerstenau and Pradip 2005). The typical oxide compositions of the red mud consist of iron, aluminium, silica, titanium and calcium (refer to Table 8.3), and they are available in mineral forms like hematite, calcite, goethite, gibbsite, sodalite, ilmenite, magnetite, perovskite and rutile. The constituent chemical and mineralogical compositions (Fe-, Al-, Ti- and Si-related oxides and minerals) of red mud clearly suggest the existence of pH-dependent variable charge and permanent charges on the surfaces of particles. As such, isomorphous substitution for Si, Al and Fe in desilication products (such as sodalite) can result in permanent charge on the surfaces of particles of red mud.

In order to further validate the finding of PZC at pH of 6.6 (refer to Fig. 8.6) for RMW, the relevant data have been searched for in the literature corresponding to different mineral types as well as for the red mud produced by different sources. The data compiled are listed in Tables 8.4 and 8.5, respectively. The values in Table 8.4 evidently highlight that minerals, particularly constituted with Fe and Al, exhibited PZC in the pH range from 6 to 8. This observation well corroborates vis-à-vis with the results reported in Fig. 8.6. As such, results depicted in Fig. 8.6 demonstrate that the red mud maintains the neutral character, which is nearly analogous to Fe and Al mineral groups (e.g. goethite, hematite, gibbsite, rutile, magnetite). Further, values

Table 8.4 The values of pH at which PZC/IEP reported for various mineral and oxide compositions present in red mud waste

Mineral/chemical oxide	pH range	References
SiO_2	1.9–2.5	Kosmulski (2002) and Liu et al. (1993)
TiO_2	5.1–6.4	Kosmulski (2009a)
Al_2O_3	7.9–9	Liu et al. (2013) and Kosmulski (2002)
Fe_2O_3	8.03	Liu et al. (2013)
Quartz	2.3–2.8	Kosmulski (2009b)
Hematite	6.0–9.2	Kosmulski (2002, 2009a)
Magnetite	5.7–6.8	Kosmulski (2002, 2009a)
Goethite	6.6–8.6	Kosmulski (2002, 2009a)
Calcite	8.2	Somasundaran and Agar (1967)
Gibbsite	6.5–8.3	Kosmulski (2002, 2009a)
Rutile	5.3–5.6	Kosmulski (2002, 2009a)
Perovskite	8.1	Hanawa et al. (1998)

Table 8.5 Values of pH at which PZC/IEP reported for red mud produced by different sources

Red mud/bauxite source	pH range	References
Weipa, Claremont	6–7.8	Chevdov et al. (2001)
CHALCO, China	7.5–8.2	Kun-yu et al. (2008)
Chinese RM (CHALCO)	7.1–8.7	Liu et al. (2013)
Rio Tinto Alcan, Yarwun refinery, Australia	6.3–6.8	Liu et al. (2013)
San Ciprian, Spain	6.9	Lopez (1998)
Overall	6–8.7	–

in Table 8.5 show an excellent agreement between the results of present study and those of red mud produced by different sources, with regard to the value of pH at which PZC/IEP occurs.

8.3.3 Particle Size Characteristics

Usually, the stability of suspensions can be assessed from the zeta potential, which in turn varies with the particle size. On the other hand, surface charge properties are also dependent upon particle size and pH of the suspension. Thus, any change in surface charge characteristics can in turn lead to change in the zeta potential, which in turn dominates the stability of particles in the suspension by forming agglomerations or dispersions. One of the means of confirming the particle affinity to agglomeration or dispersion is the measurement of their diameter. As such, the average particle diameter measured at different pH levels and is drawn against measured zeta potential is depicted in Figs. 8.7 and 8.8, respectively. The intensity/distribution of particle sizes captured as a function of pH and L/S ratios is shown in Fig. 8.9.

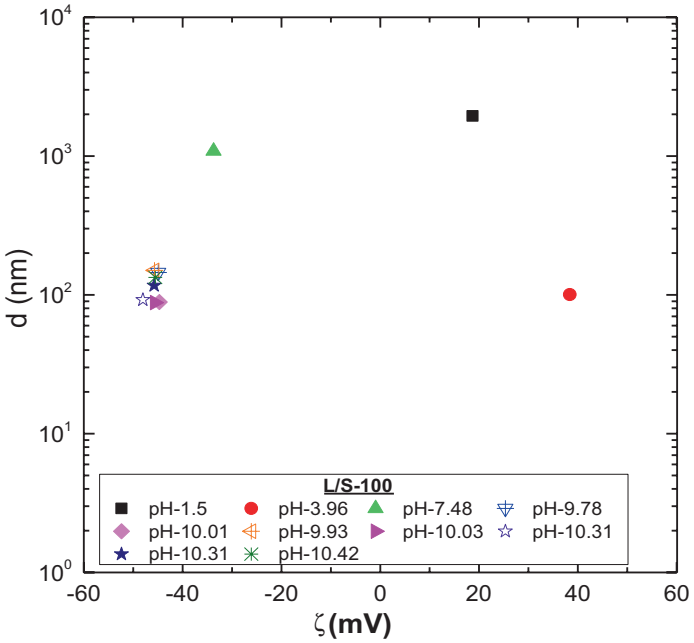

Fig. 8.7 Observed average particle diameter with zeta potential at different pH conditions

Fig. 8.8 Variation of average particle diameter at different pH conditions

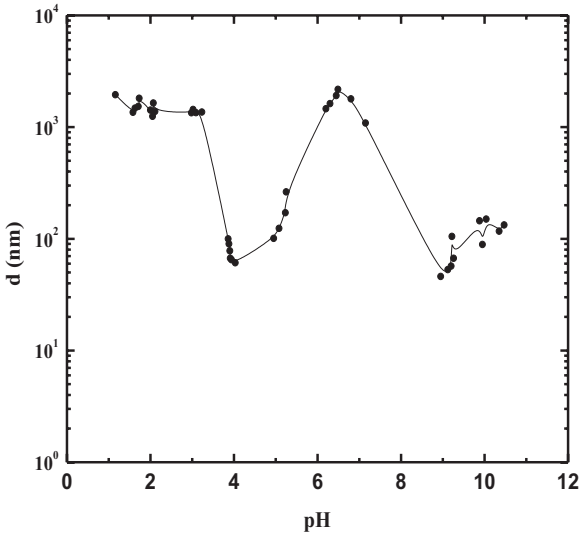

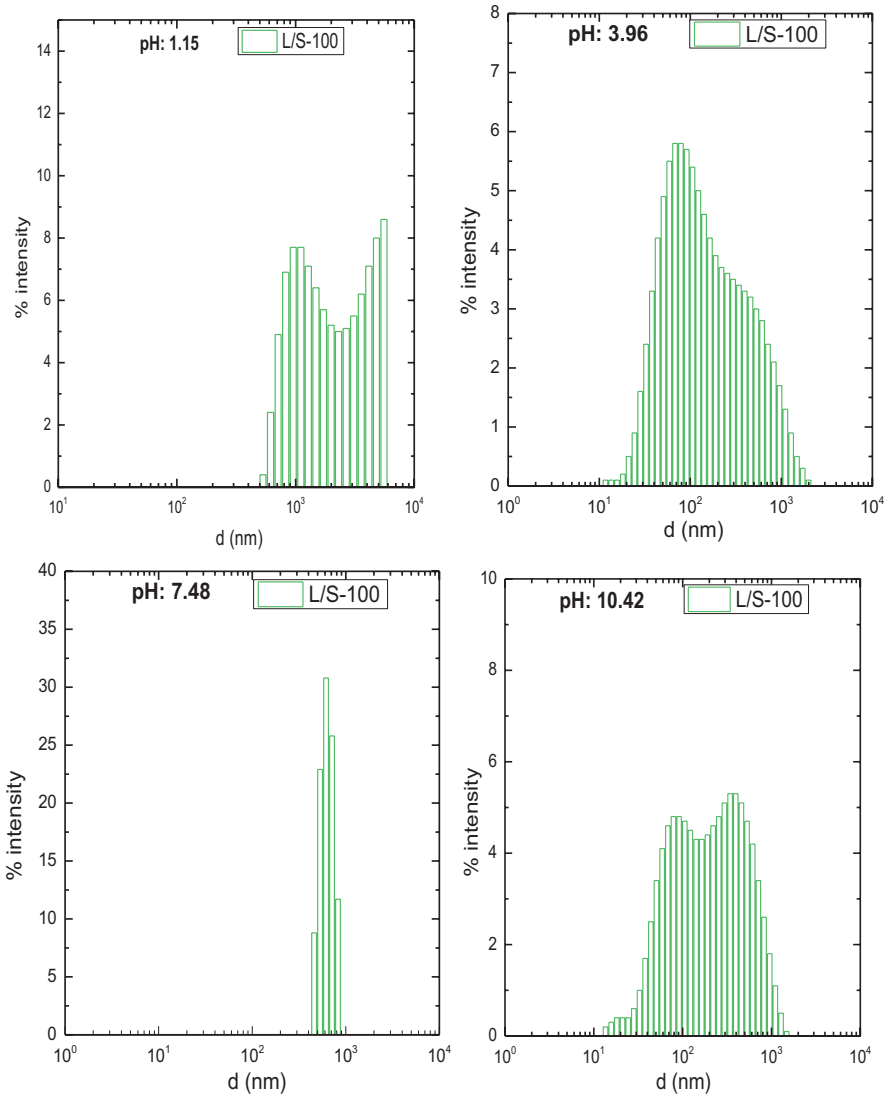

Fig. 8.9 Variation of particle intensity at different pH levels

It is apparent from Figs. 8.7 and 8.8 that at extremely low pH value (i.e. 1.15), PZC and neutral pH value (i.e. at 7.48), an average particle diameter of approximately 1660, 2176, and 1080 nm was recorded. However, for the remaining pH values, average particle diameters of 65–150 nm were observed. The lesser average particle diameter is a clear indication of the dispersive characteristics by the particles. This finding validates the inference made in Fig. 8.6 that the red mud waste particles exhibit 'good to very good dispersion' characteristics. On the other hand, the greater

average particle diameter clearly delegates the tendency of the particles to agglomerate, which could be due to coulombic attraction or van der Waals forces on the particles.

8.4 Applications and Practical Significance of Zeta Potential Measurements

- Zeta potential measurements are directly related to the character and structure of the electric double layer at the particle-liquid interface.
- Clays and clay-type materials, usually, have negatively charged faces and positively charged edges. The physical properties such as sedimentation, viscosity and structural strength are enormously responsive to the electric double layer around the particles and the affinity of the particles to aggregate. Zeta potential measurements give particularly relevant information where colloid stability and/or ion adsorption is involved.
- Zeta potential behaviour of suspension can be related to geotechnical properties such as compaction, swelling characteristics, shear strength, consolidation and material of clay-like behaviour of waste materials.
- Control of the mechanical behaviour of suspensions, using additives in the liquid phase, is also an important feature of solid and industrial waste treatment and waste neutralization and other processes of clay-like materials.

8.5 Summary

The study presents systematic investigations related to the surface charge and particle size characteristics of red mud waste from the zeta potential measurements under variable pH conditions. The following general conclusions can be drawn from the results of the study:

- The values of zeta potential found varying over a wider range from +41.8 mV to −48 mV, clearly demonstrating that the red mud waste possesses surface charge characteristics. Apparently, measurements also showed strong dependence on pH of the suspension.
- The results highlight that ζ increases with pH up to a certain pH value of 4, and thereafter, it decreased continuously with the further increase in pH.
- The PZC/IEP, which indicates the neutral character of red mud waste, was found at pH of approximately 6.6.
- The results highlight that the waste exhibits ‘good to very good dispersion’ characteristics when the pH of the suspension is maintained at 8 or above.
- An average particle diameter of 65 nm, at pH of 3.96 and above 9.00, and 1660 nm and 1080 nm, at pH of 1.5 and 7.48, was recorded.

The results reported in the study bears very practical significance pertaining to neutralization or stabilization is concerned, in selection of a suitable additive for stabilization, and in comprehending the rheological behaviour of red mud waste.

Acknowledgements Authors are highly thankful to the Department of Science and Technology (DST), Government of India, for providing financial support to carrying out this research work (Project No. SR/FTP/ETA-0297/2013). The help is greatly acknowledged.

References

Agrawal A, Sahu KK, Pandy BD (2004) Solid waste management in nonferrous industries in India. Res Conserv Recycl 42:99–120

Au PI, Leong YK (2015) Surface chemistry and rheology of slurries kaolinite and montmorillonite from different sources. Kona Powder and Part J 33:17–32

Avadiar L, Leong YK, Fourie A, Nugraha T, Clode PL (2014) Source of unimin kaolin rheological variation-Ca2+ concentration. Colloids Surf A Physicochem Eng Asp 459:90–99

Bhatnagar A, Vilar VJP, Botelho CMS, Boaventura RAR (2011) A review of the use of red mud as adsorbent for the removal of toxic pollutants from water and wastewater. Environ Technol 32(3):231–249

Chevdov D, Ostap S, Le T (2001) Surface properties of red mud particles from potentiometric titration. Colloids Surf A Physicochem Eng Asp 182:131–141

Cooling DJ (1989) Developments in the disposal of residue from the alumina refining industry. In: Light metals. TMS, Halifax, pp 49–54

Fuerstenau DW, Pradip P (2005) Zeta potential in the flotation of oxide and silicate mineral. Adv Colloid Interf Sci 114–115:9–26

Gore MS, Gilbert RB, McMilan I, Parks SLY (2016) Geotechnical characterization of compacted Bauxite residue for use in Levees. GSP, ASCE (270):299–310

Gräfe M, Power G, Klauber C (2011) Bauxite residue issues: III. Alkalinity and associated chemistry. Hydrometallurgy 108(1–2):60–79

Hanawa T, Kon M, Doi H, Ukai H, Murakami K, Hamanaka H, Asaoka K (1998) Amount of hydroxyl radical on calcium-ion-implanted titanium and point of zero charge of constituent oxide of the surface-modified layer. J Mater Sci Mater Med 9(2):89–92

Kehagia F (2010) A successful pilot project demonstrating the re-use potential of bauxite residue in embankment construction. Res Conserv Recycl 54:417–442

Kosmulski M (2002) The pH-dependent surface charging and the points of zero charge. J Colloid Interf Sci 253:77–87

Kosmulski M (2009a) Compilation of PZC and IEP of sparingly soluble metal oxides and hydroxides from literature. Adv Colloid Interf Sci 152(1-2):14–25

Kosmulski M (2009b) Surface charging and points of zero charge. CRC, Taylor & Francis, London

Kosmulski M, Gustafsson J, Rosenholm JB (1999) Correlation between the zeta potential and rheological properties of anatase dispersions. J Colloid Interf Sci 209(1):200–206

Kun-yu Z, Hui-ping H, Li-juan Z, Qi-yuan C (2008) Surface charge properties of red mud particles generated from Chinese diaspore bauxite. Trans Nonferrous Met Soc China 18:1285–1289

Li LY (1998) Properties of red mud tailings produced under varying process conditions. J Environ Eng 124(3):254–264

Liu J, Howard SM, Han KN (1993) Adsorption behaviour of cadmium and zinc ions on oxide/water interfaces. Langmuir 9(12):3635–3639

Liu Y, Naidu R, Ming H (2013) Surface electrochemical properties of red mud (bauxite residue): zeta potential and surface charge density. J Colloid Interf Sci 394:451–457

Lopez E (1998) Adsorbent properties of red mud and its use for wastewater treatment. Water Res 32(4):1314–1322
Malvern (2009) Zetasizer Nano User Manual. Manual 317(5):312
Mohapatra BK, Rao MBS, Rao BR, Paul AK (2000) Characterization of red mud generated at NALCO refinery, Damanjodi, India. In: Light metals. TMS, Nashville, pp 161–165
Newson T, Dyer T, Adam C, Sharp S (2006) Effect of structure on the geotechnical properties of bauxite residue. J Geotech Geoenviron Eng 132(2):143–151
Parekh BK, Goldberger WM (1976) An assessment of technology for possible utilization of bayer process muds. USEPA-600/2-76-30.1. Environmental Protection Agency, Cincinnati, p 154
Power G, Gräfe M, Klauber C (2011) Bauxite residue issues: I. Current management, disposal and storage practices. Hydrometallurgy 108:33–45
Prasad PM, Chandwani HK, Mahadevan H (1996) Disposal practices for bauxite tailings at the alumina refineries. Trans Indian Inst Metals 49(6):817–839
Rai S, Wasewar KL, Mukhopadhyay J, Yoo CK, Uslu H (2012) Neutralization and utilization of red mud for its better waste management. Arch Environ Sci 6:13–33
Reddy NG, Rao BH (2016) Evaluation of the compaction characteristics of untreated and treated red mud. GSP, ASCE (272):23–32
Riddick TM (1968) Control of colloid stability through zeta potential. Zeta Meter Inc., New York
Ruyters S, Mertens J, Vassilieva E, Dehandschutter B, Poffijin A, Smolders E (2011) The red mud accident in Ajka (Hungary): plant toxicity and trace metal bioavailability in red mud contaminated soil. Environ Sci Technol 45:1616–1622
Samal S, Ray AK, Bandopadhyay A (2013) Proposal for resources, utilization and processes of red mud in India-a review. Int J Miner Process 118:43–55
Shah RP, Gararia SN (1995) Upgradation of alumina refinery at Hindalco, Renukoot (India). In: Light metals. TMS, Las Vegas, pp 25–29
Snars K, Gilkes RJ (2009) Evaluation of bauxite residues (red mud) of different origins for environmental applications. Appl Clay Sci 46(1):13–20
Somasundaran P, Agar GE (1967) Surface charging and points of zero charge. J Colloid Interf Sci 24(4):433–440

Chapter 9
Sustainable Management of Dredged Sediments and Waste Using Geotextile Tube Dewatering System

Shobha K. Bhatia

Abstract In the past decade, geotextile tubes have emerged as a new technology for dewatering high-water-content dredged sediments from water bodies, by-products, and wastes. These slurry materials are often contaminated and threaten environmental resources if improperly managed. Geotextile tubes present a means to manage these materials in an environmentally responsible and sustainable manner for industrialized and developing countries alike. Keeping sustainability in mind, biodegradable materials and the viability of natural geotextiles for the dewatering and containment system need to be explored. At Syracuse University, the research team has been assessing the viability of using biodegradable geotextiles, natural flocculants, and cellulosic materials for the geotextile tube application. The results, based on both small-scale and large-scale tests, are very promising. This paper provides an overview summary of our studies.

Keywords Sustainability • Dredged sediments • Geotextile tube • Starch and natural fibers

9.1 Introduction

Numerous industries all over the world, including India and the USA, need to dewater sediments, slurries, by-products, or wastes. Dewatering serves as a precursor to disposal or further treatment by reducing the volume and weight of slurry materials, rendering them more easily transportable and disposable. Such materials include mine tailings and mineral fines, municipal sewage sludge, dredged sediments from water bodies, and wastes from agriculture, food processing, power generation, and a variety of manufacturing processes. Geotextile tubes are increasingly used for dewatering and containment applications. In addition, geotextile tubes are also used

S.K. Bhatia (✉)
Department of Civil and Environmental Engineering, Syracuse University, Syracuse, NY, USA
e-mail: skbhatia@syr.edu

G.L. Sivakumar Babu et al. (eds.), *Geoenvironmental Practices and Sustainability*, Developments in Geotechnical Engineering,
DOI 10.1007/978-981-10-4077-1_9

for shoreline protection and beach restoration. Geotextile tubes made of synthetic materials such as high-tenacity polypropylene and polyester geotextiles are most commonly used. Considering the environmental concerns and carbon foot print, geotextiles made of nature fibers, such as jute, coir, and cotton, offer the viable solutions. In addition, in projects where natural vegetation enhancement and esthetics are important criteria, it is important to evaluate viability of using biodegradable geotextile tubes made of natural fibers such as jute.

A case study on the application of biodegradable geotextile tubes to form a submerged breakwater was discussed by Gaffney (2004). The project was a coastal restoration on Dog River, Alabama, on which the previously constructed riprap was found to be ineffective in terms of facilitating vegetation, partly due to boat wake energy. To address the issue, a geotextile tube manufactured from coir, jute, and cotton of 12 m long and 4 m circumference was placed 6 m offshore, which helped in absorbing boat wake energy and allowing establishment of vegetation. The tube was hydraulically filled with sand slurry that provided a sound stability against the wave energy.

In an effort to enhance the use of biodegradable materials for the dewatering projects, Syracuse University has been conducting research on the use of biodegradable flocculants to enhance dewatering performance, cellulosic materials to retain heavy metals in geotextile tubes, and performance of jute geotextiles as a filter for dewatering applications. A brief summary of each of these studies is provided.

9.2 Green Flocculants (Cationic Starch)

Several studies (Kanchan et al. 2011, 2013, 2014, 2015) have been conducted at Syracuse University to compare the effectiveness of starch with synthetic polymers for dewatering projects. A study on Scudders pond was designed to be a biofilter for the water that is released to Hempstead Harbor in Seacliff, NY. The dewatering performance of geotextile tubes at Scudders pond was evaluated using bench-scale tests at Syracuse University and field tests at the site. Starch-based cationic flocculants were used as an alternative to the synthetic flocculent used in the dewatering project. Pressure filtration tests were conducted using the pond's sediments to predict the dewatering behavior in the field.

Pressure filtration tests were also compared with a geotextile tube demonstration test (GDT) and pressurized geotextile tube demonstration test (PGDT) at the pond site as well as in the laboratory as shown in Table 9.1 and in Fig. 9.1. Additionally, centrifuge tests were conducted to predict the final solids content and the amount of filling volume in the geotextile tubes.

Test results showed that the pressure filtration tests successfully predicted the dewatering rate of the effluent when compared with GDT and PGDT tests. Additionally, it was found that cationic starch allowed for a slightly faster dewatering rate than the synthetic flocculants (Fig. 9.1a). Figure 9.1b shows that that cationic starch that yielded the fastest dewatering in PFT also has the minimum solid content.

Table 9.1 Effluent quality during the GDT and PGDT tests

Test	Polymer	Effluent quality (NTU) collected at about 3 min	
		At pond site	In the laboratory
GDT	Control (no flocculants)	NC	144
	Synthetic	46	43
	Starch	35	49
PGDT	Starch	Not collected	11
Actual geotextile tube	Synthetic	7	

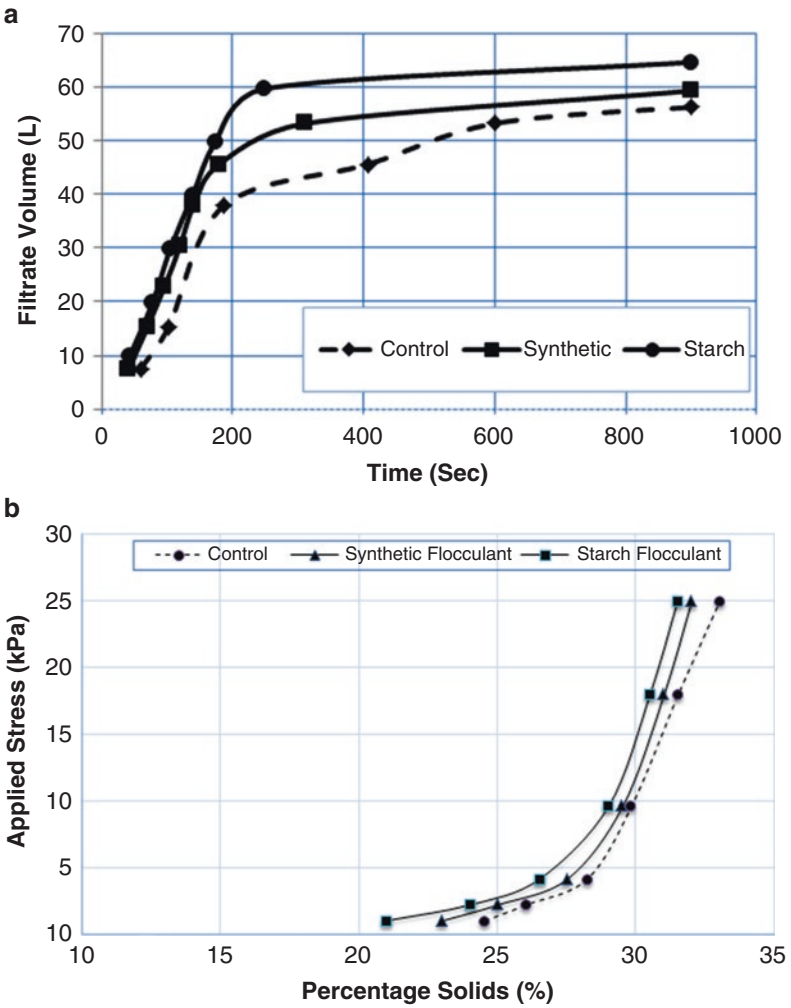

Fig. 9.1 (**a**) Dewatering rate and (**b**) centrifuge test results

The solid content results obtained from centrifuge tests, however, were higher than the results obtained from GDT and PGDT tests.

9.3 Cellulosic Materials for Enhancing Dewatering Performance

Another study (Rupakheti 2016; Rupakheti et al. 2016) conducted at Syracuse University investigated effective and sustainable measures to contain heavy metal-contaminated sediments inside a geotextile tube during the dewatering process. The efficacy of cellulosic materials (jute fibers, peanut hull, and kraft pulp) (see Fig. 9.2) on adsorption of selected heavy metals (Pb^{2+}, Cu^{2+}, Zn^{2+}, and Cd^{2+}) and dewatering performance inside a geotextile tube was studied by a series of batch adsorption and pressure filtration tests (PFT). The cellulosic materials were chosen keeping in mind their cost, accessibility, ease of handling and use, and sustainability.

Due to the presence of highly reactive clay minerals in the sediments, soils were able to adsorb and retain heavy metals (Table 9.2). However, the study on adsorption of heavy metals by cellulose materials has shown that these materials possess a heavy metal adsorption capacity as shown in Table 9.2. In addition to their potential

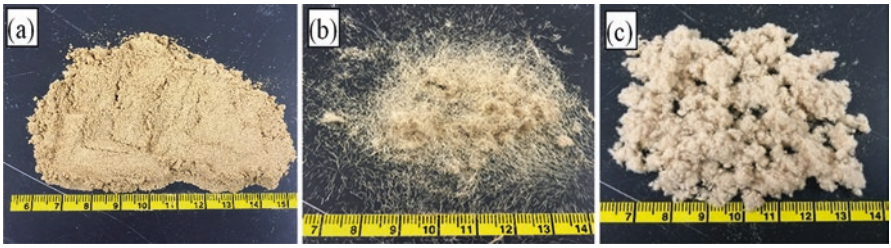

Fig. 9.2 Cellulose adsorbents: (**a**) peanut hulls, (**b**) jute fibers, and (**c**) kraft pulp

Table 9.2 Summary of % heavy metal removal (without polymer)

Conditions of contaminated Tully	% removal			
	Pb	Cu	Cd	Zn
Fines without adsorbents	99.74	98.92	88.06	83.83
Fines with peanut hulls	99.93	99.46	92.07	87.07
Fines with kraft pulp	99.88	99.56	89.08	86.03
Fines with jute fibers	99.94	99.75	91.30	87.76
Coarse without adsorbents	95.98	89.94	81.41	76.34
Coarse with peanut hulls	98.35	95.51	80.61	78.73
Coarse with kraft pulp	97.04	93.41	80.95	78.10
Coarse with jute fibers	99.37	98.37	80.22	81.59

to adsorb and retain heavy metals inside the geotextile tubes, their addition helped to improve the dewatering performance.

9.4 Jute Geotextile as a Filter

Two geotextile materials were selected for the study to make comparison on dewatering performance: one is a jute geotextile, a natural biodegradable, and the other is a polypropylene geotextile (see Fig. 9.3). The basic properties of the two materials are provided in Table 9.3.

The latest version of capillary flow porometer, Geo Pore Pro (model no. GPP-1001A), was used to measure the pore size distribution of both geotextiles. The results plotted in Fig. 9.4 show that the two geotextiles have a comparable bubble pore size.

In order to evaluate the retention and dewatering performance, pressure filtration test (PFT) was conducted using Tully silt sediment, which is classified as SM according to the Unified Soil Classification System (ASTM D2487-06). A volume

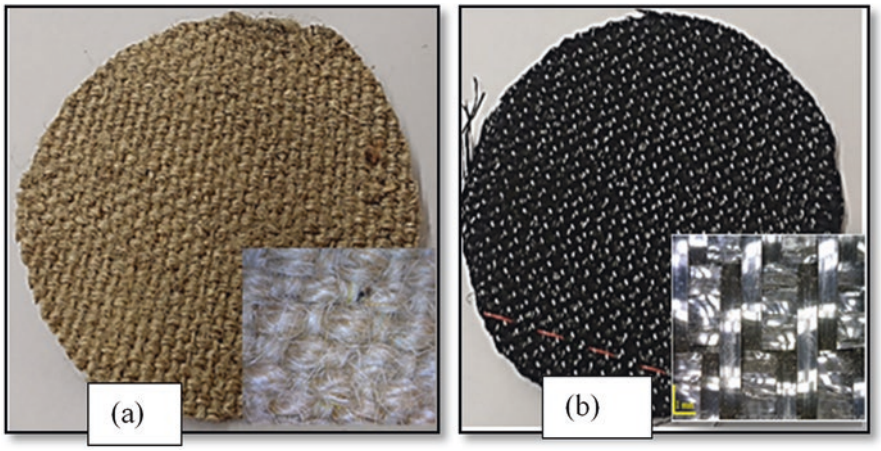

Fig. 9.3 Geotextiles tested: (**a**) jute geotextile and (**b**) synthetic geotextile

Table 9.3 Basic properties of jute and synthetic geotextiles

Name	Unit	Jute geotextile	Synthetic geotextile
Mean ultimate tensile strength (MD*XD)	kN/m	17.8 × 19.8[a]	78.8 × 109.4[b]
Mass/unit area	gm/m^2	845	585[b]
Thickness	mm	2.10	1.04[b]
Bubble pore size	microns	240–365	265–330

Note: [a]as reported by SGI testing service, [b]as reported by the manufacturer

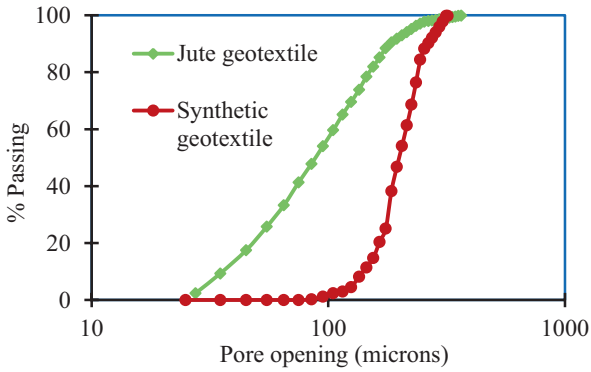

Fig. 9.4 Pore size distribution of geotextiles

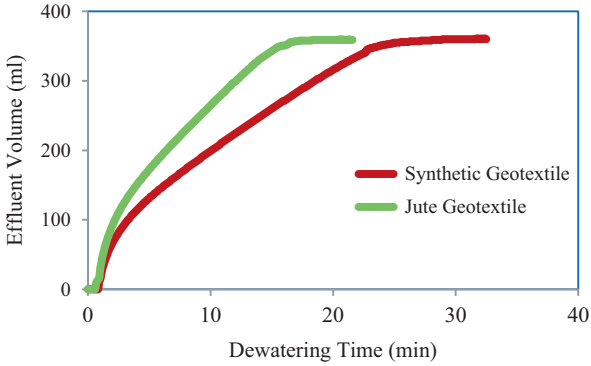

Fig. 9.5 Pressure filtration test results of jute and synthetic geotextiles

of 500 ml of 33% solid slurry was prepared, and optimum dose of 200 ppm cationic starch flocculant was added. The results plotted in Fig. 9.5 show that the jute geotextile has a better dewatering rate. For both geotextiles, the filter cake reached as high as 77% solid at the end of each test. Therefore, the jute geotextile had a comparable performance to a widely used synthetic geotextile, and it could be used for the dewatering application. Additional information will be available in our forthcoming paper (Kiffle et al. 2016).

9.5 Conclusions

The use of biodegradable materials offers a highly beneficial avenue for dewatering dredged contaminated sediments and industrial wastes. Since jute geotextiles have comparable performance to synthetic geotextiles, geotextile tubes made of the jute can be used be used for beach restoration and other dewatering projects. The addition of a small of amount of cellulosic materials is an effective way to enhance dewatering rate and heavy metal containment within the geotextiles tube.

Additionally, natural flocculants can be used instead of synthetic polymer as a viable alternative.

References

ASTM D5261-10: Standard test method for measuring mass per unit area of geotextiles. ASTM International, West Conshohocken, PA, 2010

ASTM D2487-06: Standard practice for classification of soils for engineering purposes (Unified soil classification system). West Conshohocken, PA 19428–2959, USA

Gaffney DA (2004) Advancements in tube technology for riverbank stabilization. Land and Water, the magazine of Natural Resource Management and Restoration 148(1)

Khachan MM, Bader RA, Bhatia SK, Maurer BW (2011) Comparative dewatering performance of slurries conditioned with synthetic polymers vs. eco-friendly polymers. In: Geotechnical special publication, Geo-Frontiers 2011, Dallas, TX, pp 3050–3058

Khachan MM, Bhatia SK, Zeqja E, Maio EY-S (2013) The use of cationic starch based polymers in Geotextile tube dewatering applications. In: Geosynthetics 2013 Conference, Long Beach, CA, pp 1–9

Khachan M, Bhatia S, Bader R, Cetin D, Ramarao B (2014) Cationic starch flocculants as an alternative to synthetic polymers in geotextile tube dewatering. Geosynth Int 21(2):119–136. doi:10.1680/gein.14.00003

Khachan MM, Kiffle ZB, Bhatia SK, Lebster G, Wilcox DR, Kaye P, Timpson C (2015) Evaluating geotextile tube dewatering performance at Scudders pond using cationic starches. In: Geosynthetics 2015 conference, Portland, OR, pp 1061–1069

Kiffle Z, Steele S, Bhatia K, Smith J (2016) Use of jute as a sustainable alternative for PP in geotextile tubes. In: Geotechnical frontiers 2017 conference, Orland, Florida, USA

Rupakheti P (2016) Containment and dewatering of heavy metal contaminated slurries using reactive soil minerals and cellulose materials. Thesis submitted in partial fulfillment of the requirements for the degree of master of science in Civil Engineering, Syracuse University

Rupakheti P, Bhatia SK, Jackson EK (2016) Containment and dewatering of heavy metal contaminated slurries using reactive minerals and cellulose materials in geotextile tubes, Speciality Volume in Honor of Professor Robert Koerner, Geo-Chicago 2016. Sustain Energy Geoenviron, ASCE, Illinois, August 14–18, 2016

Chapter 10
Site Characterization of Landfills Through In Situ Testing

Anirban De

Abstract In situ testing methods to obtain geotechnical engineering characterization at landfill sites present considerable opportunities and some challenges. This paper focuses primarily on the use of cone penetration test (CPT) at municipal solid waste and hazardous waste sites. Lessons learned from case histories where CPT has been used, either alone or in combination with other investigation methods, provide useful information for future work in this area.

Keywords Cone factor • CPT • In situ testing • Landfill • SASW

10.1 Introduction

Most geotechnical site characterization programs undertaken at municipal solid waste (MSW) and hazardous waste (HW) landfill sites are motivated by one of the two primary issues: (1) concern for stability of existing landfill and (2) design of structures proposed on existing landfill. The information sought are similar in the two cases, e.g., shear strength and compressibility parameters, which are usually necessary as part of bearing capacity, static and seismic slope stability, and settlement analyses (Zekkos et al. 2010). The engineering properties of waste materials within landfills are highly variable and, together with the generally toxic nature of waste material, pose significant challenges to the planning and execution of geotechnical site characterization programs.

The general challenges are first described in this paper, followed by recent advances in the field. Finally, a case history of geotechnical and geoenvironmental site characterization program at a hazardous waste disposal site is described.

A. De (✉)
Civil and Environmental Engineering Department, Manhattan College, Bronx, NY 10471, USA
e-mail: anirban.de@manhattan.edu

G.L. Sivakumar Babu et al. (eds.), *Geoenvironmental Practices and Sustainability*, Developments in Geotechnical Engineering,
DOI 10.1007/978-981-10-4077-1_10

10.2 Advantages and Challenges of In Situ Testing

Certain in situ geotechnical tests, which involve limited exposure of personnel to potentially toxic materials, have inherent advantages in site characterization at landfill sites. Standard penetration test (SPT) is the most common in situ testing method. However, this method involves the collection of sample in a split-barrel sampler and, thus, brings potentially toxic waste materials directly in contact with field personnel conducting the tests. For this reason, SPT is not preferred in landfills containing MSW or HW.

Cone penetration test (CPT) is a relatively common in situ testing method, widely used in geotechnical engineering. This method is relatively fast and does not generate any cuttings or samples, which makes this an attractive method in geoenvironmental site characterization in deposits which may pose significant risk to human health.

However, CPT is an invasive method, and the rods and cone come into contact with contaminated materials within the landfill. Potential exists for toxic gaseous material to travel through the hole and into the CPT truck when the rods are being retracted at the end of a CPT sounding. CPT soundings at MSW and HW landfills must follow proper health and safety procedures, which may require steam cleaning of rods and cone as they are extracted from the hole and air monitoring within and in close vicinity of the CPT truck.

A CPT sounding cannot be continued if either the cone tip resistance or the inclination of the rod gets close to the limit of tolerance for the piezocone instrument. Because of the intrinsic heterogeneity of waste material, it is not uncommon for the cone tip resistance to be very high at some depths within a landfill, indicating the existence of very stiff material (e.g., rocks, or rubble, or waste containers).

Spectral Analysis of Surface Waves (SASW) is a nonintrusive geophysical testing method, which measures shear wave velocities under low shear strain loading. The method does not involve any kind of penetration into the subsurface, and the results are useful in seismic response analyses. SASW has been found to be especially suitable at landfill sites, and several recent case studies have been reported in literature using this method (Kavazanjian et al. 1996: Ramaiah et al. 2016).

10.3 Cone Penetration Tests (CPTs) at Landfill Sites

Several authors have reported using CPT for geotechnical engineering characterization of landfill sites in recent years. Hinkle (1990) reported on the use of CPT at a former landfill site, located near the port of Los Angeles, where the goal was to assess the suitability of the existing material in the former unlined landfill, intended to serve as a marine container storage and repair facility. The total depth of the landfill was up to 30 m, the upper half of which was waste material and bottom half was

rubble and tires. Less than half of the CPTs were successful in penetrating the waste and reaching the desired depth.

Siegel et al. (1990) reported on the use of CPTs at nine locations on the OII Landfill in Los Angeles to delineate stratigraphy and saturated zone within the landfill as part of slope stability investigation. The CPTs ranged in depth from 4.8 to 37.5 m, with only half of the CPTs successful in penetrating more than 6.7 m. The tests had to be stopped due to excessive rod inclination, and two piezocone instruments broke off during testing.

Results from CPT indicated highly variable subsurface conditions. The authors concluded that CPTs were not particularly helpful in the particular investigation reported by Siegel et al. (1990); however, it was their opinion that CPTs might be useful in identifying relatively weak zones within landfills and changes in shear strength of waste over time.

Oakley (1990) reported using CPT to assess existing conditions at a landfill prior to placing a cap. CPT data was used to calculate anticipated settlements, which were then compared with measured actual settlements. Zhan et al. (2008) reported two CPTs conducted on a landfill in China. The tip resistances for old waste (6–13 years after disposal) were generally higher than those of the newer waste (0–7 years). Machado et al. (2010) reported on geotechnical site characterization which included five CPT soundings at two landfills in Brazil. They also reported results of soil classification based on soil behavior types, identified based on measured cone tip resistance and sleeve friction.

Ramaiah and Ramana (2014) reported results of six CPTs with pore water pressure measurements conducted at an MSW landfill in India. The maximum depth of penetration ranged from 5.7 to 13.3 m. No significant difference was noticed in the tip resistance and sleeve friction between the active phase (where the waste was less than 3 months old) and the closed phase (where the waste was 10–12 years old). The authors used the soil behavior type chart (Robertson 2009) to identify soil types consistent with the measured combination of cone tip resistance and sleeve friction for their CPT results, as well as those from several other cases reported in literature. Based on their interpretation, the authors proposed a modified zone on the soil behavior chart for landfill material, which generally spans zones representing clays, clayey silt/silty clay, and silty sand/sandy silt.

10.4 Geotechnical Site Characterization at a Hazardous Waste Site

Background De (2016) presented a case history from a Superfund hazardous waste site near the Central California coast. Five unlined hazardous waste landfills operated during the 1980s and received various chemical wastes in bulk and containers, which were separated into different landfills for disposal. Closure activity

was initiated in 1996 under US EPA oversight, and cover systems had been installed on four of the landfills by 2002.

Site-specific seismic exposure evaluation indicated that the maximum credible earthquake (MCE) at the site was a moment magnitude (M_w) 6.6 event, characterized by a peak horizontal ground acceleration (PHGA) of 0.86 g on a thrust fault underlying the site. The major concerns with respect to design of permanent cover systems at the landfills were stability (both static and seismic) and the uncertainty regarding the engineering properties of the waste material. The site characterization program was planned as a concerted effort, to synergistically utilize environmental, geophysical, and geotechnical investigation methods to evaluate the properties necessary for the design. Geotechnical investigation methods undertaken specifically in support of the static and seismic stability are discussed in this section. Detailed discussions about the scope of the investigation program are provided in De (2016).

CPT Investigation The plan view of one of the landfills (Landfill C) is shown in Fig. 10.1. Locations of CPT soundings, SASW lines, and cross sections are also shown in the figure. Twelve CPTs were advanced within the waste mass in this landfill, two were advanced through the toe buttress, and one more was advanced for the purpose of identifying the piezometric level. SASW investigation was conducted along two lines.

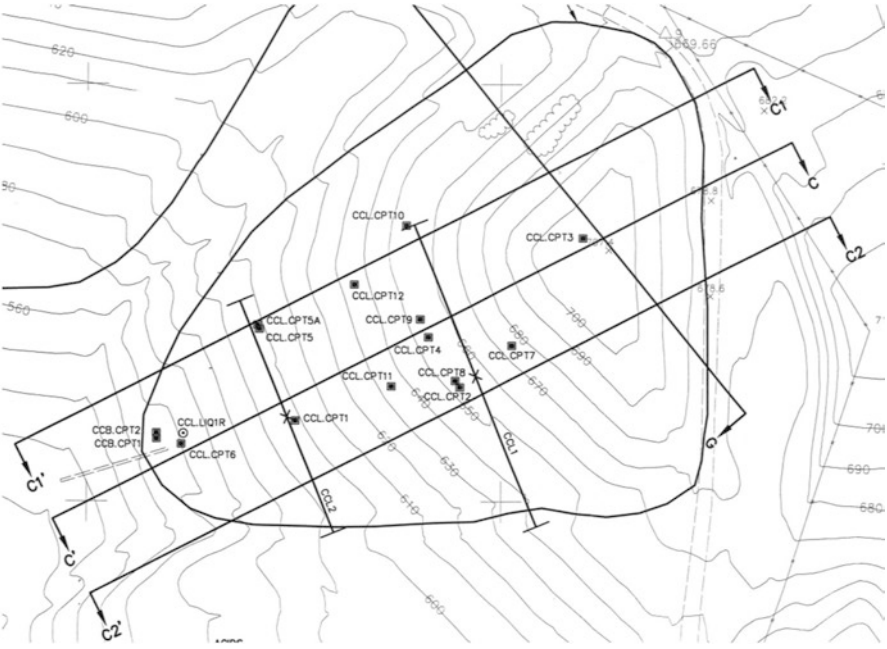

Fig. 10.1 Plan view of Landfill C, showing locations of CPTs and cross sections (Reproduced with permission from *Geotechnical Site Characterization* by Anirban De, © Momentum Press 2016)

Almost all CPT soundings penetrated through the entire depth of the landfill (up to 30 m) which included bulk and containerized waste material, interspersed with soil cover and penetrated into the natural claystone subgrade underlying the landfill.

Figure 10.2 shows cross section (CC′) through Landfill C. Note that the scales on the vertical and horizontal axes are not the same. Plots of measured cone tip resistance (q_c) from CPTs are projected at their respective locations on the cross section.

Figure 10.3 shows the plot of cone tip resistance with depth from one CPT (CPT-8) for clarity. It can be seen that the value of q_c is highly variable, with occasional high values, shown as spikes in the plot. Occasionally, very low values of q_c were recorded at certain depths (such as around 21 and 24 m below ground surface in Fig. 10.3). These indicate relatively soft material (such as sludge), most likely confined within containers (and thus protected from overburden). Spikes of high q_c above and below the low values indicate the presence of a relatively strong top and bottom surface of the containers. The q_c values increase steadily beyond 27 m, as the CPT entered the natural claystone bedrock underlying the landfill.

Displaying plots of q_c from all the CPTs on the cross section (as shown in Fig. 10.2) allows for easy identification of any potential plane of weakness, which could pass through the soft zones of all CPTs. After close scrutiny of the individual CPT plots, as well as the cross section view with superimposed plots, it was confirmed that the locations with low q_c in the different CPTs did not appear to align in any manner that would indicate the presence of a plane of potential weakness.

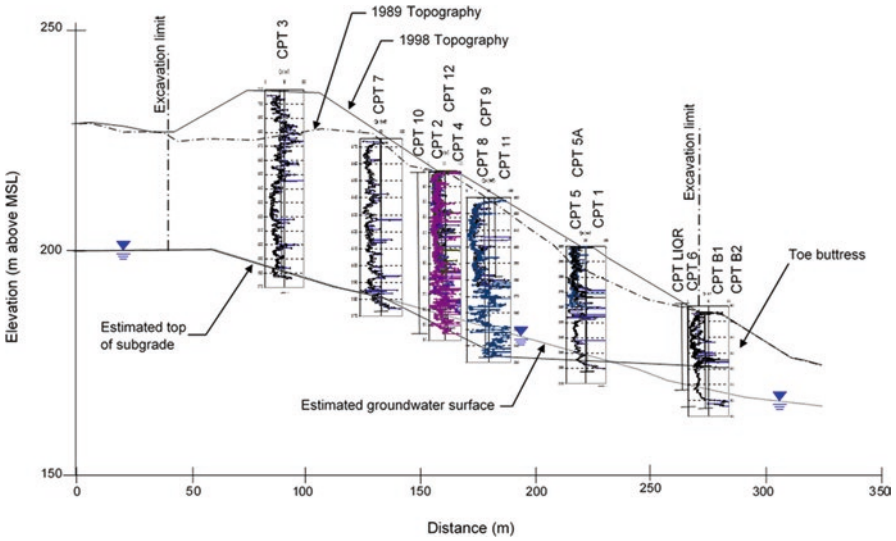

Fig. 10.2 Cross section CC′ through Landfill C, showing plots of cone tip resistance (q_c) with depth, projected on the cross section (Reproduced with permission from *Geotechnical Site Characterization* by Anirban De, © Momentum Press 2016)

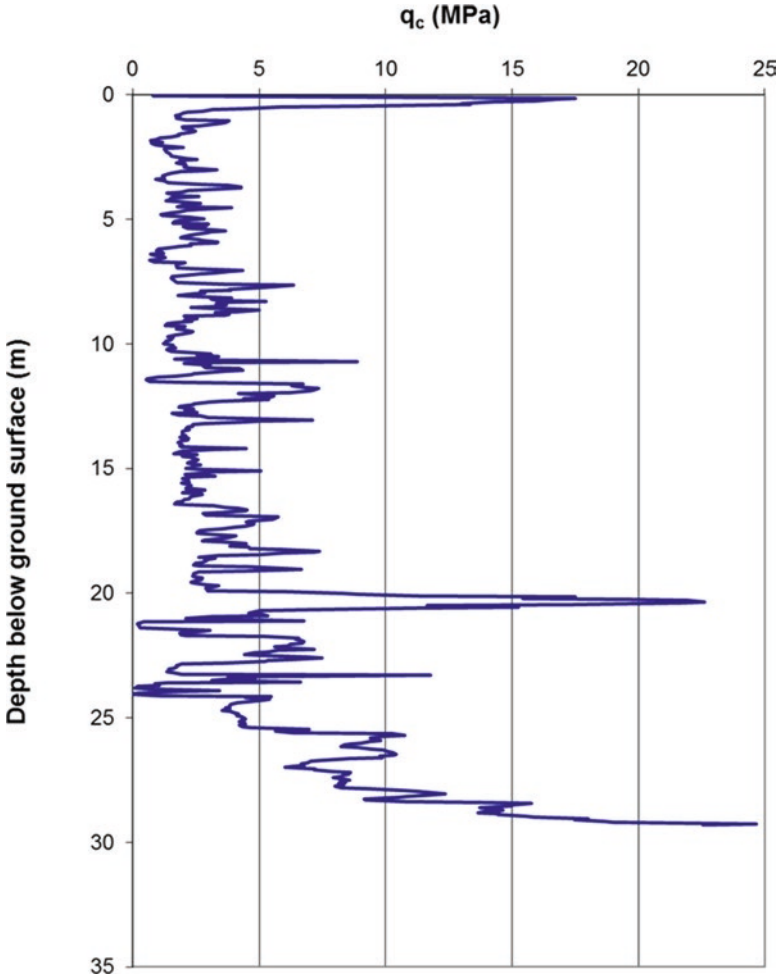

Fig. 10.3 Plot of cone tip resistance, q_c versus depth for CPT-8

The undrained shear strength (S_u) of cohesive soils can be estimated from CPT results using Eq. 10.1:

$$S_u = \frac{q_c - \sigma_{vo}}{N_k} \tag{10.1}$$

where q_c is uncorrected cone tip resistance, σ_{vo} is the total vertical overburden stress, and N_k is a cone factor.

Cone factor N_k can be estimated based on soil plasticity index (PI). This approach provided a range of N_k between 10 and 20, based on the PI of the on-site soil which had been used as daily cover. Further confirmation of the N_k was obtained by

utilizing a correlation between the shear wave velocity (V_s) measured by SASW field investigation at this site and undrained shear strength (S_u) of soft soils presented by Dickenson and Seed (1994) and a correlation between q_c and V_s reported by Mayne and Rix (1995).

10.4.1 Estimation of Shear Strength

The measured value of V_s varied from 100 to 250 m/s in the upper 10 m of the waste. The shear wave velocity (V_s) in the claystone subsurface below the landfill was almost 700 m/s. Based on comparison of q_c and V_s for soft soils, a value of cone factor (N_k) equal to 20 was found to be appropriate for use in this case. This was on the upper end of the range of 10–20, estimated based on PI and would result in conservative values of undrained shear strength, S_u. This was used in the static and seismic stability analyses of the landfills at this site and formed the basis for design and subsequent construction work. Details on the correlations are provided by Matasovic et al. (2006).

10.5 Conclusions

The presence of potentially hazardous material must be taken into account and the possibility of exposure to workers and the environment should be a major criterion in selecting suitable site characterization techniques at landfill sites. In situ field testing methods, such as CPT, have distinct advantages over other methods relative to site investigations at municipal solid waste or hazardous waste landfill sites.

In most cases, multiple geotechnical, geophysical, and environmental characterization techniques may need to be implemented to obtain a complete understanding of site conditions, in order to efficiently design the closure. An extensive site characterization program, aimed at obtaining a comprehensive understanding of the site, generally helps address any uncertainties in design. In the case history presented in the paper, cross correlation between CPT and SASW results helped engineers calculate empirical values of cone factor from which shear strength properties of waste material could be estimated for use in stability analyses.

References

De A (2016) Geotechnical site characterization. Momentum Press, New York, p 217

Dickenson SE, Seed RB (1994) Preliminary report on correlations of shear wave velocity and engineering properties for soft soil deposits in the San Francisco Bay Region, research report, Department of Civil Engineering, UCB/EERC-94, Berkeley, CA

Hinkle RD (1990) Landfill site reclaimed for commercial use as container storage facility. In: Landva A, Knowles GD (eds) Geotechnics of waste fills – theory and practice. ASTM STP, Philadelphia, 1070, pp 331–344

Kavazanjian E Jr, Matasovic N, Stokoe KH, II, Bray JD (1996) In situ shear wave velocity of solid waste from surface wave measurements. In: Proceedings of the 2nd international congress on environmental geotechnics, vol 1, Balkema, Rotterdam, The Netherlands, pp 97–102

Machado SL, Karimpour-Fard M, Shariatmadari N, Carvalho MF, Nascimento JCF (2010) Evaluation of the geotechnical properties of MSW in two Brazilian landfills. Waste Manag 30(12):2579–2591

Matasovic N, Kavazanjian E, De A, Dunn RJ (2006) CPT-based seismic stability assessment of a hazardous waste site. Soil Dyn Earthq Eng 26:201–208

Mayne PW, Rix GJ (1995) Correlations between shear wave velocity and cone tip resistance in natural clays. In: Soils and foundations, vol 35. Japanese Society of Soil Mechanics and Foundation Engineering, pp 107–110

Oakley RE III (1990) Case history: use of the cone Penetrometer to calculate the settlement of a chemically stabilized landfill. In: Landva A, Knowles GD (eds) Geotechnics of waste fills – theory and practice. ASTM STP, Philadelphia, 1070, pp 345–357

Ramaiah BJ, Ramana GV (2014) CPTu at a municipal solid waste site in Delhi, India. In: Proceedings of the 3rd international symposium on cone penetration testing, Las Vegas, Nevada, USA

Ramaiah BJ, Ramana GV, Kavazanjian E, Matasovic N, Bansal BK (2016) Empirical model for shear wave velocity of municipal solid waste in situ. J Geotech Geoenviron Eng ASCE 142(1). doi:10.1061/(ASCE)GT.1943-5606.0001389

Robertson PK (2009) Interpretation of cone penetration tests – a unified approach. Can Geotech J 46(11):1337–1355

Siegel RA, Robertson RJ, Anderson DG (1990) Slope stability investigations at a landfill in southern California. In: Landva A, Knowles GD (eds) Geotechnics of Waste Fills – Theory and Practice, ASTM STP, Philadelphia, 1070, pp 259–284

Zekkos D, Kavazanjian E Jr, Bray JD, Matasovic N, Riemer MF (2010) Physical characterization of municipal solid waste for geotechnical purposes. J Geotech Geoenviron 136(9):1231–1241

Zhan TLT, Chen YM, Ling WA (2008) Shear strength characteristics of municipal solid waste at the Suzhou landfill, China. Eng Geol 97(3):97–111

Chapter 11
Effective Management of Aged Stockpiled Solid Wastes in India

K.Y. Maillacheruvu and S.R. Asolekar

Abstract The management of municipal solid wastes (MSW) in rapidly developing economies such as India presents unique challenges as well as an opportunity to develop creative and technology-appropriate solutions, which are economically and socially sustainable in the long term. Aged wastes are defined in this paper as those municipal solid wastes which have been disposed of in dumpsites and landfills more than two decades ago. The recent 2016 fire at the Deonar dumpsite, which is the largest landfill in Mumbai, brought the spotlight on the urgent and emerging need to address the issue of aged wastes in an urban setting. This paper addresses the problem of handling and managing MSW in such settings and presents potential solutions with a focus on appropriate technological solutions. The efficacy and drawbacks of applying conventional solid waste management solutions from developed economies such as in Europe and the USA to the Indian situation are discussed. The management approaches discussed in this research may be of some relevance in the situations where the wastes are to be mined from old landfills in the USA.

Keywords Solid waste management • Waste-to-energy • Aged wastes • Appropriate technological practices • Social equity • Economic sustainability

11.1 Introduction

Management of water resources and solid wastes is emerging as a major factor impacting sustained growth in rapidly growing economies such as India. The demand for goods and services is high, and the current production models are

K.Y. Maillacheruvu (✉)
Department of Civil Engineering and Construction, Bradley University,
1501 W. Bradley Avenue, Peoria, IL 61625, USA
e-mail: kmaillac@bradley.edu

S.R. Asolekar
Center for Environmental Science and Engineering, Indian Institute of Bombay,
Powai, Mumbai 400076, India
e-mail: asolekar@gmail.com

G.L. Sivakumar Babu et al. (eds.), *Geoenvironmental Practices and Sustainability*, Developments in Geotechnical Engineering,
DOI 10.1007/978-981-10-4077-1_11

largely based on practices in the developed world. Although laws and regulations are on the books, enforcement is frequently not effective. Environmental resources are strained because of repeated use or overuse, and the impact of poor quality of environmental resources feeds into the chain of poverty and inequitable benefits of development across the population. A better understanding of how resources may be effectively used and managed with special regard to appropriate technologies rather than advanced technological solutions appears to be the key. Even a cursory analysis shows that advanced technologies by themselves may not be the answer to addressing the MSW problem in rapidly developing economies like India, especially when local conditions are not taken into account in developing and implementing management practices.

Management of solid wastes has received considerable attention over the past few decades in the USA, and several techno-centric solutions have been developed and implemented with varying degrees of success. Despite recycling efforts, the solid waste in the landfills continues to have measurable quantities of recyclables. Some communities have adopted source separation practices with some success. In contrast, the degree of recycling in solid wastes in India is quite different than what one would find in more developed countries. The calorific value of MSW, for example, is much lower in India since many recyclables are recovered prior to disposal. Perhaps more recyclables are recovered after the waste is disposed of in dumpsites! This suggests that solid waste management (SWM) practices applicable in the US and Indian contexts must be calibrated according to the prevailing customs, traditions, and practices. In both environments, however, engaging all stakeholders and creating a solution where everyone can benefit is of paramount importance. In general, when this approach has been used, the results have been generally favorable to all stakeholders.

In this paper, the issues facing SWM practices in India are discussed against the backdrop of technological solutions being implemented in the USA and other developed nations. Sustainable long-term solutions are clearly preferred. When economic and environmental issues are also addressed adequately, the holistic solution can generate jobs and other socioeconomic benefits (such as better standard of living) to the community. In seeking to create sustainable solutions, some important engineering principles are relevant, particularly as relating to material balance, energy budgets, and design principles to accelerate rejuvenation of environmental resources and receptors.

11.2 The Indian Approach

India has enjoyed growth in many industrial and technology-based sectors over the past few decades, but it remains a predominantly agricultural country. Of the more than 500,000 villages, nearly 30% are still without access to basic infrastructure including drinking water supply, electricity, and primary health support. Therefore, the priorities are bound to be different under such conditions. There are several unique challenges to continued and sustained growth. The growing population is an

obvious factor. Socioeconomic justice is another challenge. Many solutions that work elsewhere in developed countries are not likely to be effective in India. This is because the economics and subsidies that work in these developed countries are not sustainable in India. Public-private partnerships have therefore developed to support growth and to create new opportunities for the private sector, particularly in the fields of science and technology. Perhaps the most significant challenge is to creatively incorporate science and technology in crafting government policy that will promote growth and protect human health and the environment.

The policy in India with respect to solid waste management since 1999 has been to segregate at the source. The per capita production of solid waste is about 0.5 kg (including C&D waste, debris, etc.) with a broad classification of 50% w/w organic waste, 32% w/w inert and inorganic waste, and 17% recyclable waste. The typical fractionated composition of MSW in India is 47–52% biodegradable; 10–14% paper cartons and laminated packaging; 8–10% plastics, leather, and rubber; 0.5–1.0% metal; 1–1.5% glass; 1–2% cloth rags; and 18–25% inerts, debris, and C&D waste. Segregating solid waste at the generation point minimizes the need for more expensive options such as dedicated material recovery facilities (MRF). The Indian policy has been to take the energy-rich waste stream to a waste-to-energy facility. The other part of the policy is that only inert materials go to a landfill. Biodegradable materials are to be composted since that is the most energy-efficient method from a thermodynamics standpoint. The logic is that nutrients should go back to the soil. India is a predominantly agricultural country with nearly 65% of the arable land being used in this industry. When nutrients go back to the soil, this supports this agriculture-based economy, which is an engine that sustains the Indian economic growth.

11.3 Segregation of Wastes and Energy Implications

The management of solid wastes is typically associated with some degree of recycling and an adequately designed landfill. Frequently a lot of food waste and biodegradable material is disposed of in municipal landfills in developed countries. As a result, there is much effort spent on energy recovery through gas collection over the life of the landfill. For example, bioreactor landfills are designed to accelerate the biogas production cycle and recover energy in a shorter time span. The ultimate goal is production of inert materials. From a geoenvironmental standpoint, inert materials are better because settlement can be more easily predicted compared to an active landfill where biodegradation is taking place. If we take another step and ask whether it is really necessary to dispose inert material in a landfill, we then change the paradigm! This approach opens up new possibilities, which are outlined in this paper and need additional careful analysis and investigation. A holistic systems approach is preferable in managing solid wastes. Instead of investing in options such as bioreactor landfills or other accelerated energy recovery efforts, the efficacy of segregation of wastes at the source needs to be seriously considered. If wastes are segregated or separated at the source, the recycling process is likely to be more

effective. At the same time, the further management of the solid waste is likely to become considerably simpler.

The conventional definition of solid waste has to be modified in rapidly developing countries such as India because what is considered a waste in a developed economy is sometimes not considered a waste in the Indian setting. In developed countries, the approach to SWM has been to consider waste generation as a "fresh" waste, which has be to be processed (including recycling operations) and eventually disposed of in a landfill. The situation in the Deonar and Pirana dumpsites indicates that clearly the existing solid waste must first be dealt with before new managed landfills can be constructed and operated. The issue of aged waste (also called "legacy" waste) has to be addressed conclusively to create space in congested urban environments where land is at a premium. The solid waste problem can therefore be framed in the context of "fresh" solid waste and "aged" solid waste.

As long as the aged waste is present in the dumpsite, there is no room for additional solid waste. Therefore, appropriate management of aged waste is essential. The aged solid waste in dumpsites in India is typically a low-moisture waste as compared with fresh solid waste. The aged solid waste has likely undergone several years of waste decomposition or degradation under natural conditions and is likely to be inert. The aged solid waste fraction that most closely resembles soil can be mixed in with the natural soil, as long as there are no toxic chemicals in the aged soil. This will ensure that nutrients return to the soil and enrich the agricultural capacity of the native soil. The construction and demolition waste fraction of the solid waste can be recycled into the construction industry. This will create a space to construct a new landfill, if needed.

It is noted here that the state governments of Maharashtra and Gujarat have accepted Prof. Asolekar's recommendations with respect to managing solid wastes. Additionally, the Planning Commission's Task Force on Waste to Energy agreed with Prof. Asolekar's recommendation on the decision-making process for waste-to-energy initiatives. Figure 11.1 shows a proposed scheme for MSW in the Indian context.

11.4 Indian Case Studies on Solid Waste Management

In January 2016, fires were reported in the Deonar dumpsite in Mumbai. A recent report (NASA 2016) noted that the Deonar dumpsite, located by the Thane Creek in an eastern suburb of Mumbai, stretched across 132 hectares and received more than 3700 metric tons of trash per day, which accounted for one third of Mumbai's solid waste. The NASA report also noted that smoke and fire was detected by the sensors on the Terra, Aqua, and Suomi NPP satellites on January 27, 2016, and continued to burn for 4 days. *Hindustan Times* (2016) reported that air pollution was at the most severe levels since air quality data monitoring began in June 2015, with the air quality index (AQI) level rising to over 340, leading to closure of nearly 70 schools in the vicinity. Trash piles up to 30 m in height complicated the management of the

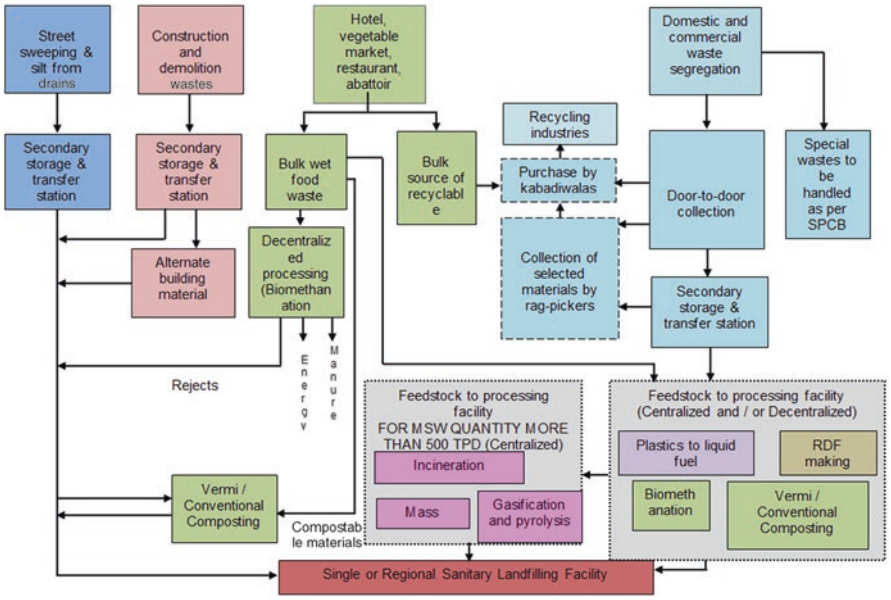

Fig. 11.1 Proposed "Integrated MSW Management System" for a large municipal corporation in India (1 to 5 million population). Source: "Report of the Task-force on Waste to Energy", April 2014 by Planning Commission of India, Gov. of India, New Delhi

situation. It is to be noted here that fires have been reported in municipal solid waste (MSW) landfills in the USA and elsewhere, although perhaps not at the same impact level as at the Deonar dumpsite, due to its urban setting.

The Deonar dumpsite is not unique. There exist other dumpsites and landfills in India and perhaps in other countries, where similar situations and complications are encountered. Prof. Asolekar is currently leading a team of experts in an effort to evaluate best management practices at the Pirana dumpsite in Ahmedabad, Gujarat. Like the Deonar dumpsite, Pirana is also an active site where solid waste continues to be disposed of every day. Preliminary site investigations and sampling at the Pirana dumpsite have revealed some interesting results, and the sampling and analysis are currently in progress. The approximately 2.5-hectare site has the most sections that are 8–16 m high and also includes areas where the solid waste has piled up to nearly 34 m. Aged solid waste at the bottom of this dumpsite has undergone transformation over at least 10–15 years.

A major challenge at the Pirana dumpsite was sampling the solid waste. After an analysis of the conditions at the site, a decision was made to collect 25 kg aliquots at seven different locations from 3-m-deep pits. Earth-moving equipment was used for the sampling operation, and the collected samples were mixed to represent a composite site sample. The collected samples are being currently analyzed for various solid waste properties, including thermodynamic properties such as calorific value. Preliminary data indicates that more than 50% of the solid waste is inert and

comprised of soil sizes less than 10 mm in diameter. No paper was recovered in the solid waste sample. Nearly 15% of the waste consisted of organic polymeric fractions such as low-density polyethylene (LDPE) wastes typically found in juice-box-type packing and other similar packing materials. The remainder was larger aggregate consisting of 0.5–8-inch material. Preliminary estimates suggest that the calorific value of the polymeric fraction is around 800 Btu/lb.

11.5 Waste Management Goals

The conventional "three R's" (reduce, reuse, and recycle) approach can be extended to the "seven R's" in a model where the goal is to achieve nearly 100% recycling or zero waste generation (El-Haggar 2007). As society moves toward the goal of zero discharge, it is of value to consider the "seven R's": reduce, reuse, recycle, recover (raw materials through sustainable management practices), rethink, renovate, and regulate. In most command-and-control type of regulatory environments that are common in industrialized countries, regulation is a significant factor in driving innovation. In a proactive sustainable culture, which may be adopted and fostered in individual manufacturing units and companies, this need not be the case – sustainability objectives are met largely before the "regulate" step and generally impact the bottom line favorably. This approach can also open a dialog with regulatory bodies and ensure that reasonable regulatory goals are being formulated. In developing countries like India, this approach is beginning to work when implemented at the single industry or manufacturing unit level, where a win-win can be created for the company and the environment (Arcievala and Asolekar 2007). Reducing waste at the source is often critical to achieving sustainability from an environmental and economic standpoint. "Upcycling" is a term used to denote a use where a by-product has a better application in another production or manufacturing process than the one where it came from (Braungart and McDonough 2002). When recycling practices can "upcycle" a by-product from a process, the economic and environmental benefit can be quite significant.

11.6 Waste Management Strategies

There are several waste management strategies that might be applicable to the Indian solid waste management problem. In fact, these same principles can be applied to developing and underdeveloped countries. Further, with some calibration, these principles are to be applied to developed economies as well. Some of these strategies are presented below, but this should not be considered an exhaustive list.

In the Indian context, the removal of aged (or legacy) waste is a top priority. In order to achieve this goal, preventive management strategies are essential. Asolekar and Gopichandran (2005) present how preventive environmental management has

been applied in Indian industries, involving greener and cleaner technologies. A systems approach, as presented in Asolekar and Gopichandran (2005), might well be the key to addressing and mitigating the solid waste problem in India. The authors also show how an effective policy for integrating policy for production and consumption can be developed and implemented.

If one follows conventional thinking and traditional design, landfills will no doubt be created, albeit at a cost that might not be sustainable in the long term. Is it really necessary to create landfills? Is there a way to eliminate aged (legacy) waste and minimize the total amount of solid waste being designated for disposal? The authors are convinced that this is indeed the case, again using preventive management strategies and challenging the norm that landfills with large area footprints are necessary to manage solid waste in India or other countries.

How can one minimize the amount of solid waste designated for disposal? An incremental approach is key. Instead of trying to build new landfills on day 1, it might be advantageous to deal with existing aged (legacy) waste. This tiered approach consists of setting some minimum and easily achievable targets. The bar is progressively raised as compliance is achieved to some average target goal. Once this goal is reached, the optimum goal can be set as a target. This tiered approach creates a ramping effect, which is essential to create capacity and sustain it in the long term. Over the past two decades, many advanced technical solutions have been hastily implemented to waste management problems in India. Frequently such projects have failed spectacularly with little to show for the investment made initially. The tiered approach addresses this management problem directly.

Some creative solutions to manage solid wastes in India include but are not limited to the following:

- Develop refuse-derived construction materials (RDCM). Create building materials from inert solid waste or aged (legacy) wastes:
  - Crush inert materials into fine material and use in construction.
  - Create precast materials and bricks from inert solid waste and residues to meet housing priorities.
  - Divert all fly ash from dumpsites and landfills, and reuse in augmenting material used in road construction.
- Develop refuse-derived fuels (RDFs) from fractions rich in volatile organics that cannot be recycled or reused. This waste can be augmented with lignin wastes, molasses wastes, and other wastes. Even if the energy content were below 1500 Btu/lb and therefore not considered suitable for incineration/burning, it is nevertheless wise to create RDFs from solid waste materials because that will eliminate the need for storage of these materials in the landfill. It will also eliminate potentially toxic organics, which might leach out as a landfill ages and potentially precious groundwater supplies.
- Recycle glass, glass wool, and metal scrap because there is a market for these recycled goods in the Indian market.
- Use a combination approach to develop the solid waste management plan.

- Recycle plastics, and convert polymers into second-, third-, and fourth-generation polymers.
- Gasify the materials that can be gasified. Use pyrolysis to produce liquid fuels from solid waste.
- Solid wastes that cannot be used in construction or as RDF can be disposed of in controlled and well-designed landfills.

Clearly these strategies and approaches require a sound understanding of science and technology principles. From a thermodynamic standpoint, for example, it is not effective to discard material like plastics in a landfill that has some recoverable energy value. Similarly if fly ash or other solid waste component materials can be utilized in construction, putting them in a landfill removes a readily available source of material and requires the use of virgin materials to produce these materials.

11.7 Summary

Recent events like the fire in the Deonar dumpsite in the city of Mumbai and the presence of large quantities of aged wastes (also sometimes referred to as legacy wastes) at sites like the Pirana dumpsite in the city of Ahmedabad have brought to the forefront some of the significant challenges in addressing the solid waste management problem in India. Unlike resource-rich economies where large landfills can be created and the waste is essentially sealed off, solid waste management has to be carried out using appropriate technologies and management strategies that can work in the Indian context. If one takes the view that solid waste contains resources that can be effectively used to produce goods and energy, albeit not at the same quality that one would expect from virgin materials, the possibilities for developing innovative solutions are immense. Further, long-term sustainability goals can be met without adversely impacting the environment or creating social inequity by avoiding the usage of virgin land and resources. Through this preventive management approach, it might be possible to eliminate aged (legacy) waste to create space for an adequately designed landfill. The authors recognize that while zero discharge is the ultimate goal, it is likely that any solution using currently available technologies and innovative preventive management strategies is likely to generate a small quantity of waste that might be appropriate to dispose of in an engineered landfill with a small area footprint.

Notes

Documentations from the following projects of Prof. Asolekar were used in preparing this article:

1. Project from UNEP in Bangladesh and Pakistan: Conceptual designing and detailing for the first national one-of-its kind integrated industrial waste management facility. Prof. Asolekar is the Lead Expert/Consultant to the UNEP, Geneva, for the multi-institutional group project (February 2016 to present).
2. Project from Ahmedabad Municipal Corporation: The AMC has awarded a short duration study project for proposing any alternative system comprising of appropriate technologies and management framework for the legacy wastes that are currently buried in the 15–25-m-tall mountains at the Pirana dumpsite (May 2016 to present).
3. Project of Municipal Corporation of Greater Mumbai: Advising Tata Consulting Engineers Ltd. (TCE) for identification of potential technologies for the proposed waste-to-energy project for disposal of municipal solid waste at Deonar dumpsite in Mumbai (April 2016 to present).
4. Member of the "Task Force" on Waste to Energy constituted in October 2013 at the behest of Prime Minister's Office (PMO) under the chairmanship of Dr. K. Kasturirangan, member of the Honorable Planning Commission of India to identify technically feasible, financially affordable, and environmentally sound processing and disposal technologies for municipal solid wastes (MSW) and assess, evaluate, and recommend systems, processes, technological options, financial mechanisms, and institutional arrangements to enhance resource recovery and promote waste-to-energy (W to E) technologies while ensuring integrated management of MSW in India. (October 2013 to April 2014).
5. Green Alang Initiative, i.e., preventive technological interventions for improving environmental attributes of ship recycling the Gujarat Maritime Board (GMB), Government of Gujarat, Gandhinagar, State of Gujarat (2010–2015).

References

Arceivala SJ, Asolekar SR (2007) Wastewater treatment for pollution control and reuse. Tata McGraw Hill Education Pvt. Ltd., New Delhi. ISBN:978-0-07-062099-5

Asolekar SR, Gopichandran R (2005) Preventive environmental management: an Indian perspective. Foundation Books Pvt. Ltd., New Delhi. ISBN:81-7596-313-1

Braungart M, McDonough W (2002) Cradle to cradle: remaking the way we make things. North Point Press, New York

El-Haggar S (2007) Sustainable industrial design and waste management. Elsevier Inc., Boston. ISBN-13:978-0-12-373623-9

Hindustan Times (2016) http://www.hindustantimes.com/india/air-quality-on-friday-worst-ever-recorded-in-mumbai/story-gXfd48EngMynqtjZ4dDR8M.html

NASA (2016) http://earthobservatory.nasa.gov/NaturalHazards/view.php?id=87429

Chapter 12
Advances in Raman Spectroscopy for the Geoenvironment

Joseph V. Sinfield

Abstract Raman spectroscopy has long offered potential for analytical specificity, sensitivity, and versatility in the study of a broad array of environmentally relevant compounds. As with other optical analytical methods, the use of the technique has been hampered by challenges in optimizing the sensor-sample interface, managing turbidity for quantitative analysis, limiting fluorescence interference, preventing biofouling (particularly for long-term monitoring), and achieving low cost. As outlined herein, research over the last several years has systematically addressed each of these factors so that Raman spectroscopy is arguably ready to be revisited as a robust and flexible field measurement technique and may now warrant targeted development effort so that it may become a more routinely employed field analysis method. In addition, the developments outlined herein are believed to be applicable to material analyses in complex, turbid, and/or fluorescence-prone settings in a broad array of fields.

12.1 Introduction

Obtaining representative measurements of in situ chemicals in the geoenvironment is challenging. Geoenvironmental settings vary on multiple scales. At the physical level, soil particles and the interparticle voids they form may range in scale from thousands of angstroms to millimeters or centimeters. The soil composition can also vary, both spatially and with depth. The extent of a zone of interest (e.g., stream, landfill, soil layer, or aquifer) may range from 10 to 100 m^2 in area to many square kilometers, and depths of interest can also vary. In addition, chemical phenomena occur over a range of time scales. For example, photochemical interactions may occur in fractions of a second, while chemical fate and transport could progress over years. This inherent variability in potential composition and broad range in spatial and temporal scale implies that in situ analyses inevitably involve a compromise between analysis time, cost, and representation of actual field conditions.

J.V. Sinfield (✉)
Lyles School of Civil Engineering, Purdue University,
550 Stadium Mall Drive, West Lafayette, IN 47907-2057, USA
e-mail: jvs@purdue.edu

G.L. Sivakumar Babu et al. (eds.), *Geoenvironmental Practices and Sustainability*, Developments in Geotechnical Engineering,
DOI 10.1007/978-981-10-4077-1_12

Overcoming the challenges of effective geoenvironmental monitoring thus requires a measurement system with sensitivity to measure low concentrations, applicability across a range of compounds, practical measurement time, minimal disturbance of the observed setting, reach over significant spatial scale, excellent spatial resolution, limited-to-no sample preparation, reusability, low cost, and robustness for field use.

Optical spectroscopic techniques, and in particular, Raman spectroscopy, a photon scattering phenomenon involving inelastic photon-molecule collisions, have for some time offered significant potential to satisfy these criteria. The energy transferred in the collision is indicative of the vibrational and rotational energy states of the bonds composing the target molecules, and thus the technique readily facilitates material identification. Further, the frequencies and relative intensities of observed scattered radiation, known as the Raman spectrum, provide insight into the bonds and stoichiometry, respectively, of the target molecule. The broad applicability of Raman therefore offers potential to assess a range of compounds in geoenvironmental settings, all with one device, potentially facilitating analysis of not only primary pollutants but also their daughter compounds, yielding insight into fate and transport processes as well as the effectiveness of remediation strategies in monitoring contexts. In addition, the relatively limited range of energy associated with molecular vibrations manifests in the Raman spectrum as Raman lines of narrow bandwidth, which often facilitates distinction of individual compounds present in mixtures. In very complex systems (as will likely be encountered in the geoenvironment), Raman bands may overlap. However, the Raman signatures of mixtures are a superposition of the signatures of the mixture constituents; and researchers have successfully applied partial least squares (PLS) or principal component analysis (PCA) to quantitatively examine and decouple the signatures of multi-compound solutions (e.g., Cooper et al. 1995; Goetz et al. 1995; Oshima et al. 2006).

Beyond general chemical detection and identification, efficient signal averaging enables quantification even at field-relevant chemical concentrations. Work to date employing compact pulsed laser Raman systems has demonstrated the ability to detect compounds such as nitrate at levels of 2 ppm, aromatic hydrocarbons such as benzene at levels of hundreds of parts per billion, and chlorinated solvents such as TCE down to ~8 ppm (e.g., Sinfield et al. 2010; Sinfield and Monwuba 2016). Opportunities exist to improve the SNR (and thus detection limits) by optimizing sampling time (to a limit), reducing laser power losses, boosting photon collection efficiency at the test point, and to some extent improving detection circuitry. When monitoring geoenvironmental processes, sampling time is typically a readily adjusted variable.

Ultimately, the real promise of Raman for geoenvironmental applications, as with other optical analytical techniques, is the fieldability achieved through recent advances in lasers, fiber optics, and detection electronics. Sensing systems can employ versatile fiber-coupled designs that provide great flexibility in the location and design of test points for a field characterization or monitoring system. In addition, because Raman spectroscopy makes use of a focused light source, target compounds can be assessed through an optically transparent window that affords

protection from the elements while in service in the field, whether below ground or immersed in water, and can also be configured for non-contact assessment.

Together, these advantages enable the analytical specificity, excellent sensitivity, and infield versatility in the study of a broad array of environmentally relevant compounds and could ultimately provide a valuable option for in situ distributed monitoring. Multiple researchers have thus explored means to employ and enhance the technique for geoenvironmental applications (e.g., Bilodeau et al. 1994; USDoE 1999; Rossabi et al. 2000). However, as with other optical analytical methods, the use of the technique has long been hampered by significant factors such as optimizing the sensor-sample interface, managing turbidity for quantitative analysis, limiting fluorescence interference, preventing biofouling (particularly for long-term monitoring), and achieving low cost.

As outlined herein, research over the last several years has systematically addressed each of these factors so that Raman spectroscopy is arguably ready to be revisited as a robust and flexible field measurement technique and may now warrant targeted development effort to improve form factor and fieldability so that it may become a more routinely employed field analysis method.

12.2 Overcoming Impediments to In-field Raman Spectroscopy

The following sections describe recent research progress on each of the heretofore outlined obstacles to effective application of Raman analysis in the field.

12.3 Optimizing the Sensor-Sample Interface

One of the primary obstacles limiting practical use of Raman spectroscopy in the field pertains to the challenge of managing the sensor-sample interface to facilitate repeatable analysis. In an in situ geoenvironmental scenario, Raman analysis is typically performed through an optical window (usually UV quartz or sapphire) that is placed in direct contact with the subsurface medium to be evaluated. Excitation energy and backscattered return are then transmitted and collected, respectively, through the window. Quantitative observations then require development of a correlation between collected signal intensity and the amount of the target analyte present in the sample volume interrogated by the system, under known excitation conditions. In a homogeneous, optically transparent setting, the sample volume can typically be approximated as a hemisphere of an empirically derived radius. However, when the sensor interface is in contact with a soil matrix, as in the context of a saturated soil volume in the geoenvironment, it is critical to account for the changes in the interrogated sample volume resulting from variations in soil-pore geometry as

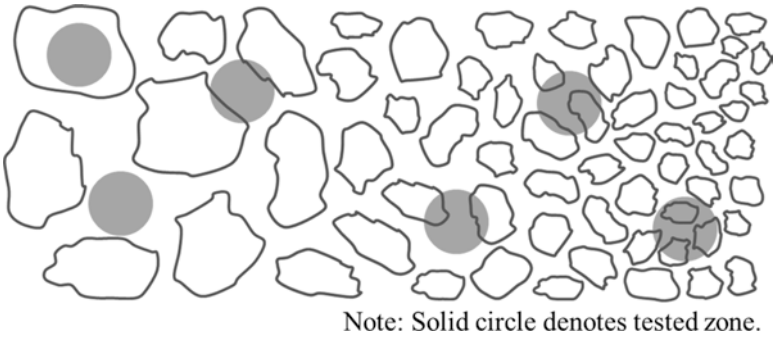

Fig. 12.1 Relationship between soil grain size and interrogated pore fluid volume (Adapted from Sinfield et al. 1999)

shown in Fig. 12.1. Depending on the size of the soil grains and pore space relative to the size of the sensor window (illustrated by the solid circle in Fig. 12.1), the sensor window may be fully occupied by pore fluid, fully occupied by a soil grain, or any fractional mix in between. This, in turn, can drive substantial variability in observed Raman intensities for a given pore fluid chemical concentration.

Work done by Sinfield et al. (1999) demonstrated that the impact of these effects becomes less variable as the dimensions of the soil grains and related pore space are reduced relative to the dimensions of the sensor window. Effectively, increasing the observation area facilitates signal averaging that reduces observation variability by maintaining a more consistent interrogation volume. For most soil systems, this can be achieved quite readily by employing a beam expander to distribute excitation energy over a larger region and utilizing a similar (or the same) optic for light collection. This benefit, however, does come at the expense of reduced signal intensity for any given pore fluid chemical concentration relative to that which would be observed in a purely liquid sample.

12.4 Managing Turbidity to Facilitate Quantitative Analysis

The presence of suspended particles in aqueous systems (i.e., turbidity) in the natural environment represents another obstacle to routine field use of the Raman technique. The particles obscure the sample volume interrogated by optical spectroscopic sensors, not unlike the soil matrix in the soil systems described above, and lead to nonlinear scattering phenomenon which hinder quantitative analysis. To address this issue, recent work has extended the above-outlined understanding of spatial variation of signal intensity in a soil-pore fluid system to develop a means to enable quantitative analysis of liquid samples containing suspended solids (Sinfield and Monwuba 2014). Empirical analysis revealed that turbidity has an equivalent effect on the intensity of analyte and bulk solvent Raman observations in mixtures at analyte concentrations typical in the environment. The correlation of these effects

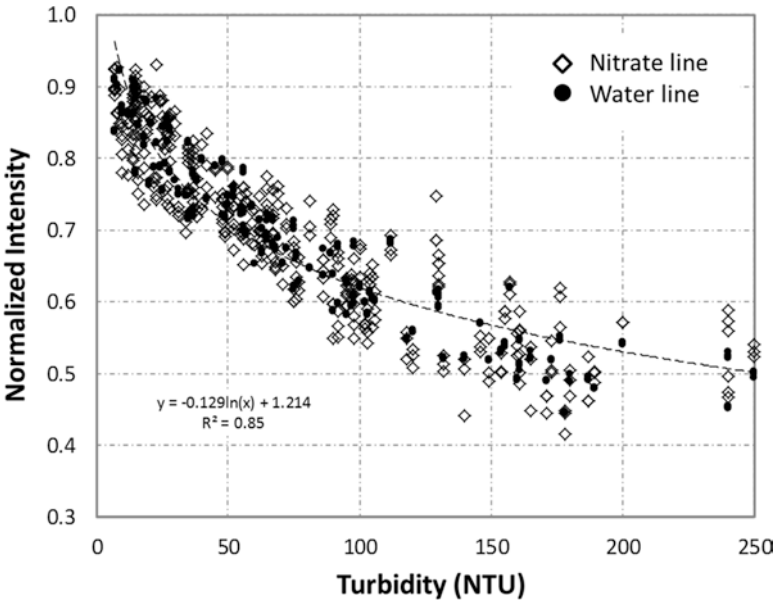

Fig. 12.2 Influence of turbidity on nitrate and water Raman line intensities (Adapted from Sinfield and Monwuba 2014)

provides a means to understand how Raman signal intensities in turbid settings relate to non-turbid settings, as changes in the signal intensity of the bulk solvent (most commonly water) in an in situ situation relative to a non-turbid volume provide a direct indicator of the change in signal intensities that can be anticipated in the same setting for any given analyte. More specifically, as shown for an example of nitrate in water in Fig. 12.2, the signal intensities for representative water and nitrate Raman lines can be predictably related to sample turbidity via a negative logarithmic relationship (note that the exact relationship varies based on soil type). Thus, a correction, based on an in situ observation of the bulk solvent, can be computed to adjust turbid sample measures back to a non-turbid baseline. Interestingly, when turbidity or a turbidity proxy (such as the observation of the solvent Raman signature) is available, ex situ derived calibration curves can be used to correct for turbidity even when turbidity effects on the analyte and solvent differ (e.g., high analyte concentrations or autofluorescence).

12.5 Limiting Fluorescence Interference

An additional challenge frequently encountered when attempting to perform Raman analysis in the geoenvironment stems from the presence of natural and/or anthropogenic fluorophores in the test medium. Natural waters frequently contain humic and fulvic

acids as well as a broad array of organic materials, which tend to emit broadband fluorescence when exposed to optical radiation within their absorption bands (typically in the ultraviolet to visible range) that can often obscure more chemical-specific Raman signatures in in situ settings. In addition, many common contaminants (e.g., aromatic hydrocarbons) also fluoresce. In the past, effort has been made to employ mid-infrared radiation to reduce or eliminate fluorescence or to use any of an array of complex and expensive techniques (such as FT-IR Raman, or shifted-excitation Raman difference spectroscopy) to combat the issue (Seasholtz et al. 1989; Cooper et al. 1995). However, these techniques can be very complex and expensive, and thus not amenable to field applications. In addition, due to the well-established $1/\lambda^4$ dependence of the Raman return, the Raman signal obtained through these methods may be significantly weaker than that attainable at shorter wavelengths, limiting detection sensitivity. Others have attempted to pursue the deep UV to avoid fluorescence altogether (Shoute et al. 2002). While an attractive future possibility, UV lasers remain far less economical than alternatives. With the above factors in mind, researchers at Purdue University developed a Raman system that employs an alternative method to limit the adverse effects of fluorescence (Sinfield and Colic 2010). Because Raman is a scattering phenomenon, and fluorescence is an emission phenomenon, Raman scattering can only occur when energy is incident, and there is a brief time difference between essentially instantaneous Raman scattering and the absorption and reemission of energy that must occur for fluorescence. This allows for the possibility to separate Raman and fluorescence in the time domain.

The Purdue time-resolved Raman spectroscopy (TRRS) system makes use of pulsed Q-switched diode laser and time-gated signal acquisition to provide a cost-effective means to obtain both Raman and fluorescence signatures, even in complex environments (Sinfield et al. 2010). With this technology, it is possible to examine the optical return from a sample as a function of time as shown in Fig. 12.3, which depicts the Raman return from benzene in an aqueous solution containing the strong fluorophore rhodamine 6G at various counting times. Here it can be seen that after an initial return of noise, the Raman peak is evident at early times and then becomes obscured in the broad fluorescence emission as time increases. Studies on compounds like gasoline (Fig. 12.4) illustrate that significant improvements in target analyte signal-to-noise ratio, and thus sensitivity, can be achieved with this technique even in complex mixtures.

12.6 Preventing Biofouling

Even once factors such as the sample interface, correction for the presence of turbidity, and fluorescence interference are addressed, the effectiveness of an optical sensing system deployed in the field can be foiled by physical interference from biotic materials – a phenomenon referred to as biofouling. Although numerous techniques are routinely employed to clean (e.g., mechanical intervention) (Manov et al. 2004; Bixler and Bhushan 2012) and/or protect surfaces (e.g., antifouling films, surface treatments, or biocides or biodispersants) (Manov et al. 2004; Yebra et al. 2004), one unique situation remains poorly addressed – that is, the biofouling of scientific instrumentation used to

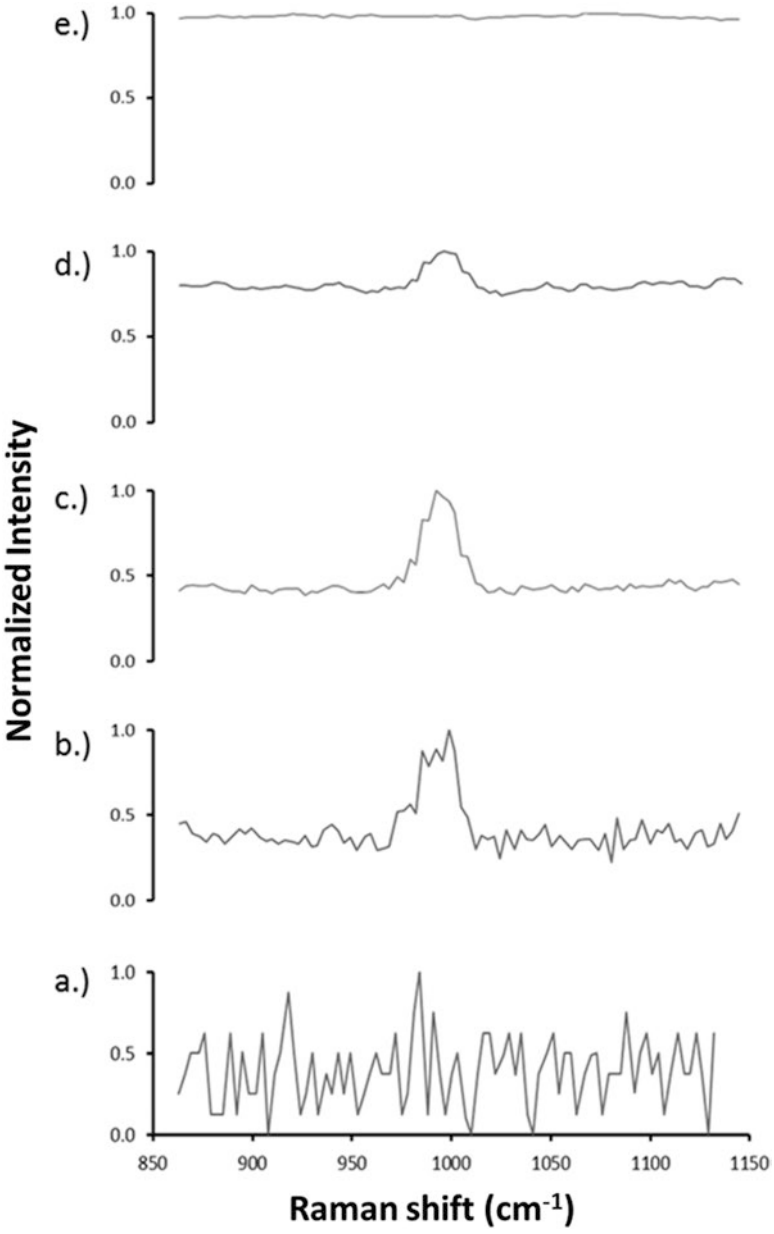

Fig. 12.3 Neat benzene Raman peak in the presence of 1×10^{-4} M rhodamine 6G as a function of counting time: (**a**) 0.1 ns, (**b**) 0.4 ns, (**c**) 0.7 ns, (**d**) 2.0 ns, and (**e**) 8.5 ns

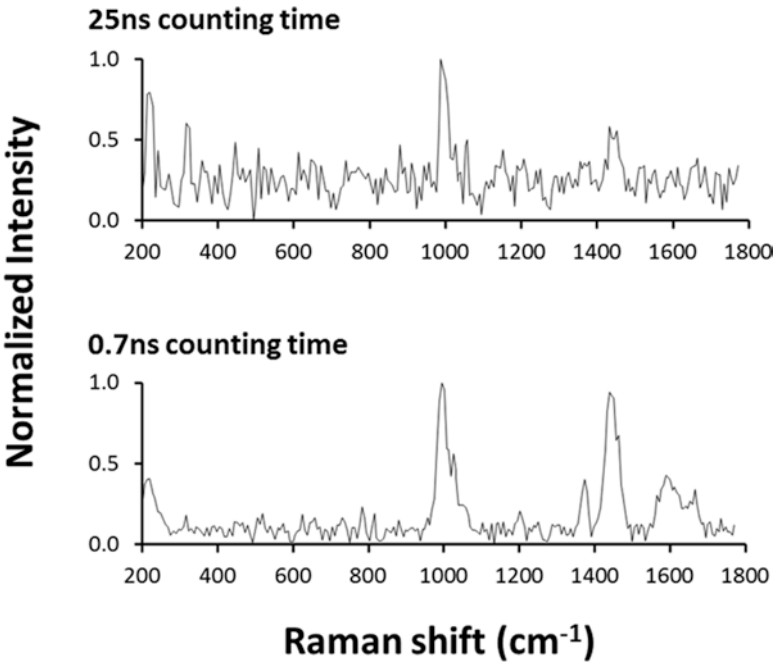

Fig. 12.4 TRRS Raman signature of gasoline (Adapted from Sinfield et al. 2010)

study natural systems, particularly when the instrumentation relies upon optical sensors, which inevitably require a window-like interface between the equipment and the environment. In this situation, mechanical action can be impractical due to access challenges, and/or the protective measures themselves can be problematic as the use of antifouling films and surface treatments can interfere with the optical path required for effective measurement and introduce chemicals, such as biocides or biodispersants, which mask or interfere with the natural environment being studied (Cloete et al. 1998). One approach that shows potential in this situation involves the use of ultraviolet light to limit or prevent the buildup of biologic film on a device's optical window. The use of UV radiation to prevent biofouling has been explored in the past at a cursory level by several researchers (e.g., Soini et al. 2002). Recent experiments at Purdue conducted on colonies of chlorella, single-celled green algae, have demonstrated that low-cost ultraviolet light sources can be employed to terminate existing algae and prevent expansion/spreading of the microorganism. Chlorella is also notably resistant to UV exposure (Pulich 1974), thus providing a broadly applicable indicator of UV treatment effectiveness. Figure 12.5 illustrates the effectiveness of this technique. The top row of the picture presents two petri dishes, each "seeded" with a controlled volume of a mixture of algal growth media and live algae and exposed to nurturing light of an equivalent intensity and duration. The bottom row of images presents the same two petri dishes after 2 days, in a scenario in which the dish on the left was continuously exposed to low levels of ultraviolet radiation and the dish on the right was not. It is clear from these images that the algae on the left

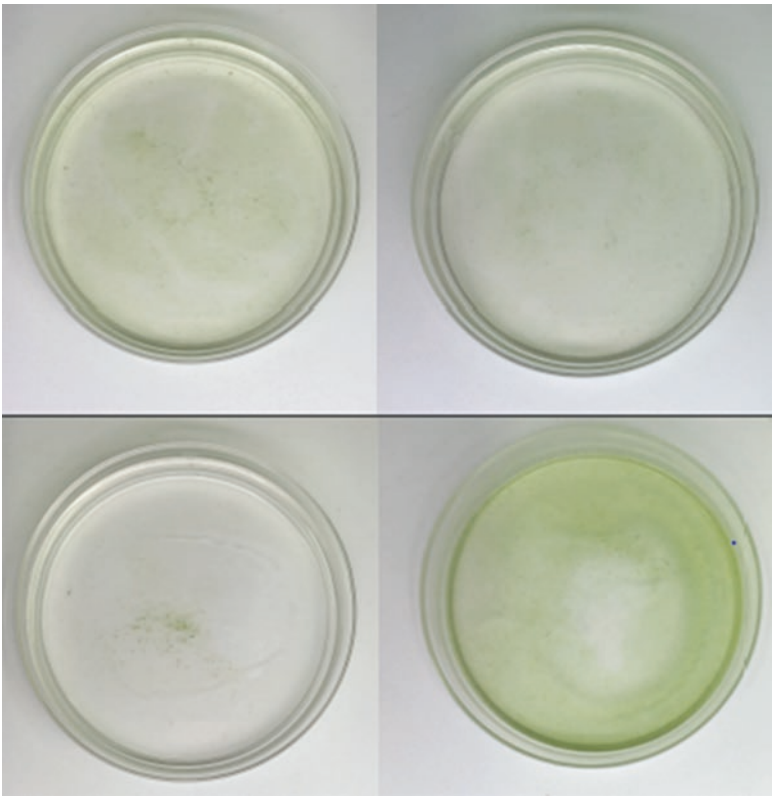

Fig. 12.5 Illustration of UV effectiveness in limiting biofouling (Image courtesy V. Sinfield)

are depleted and did not expand, while those on the right flourished, expanding both in number and areal extent. While of course not a representative of all biofouling microorganisms, these results highlight the very practical potential to employ basic UV light sources to provide long-term protection of in situ Raman sensor installations.

12.7 Achieving Low Cost

Despite the versatility of the Raman technique, and the potential to overcome the above-outlined technical hurdles, cost has also historically limited broad adoption and routine use of the method. Commercially produced Raman spectroscopic instruments have traditionally fallen into two main categories of hardware. Benchtop apparatus typically employed in research settings that occupy 1–2 m^3 of space, offer rapid test results, and cost US$200–300 k, and handheld, rapid detection systems, primarily employed for chemical identification in high-concentration settings at a cost of US$10–20 k. Achieving high sensitivity at low cost however has been elusive.

To make progress in this area, the Purdue Civil Engineering spectroscopy laboratory explored counterintuitive trade-offs in performance. Sensitivity (and cost) is primarily a function of excitation power, excitation wavelength, and detector configuration (speed, resolution). Traditional systems employ high average power continuous wave (CW) lasers, typically in the infrared region of the electromagnetic spectrum, and detect Raman scattered return using a long diffraction length monochromator and a liquid nitrogen-cooled full spectrum continuously integrated charge-coupled device. While sensitive and fast, this type of system is also very expensive (and fails to counter the challenge posed by optical fluorescence). In contrast, a new TRRS system format was devised in the Purdue Civil Engineering spectroscopy laboratory which makes use of a low average power, pulsed laser source in the visible region of the electromagnetic spectrum, a compact monochromator, and a thermoelectrically cooled photomultiplier tube (PMT) operated in photon counting mode for scanned monochromatic detection. The new system trades off resolution and speed for increased sensitivity, a reduced form factor, applicability to fluorescing media, and significantly reduced cost as shown in Table 12.1.

Table 12.1 Comparison of traditional and Purdue TRRS system components

	Laser source	Sample	Mono-chromator	Detector	ACQ	Attributes
Traditional	High avg. power	Non-fluorescing media	High resolution	Rapid full spectrum (CCD)	Continuously integrated	*Give up*
	CW	Media where NIR/ FT-IR overcome fluorescence	Full spectrum/ FFT	LN cooled	FFT de-convolution	Size
	N/M IR					Cost
						Media
						Get
						Resolution
						Speed
TRRS	Low avg. power	Non-fluorescing and fluorescing media	Low resolution	Slow mono chromatic detection (PMT)	Time resolved photon counting	*Give up*
	Pulsed		Scanning spectral coverage	TE cooled	Direct output	Resolution
	VIS					Speed
						Get
						Size/ portability
						Media
						Affordability
						VIS enhanced signal

Adapted from Sinfield et al. 2010

By operating in the visible range (in this case 532 nm), the new Raman system offers a 16- to 4.7-fold advantage in Raman intensity over traditional infrared systems (1064 and 785 nm) due to the $1/\lambda^4$ influence on Raman return. This improved return signal strength could potentially reveal features of low concentration constituents not evident in traditional infrared analyses. It is important to note that deep ultraviolet sources could provide preferable signal intensity and further reduce or eliminate the challenge of fluorescence (and are under study). However, sub-nanosecond pulsed lasers below 532 nm are not yet commercially available at comparable costs. In addition, a 532 nm source permits resolution of Raman peaks separated by as little as 17 cm^{-1} using low-cost 0.5 nm resolution spectrometers (vs ~70 cm^{-1} for deep UV), which provides an advantage that could yield deeper compositional insight into complex samples at low cost.

Accounting for custom and commercially available elements in the new design, the prototype of the new system was fabricated as a cost nearly an order of magnitude less expensive than comparable traditional instruments.

12.8 Concluding Remarks

The results of the work outlined above draw attention to the fundamental impact of environmental factors on Raman spectroscopic observations as well as specific and pragmatic advances which enable these adverse influences to be overcome. Evolution of the design of the TRRS system enabled through this work has facilitated progress toward optical spectroscopic testing and monitoring systems that can be deployed at low cost and yet provide specific analyses of a broad range of chemical compounds in nearly real time in natural settings. It is believed that the developments outlined herein have applicability in a broad range of fields involving analyses of materials in complex, turbid, and/or fluorescence-prone settings including water quality monitoring, precision agriculture, petroleum exploration, pharmaceutical quality control, analyses of biological systems, and assessment of homeland security threats and environmental disaster impact.

References

Bilodeau TG, Ewing KJ, Kraucunas IP, Jaganathan J, Nau GM, Aggarwal ID, Reich FR, Mech SJ (1994) Fiber optic Raman probe detection of chlorinated hydrocarbons in standard soils. Proc SPIE Int Soc Opt Eng 2068:258–270

Bixler GD, Bhushan B (2012) Biofouling: lessons from nature. Philos Trans R Soc Lond A Math Phys Eng Sci 370(1967):2381–2417

Cloete TE, Jacobs L, Brözel VS (1998) The chemical control of biofouling in industrial water systems. Biodegradation 9(1):23–37

Cooper JB, Flecher PE, Vess TM, Welch WT (1995) Remote fiber-optic Raman analysis of xylene isomers in mock petroleum fuels using a low-cost dispersive instrument and partial least squares regression analysis. Appl Spectrosc 49(5):586–592

Goetz MJ Jr, Cote GL, Erckens R, March W, Motamedi M (1995) Application of a multivariate technique to Raman spectra for quantification of body chemicals. IEEE Trans Biomed Eng 42(7): 728–731

Manov DV, Chang GC, Dickey TD (2004) Methods for reducing biofouling of moored optical sensors. J Atmos Ocean Technol 21(6):958–968

Oshima Y, Komachi Y, Furihata C, Tashiro H, Sato H (2006) Fluorescence-suppressed Raman technique for quantitative analysis of protein solution using a micro-Raman probe, the shifted excitation method, and partial least squares regression analysis. Appl Spectrosc 60(9):964–970

Pulich WM (1974) Resistance to high oxygen tension, streptonigrin, and ultraviolet irradiation in the green alga Chlorella sorokiniana strain ORS. J Cell Biol 62(3):904–907

Rossabi J, Riha BD, Haas JW, Eddy-Dilek CA, Kreeger AGL, Carrabba M, Hyde WK, Bello J (2000) Field tests of a DNAPL characterization system using cone penetrometer-based Raman spectroscopy. Ground Water Monit Remediat 20(4):72–81

Seasholtz MB, Archibald DD, Lorber A, Kowalski BR (1989) Quantitative analysis of liquid fuel mixtures with the use of Fourier transform near-IR Raman spectroscopy. Appl Spectrosc 43(6):1067–1072

Shoute LCT, Schmidt KJ, Hall RH, Webb MA, Rifai S, Abel P, Arboleda PH, Savage A, Bulmer JT, Loppnow GR (2002) UV Raman spectroscopy of oilsands-derived bitumen and commercial petroleum products. Appl Spectrosc 56(10):1308–1313

Sinfield JV, Colic O (2010) US Patent 8,325,337 B2 “Time Resolved Raman spectroscopy”. Washington, DC, USA

Sinfield JV, Monwuba CK (2014) Assessment and correction of turbidity effects on Raman observations of chemicals in aqueous solutions. Appl Spectrosc 68(12):1381–1392

Sinfield JV, Monwuba CK (2016) Inferential monitoring of chlorinated solvents through Raman spectroscopic observation of the vibrational modes of water. Talanta 148:7–16

Sinfield JV, Germaine JT, Hemond HF (1999) Effects of soils on laser induced fluorescence of BTX contaminated pore waters. J Geotech Geoenviron Eng ASCE 125(12):1072–1077

Sinfield JV, Colic O, Fagerman D, Monwuba CK (2010) A low cost time-resolved spectroscopic sensing system enabling fluorescence rejection. Appl Spectrosc 64(2):201–210

Soini SM, Koskinen KT, Vilenius MJ, Puhakka JA (2002) Potential of microbial growth control in water hydraulic systems by UV-irradiation and filtration. J Chem Technol Biotechnol 77(8):903–909

USDoE (U.S. Department of Energy) (1999) Raman Probe. DOE/EM-0442, July

Yebra DM, Kiil S, Dam-Johansen K (2004) Antifouling technology – past, present and future steps towards efficient and environmentally friendly antifouling coatings. Prog Org Coat 50(2):75–104

Chapter 13
Sustainable Design of Monopile-Supported Offshore Wind Turbine Considering Climate Change

Swagata Bisoi and Sumanta Haldar

Abstract Global warming may change the wind and wave pattern, thus altering the dynamic behavior of offshore wind turbine (OWT). This study examines the impact of climate change on the sustainable design and wind energy production of monopile-supported OWT in soft clay incorporating future wind speed, wave height, and period. Two offshore locations, namely, at east and west coasts in India, are selected. For both the locations, wind speed, wave height, and wave period are obtained from the buoy deployed by the Indian National Centre for Ocean Information Services (INCOIS) from 1998–2006. Statistical downscaling method is used to predict the future wind speed, wave height, and wave period due to climate change for the period of 2006–2040. The observed data is compared with the downscaled data from the National Centers for Environmental Prediction (NCEP) reanalysis data to calibrate the statistical downscaling model. The general circulation model (GCM) predictor variables for various global carbon dioxide emission scenarios are used for future climate change. This study shows that the modification in design of OWT is required due to change in dynamic behavior of OWT considering future climate.

Keywords Climate change • Monopile • Offshore wind turbine • Soil-structure interaction • Statistical downscaling method

13.1 Introduction

Design of monopile-supported offshore wind turbine (OWT) primarily requires the estimation of the fundamental frequency to avoid resonance due to rotor frequency (1P), blade-passing frequency (3P), and wave frequency (Bhattacharya 2014). Serviceability limit state (SLS) and fatigue limit state (FLS) criteria are also needed

S. Bisoi (✉) • S. Haldar
Department of Civil Engineering, School of Infrastructure, Indian Institute of Technology Bhubaneswar, Bhubaneswar 751013, India
e-mail: sb17@iitbbs.ac.in; sumanta@iitbbs.ac.in

G.L. Sivakumar Babu et al. (eds.), *Geoenvironmental Practices and Sustainability*, Developments in Geotechnical Engineering,
DOI 10.1007/978-981-10-4077-1_13

to be checked for safe design (Bhattacharya 2014). Fluctuating wind speed and wave height are the primary cause to change in dynamic behavior of monopile-supported OWT which affects the wind energy generation. Considering the past 3 years (1998–2000) observed data, Deepthi and Deo (2010) forecasted wind speed for the period 2009–2100 at offshore location near west coast India. They showed that 100 years return period wind speed is going to be increased by about 40–70% due to climate change at the Indian offshore locations using GCM-A2 scenario. Kulkarni et al. (2013) also projected, due to climate change, about 8% increase in wind speed at west and east coasts of India. Wave height and wave period also change due to fluctuating wind speed which may affect the performance and energy production of OWT (Grabemann and Weisse 2008). Radhika et al. (2013) reported about 8–44% increase in significant wave height observed in east and west coasts of India because of future climate accounting for A1B, A2, and B1 emission scenarios. Hence, wind and wave loading on offshore structure may alter significantly due to the effect of climate change (Harrison and Wallace 2005). Sailor et al. (2008) reported about 40% reductions in future wind power production than the present scenario. Previous studies examined impact of climate change on future wind and wave climate; however, possible impact on future design of OWT, when such changes would occur with respect to those from the present loading condition, was not studied.

In this study, effect of climate change on 50 years return period wind speed, wave height, and wave period is assessed for safe and sustainable OWT along the west and east coasts of India. The past wind speed, wave height, and period data are collected from INCOIS for the period of 1998–2006. The statistical downscaling model is calibrated with NCEP reanalysis data of wind speed, wave height, and wave period. The future values are downscaled considering GCM model considering A1B, A2, and B1 emission scenarios. The wind and wave loads are evaluated based on 50 years return period of wind speed and wave height and using Gumbel and generalized extreme value (GEV) distributions for various scenarios. Monopile foundation is found to be cost-effective at shallow water depth; hence, a 5 MW OWT embedded in clay is considered, and SLS criterion is evaluated due to the impact of climate change. The OWT structure is modeled as Euler-Bernoulli beam, and soil resistance is modeled as API (2011)-based cyclic *p-y* curve.

13.2 Study Region and Data Collection

The buoy data of daily maximum wind speed and corresponding wave height and wave period are collected from INCOIS server for the period of 1998–2006 for two offshore locations in India: (1) near Mormugao which is off Goa along the west coast denoted as SW03 and (2) near to Mullakadu which is off Tamilnadu along the east coast denoted as SW05. The latitude and longitude of the selected regions are 15.39°N and 73.76°E, respectively, for SW03 and 8.7°N and 78.23°E, respectively, for SW05. The SW03 and SW05 locations are 28 km and 13 km away from the shore, respectively, and the water depth is assumed to be 20 m.

NCEP reanalysis predictor variables considered as high-resolution data compared to GCM data are used to calibrate the downscaling model using the observed data as input. Five predictor variables, namely, zonal wind speed, meridional wind speed, air temperature at 2 m high, specific humidity at 2 m high, and sea level pressure, are obtained at both locations from NCEP for the period of 1998–2006. The predictor variables are downloaded for an area corresponding to 25 grid points distributed as 5 × 5 grids (1.905° and 1.875° interval for latitude and longitude, respectively) around the selected locations to obtain more realistic estimate of the nearest climate. The extent of the latitudes and longitudes is 10.48°–18.09° N and 69.38°–76.88°E, respectively, for SW03 and 6.67°–14.29° N and 73.13°–80.63°E, respectively, for SW05. The NCEP data are downloaded for 25 grid points, and weighted average method is used to estimate the predictor variables at the selected location from the adjacent grid points (Wilby et al. 2004).

GCM predictors of various scenarios such as A1B, A2, and B1 are considered for analysis. The global carbon dioxide emossions in A1B, A2 and B1 scenario are about 500 ppm, 500 ppm and 470 ppm respectively by year 2050, whereas, 720 ppm, 850 ppm and 550 ppm by year 2100 according to Canadian Centre for Climate Modelling and Analysis (http://www.cccma.ec.gc.ca/data/cgcm3/cgcm3_forcing.shtml). Predictors are downloaded for all the scenarios. The grid size of GCM predictors is 2.81° × 2.81° which is re-gridded to match with the NCEP data (1.875° × 1.905°) using bilinear interpolation method. After re-gridding, weighted average method is used to estimate the data for selected locations for the period of 2001–2100. Bias correction is carried out for all predictor variables for the predefined baseline period of 1998–2014 and 2001–2014 for NCEP and GCM predictors, respectively.

13.3 Methodology

13.3.1 Prediction of Future Wind and Wave Climate

Statistical downscaling model (*SDSM*) proposed by Wilby and Dawson (2007) is used for predicting future wave and wind climate. The *SDSM* model is used to correlate the predictors and predictands (e.g., wind speed). The stochastic weather generator and transfer function method are adopted for downscaling using the first-order Markov chain approach (Wilby et al. 2004) for future wind speed, wave height, and wave period. The bias-corrected data are used further to validate the model using observed data and downscaled data derived from NCEP. Wind speed and wave height corresponding to 50 years return period at 95% confidence level are obtained considering Gumbel and GEV distributions using GCM predictors. Various design guidelines suggest evaluation of safety of OWT corresponding to 50 years return period loads (DNV-OS-J101 2010). The 50 years return period wind speed, wave height, and wave period are predicted using Gumbel and GEV distributions for past climate to compare the effect of climate change. Accuracy of return period wind

Table 13.1 Performance of statistical downscaling model

Location	Statistics	Wind speed (m/s)	Wave height (m)	Wave period (s)
SW03	Correlation coefficient	0.6	0.87	0.82
	Mean absolute error	1.7	0.24	0.47
SW05	Correlation coefficient	0.65	0.73	0.71
	Mean absolute error	1.7	0.24	0.99

speed and wave height may be improved considering longer-duration past dataset, which is the future scope of study.

Cross validation method is adopted to check the credibility of the downscaled model. Downscaling model is driven by NCEP reanalysis predictors with observed data for the period of 1998–2006 for both locations. Table 13.1 shows the correlation coefficient and mean absolute error of wind speed, wave height, and wave period between observed and predicted data. It is observed that the correlation coefficients of wind speed are 0.6 and 0.65 for SW03 and SW05, respectively, compared to wave height and wave period; however, it can be regarded as reasonably good prediction for simulating the natural phenomena (Kulkarni et al. 2014).

13.3.2 Finite Element Model

The monopile-supported OWT is assumed to be embedded in a uniform deposit of marine soft clay which is mostly found at Indian offshore location (Basack and Purkayastha 2009). The monopile and tower are modeled as an Euler-Bernoulli beam which is discretized into beam elements. A uniform cross section for the monopile (i.e., sea level to monopile tip) and a tapered section of the tower (above MSL) are assumed. The diameter of tower at hub height is considered as half of the tower base diameter. A uniform thickness of tower and monopile is considered for simplicity. The RNA mass is assumed as a point mass attached on the top of the tower (M_{RNA}) with a rotary inertia (J_{RNA}) (cf. Fig. 13.1). The lateral soil resistance is modeled by a series of soil springs following API (2011)-based nonlinear *p*-*y* curves. API-based cyclic *p*-*y* curves are evaluated for small-diameter flexible pile and low-load cycles (DNV-OS-J101 2010). Despite of limitation it is widely used for the design of OWT in the offshore industries and also recommended in several design guidelines. More appropriate model for clay considering stiffness degradation effect may be addressed in the future study. Monopile foundation is assumed to be resting on rigid base; hence, a roller support is introduced at the base. The *p*-*y* curves are generated based on three parameters: (1) undrained shear strength of soil (s_u), (2) strain corresponding to one-half the maximum stress on laboratory undrained compression tests of undisturbed soil (ε_c), and (3) an empirical dimensionless constant (J). Ashour et al. (1998) graphically showed a relationship between ε_c and s_u. Based on this, an average $\varepsilon_c \varepsilon_c$ is estimated for the given value of s_u. A constant value of $J = 0.5$ is used for all cases.

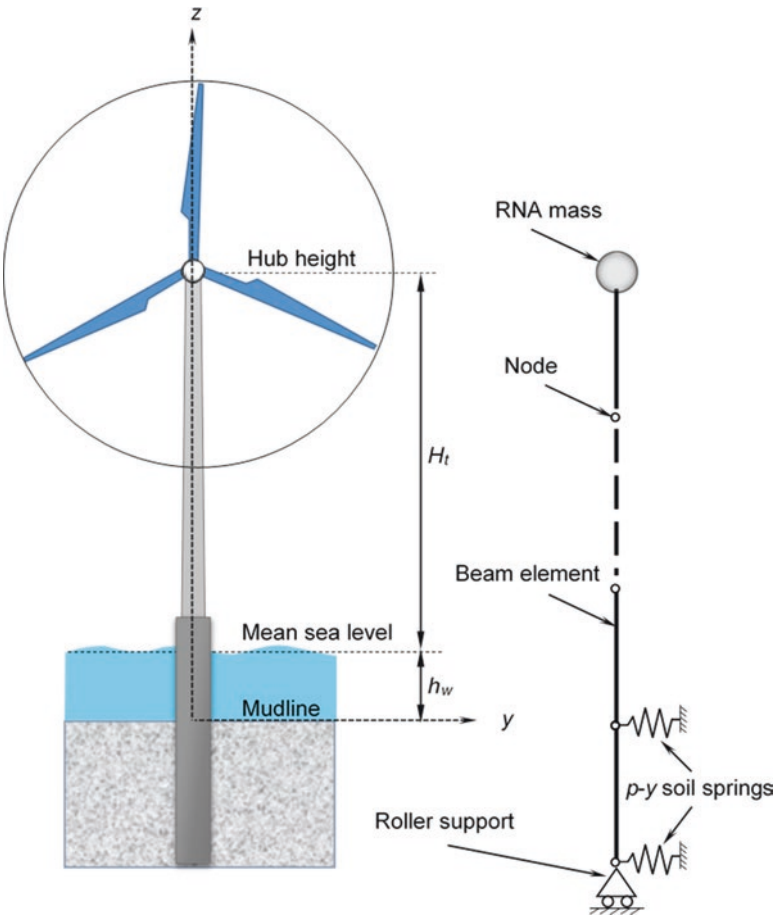

Fig. 13.1 Schematic diagram of finite element model of OWT system in clay

Overall 12% damping is considered in this study based on the literature (GL 2005). Dynamic analysis is carried out in time domain using finite element method in COMSOL Multiphysics® (COMSOL 2013). Numerical model is validated comparing the fundamental frequency of the system with the measured frequency of the installed wind turbine tower-monopile-soil system (Bisoi and Haldar 2014).

13.4 Estimation of Wind and Wave Loads

The total wind load acting on the OWT structure is divided into two components, namely, the load acting on the turbine blades and the load acting on the turbine tower. The load acting on the turbine blades (F_b) is estimated as (Jara 2006)

$$F_{\mathrm{b}} = 0.5\rho_a \pi R_T^2 V_{hub}^2 C_T\left(\lambda_s\right) \tag{13.1}$$

where F_{b} is the wind load acting on the hub in N, V_{hub} is the wind speed at the hub height in m/s, R_T is the rotor radius in m, ρ_a is the air density which equals to 1.23 km/m^3 at 15 °C at 1 atm, and $C_T(\lambda_s)$ is the thrust coefficient which is a function of the tip speed ratio ($\lambda_s = V_r R_T/V_{hub}$, V_r is the rotor speed in rad/s). The frequency of wind load is same as the rotor frequency (f_r), and it is applied as lateral point load at RNA, which is $F_{\mathrm{b}}\sin(2\pi f_r t)$, where t is the dynamic time. Wind load acting on turbine tower is estimated based on wind load profile as (ABS 1997; DNV-RP-C205 2010)

$$F_{\mathrm{tower}}\left(z\right) = 0.61\left(U_{10}/\ln\left(10/z_0\right)\cdot\ln\left(z/z_0\right)\right)^2 C_s D\left(z\right) \tag{13.2}$$

where F_{tower} is the wind load acting on the tower in N/m, C_s is the shape coefficient (=0.5), $D(z)$ is the tower diameter at tower height z from the mean sea level (MSL), z_0 is a terrain roughness parameter which is equal to 0.0001 m in the open sea without waves, and U_{10} is the 10 min average wind speed at 10 m height from MSL. Load on tower obstructed due to blade rotation (3P loading) ($F_{1\ \mathrm{tower}}\sin(6\pi f_r t)$) is estimated by integrating Eq. (13.2) up to the blade length and applied as lateral point load at the center of gravity. Load on tower uncovered by the blade is applied as static equivalent point lateral load ($F_{2\mathrm{tower}}$) at the center of gravity.

The wave force (F_{wave}) on the OWT is estimated using Morison's equation:

$$\begin{aligned} F_{\mathrm{wave}}\left(t\right) = F_M\left(t\right) + F_D\left(t\right) = C_M \rho \pi D^2/4 \int_{\eta(t)}^{-d_w} \ddot{u}\left(t\right) dz_1 \\ + C_D \rho D/2 \int_{\eta(t)}^{-d_w} \dot{u}\left(t\right)\left|\dot{u}\left(t\right)\right| dz_1 \end{aligned} \tag{13.3}$$

where F_M = inertia force, F_D = drag force, d_w = water depth in m, C_D = drag coefficient, C_M = mass coefficient, ρ = mass density of the sea water (1030 kg/m^3), D = diameter of the tower and monopile in m, $\dot{u}$ = wave-induced velocity of water, $\ddot{u}$ = wave-induced acceleration of water which are given in DNV-OS-J101 (2010), and $\eta(t)$ = surface wave profile = 0.5 $h_w \cos(\omega_w t)$. Wave load is applied as lateral point load at MSL with the wave frequency (ω_w).

Owing to nonavailability of information pertains to wind speed; annual maximum wind speed is assumed as 10 min average wind speed at 10 m height (U_{10}) from daily wind speed data for the year 2006–2040. Wind speed profile along the tower is derived using DNV-RP-C205 (2010). Wind speed at hub height is derived from the wind speed profile, and wind load at hub height is estimated from Eq. (13.1). Loads on tower ($F_{1\mathrm{tower}}$ and $F_{2\mathrm{tower}}$) are estimated by integrating Eq. (13.2) over the tower height. Wave load is calculated using Eq. (13.3) from the annual wave height and

wave period corresponding to annual maximum wind speed data. Loads are also estimated for the past climate, which is estimated based on the annual maximum wind speed and corresponding wave height and wave period for the period of 1998–2006.

13.5 Modeling Parameters

In this study, a 5 MW OWT is considered, and the parameters are obtained from literature (4C-Offshore 2013). Tower height (H_t) = 80 m embedded monopile length (L_p) = 55 m, which is installed in soft clay (s_u = 25 kPa, ε_c = 0.01) at west coast and east coast offshore locations of India. Diameter and thickness of tower and monopile, D = 8 m and t_w = 0.043 m, respectively. The water depth is considered as 20 m. The rotor frequency is considered as 0.25 Hz for the analysis. A typical value of RNA mass (M_{RNA}) and rotor diameter (D_r) is considered as 350 ton and 126 m, respectively. Young's modulus of the tower and monopile is assumed as 2.1×10^5 MPa, and mass moment of inertia (J_{RNA}) is considered as 4×10^7 kg-m^2.

13.6 Results and Discussion

13.6.1 Effect of Climate Change on Future Wind and Wave Climate

The wind speed and wave height based on 50 years return period for A1B, A2, and B1 scenarios are assessed in order to examine the effect of climate change on the design of OWT. The wind speed and wave height are derived for 50 years return period considering Gumbel and GEV distributions. No design guidelines outlined on 50 years return wave period; hence, average wave period is taken from the time series of downscaled wave period based on projected climate (2006–2040) and past climate (1998–2006) for both locations. Figures 13.2 and 13.3 present 50 years return period wind speed and wave height for all the three scenarios and both locations. Figure 13.2 shows that, at SW03, wind speed is increased by about 19%, 14%, and 20% for the A1B, A2, and B1 scenarios, respectively, for GEV distribution due to climate change. However, wind speed is increased by about 17–26% for Gumbel distribution and 83–98% for GEV distribution considering future climate variation as compared to past climate (Fig. 13.2a). Wind speed at SW05 is decreased by about 2–7% for A2 and B1 scenarios considering Gumbel distribution, respectively, and 2–19% for GEV distribution, respectively, (Fig. 13.2b). However, wind speed is increased marginally for A1B scenario for Gumbel and GEV distributions. It is observed that GEV distribution predicts higher 50 years return period wind speed than that of Gumbel distribution for both locations.

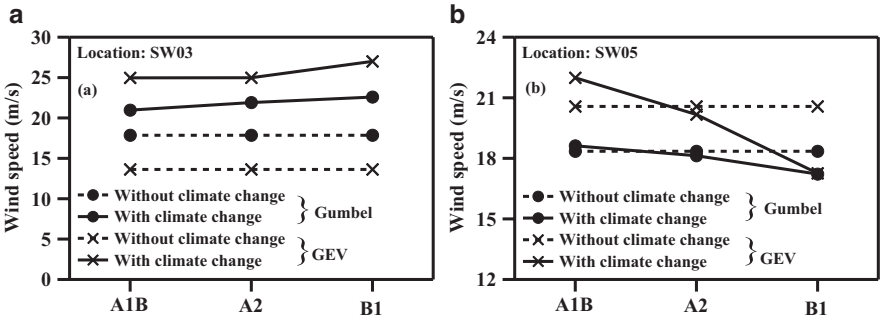

Fig. 13.2 The wind speed variation based on 50 years return period for the locations of (**a**) SW03 and (**b**) SW05 for Gumbel distribution and GEV distribution

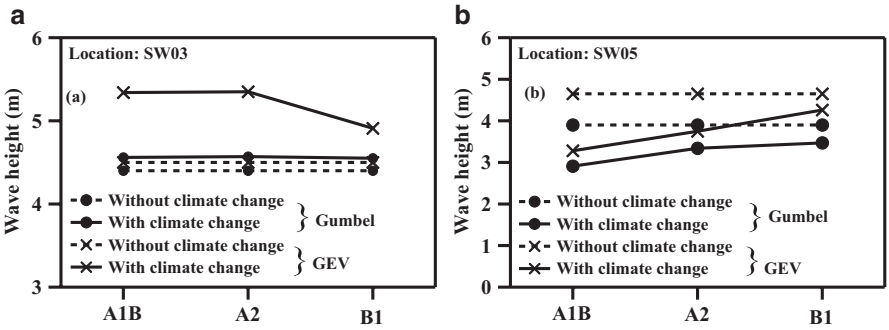

Fig. 13.3 Fifty years of return period wave height for the locations (**a**) SW03 and (**b**) SW05 using Gumbel and GEV distribution

Figure 13.3a shows the variation of wave height for 50 years return period along the west coast of Indian offshore location (i.e., SW03). It is observed that wave height is increased at SW03 and decreased at SW05 considering Gumbel and GEV distributions in future climate as compared to past climate. The wave height is increased by about 4–19% for Gumbel and GEV distribution, respectively. Whereas, the wave height is decreased up to 14–25% for Gumbel distribution and 15–28% considering GEV distribution at SW05 (Fig. 13.3b).

13.6.2 Effect of Climate Change on OWT Responses

The impact of climate change on the responses of OWT structure is assessed based on wind and wave loads. Loads are derived from 50 years return period wind speed, wave height, and average wave period considering Gumbel distribution. Maximum rotation at tower top ($\theta_{\text{Tower,max}}$) and monopile at mudline ($\theta_{\text{Pile,max}}$) are evaluated

Table 13.2 Summary of loads and responses of OWT at SW03

Parameter	Without climate change effect	With climate change effect		
		A1B	A2	B1
U_{10} (m/s)	17.86	20.97	21.91	22.59
F_b (N)	1.67×10^6	2.01×10^6	2.16×10^6	2.22×10^6
$F_{1\text{tower}}$ (N)	6.61×10^4	9.12×10^4	9.96×10^4	1.06×10^5
$F_{2\text{tower}}$ (N)	1.77×10^4	2.44×10^4	2.66×10^4	2.83×10^4
h_w (m)	4.4	4.56	4.57	4.55
T_w (s)	5.98	6.16	5.36	5.36
F_{wave} (N)	1.71×10^6	1.79×10^6	1.96×10^6	1.95×10^6
$\theta_{\text{Tower,max}}$ (deg)	1.82	2.29	2.3	2.38
$\theta_{\text{Pile,max}}$ (deg)	0.46	0.59	0.61	0.64

Table 13.3 Summary of loads and responses of OWT at SW05

Parameter	Without climate change effect	With climate change effect		
		A1B	A2	B1
U_{10} (m/s)	18.35	18.62	18.13	17.22
F_b (N)	1.71×10^6	1.73×10^6	1.69×10^6	1.62×10^6
$F_{1\text{tower}}$ (N)	6.98×10^4	7.19×10^4	6.82×10^4	6.15×10^4
$F_{2\text{tower}}$ (N)	1.87×10^4	1.92×10^4	1.82×10^4	1.64×10^4
h_w (m)	3.9	2.91	3.34	3.47
T_w (s)	5.57	7.62	7.72	7.59
F_{wave} (N)	6.25×10^5	1.01×10^6	5.45×10^5	1.56×10^6
$\theta_{\text{Tower,max}}$ (deg)	1.71	1.71	1.67	1.57
$\theta_{\text{Pile,max}}$ (deg)	0.43	0.44	0.41	0.4

considering climate change and past climate for three different scenarios (Tables 13.2 and 13.3). The allowable rotation of monopile at mudline is 0.5° (DNV-OS-J101 2010). It is observed that $\theta_{\text{Tower,max}}$ is increased for the location SW03 by about 25–30% (Table 13.2) and decreased by about 2–8% for SW05 (Table 13.3) due to climate change. Similar observation is observed for monopile rotation at mudline. For example, $\theta_{\text{Pile,max}}$ is increased by about 28–40% at SW03, whereas it is decreased by about 5–7% at SW05 when climate change is taken into account. Variation in $\theta_{\text{Tower,max}}$ and $\theta_{\text{Pile,max}}$ is marginal for three different scenarios since variation of wind and wave loads is found to be marginal.

Wind energy production in terms of available wind power and safety margin for $\theta_{\text{Pile,max}}$ is evaluated for past and future climate variation. The available wind power per unit area of flow (W/m^2) is estimated as $0.5\,\rho V^3$, where ρ is air density (kg/m^3) and V is the hub height wind speed. The safety margin of OWT is estimated as $(0.5° – \theta_{\text{Pile,max}})/0.5° \times 100\%$, which indicates how much of the OWT serviceability limit held in reserve. Figure 13.4a shows the safety margin of OWT considering past and future climate. It is observed that safety margin is positive when climate change is not accounted for analysis for both locations. For location SW03, safety margin becomes negative (i.e., $\theta_{\text{Pile,max}} \leq 0.5°$) considering future climate variation

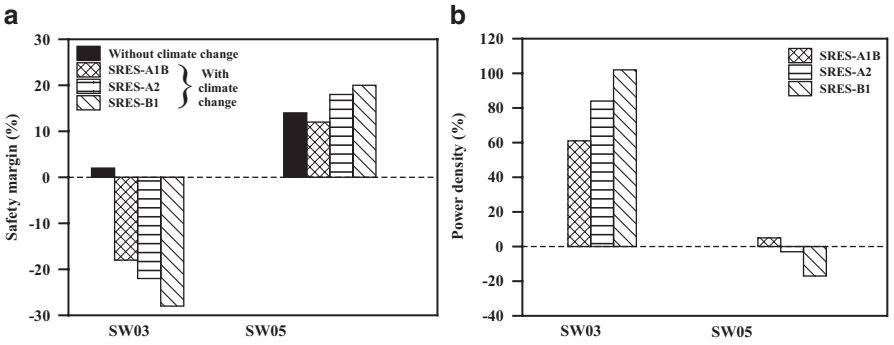

Fig. 13.4 Impact of climate change on (**a**) safety margin of pile and (**b**) power output of OWT based on 50 years return period

for all the scenarios. Interestingly, wind energy density increases substantially for this location due to increased wind speed. For the location SW05, safety margin improves because of reduced wind speed when future climate change is taken into account; however, wind energy density is found to be decreased marginally (Fig. 13.4b).

13.7 Conclusions

The impact of climate change on the design of OWT is carried out considering 50 years return period wind and wave loads. The statistical downscaling model is used to predict future wind speed, wave height, and wave period using GCM for A1B, A2, and B1 emission scenarios. The safety margin and power output are assessed due to climate change. It is observed that wind load on OWT is increased for all three scenarios at west coast of India and decreased at east coast of India considering Gumbel and GEV probability distributions. Future wave height is increased at the east coast and decreased at the west coast of Indian offshore locations both for Gumbel and GEV distributions. At west coast location, an OWT structure which is designed to be safe without considering climate change found to be unsafe due to serviceability criterion when climate change is taken into account. The OWT is found to be safe at the east coast considering climate change effect; however, wind energy production is found to be decreased marginally. This aspect is important for the selection of a strategic location of an OWT in order to improve wind energy production in conjunction with safety for its serviceable life in a sustainable manner.

Acknowledgments This work was supported by a grant from the Department of Science and Technology (DST Grant No. SR/FTP/ETA-08/2012), India, to the second author. The source of support is greatly appreciated.

References

4C-Offshore. Offshore turbine database (2013) www.4coffshore.com/windfarms/turbines.aspx
ABS (1997) Rules for building and classing offshore installation. American Bureau of Shipping, New York
API (2011) Petroleum and natural gas industries-specific requirements for offshore structures. Part 4 – Geotechnical and foundation design considerations. American Petroleum Institute, Washington, DC
Ashour M, Norris G, Pilling P (1998) Lateral loading of a pile in layered soil using the strain wedge model. J Geotech Geoenviron Eng ASCE 124(4):303–315
Basack S, Purkayastha RD (2009) Engineering properties of marine clays from the eastern coast of India. J Eng Technol Res 1(6):109–114
Bhattacharya S (2014) Challenges in design of foundations for offshore wind turbines. Eng Technol Ref 1:9. doi:10.1049/etr.2014.0041
Bisoi S, Haldar S (2014) Dynamic analysis of offshore wind turbine in clay considering soil-monopile-tower interaction. Soil Dyn Earthq Eng 63:19–35
COMSOL multiphysics user guide (2013) Version 4.3b edition, COMSOL AB, USA
Deepthi R, Deo MC (2010) Effect of climate change on design wind at the Indian offshore locations. Ocean Eng 37:1061–1069
DNV-OS-J101 (2010) Design of offshore wind turbine structures. DET NORSKE VERITAS
DNV-RP-C205 (2010) Environmental conditions and environmental loads. DET NORSKE VERITAS
GL (2005) Guideline for the certification of offshore wind turbines. Germanischer Lloyd, Hamburg
Grabemann I, Weisse R (2008) Climate change impact on extreme wave conditions in the North Sea: an ensemble study. Ocean Dyn 58:199–212
Harrison GP, Wallace AR (2005) Climate sensitivity of marine energy. Renew Energy 30(12):1801–1817
Jara FAV (2006) Model testing of foundations for offshore wind turbines. Ph.D. thesis, University of Oxford
Kulkarni S, Deo MC, Ghosh S (2013) Impact of climate change on local wind conditions. Proceedings of HYDRO 2013 International, IIT Madras, India
Kulkarni S, Deo MC, Ghosh S (2014) Changes in the design and operational wind due to climate change at the Indian offshore sites. Mar Struct 37:33–53
Radhika S, Deo MC, Latha G (2013) Evaluation of the wave height used in the design of offshore structures considering the effects of climate change. Proc Inst Mech Eng Part M J Eng Marit Environ 227(3):233–242
Sailor DJ, Smith M, Hart M (2008) Climate change implications for wind power resources in the Northwest United States. Renew Energy 33:2393–2406
Wilby RL, Dawson CW (2007) SDSM 4.2 – a decision support tool for the assessment of regional climate change impacts. User manual
Wilby RL, Charles SP, Zorita E, Timbal B, Whetton P, Mearns LO (2004) Guidelines for use of climate scenarios developed from statistical downscaling methods. Supporting material of the IPCC, available from the DDC of IPCC TGCIA, 27

Chapter 14
Axial Stress Distribution in Geothermal Energy Pile Group in Sand

Rajni Saggu and Tanusree Chakraborty

Abstract The integration of geothermal heat exchange techniques in structural pile foundation is gaining acceptance to cater the heating and cooling requirements of a building. The purpose of the present study is to analyze the response of energy pile foundations subjected to heating and cooling cycle through numerical investigations. For this purpose, a highlight of finite element method is used to simulate energy pile group. The interaction between the piles in a group is analyzed during thermal cycle and constant mechanical loading of the piles. The pile response is considered to be linear elastic. The soil behavior is reproduced using a constitutive model CASM, based on concepts of critical-state soil mechanics. The CASM model has been implemented in finite element software Abaqus through user-defined material subroutines. In the present study, the axial stress distribution in the piles in a group of six piles is analyzed. It is observed from the results that the thermal piles are subjected to heating-induced excess load in addition to the axial mechanical load from the superstructure. However, for nonthermal piles, unloading of the piles happens during heating of the thermal piles. Heating of the thermal piles causes an increase in the axial stress in the thermal piles and decrease in axial stress in the nonthermal piles. However, the cooling of the piles causes decrease in axial stress in thermal piles and an increase in axial stress in nonthermal piles. At the end of cooling, there is a setup of additional axial stress in the thermal piles as compared to the nonthermal piles. The analysis results conclude that the thermally induced axial stress should be taken into consideration for the geotechnical design of energy piles.

Keywords Axial stress • CASM • Pile cap • Thermomechanical loading • Thermal piles

R. Saggu (✉)
Department of Civil Engineering, Amity School of Engineering and Technology, Amity University Uttar Pradesh, Sector – 125, Noida 201313, Uttar Pradesh, India
e-mail: rsaggu@amity.edu

T. Chakraborty
Department of Civil Engineering, Indian Institute of Technology (IIT) Delhi, Hauz Khas, New Delhi 110016, India
e-mail: tanusree@civil.iitd.ac.in

G.L. Sivakumar Babu et al. (eds.), *Geoenvironmental Practices and Sustainability*, Developments in Geotechnical Engineering,
DOI 10.1007/978-981-10-4077-1_14

14.1 Introduction

The innovative geothermal energy technology can contribute to sustainability of civil infrastructure by reducing nonrenewable energy use and minimizing the carbon footprint of built structures. Geothermal energy piles are subjected to thermal loading in addition to axial mechanical loading. Therefore, to maintain the structural integrity of geothermal energy piles, the effect of temperature on geotechnical capacity needs to be studied. The geothermal piles are used as a group in major construction projects. All or only certain number of piles in the group may be installed as thermal piles (Koene and Geelen 2000; Salciarini et al. 2013). In the present literature, the scientific studies on geothermal pile groups are rare due to the complexity involved in experimental and numerical investigation of the pile groups. Brettmann and Amis (2011) presented the results of thermal conductivity tests of geothermal energy pile group, and they reported increase in soil temperature surrounding the pile during heating of the pile; however, the soil temperature remains unchanged at the center between the two piles. Dupray et al. (2014) carried out two-dimensional thermo-hydro-mechanical finite element analyses of a pile group in clay and reported that heating and cooling of the piles in a group have a positive impact on the mechanical behavior of piles in comparison to heating and cooling of isolated piles. Saggu and Chakraborty (2016a) have performed numerical investigation of geothermal energy pile groups and stated that adequate pile spacing should be considered while designing the geothermal energy piles. The geotechnical behavior of energy pile groups under combined thermal and mechanical loading is currently not fully understood, especially when the pile groups contain thermal and nonthermal piles altogether under single pile cap. Saggu and Chakraborty (2015) have investigated a single pile subjected to cyclic thermal loading. They have shown that the shaft capacity of the geothermal energy piles does not change significantly as compared to the piles under only mechanical load, whereas axial stress in the pile and pile base displacement increase with increase in temperature in the pile. Therefore, in the present work, effort has been given in understanding the axial stress distribution in geothermal energy pile group as compared to the pile group subjected to only mechanical loading.

In order to gain insight into geothermal energy pile behavior, three-dimensional nonlinear finite element analyses of geothermal energy pile groups with six piles in the group have been carried out using the finite element software Abaqus (Abaqus Manual Version 6.11). The piles have been considered to behave linear elastically. The soil behavior has been reproduced using a constitutive model CASM (Yu 2006) which is based on concepts of critical-state soil mechanics. The constitutive model has been implemented in Abaqus through two user-defined material subroutines: UMAT for defining the mechanical stress-strain response of soil and UMATHT for defining the soil thermal parameters. A uniform temperature change is applied over the entire length of the pile as reported in Laloui et al. (2006).

14.2 Details of Numerical Analyses

14.2.1 Finite Element Model

The analyses reported in the present study employed the software Abaqus/standard for finite element simulation of pile groups. The sensitivity analyses were conducted for (1) different pile configurations for thermal and nonthermal piles in a group and (2) pile spacing. In these analyses, separate parts are created for the pile, pile cap, and soil geometries. The pile and the pile cap are assumed to be made of concrete with ultimate compressive strength of 45 MPa. The stress-strain response of concrete is assumed to be linear elastic with Young's modulus (E) = 33.7 GPa and Poisson's ratio (ν) = 0.2. The thermal parameters of concrete, thermal conductivity, k = 2.1 W/m °C; specific heat, C = 800 J/ °C; and coefficient of thermal expansion, $\alpha = 10^{-5}$/ °C, are taken from Laloui et al. (2006). The soil considered herein is Ottawa sand. The CASM model and thermal parameters for Ottawa sand are presented in Table 14.1.

Tie constraint has been considered between the pile cap and the piles to tie the vertical and the horizontal degrees of freedom. The stress-strain response of Ottawa sand has been simulated using constitutive model CASM. Figure 14.1 shows typical finite element mesh of the pile cap, six piles, and the soil surrounding the piles. Here, each pile is 20 m long with 1 m diameter. The pile cap is of 15.5 m length, 12.9 m width, and 1.2 m thickness. The vertical far-field soil boundaries have been placed at a distance of 6.5 m from the side of the pile cap along the shorter dimension of the pile cap and 7.5 m, along the longer dimension as shown in Fig. 14.1. The bottom soil boundary is considered at a distance of 20 m from the bottom of the

Table 14.1 CASM model and thermal parameters for Ottawa sand

Parameter	Value	References
Slope of critical-state line in e-ln(p') space (λ)	0.02	Sasitharan et al. (1994)
		Carraro (2006)
		Loukidis (2006)
Slope of unloading-reloading line in e-ln(p') space (κ)	0.005	Yu (2006)
Critical-state line intercept at 1 kPa pressure (Γ)	0.8	Model simulation
Reference-state parameter (ξ_R)	0.075	Yu (2006)
Model parameter (n)	4.5	Model simulation
Slope of critical-state line in q-p' space (M_{cc})	1.2	Yu (2006)
		Loukidis (2006)
Poisson's ratio (υ_s)	0.3	Yu (2006)
Shear modulus (G)	32.6 MPa	Laloui et al. (2006)
Bulk modulus (K)	15 MPa	
Thermal conductivity (k_s)	0.274 W/m °C	Tarnawski et al. (2009)
Specific heat (C_s)	722 J/°C	
Coefficient of thermal expansion (α_s)	10^{-4}/°C	

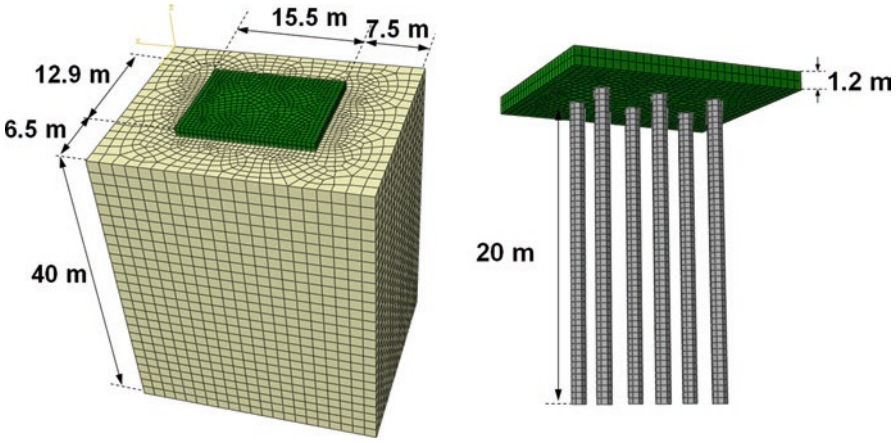

Fig. 14.1 Finite element mesh for pile cap, geothermal pile group of six piles, and soil

piles. A pinned boundary condition has been applied to restrict the vertical and horizontal displacements at the bottom soil boundary and a roller boundary condition to restrict the horizontal displacements at the far-field vertical soil boundaries. The initial stress state in the pile and the soil has been assumed to be geostatic. Among the thermal boundary condition, the heat is allowed to flow through the far-field sides of the mesh and through the bottom boundaries of the mesh. The initial temperature in the energy pile and soil is considered as 15 °C (Laloui et al. 2006). The pile and soil domain has been discretized using eight-node thermally coupled brick, trilinear displacement, and temperature element (C3D8T). Extra fine mesh is used to characterize the soil elements near pile-soil interface with minimum element size in soil domain as 0.5 mm surrounding the pile and the maximum element size as 1.5 mm in the far-field regions. To model the interfaces between the pile and the soil surfaces, a frictional contact in the tangential direction with a coefficient of friction μ (= tanδ) between soil and concrete of 0.55 is considered for the analyses. In the normal direction, hard contact has been considered between the pile and soil.

Heat conduction between pile and soil has been made possible by defining a thermal conductance at the pile-soil interface same as the soil thermal conductance.

14.2.2 Sand Constitutive Model CASM

To determine the CASM model parameters for the present study, a FORTRAN code has been written for drained and undrained triaxial compression test simulation of Ottawa sand. The model parameters have been determined for minimum void ratio e_{min} = 0.48 and maximum void ratio e_{max} = 0.78 (Murthy et al. 2006). The thermal constitutive model is implemented in Abaqus through user-defined material subroutine UMATHT. The thermal behavior of pile-soil system is considered to follow the energy balance equation given by (Green and Naghdi 1992):

$$\int_V \rho \dot{U} dV = \int_V r dV + \int_S q_H dS$$

where ρ is the density of the material; $\dot{U}$ is the material time rate of the internal energy; V and S are the volume and surface area of solid material, respectively; q_H is the heat flux per unit area of the body; and r is the heat supplied externally into the body per unit volume.

14.3 Finite Element Simulation of Pile Group

Three-dimensional nonlinear finite element analyses of four pile groups with six piles in each group have been performed under thermomechanical loading using Abaqus. The analyses are performed in two steps: (1) a static step for applying the gravity loading and to bring the model in geostatic equilibrium and (2) a coupled temperature-displacement step for applying the thermal and mechanical loads. The analyses have been carried out for four different pile combinations, e.g., (1) all piles are geothermal, (2) only the corner piles are geothermal, (3) only the middle piles are geothermal, and (4) no piles are geothermal. To understand the effect of pile spacing on geotechnical behavior of piles, the analyses are carried out for pile spacing of 4 m center to center and 2.5 m center to center. An axial load Q of 6000 kN is applied on the pile cap instantaneously and maintained during the analysis. The temperature change, $\Delta T = 21$ °C (Laloui et al. 2006), is applied to the pile with 12 days of heating and 16 days of cooling. The initial ambient temperature of 15 °C is considered for soil domain. The analyses have been carried out for sand with different relative densities $D_R = 40\%$ and 50%. Ottawa sand is modeled using CASM constitutive model. The lateral earth pressure coefficient at rest (K_0) is assumed to be 1 for all analyses. For the analyses, tensile axial stress and upward displacement are considered as positive; depth is considered positive in the downward direction from the ground surface.

14.4 Analysis Results and Discussion

14.4.1 Axial Stresses in the Pile

Figure 14.2a through 14.2c shows the axial stresses induced due to thermomechanical loading of the piles.

The results are plotted along depth for piles with 4 m center-to-center spacing for two different soil relative densities, $D_R = 40\%$ and 50%. In order to understand the permanent setup of thermally induced axial stress, results have been plotted (1) at the end of heating and (2) at the end of cooling. Similarly, Fig. 14.3a through 14.3c presents axial stresses induced due to thermomechanical loading of the piles. The results are plotted along depth for piles placed at 2.5 m center-to-center spacing for soil relative densities, $D_R = 40\%$ and 50%

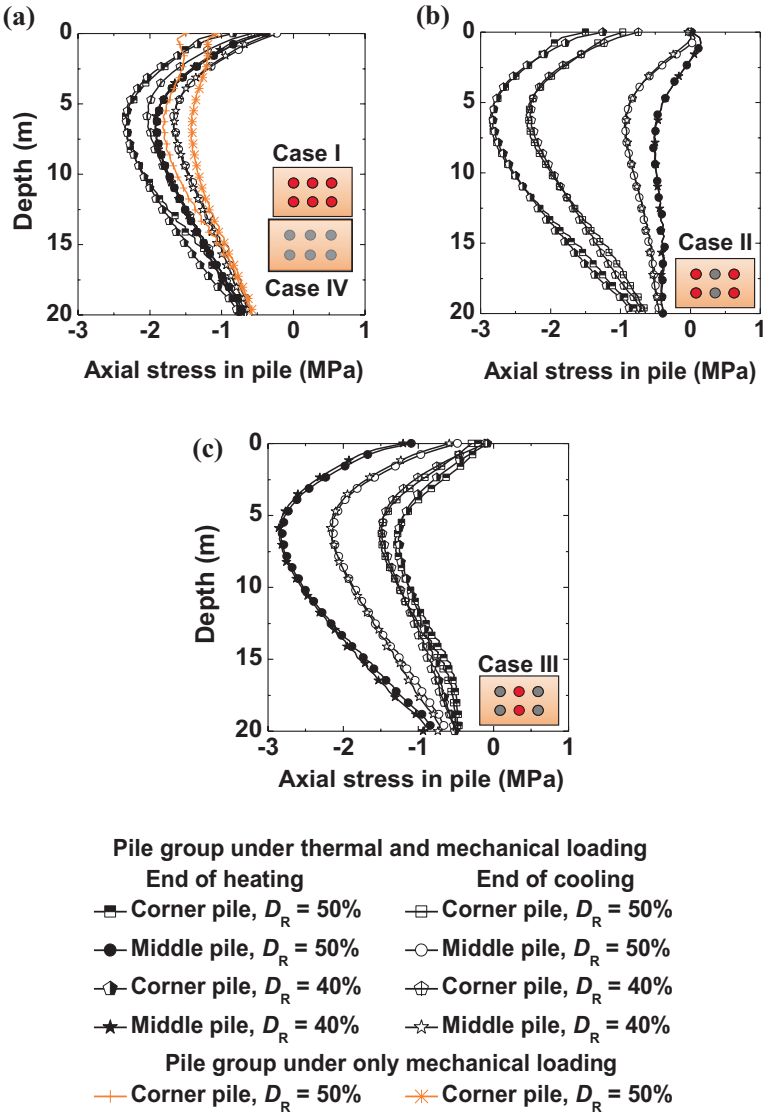

Fig. 14.2 Axial stress generated in piles with 4 m center-to-center spacing

It is concluded from the figures that the thermal loading of the piles causes expansion of piles at pile ends and the axial stress tends to increase at the end of heating. Upon thermal unloading, the axial stress tends to decrease. For all the piles, the axial stress is higher at the end of heating than that at the end of cooling. Moreover, the thermal piles exhibit higher axial stress than the nonthermal piles due to thermally induced axial stress generated in the piles in addition to that caused due to axial mechanical loading of the piles. The corner piles exhibit higher axial stress

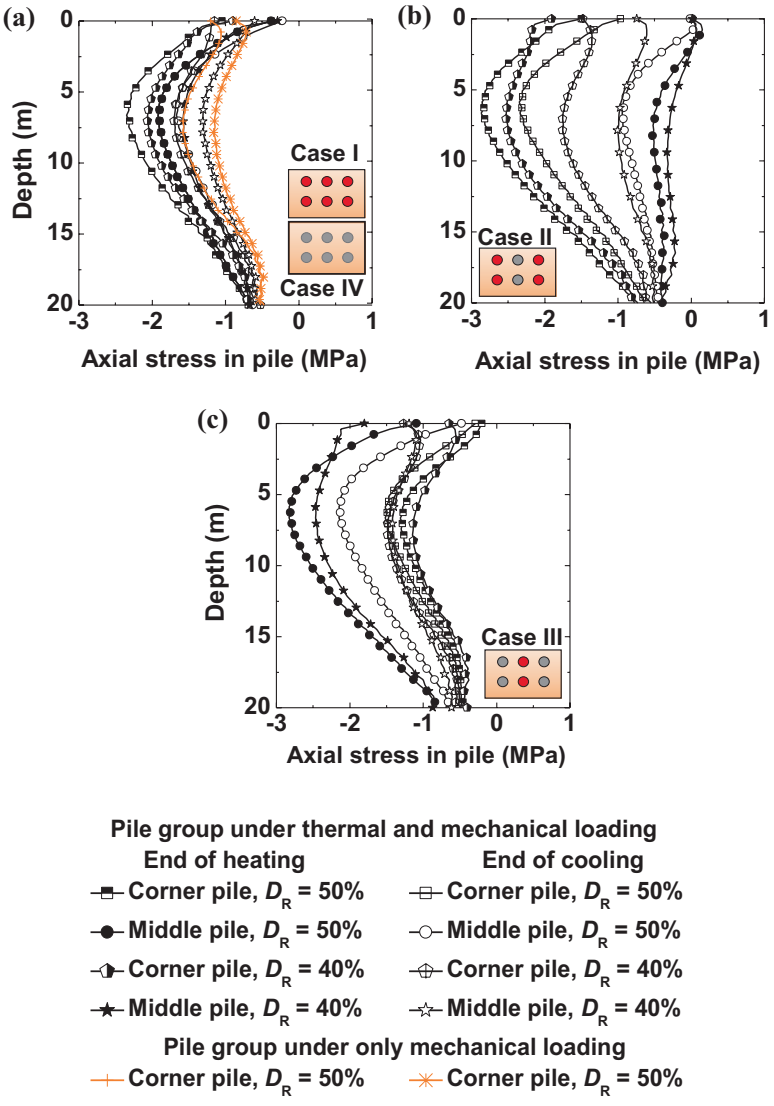

Fig. 14.3 Axial stress generated in piles with 2.5 m center-to-center spacing

than the middle piles which happen due to nonuniform load distribution on the piles through the raft as a result of thermal expansion of the piles. It is also observed from the figures that the effect of soil relative density is not significant for the floating piles placed at 4 m center to center as also observed by Saggu and Chakraborty (2016b) for a single thermal pile. However, for thermal piles placed at 2.5 m center to center, the piles in soil with $D_R = 50\%$ experience higher magnitude of axial stress

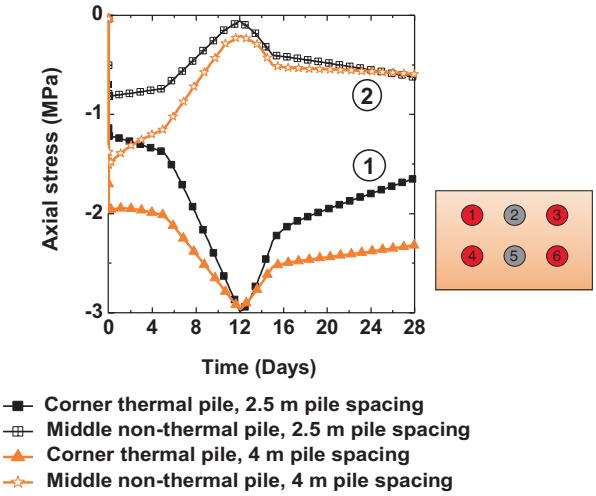

Fig. 14.4 Axial stress-time history in a corner thermal pile and a middle nonthermal pile for Case II

as compared to the piles in sand with $D_R = 40\%$ which may be attributed to the relatively denser soil which offers lesser pile base displacement.

To analyze the effect of nonuniform load distribution on the piles due to heating and cooling of the piles, the results are compared for axial stress-time history of one corner and one middle pile as presented in Fig. 14.4. The results are presented for axial stress-time history at the top of the piles for analysis of Case II for pile groups with both 4 m and 2.5 m spacing, wherein only corners are the thermal piles. Initially, the axial stress on the pile for both corner and middle piles increases under mechanical axial load. Heating of the thermal piles causes an increase in axial stress in the thermal piles and decrease in axial stress in the nonthermal piles. Conversely, the cooling of the thermal piles results in decrease in axial stress in thermal piles and increase in axial stress in nonthermal piles. However, at the end of cooling, higher axial stress is exhibited by the thermal piles as compared to the nonthermal piles.

14.5 Conclusions

This paper summarizes the results of numerical investigation of geothermal energy pile groups. Thermomechanical behavior of geothermal energy pile groups with pile cap has been investigated herein using three-dimensional nonlinear finite element analysis procedure using software Abaqus (Abaqus Manual Version 6.11 (2011)). The axial stresses generated in the piles are analyzed for different combinations of thermal and nonthermal piles in a single layer of Ottawa sand. The piles and raft have been considered as linear elastic. The stress-strain response of sand has been reproduced using a state parameter-based constitutive model CASM. The axial stress in

the piles in the group under thermomechanical loading has been investigated for different pile spacing, 4 m and 2.5 m center to center. Heating of thermal piles causes expansion of these piles in upward direction at the pile head, thus, the piles pushing the raft along with it in the upward direction. As a result, redistribution of axial load occurs on the piles due to heating and cooling. The load on nonthermal piles decreases, and the load on thermal piles increases. The thermal piles experience higher magnitude of axial stress at the end of heating than at the end of cooling. Moreover, thermal piles exhibit higher axial stress than the nonthermal piles. The axial stress in the thermal piles increases, and axial stress in the nonthermal piles decreases due to heating of thermal piles. However, the axial stress in thermal piles decreases, and the stress in nonthermal piles increases due to cooling of thermal piles.

References

Abaqus/Standard User's Manual, Version 6.11 (2011) Dassault Systèmes Simulia Corporation, Providence, Rhode Island, USA

Brettmann T, Amis T (2011) Thermal conductivity evaluation of a pile group using geothermal energy piles. Geo-Front, ASCE 2011:499–508

Carraro JAH (2006) Mechanical behavior of silty and clayey sands. Ph.D. dissertation, Purdue University, USA

Dupray F, Laloui L, Kazangba A (2014) Numerical analysis of seasonal heat storage in an energy pile foundation. Comput Geotech 55:67–77

Green AE, Naghdi PM (1992) On undamped heat waves in an elastic solid. J Therm Stresses 15:253–264

Koene F, Geelen C (2000) Energy piles as an efficient way to store heat. CADDET energy efficiency special issue on Netherlands 2000

Laloui L, Nuth M, Vulliet L (2006) Experimental and numerical investigations of the behavior of a heat exchanger pile. Int J Numer Anal Methods Geomech 30:763–781

Loukidis D (2006) Advanced constitutive modeling of sands and applications to foundation engineering. Ph.D. dissertation, Purdue University, USA

Murthy TG, Loukidis D, Carraro JAH, Prezzi M, Salgado R (2006) Undrained monotonic response of clean and silty sands. Géotechnique 57(3):273–288

Saggu R, Chakraborty T (2015) Cyclic thermo-mechanical analysis of energy piles in sand. Geotech Geol Eng 33:321–342

Saggu R, Chakraborty T (2016a) Thermo-mechanical response of geothermal energy pile group in sand. Int J Geomech. doi:10.1061/(ASCE)GM.1943-5622.0000567

Saggu R, Chakraborty T (2016b) Thermo-mechanical behavior of geothermal energy piles in sand. Proceedings of geotechnical and structural engineering congress, 14–17 February 2016, Phoenix, Arizona, pp 921–930

Salciarini D, Ronchi F, Cattoni E, Tamagnini C (2013) Some remarks on the thermomechanical effects induced by energy piles operation in a small piled raft. Int J Geomech. doi:10.1061/(ASCE)GM.1943-5622.0000375

Sasitharan S, Robertson PK, Sego DC, Morgenstern NR (1994) State-boundary surface for very loose sand and its practical implications. Can Geotech J 31(3):321–334

Tarnawski VR, Momose T, Leong WH, Bovesecchi G, Coppa P (2009) Thermal conductivity of standard sands. Part I. Dry state conditions. Int J Thermophys 30(3):949–968

Yu HS (2006) Plasticity and geotechnics. Springer, New York

Chapter 15
Importance of Non-stationarity in Sustainability and Resilience of Geo-Infrastructure

Sumanta Haldar and Dipanjan Basu

Abstract The importance of non-stationarity in loads and resistances of geo-infrastructure is pointed out in this paper. Temporal variations of loads and resistances are now becoming an inherent aspect of civil infrastructure systems, particularly because of the effect of climate change. Non-stationarity of loads and resistances affects the sustainability and resilience of geo-systems and, if not taken into account properly, may lead to unsustainable outcomes. Inherent in the concept of resilience is the aspect of temporal variation, and therefore time-dependent reliability estimation of a system can be related to its resilience. An example of time-dependent reliability calculation for an offshore wind turbine (OWT) foundation is presented. How such calculations can be related to the resilience and sustainability of OWTs is conceptually outlined.

15.1 Sustainability

Sustainability is a normative concept that focuses on managing resources in such a way that guarantees welfare and promotes equity of current and future generations (Brundtland 1987; Basu and Puppala 2015a, b). Naturally, sustainability attempts to prevent the detrimental effects of anthropogenic development on the environment and society at multiple levels and promotes development that balances the three Es – the environment, economy, and equity. However, achieving sustainable

S. Haldar (✉)
Department of Civil Engineering, School of Infrastructure, Indian Institute of Technology Bhubaneswar, Jatni, 752050 Bhubaneswar, Odisha, India
e-mail: sumanta@iitbbs.ac.in

D. Basu
Department of Civil and Environmental Engineering, University of Waterloo, 200 University Avenue W, Waterloo, ON N2L 3G1, Canada
e-mail: dipanjan.basu@uwaterloo.ca

G.L. Sivakumar Babu et al. (eds.), *Geoenvironmental Practices and Sustainability*, Developments in Geotechnical Engineering,
DOI 10.1007/978-981-10-4077-1_15

development is not a simple, linear process because the world is a "giant organism" consisting of innumerable subsystems interacting with each other, with several layers of heterogeneity and complexity embedded in each of them. Sustainable development in one system may imply unsustainable outcomes for another system, and often these outcomes are not even clear in the first place. Geotechnical engineers can hardly deal with complex, global sustainability issues. However, they cannot remain indifferent either, because geotechnical constructions have a significant impact on the environment, economy, and society. The environmental impact of geotechnical constructions is quite apparent because of vast exploitation of natural resources like geo-materials (e.g., clay, sand, and stone reserve) and fossil fuel (e.g., diesel used in construction equipments and hauling trucks) in the construction activities, and the resulting environmental pollution caused by related off-site operations (e.g., wastes generated from manufacturing of cement and geosynthetics) and on-site activities (e.g., carbon emissions and dust and noise pollution generated by construction machineries). What are perhaps not that apparent are the societal and economic implications of geotechnical constructions. A poorly designed or inappropriately constructed road embankment can lead to significant restoration and maintenance costs that create financial burden on the local authorities and may cause serious accidents. On the other hand, a properly executed geotechnical work, e.g., low-volume roads in a remote community, may help develop the local economy and add to social well-being.

Significant efforts have been made in geotechnical engineering research and practice to promote sustainable development by using nonconventional materials (e.g., recycled or recyclable materials), designing new products (e.g., geothermal energy piles), and adopting novel construction techniques (e.g., new deep mixing technologies) that reduce cost, minimize the use of natural resources, and restrict pollution and carbon emissions (Basu et al. 2015). At the same time, reasonable progress has been made in developing sustainability assessment tools in geotechnical engineering (e.g., life cycle assessment-based assessment tools).

An equally important aspect of sustainability that has not been considered in mainstream geotechnical practice is accounting for the changing demands on and expectations from an engineering solution. Unless such non-stationarity in loads (i.e., temporal variability of loads) is taken into account in geotechnical practice, sustainable development cannot be fully achieved. For example, the changing climate pattern because of global warming has led to unprecedented drought in some places and more intense and frequent storm events and floods in other places. Changing economies and lifestyle have led to rapid urbanization in the last decade associated with severely increased demands on the civil infrastructure. These excess demands that were unanticipated have led to failures or reduction of life span of geo-infrastructure. Unanticipated failures resulting in loss of life or property and the associated repair, redesign, and reconstruction have negative environmental, societal, and economic impacts and do not support sustainable development.

15.2 Resilience

Resilience is a descriptive concept often closely associated with sustainability. Resilience is mostly understood as the ability of a system to "bounce back" to normal functionality when subjected to disruptions. In the context of infrastructure, resilience can be understood as the ability of a system to withstand disruptions and continue to function by rapidly recovering from and adapting to the disruptions (National Infrastructure Advisory Council 2009). It is necessary to develop resilience in civil infrastructure systems as the effects of climate change are becoming more and more apparent and the frequency of natural disasters are increasing. Climate change gradually alters the load and resistance of physical infrastructure systems that can accelerate the deterioration of the physical structures. Disasters, either natural or man-made, have the capability to destroy critical infrastructures and cause detrimental effects to societies.

Incorporation of resilience thinking in infrastructure management can improve preparedness and response against disruptive events. For example, the reliability and robustness of infrastructure systems can be enhanced so that the ability to absorb external shocks can be increased; systems can be designed to improve redundancy in order to maintain their operability and rapidly recover even after disruptions occur; and tactical responses regarding emergency management and resource allocation can be planned in advance to better cope with future potential disruptions. Preparedness is mostly associated with the abilities to proactively mitigate the effects of the disruptive events by arranging adequate resources and devising strategies prior to the disruption. Three types of responses – absorption, recovery, and adaptation – can be expected after the event of disruption (Francis and Bekera 2014). Absorption is the immediate response of an infrastructure system in which the system withstands the disruption; recovery is the organizational efforts to rapidly repair the damaged system and mitigate the consequential effects propagated to other systems (e.g., communities); and adaptation is the ability to adjust to future disruptions by undertaking changes aimed for enhanced responses. Considering the fact that impacts of damaged infrastructure are significant and that there will always be only a finite amount of resources available for repair and recovery, the resilience of an infrastructure system needs to be improved by increasing its preparedness and improving its response to disruptions with optimized efficiency (e.g., efficient use of resources, maximum environmental protection, and minimum recovery time).

The complex aspects of resilience can be expressed in a simplified way in terms of the "resilience triangle," as shown in Fig. 15.1, where the loss of resilience or quality of system functionality is expressed as a function of time (Bruneau et al. 2003; Bocchini and Frangopol 2011). In Fig. 15.1, absorption of shocks is reflected by the degradation of the system functionality at the event of disruption from time t_d to t_a. The recovery efforts can be initiated immediately post-disruption; however, the system functionality can be unchanged for a certain period of time (from time t_a to t_r) until adequate resources are collected and response strategies are organized. Ultimately, it is expected that the system functionality recovers to an acceptable

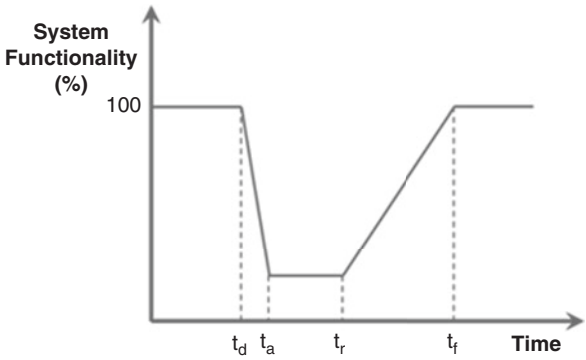

Fig. 15.1 Schematic of typical resilience loss over time

level for its normal operation from time t_r to t_f. Adaptation is the learning process that has been acquired during the disruptive event to better prepare, mitigate, and respond to potential disruptive events in the future.

Resilience can be further described by four properties: robustness, rapidity, resourcefulness, and redundancy (Bruneau et al. 2003). Robustness refers to the strength of systems to withstand a given level of stress or demand without suffering a loss of functionality. Rapidity is the capacity to meet priorities and achieve goals in a timely manner in order to contain losses and avoid future disruption. Resourcefulness is the capacity to identify problems, establish priorities, and mobilize resources (i.e., monetary, physical, technological, and informational resources). Redundancy indicates the extent to which existing elements or systems are substitutable.

It is evident from the foregoing discussion that non-stationarity in loads and resistances affects sustainable development and can be directly linked to the resilience of a system. The changing demands and supplies pertaining to a system may alter the system performance gradually or rapidly depending on the rate at which the supplies and demands (i.e., resistances and loads) change. It is necessary to account for this temporal change in resilience thinking.

15.3 Incorporating Non-stationarity

Robustness, as described with reference to resilience, is the ability of a system to withstand shocks and still perform, even if with reduced functionality. It is related to reliability because reliability is a measure of the "distance" of the "design state" of a system from its "failure (limit) state." Thus, the greater the reliability of a system, the greater is its robustness. It is therefore important to assess the reliability of a system under temporally varying loads and resistances because this gives an indication of the robustness under temporally changing conditions. Indeed, reliability can be calculated as a function of time for systems in which the loads and resistances change over time. Therefore, the changing resilience of a system under

non-stationary loads can be partially estimated if the reliability of a system is known as a function of time.

Resilience in civil infrastructure contributes to its sustainability as well. Therefore, time-dependent reliability estimation gives an idea about how sustainable a system remains over time. Clearly, incorporating non-stationary loads and resistances in reliability calculations enhances the quality of estimation of resilience and sustainability of geo-infrastructures and is essential for ensuring their long-term satisfactory performance.

15.4 Time-Dependent Reliability of a Wind Turbine System

An example of time-dependent reliability calculation is shown in this chapter for offshore wind turbine (OWT) foundations. Future wind and wave loads on OWTs may alter because of fluctuations in climatic conditions. Hence, the time-dependent reliability of an OWT structure founded in sand is investigated for the period 2015–2050 – reliability calculations are performed for the serviceability limit state of maximum allowable mudline rotation. The OWT system is modeled as a beam supported laterally by a nonlinear Winkler foundation characterized by the American Petroleum Institute (API 2011) recommended cyclic *p-y* relationship for sand. The uncertainties in soil properties and wind and wave loads are incorporated in the analysis. Future wind speed and wave height and period are generated for a location at a distance of approximately 28 km off the west coast of India using an open-source program called statistical downscaling model (SDSM) (Wilby et al. 2002). According to DNV-OS-J101 (2010), the serviceability limit for monopile head rotation is 0.5° at the mudline. The instantaneous probability of failure $p_f(t)$ over the design life of an OWT structure can be defined as

$$p_f(t) = \mathrm{P}\left(0.5^\circ \le \left|\theta_{\text{mudline}}(t)\right|\right) \tag{15.1}$$

where $\theta_{\text{mudline}}(t)$ is the rotation of monopile at mudline in degrees, and it depends on future loading and soil and monopile properties and changes with time t. The time-dependent reliability index of OWT with a design life T can be divided into finite number of time segments (e.g., month, year, etc.) as

$$\beta(T) = \Phi^{-1}\left(\prod_{N}^{i=1}(1-p_i)-1\right); \quad N = 1,2,\ldots,50 \tag{15.2}$$

where $\Phi^{-1}(\cdot)$ is the inverse of cumulative density function of the standard normal variate, p_i is the probability of failure for the ith time step, and N is the number of time segments. In this study, p_i is estimated annually using Eq. (15.1) considering the annual maximum θ_{mudline} value for a 50-year time period (2001–2050) after incorporating the effects of climate change. The value of p_i is also estimated based

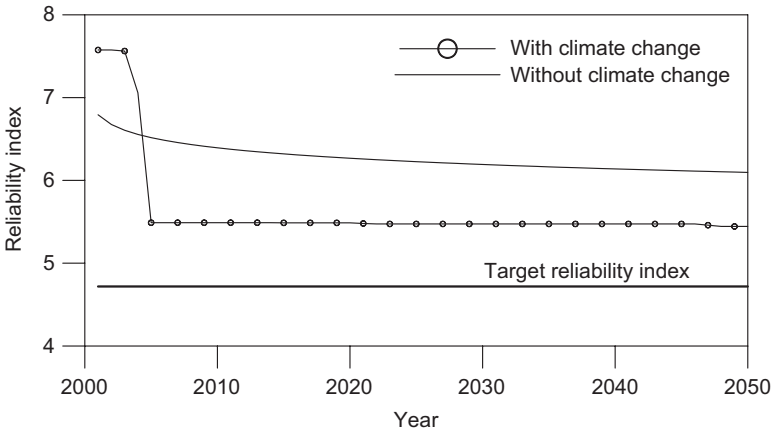

Fig. 15.2 Reliability of offshore wind turbine for different design lives considering present and future climate conditions

on the present climate conditions in which the maximum θ_{mudline} value is estimated for the period of 1998–2001. The mean and standard deviation of θ_{mudline} is obtained by ensemble averaging of 1000 Monte Carlo simulations. A first-order second-moment (FOSM) reliability method was used to estimate the annual probability of failure and reliability index for the serviceability criterion. A summary of the results is presented in Fig. 15.2 for different values of T. The estimated time-dependent reliability index considering climate change effects for different design lives is found to be less than that of the case where climate change effect is not taken into account in the analysis.

15.5 Conclusions

Geotechnical engineering contributes significantly toward the sustainability and resilience of civil infrastructure systems. An important aspect of both sustainability and resilience is the time-dependent variation of applied loads and resistances. Such non-stationarity, if not taken into account in planning, design, construction, and monitoring of geo-infrastructures, may lead to failures resulting in loss of life and property. One way of estimating the effect of this non-stationarity is through the calculation of the reliability index of a system as a function of time. An example of time-dependent reliability index calculation is provided for an offshore wind turbine foundation. Such calculations can provide a better estimation of the sustainability and resilience of geo-infrastructures.

References

API. American Petroleum Institute (2011) Petroleum and natural gas industries-specific requirements for offshore structures. Part 4 – Geotechnical and foundation design considerations. American Petroleum Institute, Washington, DC

Basu D, Puppala A J (2015a) Principles of sustainability and their applications in geotechnical engineering. In: Proceedings of 15th Pan-American conference on soil mechanics and geotechnical engineering, Buenos Aires, Argentina, November 2015 (keynote paper)

Basu D, Puppala A J (2015b) Sustainability: an emerging discipline within geotechnical engineering. In: Proceedings of 16th European conference on soil mechanics and geotechnical engineering, Edinburgh, UK, September 2015

Basu D, Misra A, Puppala AJ (2015) Sustainability in geotechnical engineering: perspectives and review. Can Geotech J 52:96–113

Bocchini P, Frangopol DM (2011) Resilience-driven disaster management of civil infrastructure. COMPDYN 2011, ECCOMAS, Corfu, Greece 1:1–11

Brundtland GH (1987) Our common future: report of the world commission on environment and development. Oxford University Press, Oxford

Bruneau M, Chang SE, Eguchi RT, Lee GC, O'Rouke TD, Reinhorn AM, Shinozuka M, Tierney K, Wallace WA, Winterfeldt D (2003) A framework to quantitatively assess and enhance the seismic resilience of communities. Earthquake Spectra 19(4):733–752

DNV-OS-J101 (2010) Design of offshore wind turbine structures. DET NORSKE VERITAS

Francis R, Bekera B (2014) A metric and frameworks for resilience analysis of engineered and infrastructure systems. Reliab Eng Syst Saf 121:90–103

National Infrastructure Advisory Council (2009) Critical infrastructure resilience. National Infrastructure Advisory Council, Washington, DC

Wilby RL, Dawson CW, Barrow EM (2002) SDSM – a decision support tool for the assessment of regional climate change impacts. Environ Model Softw 17:147–159

Chapter 16
Reliability-Based Sustainable Design of Piled Raft-Supported Structure

Rajib Saha, Diptesh Chanda, and Sumanta Haldar

Abstract Past failures of pile foundation-supported structures during earthquake had lead engineering community to develop sustainable design guideline. Dynamic soil-structure interaction (DSSI) is important in seismic design because it leads to increased or decreased response that of conventional fixed base design. Inherent variability of soil parameters and modeling considerably affects the dynamic response of structure which leads to precise estimation of safety factor. This study attempts to propose a reliability-based design solution for piled raft foundation considering interaction among soil-pile and superstructure under seismic loading. In situ variability of undrained shear strength of soil and different DSSI modeling is incorporated. Response statistics of an idealized structural system supported on piled raft foundation embedded in homogenous soft clay is calculated using Monte Carlo simulation (MCS). Probability of failure is assessed and design implications are also suggested. Finally, this study highlights importance of reliability-based design of piled raft foundation and rational choice of DSSI modeling which may help sustainable design of piled raft foundation.

Keywords Reliability • Dynamic soil-structure interaction • Seismic • Pile foundation • Monte Carlo simulation

16.1 Introduction

Reliability-based design of structure and foundation considering dynamic soil-pile foundation-structure interaction (SPFSI) is considered as primary step toward sustainable design. Ensuring safety and economy with minimum material use is the basic attribute of a sustainable design guideline. In fact, pile foundation is considered as highly engineered and robust foundation system to support heavy structural load

R. Saha (✉) • D. Chanda
Civil Engineering Department, NIT Agartala, Tripura (w) 799046, Tripura, India
e-mail: rajib.civil@nita.ac.in

S. Haldar
School of Infrastructure, IIT Bhubaneswar, Bhubaneswar, Odisha 750013, India

G.L. Sivakumar Babu et al. (eds.), *Geoenvironmental Practices and Sustainability*, Developments in Geotechnical Engineering,
DOI 10.1007/978-981-10-4077-1_16

in soft and loose soil deposit. Failures of several pile-supported structures, such as bridge, buildings, flyovers, etc., during past earthquake events (e.g., 1964 Niigata; 1989 Loma Prieta; 1995 Kobe earthquake) have given a strong lesson and insisted practicing engineer and researchers to modify the existing seismic design guidelines of foundation and structural system. Ex post facto analysis of failure of such structures indicated that the behavior of pile-supported structure embedded in soft soil during seismic excitation is a dynamic soil-structure interaction (DSSI) problem. However, the conventional practice of seismic design is based on fixed base consideration of structure with an anticipation of beneficial attributes of DSSI as reported in previous codal guidelines (NEHRP 1997). Incorporation of DSSI may result in increased or decreased forces in superstructure and foundation as compared to fixed base condition. Further, DSSI in design may result to significant uncertainties in response of the system due to in situ variability of soil strength and stiffness parameters even in distinct homogenous layer which lead to a reliability-based problem (Das et al. 2016). Inherent variability is reported as one of the primary sources of soil uncertainty (Phoon and Kulhway 1999). Thus, precise estimation of safety margin is required for sustainable design of such foundations under uncertain loads like seismic events with an acceptable risk. Previous studies have addressed probabilistic seismic design of pile with an emphasis on different reliability-based approaches (e.g., Tandjiria et al. 2000; Haldar and Babu 2008; Pula and Rozanski 2012).

Present study is an attempt to propose a reliability-based design guideline for pile foundation considering dynamic interaction among whole system, i.e., soil, pile foundation, and superstructure attributing in situ variability of Young's modulus and undrained cohesion in very soft clay. Effects of in situ variability on safety factor are examined considering different Winkler-based soil-structure interaction (SSI) modeling which may provide significant input in reliability-based design. Monte Carlo simulation (MCS) is used to carry out the probabilistic analysis. Response statistics is obtained for an idealized structural system having fundamental period of 2.0 s supported on piled raft foundation embedded in homogenous soft clay. Probability of failure considering ultimate limit state and serviceability criteria are assessed using first-order reliability methods. Further, design implications are suggested in the form of percentage steel required for pile foundation attributing different SSI models. This study shows that selection of SSI model may have considerably affected estimation of safety factors.

16.2 Idealization of Structural System

A representative long period structure with fundamental period (T_{fixed}) of 2.0 s (resembles a 20-story building) is designed to be supported by 9 × 9 RCC piled raft foundation embedded in very soft homogenous clay. The pile tip is assumed to be supported on a hard soil deposit (cf. Fig. 16.1a). The pile group is designed based on dead load of 8.0 kN/m^2 at each floor having single bay size of 8.5 m × 8.5 m along with self-weight of raft slab. The spacing (S) to diameter (d) ratio (S/d) of pile is 3 and length (L) to diameter (d) ratio of pile is 60. Further details of pile and soil are given in Table 16.1.

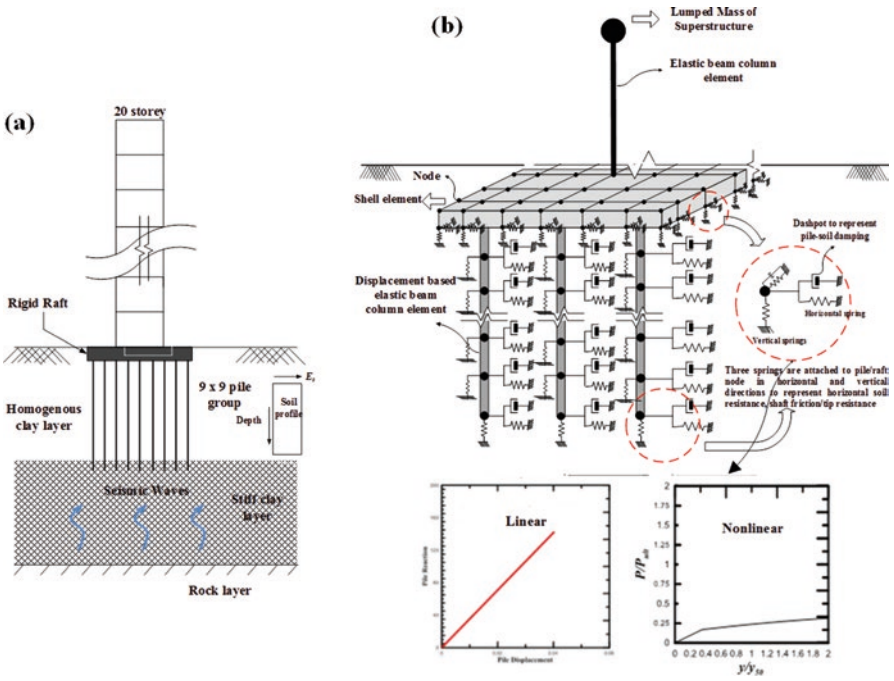

Fig. 16.1 (**a**) Structural system and (**b**) finite element model of soil-piled raft-structure

Table 16.1 Pile and soil data used for deterministic analysis

Pile data	Value	Soil data	Value
Pile diameter, d (m)	0.3	Soil consistency	Very soft
Pile length, L (m)	18	Undrained cohesion, C_u (kN/m^2)	9.80
Young's modulus, E_p (kN/m^2)	21.78×10^6	*SPT N* value	1
Poisson's ratio of concrete	0.17	γ_{sat} (kN/m^3)	13.50
Section modulus, Z (m^3)	0.0045	Young's modulus, E_s (kN/m^2)	2500
Flexural strength, F_y (kN/m^2)	3050	Poisson's ratio	0.4
Flexural moment, M_y (kN m)	13.725	Undrained cohesion at tip, C_d (kN/m^2)	100.0

16.3 System Modeling

Superstructure is idealized as a single-story lumped mass stick model structure having single degree of freedom. Column is modeled using an elastic beam-column element, and stiffness of the column is adjusted to obtain $T_{\text{fixed}} = 2.0$ s. Response of the superstructure is obtained for considering both fixed base and SSI condition. Raft is modeled as four-noded shell element, having six degrees of freedom at each node. Plan dimension of raft is considered as 10 m × 10 m which is discretized into 0.5 m × 0.5 m small elements based on a convergence study. A moderately rigid raft

is selected in this study considering the relative stiffness of raft and soil (k_{rs}) as suggested by Horikoshi and Randolph (1998):

$$k_{rs} = 4E_r B_r t_r^3 (1-\nu^2) / 3\pi E_s L_r^4 (1-\nu_r^2) \tag{16.1}$$

where E_r and E_s = Young's modulus of raft and soil, respectively; L_r and B_r = raft length and breadth, respectively; t_r = raft thickness; and ν and ν_r = Poisson's ratio of soil and raft, respectively. The value of $k_{rs} = 1$ denotes a moderately rigid raft, hence used for analysis. Pile is modeled using displacement-based elastic beam-column element having six degrees of freedom at each node. Each pile is meshed into 0.9 m interval from a convergence study. Pile head is attached to the raft node by a rigid link to follow the same degrees of freedom of raft element. Plate on Winkler foundation and beams on Winkler foundation (BWF) model are used to model the raft-soil and pile-soil interaction, respectively. Raft-soil and pile-soil interaction is modeled considering both linear and nonlinear idealization of load-deformation behavior of soil. Finite element model of soil-piled raft-structure system is presented in Fig. 16.1b.

Raft-soil interaction is modeled as linear spring (Gazetas 1991; Dutta et al. 2009; Makris and Gazetas 1992), and the details are available in Das et al. (2016). It is denoted as "linear" for the sake of brevity in next sections. Nonlinear piled raft-soil modeling in clay soil is carried out using cyclic *p*-*y*, *t*-z, and *q*-z springs as suggested by Boulanger et al. (1999) and Curras et al. (2001) based on benchmark stiffness curve proposed by Matlock (1970). However, present study proposes a modification in the backbone *p*-*y* curve for soft clay suggested by Matlock (1970) to incorporate the effect of spatial variability in ε_{50}. In Matlock (1970) curve, the critical displacement y_c is a function of strain parameterε_{50}, and the value was suggested based on laboratory triaxial test. Present study proposes ε_{50} as a function of undrained cohesion (C_u) based on Evans and Duncan (1982) which seems to be more rational from the point of view on predicting the accurate response of soil-pile foundation-structure system. The relationship between mean values of ε_{50} and C_u is found to be best fitted with power-based equation. The modified expression is given below. This modified Matlock soil model is represented as "nonlinear" in next sections:

$$\varepsilon_{50} = \left(\frac{0.1796}{\log_{10} C_u} \right)^{\frac{1}{1.1841}} \tag{16.2}$$

$$y_c = 2.5 \times d \times \left(\frac{0.1796}{\log_{10} C_u} \right)^{\frac{1}{1.1841}} \tag{16.3}$$

Soil damping is idealized as linear dashpots which are connected as parallel to the soil springs for raft and pile. This study considers 5% of critical damping in each mode regardless of structural support condition. Sinusoidal acceleration with a frequency equal to the fundamental frequency of the system having an amplitude of

0.02 g is applied at the base of structure. Dynamic analysis is carried out using OpenSees (Mazzoni et al. 2007).

16.4 Modeling of Soil Uncertainty and Probabilistic Analysis

In this study, the spatially variable undrained soil shear strength (C_u) and Young's modulus (E_s) of soil are modeled by random field. The random field is generated following Haldar and Babu (2008) within the finite element grids by assigning C_u or E_s at each grid location which is not presented herein due to brevity. Undrained soil shear strength (C_u) and Young's modulus (E_s) are considered as lognormally distributed random variable represented by parameters mean μ_{Cu}, standard deviation σ_{Cu}, and spatial correlation distance $\delta_z = 1.5$. Deterministic soil parameters presented in Table 16.1 are assumed as mean values for probabilistic analysis. The probability analysis is conducted for a range of variability and a correlation parameter of soil. The range of values is selected based on the typical range for coefficient of variation (COV) of shear strength (10–50%) as suggested by Phoon and Kulhway (1999). Monte Carlo simulation (MCS) is adopted in present study for probabilistic analysis. Based on a convergence study (Das et al. 2016), the number of sample realizations for MCS analysis is considered as 200. The range of coefficient of variation (COV_{Cu} or COV_{Es} %) is considered as 10, 30, and 50.

16.5 Results and Discussion

16.5.1 Assessment of Probabilistic SSI Period and Probability of Failure

Time history analysis is performed to obtain the dynamic response of the finite element model of soil-piled raft-structure system and fixed base structural system. Newmark's $\beta - \gamma$ method ($\beta = 0.5$ $\gamma = 0.25$) considering a small time step of $T/100$ is used to solve the dynamic motion of equation, where T is the fundamental time period of the structure. First, the mean fundamental period of vibration ($T_{ssi(mean)}$) is calculated for linear and nonlinear idealization of soil behavior by eigenvalue solution, and the normalized period (i.e., $T_{ssi(mean)}/T_{fixed}$) is presented in Fig. 16.2. It is observed that $T_{ssi(mean)}$ obtained considering linear and nonlinear model gives relatively higher prediction in order of 25% and 7.5%, respectively, as compared to fixed base period for this long period structure which indicates that the variability effect is higher on period lengthening in case of linear soil behavior.

Table 16.2 presents the probability of failure (POF) considering flexural failure and serviceability criteria attributing different SSI models and fixed base condition. POF is calculated using first-order reliability method (FORM) as it may give precise

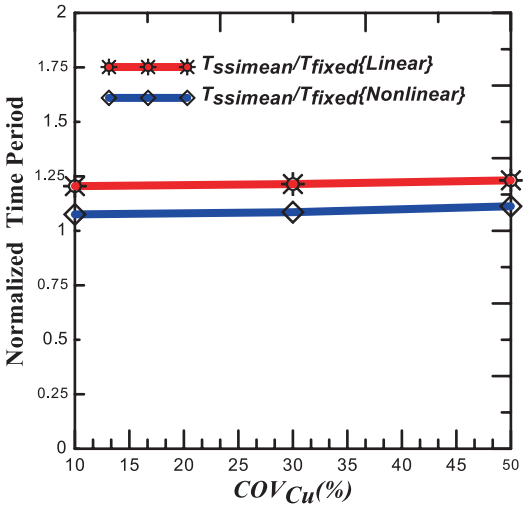

Fig. 16.2 Normalized period with respect to COV for different SSI models

Table 16.2 Probability of failure and reliability index using FORM

	POF (in %)							
	Flexural failure criteria				Serviceability			
SPFSI modeling	Deterministic	10%	30%	50%	Deterministic	10%	30%	50%
Fixed base	0	–	–	–	0	–	–	–
Linear	–	12	14	17	–	41.6	42.7	43.8
Nonlinear	–	100	100	100	–	0	0	0

estimation in case of higher values of probability of failure (Haldar and Basu 2013). A pile is considered to be unserviceable if the mean maximum deflection exceeds the tolerable displacement of 30 mm. Likewise, a pile may lead to flexural failure if it exceeds the corresponding yield capacity of 13,725 N-m for the pile dimension considered herein. It is observed that the POF is found to be zero irrespective of criteria if pile design is made based on fixed base condition. While, SSI model with linear and nonlinear idealization exhibits a different scenario of POF in order of maximum 17% and 100%, respectively, considering flexural failure criteria. Further, linear model exhibits maximum POF of 44% as per displacement criteria. Hence, the results clearly indicate that coupled analysis of soil-pile foundation-structure system gives precise and safe estimation of POF. While, the nonlinear model may give reasonably accurate prediction of safety factor for pile design under lateral load. Hence, the selection of SSI modeling may have a significant role to predict the accurate reliability index which may be further confirmed by a detailed study.

Table 16.3 Percentage of longitudinal steel required for a single pile

	Mean bending moment (kN-m)				% of steel			
Modeling	Deterministic	10%	30%	50%	Deterministic	10%	30%	50%
Fixed base	12.35	–	–	–	0.55	–	–	–
Linear	–	116.35	116.413	116.564	–	4.7	4.7	4.8
Nonlinear	–	170.199	171.342	172.366	–	5.2	5.3	5.4

16.5.2 Design Implications

Finally, the design implication in the form of percentage of design longitudinal steel for pile is presented in Table 16.3 for each modeling cases. Structural design of pile design is performed following SP 16 (1980) considering a long column problem with biaxial load combinations. It clearly indicates that the percentage of steel in a single pile may be significantly underestimated if design response is obtained from decoupled analysis, i.e., fixed base modeling. On the other hand, coupled analysis incorporating DSSI effect with linear and modified nonlinear SSI model gives a significantly higher prediction of design response which may be anticipated during earthquake event. While, the nonlinear model results to relatively higher percentage of steel required for pile as compared to fixed base design.

16.6 Conclusions

Summarily, present study proposes a reliability-based design guideline for pile foundation considering coupled seismic analysis of soil-piled raft-structure system attributing DSSI effect. It is found that the nonlinear SSI model may give safe, precise, and accurate estimation of probability of failure of the structure. Further, design implication in the form of percentage steel required for pile design is calculated to highlight the importance of DSSI along with SSI modeling issues. Hence, the outcome of this study gives an input toward sustainable design solution of such heavy structural system.

References

Boulanger RW, Curras CJ, Kutter BL, Wilson WD, Abghari AA (1999) Seismic soil-pile-structure interaction experiments and analyses. J Geotech Geoenviron Eng 125(9):750–759

Curras JC, Boulanger WR, Kutter BL, Wilson DW (2001) Dynamic experiments and analysis of a pile-group-supported structure. J Geotech Geoenviron Eng 127(7):585–596

Das B, Saha R, Haldar S (2016) Effect of in-situ variability of soil on seismic design of piled raft supported structure incorporating dynamic soil-structure-interaction. Soil Dyn Earthq Eng 84:251–268

Dutta SC, Bhattacharya K, Roy R (2009) Effect of flexibility of foundations on its seismic stress distribution. J Earthq Eng 13:22–49

Evans Jr LT, Duncan GM (1982) Simplified analysis of laterally loaded piles. Rep. No. UCB/GT/82-04, University of California, Berkeley, California

Gazetas G (1991) Formulas and charts for impedances of surface and embedded foundations. J Geotech Eng 117(9):1363–1381

Haldar S, Babu GLS (2008) Effect of soil spatial variability on the response of laterally loaded pile in undrained clay. Comput Geotech 35:537–547

Haldar S, Basu D (2013) Response of Euler-Bernoulli beam on spatially random elastic soil. Comput Geotech 50:110–128

Horikoshi K, Randolph MF (1998) A contribution to optimum design of piled rafts. Geotechnique 48(3):301–317

Makris N, Gazetas G (1992) Dynamic pile-soil-pile interaction. Part II: Lateral and seismic response. Earthq Eng Struct Dyn 21:145–162

Matlock H (1970) Correlations for design of laterally loaded piles in soft clay. In: Proceedings of 2nd annual offshore technology conference 1:577–594

Mazzoni S, Mckenna F, Scott MH, Gregory L, Fenvas (2007) OpenSees, open system for earthquake engineering simulation user command- language manual. Available online: http://opensees.berkeley.edu

NEHRP (1997) Recommended provisions for seismic regulations for new buildings and other structures: parts 1 and 2. Building Seismic Safety Council, Washington, DC

Phoon KK, Kulhawy FH (1999) Characterization of geotechnical variability. Can Geotech J 36:210–238

Pula W, Rozanski A (2012) Reliability of rigid piles subjected to lateral loads. Struct Saf 12:205–218

SP 16 (1980) Design aids for reinforced concrete to IS: 456-1978. Bureau of Indian Standards

Tandjiria V, Teh CI, Low BK (2000) Reliability analysis of laterally loaded piles using response surface methods. Struct Saf 22:335–355

Chapter 17
Quality Control and Quality Assurance for Large Infrastructure Projects

S. Bandi

Abstract INTERRA provided quality control (QC) or quality assurance (QA) for large infrastructure projects spanning transportation, storm damage risk reduction, and environmental remediation areas. Quality assurance and control have assumed increased significance in creating a green and sustainable economy.

17.1 Introduction

Lately, the QA and QC have assumed more significance in light of environmental stewardship being a major focus area of governmental agencies. First, the process of making or building something should consume the least amount of natural resources. A good QA/QC program will ensure the project is built right and minimize waste that would otherwise happen with out-of-spec materials brought to the site or construction that does not meet specifications and needs to be redone. Second, the service life of a project should be the longest possible. To this end, a good QA/QC program will ensure that projects will be built correctly, and the cost and resource consumption will be minimal in maintaining and replacing the constructed project through its service life. Third, maximum use of reclaimed materials in construction projects will reduce the need for scarce natural resources and the transportation associated with those. A robust QA/QC program will ensure the reclaimed or recycled materials meet the project specifications.

The American Association of State Highway and Transportation Officials (AASHTO) defines QA as "(1) All those planned and systematic actions necessary to provide confidence that a product or facility will perform satisfactorily in service; or (2) making sure the quality of a product is what it should be."

Historically, the term QC/QA is used with QC referring to the contractor's role and QA to the owner's role. This term implied that QC and QA are separate

S. Bandi (✉)
INTERRA, 600 Territorial Drive, Suite G, Bolingbrook, IL, USA
e-mail: sbandi@interraservices.com

G.L. Sivakumar Babu et al. (eds.), *Geoenvironmental Practices and Sustainability*, Developments in Geotechnical Engineering,
DOI 10.1007/978-981-10-4077-1_17

functions; in fact, QA refers to the overall system for assuring project quality, with QC being one element of a comprehensive QA program.

FHWA's Transportation Construction Quality Assurance Reference Manual defines QC as "The system used by a contractor party to monitor, assess, and adjust their production or placement processes to ensure that the final product will meet the specified level of quality."

The Federal Highway Administration (FHWA) supports and promotes the use of recycled highway materials in pavement construction in an effort to preserve the natural environment, reduce waste, and provide a cost-effective material for constructing highways. In fact, the primary objective is to encourage the use of recycled materials in the construction of highways to the maximum economical and practical extent possible with equal or improved performance. The recycled materials include portland cement concrete (PCC), reclaimed asphalt pavement (RAP), reclaimed asphalt shingles (RAS), and crushed composite pavement (CCP). The recycled materials require increased frequencies of QA and QC inspection and testing to ensure that the final product with recycled materials meets or exceeds the performance of product made with virgin materials.

INTERRA has worked on a number of large infrastructure projects in transportation, storm damage risk reduction, and environmental remediation projects. Services provided by INTERRA included field and plant inspection and testing of PCC and HMA, inspection and testing of structural steel, field inspection and testing of soils, and laboratory testing on PCC, HMA, and soils. INTERRA's laboratories have been accredited by the State DOTs, Army Corps of Engineers, and the AASHTO. It maintains a 13,000 SFT state-of-the-art laboratory in Bolingbrook, Illinois, in addition to branch laboratories in Michigan and Wisconsin. INTERRA is also at the forefront of developing systems and processes to automate construction materials testing and scheduling and report delivery to clients using bar-coded samples, data forms, and smartphone devices.

17.1.1 LPV 111: New Orleans East Back Levee, New Orleans, LA

Archer Western-Alberici JV was tasked by USACE to reconstruct, elevate, and reinforce more than 5 miles of levee outside of New Orleans at an approximate cost of

$350 million. The project is a part of the federal government's efforts to protect New Orleans from hurricanes.

The team also constructed more than 2000 lineal feet of concrete flood wall. In addition, the team raised the elevation of the levee from an average of +14 to +26 ft. using approximately 1.7 million cubic yards of clay embankment in an 18-month period.

Soil below the levee was strengthened through the use of deep soil mixing, a technology which uses large augers to drill holes in which cement is mixed with the soil to create a column of soil and cement that is left in place.

17.1.2 Chalmette Loop Levee (LPV 146), Bayou Dupre to Hwy 46, Reach 146, Saint Bernard, LA

Saint Bernard Levee Partners constructed the $273 million, approximately 8-mile long concrete T-wall levee from Bayou Dupre to Hwy 46 in Saint Bernard, LA. INTERRA provided complete construction material testing and inspection for soils, concrete, asphalt, and steel. More than 100,000 cubic yards of concrete was used to build the T-wall. To accomplish this high-profile, fast-tracked project within the aggressive schedule, INTERRA established an on-site laboratory and had it successfully accredited by the USACE in matter of weeks. The on-site laboratory not only maintained required quality standards over the course of the project but was able to accurately process and document a dramatically large number of widely varied tests.

17.1.3 Elgin O'Hare Western Access (EOWA) Project: Illinois Tollway

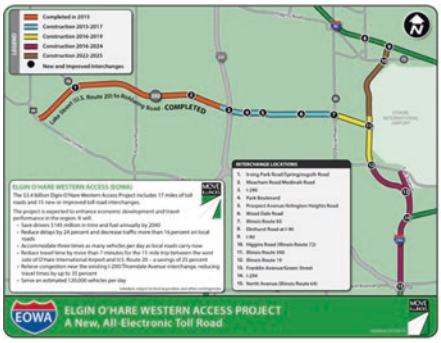

Designated a "Project of National and Regional Significance" by federal transportation legislation, the $3.4 billion Elgin O'Hare Western Access Project includes 17 miles of new roads with 15 new or improved interchanges as part of a new, all-electronic toll road that includes rehabilitating and widening Illinois Route 390, formerly known as the Elgin O'Hare Expressway, and extending it east along Thorndale Avenue to O'Hare and building a new roadway around the western border of O'Hare linking the Jane Addams Memorial Tollway (I-90) and the Tri-State Tollway (I-294). The Illinois Tollway is committed to "building green" and minimizing the environmental impact of construction by reducing, recycling, and reusing materials. To that end, the tollway requires 100% recycling of concrete and asphalt pavements with reconstruction. For example, existing aggregate subbases were recycled, subgrade undercuts were eliminated or minimized, old concrete was recycled as new porous base, and old asphalt was recycled for many applications.

INTERRA's scope of work includes providing independent assurance (IA) services consisting of independent verification of the tollway's quality control/quality assurance (QC/QA) roadway materials program in addition to direct assistance for tollway materials to help resolve material-related issues.

17.1.4 O'Hare Modernization Program (OMP), Chicago, IL

The O'Hare Modernization Program (OMP) will reconfigure O'Hare International Airport's intersecting runways into a more modern, parallel layout. The $6.6 billion program will substantially reduce delays in all weather conditions and increase capacity at the airfield, allowing O'Hare to meet the region's aviation needs well into the future.

The scope of work included reconfiguring intersecting runways into a parallel layout to increase efficiency and capacity, designing and constructing three new runways, relocating 3 miles of existing Union Pacific Railroad tracks, and relocating the water detention basin on the south airfield. INTERRA has been providing quality assurance services as part of the large team on this mega project.

The Chicago Department of Aviation (CDA)'s Earthwork Management Plan has kept soil on-site and out of landfills, helping the CDA achieve the triple bottom line by being economically viable, socially responsible, and environmentally sound. Soil has been reused as part of new projects or stockpiled for future use, saving over $150 million. By keeping soil on-site, the CDA has also saved more than 630,000 truck trips and more than 73,000 tons of carbon dioxide.

17.1.5 Fullerton Theater on the Lake, Chicago, IL

The Chicago Shoreline Protection Project: Fullerton Parkway/Theater on the Lake project has added nearly six acres of land by filling in Lake Michigan with dredged material near Fullerton Avenue Beach. This stretch of lakefront was transformed into a lush park designed to withstand severe storms and enhance the safety of locals and tourists. INTERRA provided QA and inspection services for the project.

17.1.6 Dan Ryan Expressway: 31st Street to I-57, Chicago, IL

INTERRA provided construction inspection, management, and material (QC/QA) services for the reconstruction of the $725 million Dan Ryan Expressway reconstruction project for the full duration from 2004 to 2007. The Illinois Department of Transportation (IDOT) reconstructed the Dan Ryan Expressway between the 31st and the I-57 interchange. The vastly improved expressway included an additional lane in each direction, a reconfigured skyway interchange, and significant enhancements to the local access roads that run parallel to the expressway.

The new pavement consists of a 24-inch recycled gravel subbase, a 6-inch asphalt base, and 14 in of continuous steel reinforced concrete. The project has also been recognized as one of the largest "green" construction projects in the nation, by requiring the use of ultralow sulfur diesel fuel or retrofit construction equipment to reduce emissions, limiting idling of trucks.

As a member of the project team, INTERRA contributed its expertise and inspection and testing services to help ensure that this highly complex, long-term project was completed on schedule, with minimum disruption to one of the highest volume routes into and out of the City of Chicago.

17.2 Conclusions

INTERRA firmly believes that QA/QC is an integral part of a green and sustainable economy. Good QA/QC program is essential to large infrastructure projects to reduce waste, minimize rework, extend service life, and incorporate reclaimed and recycled materials in those projects.

References

Chicago Department of Aviation (CDA) website at www.flychicago.com
Illinois Tollway website at www.illinoistollway.com
INTERRA's website at www.interraservices.com
Rafalowski M (2012) Construction quality assurance for design-build highway projects. FHWA Publication No.: FHWA-HRT-12-039

Chapter 18
Risk Management: Challenges and Practice for US Dam and Levee Safety

Kevin S. Richards and Nathan J. Snorteland

18.1 Introduction

One of the earliest research efforts on internal erosion was funded by the Government of India in 1895 at Thomason Civil Engineering College, Roorkee (Clibborn 1902). The research was primarily an effort to better understand the 1885 failure of the Khanki Weir and use this information to refine design guidance. This led to early improvements in the analysis and design of defensive measures to prevent piping failures of dams, as well as enabling the prediction of the failure of Narora Weir in 1898. Risk assessment is the process of evaluating what may go wrong and how likely it is to go wrong, how frequently it might fail, and the magnitude of consequences due to failure. The product of all these quantities is defined as "risk." Probabilistic risk assessments grew out of fault tree analysis methods used to evaluate aircraft equipment failures in the early 1970s (Wellock 2011). Qualitative considerations of risk began in the 1950s with the advent of nuclear power, expanded into the aerospace program during the 1960s, and into dam safety, transportation, and the environmental fields in the 1970s. The Nuclear Regulatory Commission (NRC 1975) first employed probabilistic risk assessments in 1975. The probabilistic approach was different than reliability analyses employed during design, in that it considers low-frequency high-consequence scenarios not previously considered during design (NASA 2011). From the beginning, risk assessments identified the critical potential failure modes, the likelihood of failure, and frequency that they might occur and

K.S. Richards (✉)
Risk Management Center, U.S. Army Corps of Engineers,
1000 Liberty Avenue, Pittsburgh, PA 15222, USA
e-mail: kevin.s.richards@usace.army.mil

N.J. Snorteland
Risk Management Center, U.S. Army Corps of Engineers,
12596 W. Bayaud Avenue, Suite 400, Lakewood, CO 80228, USA

G.L. Sivakumar Babu et al. (eds.), *Geoenvironmental Practices and Sustainability*, Developments in Geotechnical Engineering,
DOI 10.1007/978-981-10-4077-1_18

considered the consequences of failure. The approach has been refined over the years with the development of better methods to inform estimates of the likelihood of failure, loading frequency, and consequences (Reclamation-USACE 2015).

Over the past 15 years, improvements in risk assessment methodologies for dams and levees have been significant, although there is much room for further advancements. New tools have been developed for rapid evaluation of dams or levees, such as the potential failure mode analysis (FERC 2005) or the semiquantitative risk assessment (USACE 2014). The US Bureau of Reclamation and the US Army Corps of Engineers recently began collaborating to develop and maintain current guidance for performing quantitative risk assessments for dams and levees, including recommendations and references to assist with estimating likelihood of failure for various failure modes (Reclamation-USACE 2015). There currently is no standardized method for estimating likelihood of failure for any given failure mode, and much engineering judgment is required when performing a risk assessment. Some of the available methods and statistics are based on little research and could be further improved with more work.

18.2 Risk Assessment for Dams and Levees

Not all federal agencies in the USA have adopted the quantitative risk assessment method in their dam safety programs, although most are using some level of risk-informed decision process to help prioritize expenditures. Qualitative or semiquantitative methods portray likelihood of failure and consequences for potential failure modes (PFM) within an order of magnitude (Fig. 18.1) so a decision can be made to either (a) prioritize immediate actions to achieve maximum risk reduction or (b) prioritize need for a more in-depth evaluations while implementing interim risk reduction measures.

A semiquantitative risk assessment (SQRA), while informative, might be too approximate to justify immediate remediation. If the remediation is very costly or the potential consequences are significant, a more detailed quantitative risk assessment may be warranted to ensure all risks have been identified and accurately assessed. SQRAs are typically done fairly rapidly using existing information. Their purpose is mostly as a screening tool. If a deficiency is found during an SQRA, more data or analyses may need to be developed to better characterize risk before selecting an appropriate risk management strategy. Quantitative risk assessments are currently being used by the Reclamation and the USACE to fill this need.

Quantitative risk assessments require a clear understanding of the potential failure mode and the sequence of events that lead to failure. Additional analyses and data are prepared in advance of the assessment to provide a more accurate assessment of the likelihood of failure, loading frequency, and potential consequences. In practice, the first step of a quantitative risk assessment requires defining the sequence of events (event tree) that are required to lead to failure for each of the critical potential failure modes that were identified during the screening phase (Fig. 18.2).

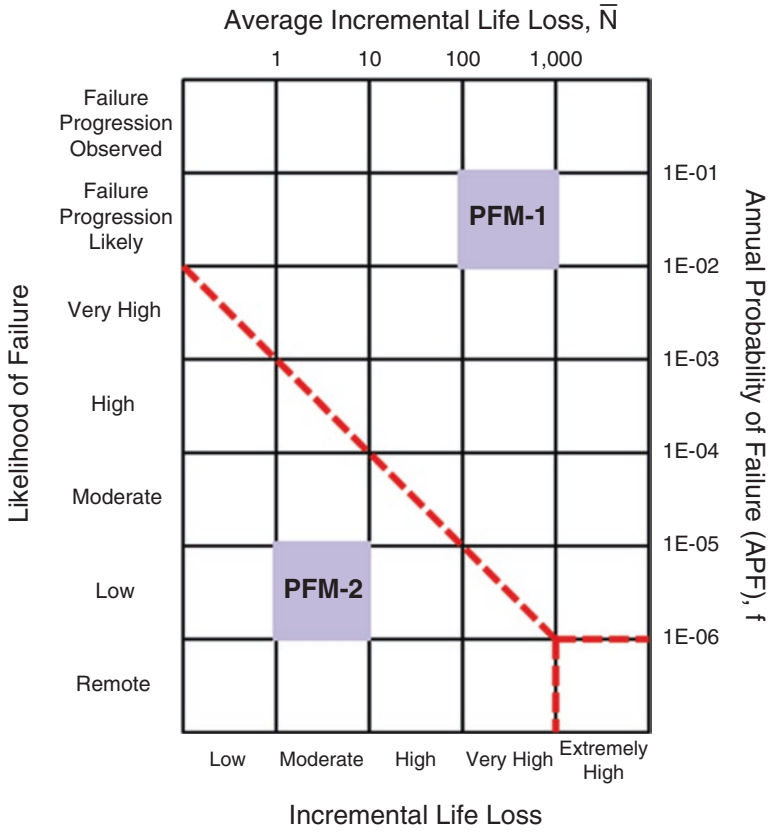

Fig. 18.1 Example of semiquantitative method of portraying risk

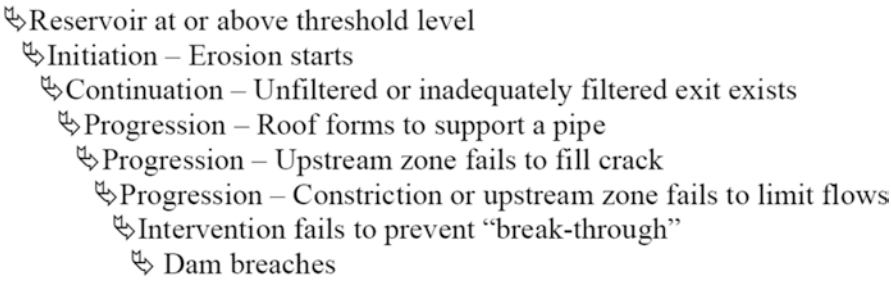

Fig. 18.2 Example of an event tree for internal erosion (Reclamation-USACE 2015)

The event tree includes the loading condition, in which an annual frequency is required to annualize the probability of failure. Probability of failure for each of the other nodes of the tree is estimated using whatever information can be gathered to help inform the estimate and is expressed as some decimal less than 1.0.

Predicting event trees requires not only a clear understanding of the existing conditions and materials at a project but also a clear understanding of the failure process that is most likely to take place. Unfortunately, there are a number of case histories where event trees were more complex than simple conceptual models might predict. This is an area where further research and collaboration could improve our ability to predict events leading to dam failures. A problem with many existing dam failure case histories is that there are not that many well-documented cases. Where dams have failed, much of the evidence that could be used to reconstruct an event tree is usually destroyed or poorly documented, leading to alternate interpretations of root causes. Also, in some well-studied cases such as Teton Dam failure, there are many elements of various internal erosion failure modes that may have been at work simultaneously (such as backward erosion piping through the embankment with concentrated leak erosion into fractured bedrock and stoping into the reservoir). Current practice is to make event trees as simple as necessary to reflect most likely failure modes; however, reality is often more complex.

Once an event tree is defined for each of the most critical failure modes, a quantitative risk assessment is completed by assigning the likelihood/probability for each node in the event tree for each failure mode, computing the annualized total probability of failure for each failure mode with an applied loading frequency curve, multiplying load increments by consequences to determine risk for each failure mode, and summing all the failure modes with appropriate adjustments to come up with the total project risk. The likelihood of failure for each of the event tree nodes is an area where much research is needed. There are many failure modes where information is needed to better inform estimates for the probability of failure for each event tree node.

Some areas of possible study to address current challenges with this method include; improved paleoseismicity methods, predicting likely seismic/source energy characteristics from known seismic sources, characterizing in situ stress states, nonlinear deformation characteristics of soil structures in response to seismic loads, and characterization of liquefaction characteristics of gravel and other mixed soils, predicting cracking characteristics of soils, hydraulic properties and erodibility of cracked soils; prediction methods for initiation, continuation, and progression nodes for internal erosion; methods for single-point and local-area characterization of site seepage conditions. Other areas of research are also needed, such as; creating innovative seepage monitoring methods for dam safety, advanced geotechnical site characterization tools for risk assessments, differentiation of benign from hazardous boils and prediction of boil response to changing seepage conditions; and improved remote sensing or geophysical methods for levee seepage characterization. Finally, more research is needed to help assess the magnitude of changes to future hydraulic loading conditions considering climate change, and improved system approaches to risk management, just to name a few.

Once a quantitative risk assessment is completed, the potential failure modes are typically plotted on chart and the total risk is computed (Fig. 18.3) and compared to tolerable risk. Another limitation is that when choosing which potential failure modes to assess, the risk assessment team must simplify their risk estimates to focus

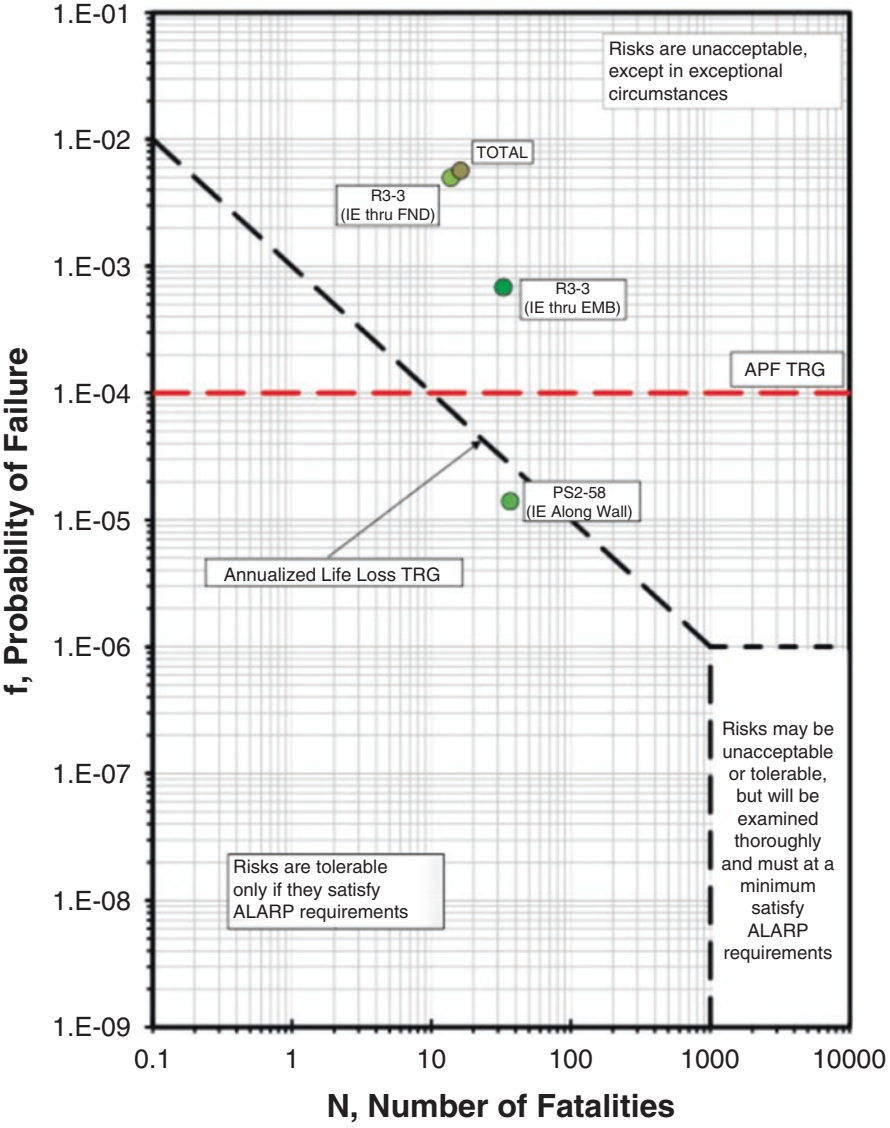

Fig. 18.3 Example of quantitative method of portraying risk

only on the perceived "critical" failure modes. Although many failure modes contribute to the total project risk, most will only contribute a very small amount to the total. This simplification requires engineering judgment by the risk assessment team, and better knowledge of potential failure modes, site conditions, and case histories of failures would focus risk assessment teams on those failure modes that contribute the majority of the total project risk.

In some cases, more effort is required to estimate the total risk for a particular project, for example, on levee systems where the extent of the project may influence the total project risk by increasing the likelihood of encountering flaws in the foundation or structure. These types of studies require consideration of length effects. Proper consideration of length effects requires an ability to divide a lengthy project into its "characteristic" sections with similar risk characteristics within each section. Early studies defined the characteristic section as being 1600 ft. in length because this was the approximate average length of dams that were used to develop early dam failure statistics. However, more recent studies have used autocorrelation or other more site-specific information to try to define the characteristic sections (Bowles et al. 2012). The sum of risk for each of the characteristic sections captures the overall project risk, but due to the complexity of loading conditions, dependence or independence of failure modes, or overlapping consequence centers, new computational tools and methods would help facilitate the division of a project into its characteristic sections and to compute the total risk for such projects.

De Morgan's rule is commonly used to adjust total risk where the risk from multiple PFMs is summed in a system. However, improved mathematical methods are still needed to define independent from dependent failure modes to avoid double counting and more accurately sum complex systems of failure modes to estimate total risk. For example, based on dam or levee failure statistics, how likely are multiple breaches to occur simultaneously for a given consequence center and does the total risk systematically depend on the number of critical failure modes under consideration? Should they be weighted and summed the same if only two or if two hundred failure modes are considered? More work is needed to investigate best methods for rolling up risk when length effects are considered and when improbable simultaneous events may be included in the total risk computation.

18.3 Conclusions

Risk assessments have found wider usage in engineering practice during the past 50 years in the USA. Techniques have more recently been develop for application of risk assessments in the dam and levee safety fields, but there is further research needed to further refine these methods. Risk assessments can be employed for screening level work, such as a potential failure mode analysis or semiquantitative risk assessment to identify and quickly assess the most likely and most damaging failure modes. Alternatively, risk assessments can be employed to guide risk management decisions for projects with excessive risk, such as with a quantitative risk assessment. Although risk management activities have improved immensely with the advent of risk assessment methodologies, there are a number of areas where additional improvements would improve our ability to characterize and portray risk.

References

Bowles DS, Chauhan SS, Anderson LR, Grove RC (2012) 2012 – Baseline risk assessment for Herbert Hoover Dike. ANCOLD proceedings of technical groups. http://www.ancold.org.au/?product=2012-baseline-risk-assessment-for-herbert-hoover-dike

Clibborn LCJ (1902) Experiments on the passage of water through sand, Government of India technical paper no. 97. Thomason College, Roorkee

FERC (2005) Engineering guidelines for the evaluation of hydropower projects – chapter 14 dam safety performance monitoring program. Federal Energy Regulatory Commission, Washington, DC . http://www.ferc.gov/industries/hydropower/safety/guidelines/eng-guide.asp

NASA (2011) Probabilistic risk assessment procedures, guide for NASA managers and practitioners, NASA/SP-2011-3421, Second edn. NASA Center for AeroSpace Information, Hanover . http://www.hq.nasa.gov/office/codeq/doctree/SP20113421.pdf

NRC (1975) Reactor safety study: an assessment of accident risks in U.S. commercial nuclear power plants, WASH-1400, NUREG/75-014. Nuclear Regulatory Commission, Rockville

Reclamation-USACE (2015) Best practices in dam and levee safety risk analysis. U.S. Bureau of Reclamation, Denver . http://www.usbr.gov/ssle/damsafety/risk/methodology.html

USACE (2014) Safety of dams – policy and procedures, ER 1110-2-1156. U.S. Army Corps of Engineers, Washington, DC . http://www.publications.usace.army.mil/Portals/76/Publications/EngineerRegulations/ER_1110-2-1156.pdf?ver=2014-04-10-153209-550

Wellock T (2011) The reactor safety study: the birth, death and rebirth of PRA. NRC Historian blog, U.S.NRC. https://public-blog.nrc-gateway.gov/2011/11/15/the-reactor-safety-study-the-birth-death-and-rebirth-of-pra/

Chapter 19
Energy Geotechnics: Toward a Sustainable Energy Future

James M. Tinjum

Abstract Economic development over the past century has been powered largely by fossil fuels. Large, centralized coal plants provided the opportunity for increased population density and job growth, resulting in improved manufacturing capacity and prosperity. Our increasing use of oil allowed us to travel farther, transport goods faster, and develop innovative supply chains. However, not every country followed this same development pattern—30% of the world's rural population still lacks access to electricity per *The World Energy Outlook*. To put this into perspective, if those in India without electricity constituted the populace of a country, it would be the fourth largest in the world. Without electricity, many people are denied many necessities and luxuries, one of these being access to the wealth of information via the Internet. Providing clean energy that enables economic development and lifts communities to a better living standard while protecting the climate is the seminal challenge for a world of nearly ten billion people. This paper showcases the use of large-scale, energy production from wind and efficiency offered by geothermal exchange by highlighting the use of applied wind energy geotechnics and thermal geotechnics—both of which are elements of the emerging discipline of *Energy Geotechnics*.

Keywords Geothermal exchange • Energy geotechnics • Wind balance of plant • District-scale geothermal • Turbine foundation

19.1 Introduction

From 2000 to 2010, world energy consumption increased by 23% and is projected to grow by 56% between 2010 and 2040 (EIA 2013). Meanwhile, the burning of fossil fuel has been directly tied to the exponential increase that has occurred in atmospheric CO_2 levels since the Industrial Revolution (Etheridge et al. 1996). Fossil fuels (coal, petroleum, and natural gas) are burned to produce 80% of world's

J.M. Tinjum (✉)
University of Wisconsin-Madison, 432 N Lake St, Madison, WI 53706, USA
e-mail: jmtinjum@wisc.edu

G.L. Sivakumar Babu et al. (eds.), *Geoenvironmental Practices and Sustainability*, Developments in Geotechnical Engineering,
DOI 10.1007/978-981-10-4077-1_19

energy, and 77.5% of that is produced in the USA. CO_2 concentrations are now at a record high of 397 parts per million (Tans and Keeling 2014), and, at the current growth rate, the burning of fossil fuels alone is projected to increase emissions by 46% by 2040 (EIA 2013). Extensive climate research has demonstrated the connection between increased CO_2 concentrations and global temperature rise, shifting rainfall and snowfall patterns, and extreme climate events, among other effects (EPA 2013). The superposition of these issues and concerns has created an urgent, worldwide call to develop innovative renewable energy solutions and integrate them into all sectors of society. The World Economic Forum (2012) has determined that, to meet the United Nations' goal to mitigate the effects of global warming, $700 billion must be spent annually on renewable power, low-carbon transport, and energy efficiency research and technology implementation.

Wind Energy Geotechnics Wind energy is one of the fastest growing sectors of renewable energy in the USA. In 2015, wind turbines generated 4.7% of the total electricity used in the USA, which is equivalent to the annual electricity use of about 17 million households (EIA 2016). This growth in wind energy production has been fueled by the increase in the number of in-service turbines, the capacity and size of turbines, and improvements in the average electrical energy produced by wind turbines. This trend is predicted to continue in the foreseeable future, and the anticipated rated capacity of wind turbine generators (WTGs) will be greater than 5 MW by the end of the decade (Fig. 19.1a – IEA 2013). Recent publication of USEPA's Clean Power Plan (40 CFR Part 60) will accelerate the trend of increased wind energy penetration as the USEPA has established state-specific interim and final reductions in emissions of CO_2 from electrical power plants by 2022 and 2030, respectively.

WTG structures are typically supported on massive octagonal gravity-based foundations (Fig. 19.1b). The size of these shallow foundations is proportional to the capacity of WTGs and height of the tower (Morgan and Ntambakwa 2008). For example, an increase in the generation capacity of a WTG from 1.5 to 3.0 MW may require an increase in the concrete volume of the foundation from 180 to about 350 m^3. This foundation size is required to accommodate greater overturning moments as determined by design approaches that in most cases are overconservative and developed from conventional design of shallow footings (Fig. 19.2). In addition to increasing the foundation cost, manufacture of Portland cement contributes significantly to global GHG emissions (about 5% – Rubenstein 2012). That is, part of the benefits obtained by using a clean energy source such as wind energy would be offset by using more concrete and steel for the construction of the infrastructure. Despite the rapid increase of the sizes of the shallow WTG foundations and special design considerations such as foundation stiffness, engineering models used to assess the stress and strain distributions under the foundations have not been updated and still do not fully characterize the response of foundation soils (Cerato and Lutenegger 2007; Svensson 2010) as required for WTGs. This lack of characterization, understanding, and modeling of foundation soil responses under massive shallow foundations used in WTG structures leads to overconservative

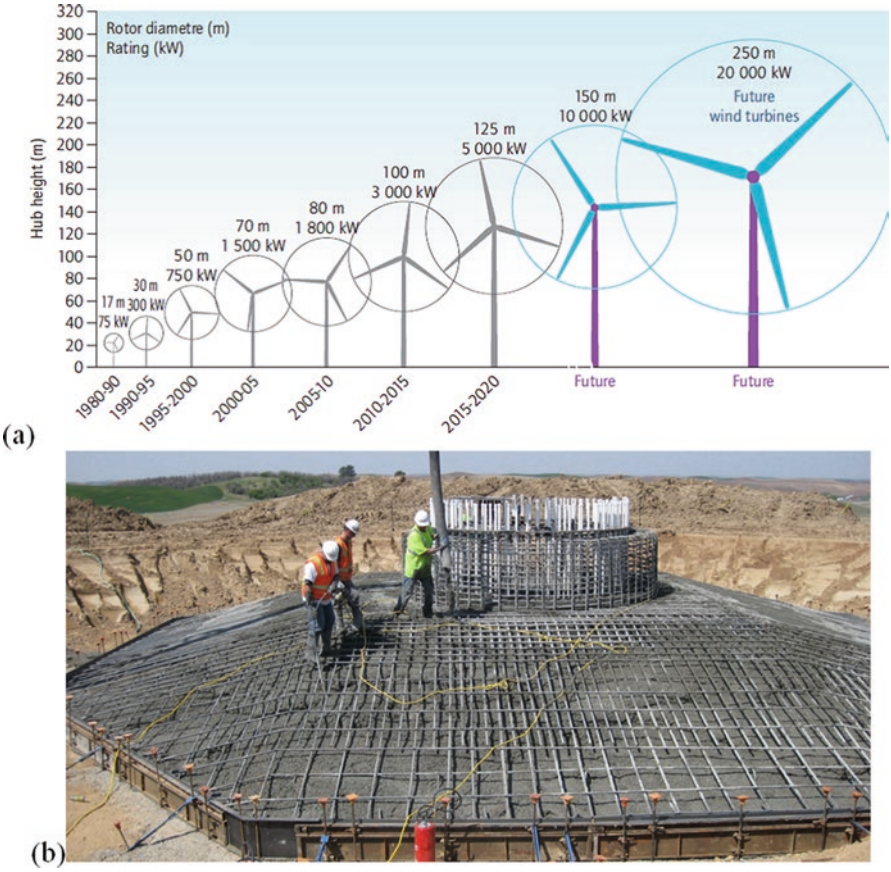

Fig. 19.1 (**a**) Size increase of wind turbines from 1980 to 2020 (IPCC 2011) and (**b**) shallow foundation of a typical WTG

designs that affect financial and sustainable development of wind energy infrastructure. Therefore, a life-cycle analysis of the system may make this alternative energy system less attractive (Rajaei and Tinjum 2013). The development of a framework for mechanistic-based design of WTG foundations requires answering scientific and engineering questions that will advance research in soil dynamics, unsaturated soil mechanics, and foundation engineering.

Geothermal Exchange Presently, space heating and cooling accounts for 48% of energy use worldwide; when the energy used to heat water is included, this figure rises to 66% in the USA (EIA 2009). Burning fossil fuels such as natural gas for heating applications directly contributes to GHG emissions. Ground-source heat pump (GSHP) systems use the thermal energy stored in the Earth and can be applied nearly anywhere to create an environmentally friendly, low-cost, and sustainable source for heating and cooling. With the adoption of innovative GSHP systems, the

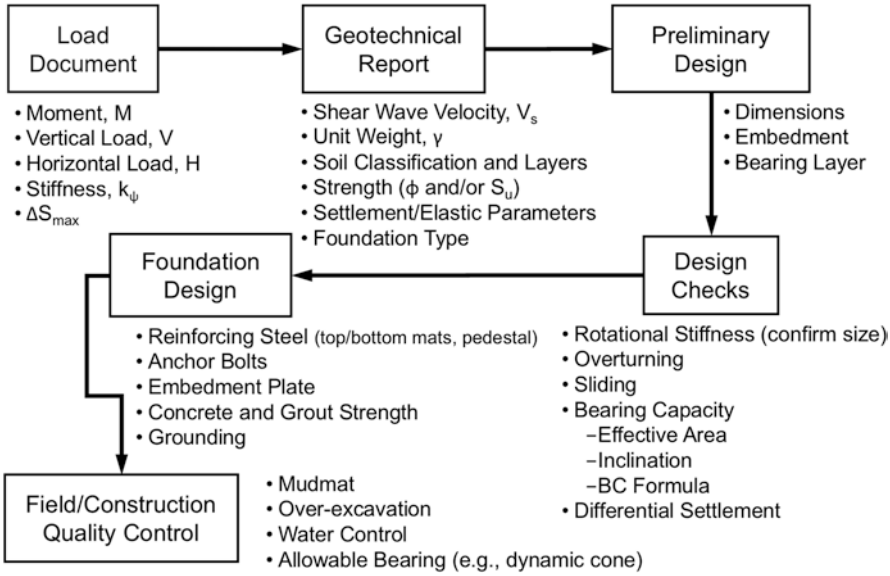

Fig. 19.2 General design flow for a WTG foundation (Tinjum and Lang 2012)

USA would reduce the demand for conventional sources of energy. Adopting this technology also increases economic development because the systems are typically designed, drilled, manufactured, and installed using domestic resources, labor, and talent. A GSHP system can reduce GHG emissions by as much as 44%, as compared to a conventional air-source heat pump, up to 72% in comparison to electric resistance heating, and almost 40% in comparison to a conventional gas boiler (Jenkins et al. 2009; EPA 2013). Equipping 100,000 homes with GSHP systems would reduce oil consumption by 2.15 million barrels per year (EPA 2013).

A GSHP can be applied anywhere, even in areas of low geothermal gradient (ASHRAE 2011). GSHP systems rely on a relatively constant subsurface temperature to about 50 m deep (Hart and Couvillion 1986). Within the near surface, the subsurface temperature will be higher than that of ambient air in the winter and lower in the summer and will remain relatively constant—the result of homeostatic heat flux entering the ground from above (the sun) and below (radioactive decay within the earth's interior). In the shallow subsurface (<10 m deep), the temperature fluctuates due to the atmospheric boundary. At depths greater than 50 m, temperature approaches the natural geothermal gradient of about 30 °C/km (Grant et al. 1982).

Vertical GSHPs are low-enthalpy systems used for space heating and cooling, and they range in depth from 23 to 150 m with a diameter between 0.075 and 0.15 m (Diao et al. 2004; NRC 2009). GSHP systems typically include ground-heat exchangers (GHXs) that involve a sealed loop of U-pipe made of high-density polyethylene (HDPE) that is buried in the ground and connected to a heat pump through which a carrier fluid is circulated. When space is limited, as occurs with district-scale systems or in urban areas, a vertical borehole configuration is usually

preferred over a horizontal trench system because less area is required to provide the same heat transfer (Wu et al. 2014). In residential systems, boreholes are rarely deeper than 100 m because drilling deeper through bedrock becomes increasingly more difficult. In the USA, the space between the GHX and the borehole is grouted to provide better thermal contact between the pipe and the surrounding soil/rock and to prevent groundwater contamination. The closed-loop system delivers relatively warm (or cool) carrier fluid to water-air or water-water heat exchangers that are used to regulate building temperature.

The coefficient of performance (COP) of a properly designed and installed GSHP system will be three or greater, meaning that for every 1 $kWh_{electricity}$ put into the system, ≥3 kWh_{heat} will be produced (or ejected). This higher COP results because the GSHP system maintains a source/sink earth temperature that remains roughly constant, as compared to the variable air temperature. In addition, water has a relatively high capacity to hold heat and can therefore transfer heat more efficiently, resulting in a system with greater heat transfer ability than that of an air-source heat pump. GSHP systems transfer heat rather than generate heat and can provide an equivalent temperature environment for as little as one quarter of the cost of operating a conventional heating, ventilating, and air-conditioning (HVAC) system. Although the number of commercial and residential GSHP installations is expected to continuously grow (Akella et al. 2009; Lo Russo et al. 2009; Blum et al. 2010), these systems are still not widely used in comparison to conventional HVAC systems because of the higher initial costs associated with installation (drilling), the borefield space requirements, the limitations in installation and business planning infrastructure, and a lack of reliable system design and tools (Hughes 2008).

19.2 Instrumented Field Sites

Wind Turbine Generator Foundation Contact pressure cells and soil deformation meters were installed under a WTG foundation prior to construction at two sites located in the Midwest region of the USA (Fig. 19.3). The instrumentation at the two sites is identical and used the predominant wind direction at the WTG site for positioning the gauges. The behavior of soil underlying the foundations under vertical (static) and horizontal (dynamic) loadings has been monitored for over 3 years, with long-term monitoring continuing. The distribution of stress and strain both in plan and in depth is being investigated.

Pressure Measurement System Nine hydraulic contact earth pressure cells (Geokon Model 3500 Earth Pressure Cell) were installed as shown in Fig. 19.3a. Five sensors were oriented along the predominant wind direction axis. Two pressure cells (PG) were installed along two lines 70° from the predominant wind direction to measure contact stress distribution under the WTG foundation. Nine shallow excavations (>0.2 m in width and approximately 0.03 m in depth) were dug below foundation grade, and the pressure cells were carefully placed into these pockets.

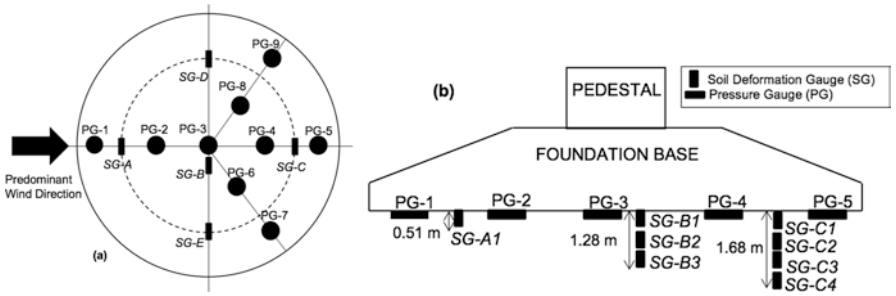

Fig. 19.3 Instrumentation layout underlying WTG foundation: (**a**) plan view and (**b**) cross-sectional view

Soil Strain Measurement System Ten soil deformation gauges (Geokon 4430 vibrating wire deformation meters) were installed beneath each WTG foundation. The main purpose of the soil strain gauges (SG) was to measure the deformation of the underlying soil at different locations and depths. The instruments can measure displacement up to 12.5 mm, and the total length of the deformation meter is 300 mm; thus, the maximum strain measurement is 4.17%. Soil strain gauges were also installed in consideration of the predominant wind direction. Eight deformation gauges were installed along the predominant wind direction axis, and two were placed perpendicular to the predominant wind direction. Three deformation gauges were located at the center of the foundation at different depth, and four were placed at varying depths on the leeward site as shown in Fig. 19.3b.

District-Scale Geothermal Exchange District-scale geothermal fields—which include closed-loop systems at Ball State University, Missouri School of Science and Technology, and Epic Systems in Wisconsin—may have 3000+ boreholes. Indeed, Epic's system has grown from 564 boreholes in 2006 to more than 6000 in 2016 (see Fig. 19.4) and achieves significant (40%) energy savings (Brandherm 2013). Epic operates a district-scale, cooling-dominated GSHP system that includes 25 km of underground piping, 12 ML of closed-loop, circulating water, and over 6150 in-service geothermal wells (100–160 m in depth), and the system has a capacity of 40 MW—enough energy to power 4000 homes. With Borefield No. 4 now on line, Epic expects its 9500-person campus to become energy neutral because of contributions from the company's solar fields, wind turbines, and GHX fields. This site provides an opportunity to create a *natural laboratory* with a great number of research advantages. The facility is well monitored to allow the proper evaluation of the energy balance; has been operational for more than 5 years; includes complex, near-surface geology; and an innovative company that actively seeks to enhance the system's performance and sustainability operates it. Recently, we have drilled and instrumented two 150-m-deep GHX wells (standard U-loop and pipe-within-pipe loop), six internal sentry wells, and five external monitoring wells that will accommodate several different devices that will keep track of borehole geophysics and

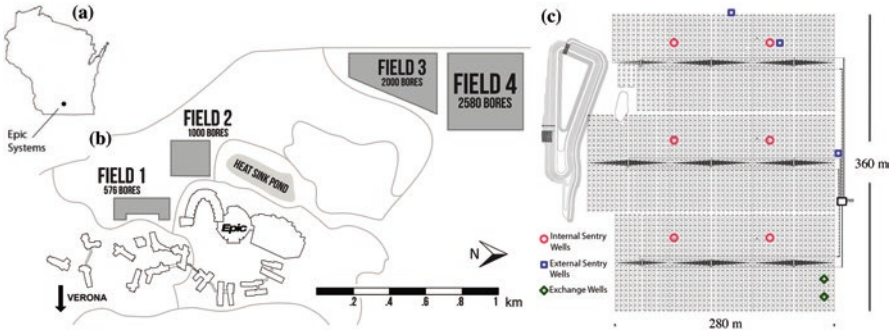

Fig. 19.4 Site: (**a**) Geographic location, (**b**) district-scale geothermal exchange fields relative to campus, and (**c**) Borefield No. 4 layout and monitoring points

allow for fiber-optic distributed temperature sensing (DTS) arrays to monitor site performance (Fig. 19.4c).

19.3 Conclusions

Energy Geotechnics is an emerging discipline in which geotechnical and geological engineers, geologists, and other scientists/engineers employ the principles of engineering physics and soil mechanics for the advancement of energy systems. At our project sites, diverse teams of students, faculty, and industrial partners are working on field, laboratory, and modeling research to study foundation soil response for wind turbine generators and heat transfer in district-scale geothermal exchange fields. To date, we have engaged over 30 undergraduate and graduate students and introduced them to academic research related to energy geotechnics. Some of the unique techniques and studies developed at these field sites include the interpretation of borehole geophysical results, distributed thermal response and temperature sensing systems, measurement of thermal conductivity of rocks and soils, and life-cycle analysis of GHG emissions for both wind energy and geothermal exchange sites.

References

American Society of Heating, Refrigerating and Air-Conditioning Engineers (ASHRAE) (2011). HVAC applications handbook. Chapter 34, Geothermal energy

Akella AK, Saini RP, Sharma MP (2009) Social, economical and environmental impacts of renewable energy systems. Renew Energy 34(2):390–396

Blum P, Campillo G, Munch W, Kolbel T (2010) CO_2 savings of ground source heat pump systems – a regional analysis. Renew Energy 35(1):122–127

Brandherm B (2013) Personal communication with James Tinjum

Cerato A, Lutenegger A (2007) Scale effects of shallow foundation bearing capacity on granular material. J Geotech Geoenviron Eng 133(10):1192–1202

Diao N, Li Q, Fang Z (2004) Heat transfer in ground heat exchangers with groundwater advection. Int J Therm Sci 43(12):1203–1211
Energy Information Administration (EIA) (2009) Residential energy consumption survey (RECS). Energy Information Administration (EIA), Washington, DC
Energy Information Administration (EIA) (2013) International energy outlook. Energy Information Administration (EIA), Washington, DC
Energy Information Administration (EIA) (2016) Electricity net generation from renewable energy by energy use sector and energy source. Energy Information Administration (EIA), Washington, DC
Environmental Protection Agency (EPA) (2013) Inventory of U.S. greenhouse gas emissions and sinks: 1990–2011. U.S. Environmental Protection Agency, Washington, DC
Etheridge D, Steel L, Langenfelds R, Francey R, Barnola J, Morgan V (1996) Natural and anthropogenic changes in atmospheric CO_2 over the last 1000 years from air in the Antarctic ice and firn. J Geophys Res Atmos 101(D2):4115–4128
Grant MA, Donaldson IG, Bixley PF (1982) Geothermal reservoir engineering. Academic, San Diego, 369 p
Hart DP, Couvillion R (1986) Earth-coupled heat transfer. National Water Well Association, Dublin, 192 p
Hughes PJ (2008) Geothermal heat pumps: market status, barriers to adoption, and actions to overcome barriers. Oak Ridge National Laboratory/U.S. Department of Energy, Oak Ridge, 42 p
International Energy Agency (IEA) (2013) Technology roadmap–wind energy. http://www.iea.org/publications/freepublications/publication/Wind_2013_Roadmap.pdf. Accessed 15 Feb 2015.
IPCC (2011) Report from the Intergovernmental Panel on Climate Change. Cambridge University Press, Inc., New York
Jenkins D, Tucker R, Rawling R (2009) Modelling the carbon-saving performance of domestic ground-source heat pumps. Energy Buildings 41:587–595
Lo Russo S, Boffa C, Civita MV (2009) Low-enthalpy geothermal energy: an opportunity to meet increasing energy needs and reduce CO_2 and atmospheric pollutant emissions in Piemonte, Italy. Geothermics 38(2):254–262
Morgan K, Ntambakwa E (2008) Wind turbine foundation behavior and design considerations. AWEA WINDPOWER conference, Houston, TX, pp 1–14
National Resources Canada (NRC) (2009) Heating and cooling with a heat pump. http://oee.nrcan.gc.ca/publications/residential/heating-heatpump/7158: Office of Energy Efficiency
Rajaei M, Tinjum JM (2013) Life cycle assessment of energy balance and emissions of a wind energy plant. Geotech Geol Eng 31(6):1663–1670
Rubenstein M (2012) Emissions from the cement industry. State of the Planet. Columbia University. URL: http://blogs.ei.columbia.edu/2012/05/09/emissions-from-the-cement-industry/. Accessed on 31 Aug 2015
Svensson H (2010) Design of foundations for wind turbines. MS thesis, Division of Structural Mechanics, LTH, Lund University, Box 118, SE-221 00 Lund, Sweden
Tans P, Keeling R (2014) Recent monthly average Mauna Loa CO_2. National Oceanic and Atmospheric Administration/ESRL (www.esrl.noaa.gov/gmd/ccgg/trends/) Scripps Institution of Oceanography
Tinjum JM, Lang P (2012) Wind energy geotechnics. Geo Strata 2012:18–26
World Economic Forum (2012) Global competitiveness report 2012–2013. http://www3.weforum.org/docs/WEF_GlobalCompetitivenessReport_2012-13.pdf
Wu R, Tinjum J, Likos W (2014) Finite-element modeling of coupled heat and moisture transfer in unsaturated soils for shallow horizontal geothermal ground loops. Geotech Geol Eng. doi:10.1007/s10706-014-9811-2

Chapter 20
Performance Evaluation of Coal Ash-Based Barriers of Landfill Covers

B.V.S. Viswanadham

Abstract The objective of this paper is to evaluate the performance of coal ash-based barriers subjected to continuous differential settlements in a geotechnical centrifuge. Motor-based differential settlement simulator was used to induce differential settlements with a distortion level up to 0.125 at 40 gravities in a 4.5 m radius large beam centrifuge facility available at the Indian Institute of Technology Bombay, India. A short series of centrifuge model tests were conducted by varying the thickness of coal ash-based barriers. All the developed coal ash-based barriers were subjected to an overburden of 25 kN/m^2 equivalent to that of the landfill cap covers. All the models were thoroughly instrumented with linearly variable differential transformers (LVDTs) and Pore pressure transducers (PPTs) to measure vertical settlements and pore water pressure. Digital image cross-correlation (DIC) technique was adopted to arrive at deformation profiles of coal ash-based barriers and strain distribution along the topmost surface of the tested barrier during all settlement stages. The water sealing efficiency was assessed in terms of limiting distortion level and strain at water breakthrough. A 0.6 m-thick coal ash-based barrier with an overburden of 25 kN/m^2 was observed to experience a limiting distortion level of 0.068 and a strain at breakthrough of 0.98%. In comparison, a 1.6 m-thick coal ash-based barrier has not registered any water breakthrough and been noted to sustain large deformations. This centrifuge study demonstrates that coal ash-based barriers of an adequate thickness can be used as impervious barriers in landfill cap covers.

Keywords Coal ash • Landfills • Covers • Model tests • Centrifuge modelling

B.V.S. Viswanadham (✉)
Department of Civil Engineering, Indian Institute of Technology Bombay, Powai, Mumbai 400 076, India
e-mail: viswam@civil.iitb.ac.in

G.L. Sivakumar Babu et al. (eds.), *Geoenvironmental Practices and Sustainability*, Developments in Geotechnical Engineering,
DOI 10.1007/978-981-10-4077-1_20

20.1 Introduction

Because of their low hydraulic conductivity and high adsorption capacity, compacted clay soils are traditionally used in landfill waste containment systems. The desirable characteristics, such as low hydraulic conductivity, of a clay-based barrier of landfill waste containment systems may change due to ongoing bio-decomposition of the municipal solid waste and temperature and moisture fluctuations. Furthermore, clay barrier materials can also be susceptible to chemical attack by permeating contaminants (Kaya and Durukan 2004). Two predominant causes of failures of clay barriers are (1) desiccation cracking due to moisture fluctuations and (2) cracking due to excessive differential settlements. Imperviousness of clay barriers is essential, especially in municipal solid waste landfills and cap covers of low-level radioactive waste containment sites. The problem of cracking of clay barriers of waste containment systems was addressed by several investigators through a variety of research efforts. Morris et al. (1992) and Miller et al. (1998) have reported that the hydraulic conductivity of clay barriers having desiccation cracks has increased considerably. In addition, especially in compacted clayey soils at low overburden, thermally induced moisture changes in the clay barrier can cause a reduction in plastic deformability and desiccation cracks. Differential settlement of clay-based cap covers is caused by MSW stored in landfills undergoing bio-decomposition and the collapse of cavities within the waste or between waste packages or toppling of waste containers (Gourc et al. 2009). Differential settlement and subsidence can result in a catastrophic loss of performance of the landfill cap covers. Excessive differential settlements can result in tension cracks in the zone of sharp curvatures, thereby resulting in loss of integrity of the cap cover system.

Sometimes, it may be difficult to obtain clay barrier materials having the physicochemical characteristics mentioned above to be used as a landfill barrier with low cost. In such situations, the use of coal ash-based barriers in waste containment systems is a viable option. Large quantities of coal ashes are being produced by coal-fired thermal power plants all over the world. The need of the day is to have practical engineering applications which involve the safe disposal of such so considered hazardous materials. Coal ashes have been shown to have beneficial properties such as low specific gravity, lower compressibility, higher rate of consolidation, high strength, high California bearing ratio, high volume stability, water insensitiveness to compaction and pozzolanic reactivity. Coal ash has been used successfully as a structural fill material for constructing highway embankments throughout the world (Faber and Digioia 1976; Toth et al. 1988; Chand and Subbarao 2007). To date, very few studies have been conducted to evaluate the potential engineering applications of coal ash as landfill liners/waste containment systems (Bowders Jr. et al. 1987; Edil et al. 1987; Prashanth et al. 2000; Kaya and Durukan 2004; Cokca and Yilmaz 2004). In some cases, hydraulic conductivity values less than 10^{-7} m/s have been measured in the laboratory on the specimens of coal ash and stabilized fly ash, with differences in hydraulic conductivity values being attributed to the type

and amount of fly ash (ASTM Class C or F), admixture and/or stabilizer, among other factors. Prashanth et al. (2000) studied the potential of a pozzolanic coal ash as a hydraulic barrier in landfill liners. They evaluated the shrinkage, compaction, permeability, consolidation and strength characteristics of three different coal ashes. Kaya and Durukan (2004) studied the utilization of bentonite-embedded zeolite (BEZ) as a clay liner. Adsorption characteristics, cation exchange capacity, volumetric shrinkage, compaction characteristics and hydraulic conductivity of the mixtures were investigated. It was also found that the hydraulic conductivity of BEZ with 10% bentonite is less than 1×10^{-9} m/s. Cokca and Yilmaz (2004) studied the feasibility of utilizing coal ash, rubber and bentonite as a low permeability liner material. Hydraulic conductivity, leachate analysis, unconfined compression, split tensile strength, one-dimensional consolidation, swell and freeze/thaw cycle tests were performed. It was found that hydraulic conductivity increases as rubber percent increases and bentonite content decreases. Coal ash with up to 10% rubber and 10% bentonite was found to be suitable for construction of a liner.

Considering the requirement of a new landfill barrier material, a barrier material comprising 80% coal ash blended with 20% bentonite (by dry weight) was formulated. The performance of coal ash-based barriers having two different thicknesses (0.6 and 1.6 m) subjected to continuous differential settlements was evaluated in a 4.5 m radius large beam centrifuge available at the IIT Bombay, India. Motor-based differential settlement simulator developed at the IIT Bombay was used to induce differential settlements with a distortion level up to 0.125 at 40 gravities. During centrifuge testing, the centripetal acceleration is induced on a small-scale model, thereby increasing the unit weight of the soil, so as to make the identical stress-strain behaviour of the soil in the model and prototype. Thus, the centrifuge modelling technique can be adopted to assess the response of coal ash barriers to continuous differential settlements simulated in a centrifuge.

20.2 Centrifuge Model Tests on Coal Ash-Based Barriers

20.2.1 Development of Coal Ash-Based Barrier

20.2.1.1 Coal Ash

The coal ash used in the present work was collected from an ash pond dam in Kahalgaon thermal power plant in the Bihar state in India and is classified as ASTM Class F coal ash according to Sridharan et al. (2000). It has an average particle size of 0.09 mm, coefficient of uniformity of 32.5 and coefficient of curvature of 0.931 and is classified as ML according to the Unified Soil Classification System. The coefficient of permeability of coal ash was found to be 1.61×10^{-7} m/s.

20.2.1.2 Bentonite

The sodium-based bentonite used in the model tests was obtained from a company in the State of Gujarat in India. The X-ray diffraction spectra show that it is predominantly a montmorillonite with magnetite, hematite, anatase, calcite and kaoline traces and chemical composition of bentonite determined by X-ray fluorescence spectroscopy, which also confirms the presence of sodium-based montmorillonite. The clay content in the bentonite was found to be 86%, as per the methylene test. The specific gravity of the bentonite was found to be 2.94. The liquid limit and the plasticity index are 395% and 353%, respectively.

20.2.1.3 Properties of Bentonite-Blended Coal Ash

Considering the need for ensuring the permeability less than 1 x 10^{-9} m/s, several blends of coal ash and bentonite were tried. Coal ash content varied from 90% to 80%. The coal ash content signifies the percentage of dry weight of coal ash with respect to total dry weight of combined mixture. In this paper, results of 80% coal ash blended with 20% bentonite (by dry weight) were reported. Bentonite-blended coal ash was found to have a liquid limit of 81% and plasticity index of 36%. The maximum dry unit and optimum moisture content (according to the standard Proctor compaction) are 13.74 kN/m^3 and 20.94%, respectively, and the bentonite-blended coal ash is classified as CH according to the Unified Soil Classification System. The swell potential of the bentonite-blended coal ash was found to be 10% under a normal stress of 25 kPa, and the coefficient of permeability determined by performing falling head tests in an oedometer in the laboratory was found to be 1x10^{-9} m/s. The falling head permeability test was conducted after subjecting bentonite-blended coal ash sample for swelling for about 7 days under a normal stress of 25 kPa, and then falling head permeability tests were carried out over a period of 7 days. This was carried out considering the presence of bentonite in bentonite-blended coal ash and the presence of normal stress in the form of overburden in the cover of the order of 25 kPa.

20.2.1.4 Model Test Package

A strong box having internal dimensions of 720 mm in length, 450 mm in width and 440 mm in height was used in the present study. A transparent Perspex glass sheet of 50 mm thickness placed towards the front side of the container enabled to view the model during flight. The motor-based differential settlement simulator developed at the IIT Bombay was used in the present study (Rajesh and Viswanadham 2010). The MDSS system works on a simple mechanism in which the rotational movement is converted to translational movement. It comprises of a motor, controller, screw jack, central platform, gear trains, connecting shaft and bearings. It has a capability of inducing a maximum central settlement of 25 mm with a distortion

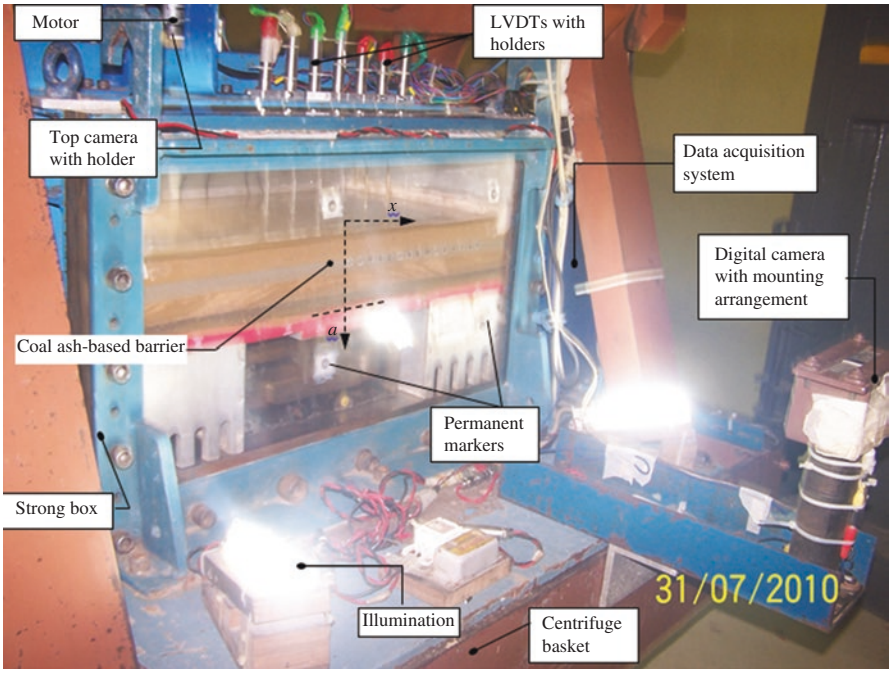

Fig. 20.1 Model test package mounted on the swing basket

level (defined as a central settlement over an influencing length) of 0.125. After placing the MDSS within the strong box, the surface area of the coal ash-based barrier is 720 mm in length and 360 mm in breadth, and this corresponds to 415 m^2 in the field at 40 gravities. Figure 20.1 shows the perspective view of the model test package mounted on the swing basket. Details of the model test package are given by Viswanadham (2012). Various accessories like data acquisition system, digital photo camera to view front elevation of the model and illumination arrangement can be noticed.

Model preparation commences with the placement of side, rear and central support system within the strong box and provision of non-woven geotextile sheet strips and bentonite paste on all around the sides of the container. A 30 mm-thick coarse sand layer followed by a 30 mm-thick fine sand layer was placed in dry state by raining technique at a relative density of 55%. These layers were introduced to eliminate stress concentration, which may arise due to abrupt discontinuity at hinge locations. These layers are referred herein as sacrificial layers. The sacrificial sand layers are pre-saturated and drained for about 9–10-h duration in 1 g. The coal ash-bentonite mixture was moist-compacted towards the wet side its optimum and corresponding dry unit weight. Figure 20.2 shows the plan view of the various stages of construction of a coal ash-based barrier blended with 20% bentonite. This blend was selected according to Viswanadham (2012). In order to avoid the leakage of water between sides of the container and the coal ash-based barrier, a water tight

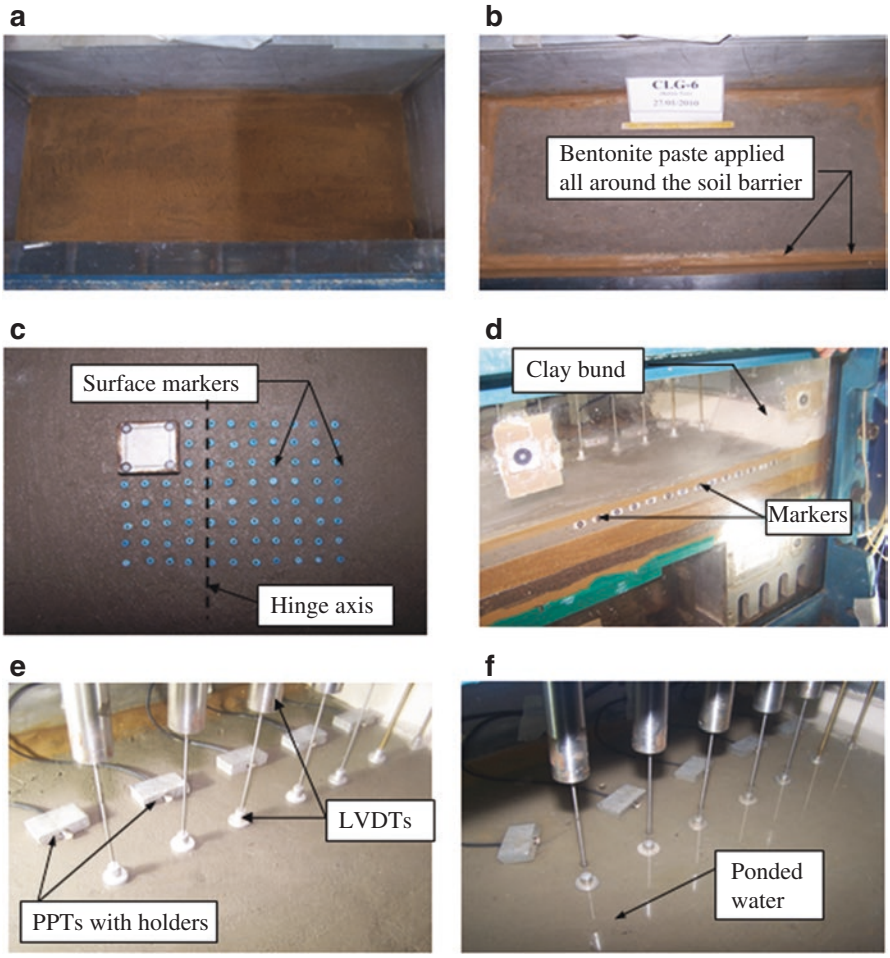

Fig. 20.2 Plan view of various stages of constructing coal ash-based soil barrier. (**a**) Stage 1 (pre-saturated and drained sand layers), (**b**) Stage 2 (compaction of coal ash-based barrier), (**c**) Stage 3 (placement of markers on the surface of coal ash-based barrier), (**d**) Stage 4 (preparation of bund on both sides along with placement of markers), (**e**) Stage 5 (placement of PPTS), (**f**) Stage 6 (ponding with water on the coal ash-based barrier)

seal made out of a thick bentonite paste was applied all along the sides of the soil barrier (Stages 2 and 4). Markers were placed along the surface of the coal ash barrier to measure integral displacements of these markers during various stages of the test. A 20 mm square grid of markers was placed on the model coal ash barrier surface along the zone of maximum curvature, as shown in Fig. 20.2e. Five pore pressure transducers (PPTs) were placed above the prepared coal ash barrier surface for measuring the water breakthrough at the onset of differential settlements. Further, seven LVDTs were placed above the coal ash barrier surface (or on the sand

placed for overburden pressure) to measure the deformation profiles at various stages of central settlement (Stages 5 and 6). One digital camera was placed to view the right-hand portion of front elevation of the model, and one CCD camera was placed to view the portion of the top surface of the coal ash barrier to monitor the performance during the centrifuge test.

In the present study, thickness of the coal ash-based barrier selected is 0.6 m and 1.6 m. Since, in the present study, the gravity level was fixed at 40 g, a 1.6 m-thick coal ash-based barrier in the prototype scale was modelled as 40 mm-thick model coal ash-based barrier layer. In majority of landfill sites, thickness of the cover soil and water drainage layer placed above the soil barrier in the cover system ranges from 1 to 1.5 m. This cover soil can induce an overburden pressure of 25 kPa. In order to observe the effect of overburden on the deformation behaviour of coal ash-based barriers, overburden pressure was maintained at 25 kPa. This was achieved by pluviating dry sand of 27 mm thickness with a dry unit weight of 15 kN/m^3, and thereafter it was inundated with water up to 10 mm height above the sand surface. A settlement rate s_{rm} (in model dimensions) of 1 mm/min was maintained for all centrifuge tests performed using the MDSS system. The settlement rate may not be realistic when projected to the prototype dimensions, but to some extent represents excessive settlements near the drains in bioreactor landfills, localized depression or collapse of the waste containers or ground subsidence in waste disposal sites. The projected prototype settlement rate at 40 gravities (s_{rp}) is 36 mm/day. Figure 20.3 shows the front elevation of coal ash-based barrier during centrifuge test at 40 g. When the horizontal distance from centre of the coal ash-based barrier x is zero, the value of settlement is termed as a central settlement a (Fig. 20.3a), and it is referred herein as maximum central settlement a_{max}, if the induced central settlement equals to 25 mm.

The nature of induced deformation in the coal ash-based barrier can be explained using parameters like settlement ratio and distortion level. Settlement ratio, a/a_{max}, is defined as the ratio of central settlement a at any stage of deformation to the maximum central settlement a_{max}. Distortion level, a/l, is defined as the ratio of central settlement a to the influence length l within which differential settlements are induced (Fig. 20.3a). The influence length l is defined herein as a horizontal distance from the centre of the soil barrier to a point where induced settlements cease to be negligible. An influence length l which equals to 200 mm (in model dimensions) from the centre of the soil barrier was adopted uniformly in all centrifuge tests. This was fixed based on the measured deformation profiles in a number of tests. The MDSS setup can induce a maximum distortion level of 0.125 with a maximum strain value of 5%. Analysis and interpretation of centrifuge model tests are discussed in detail by Viswanadham (2012).

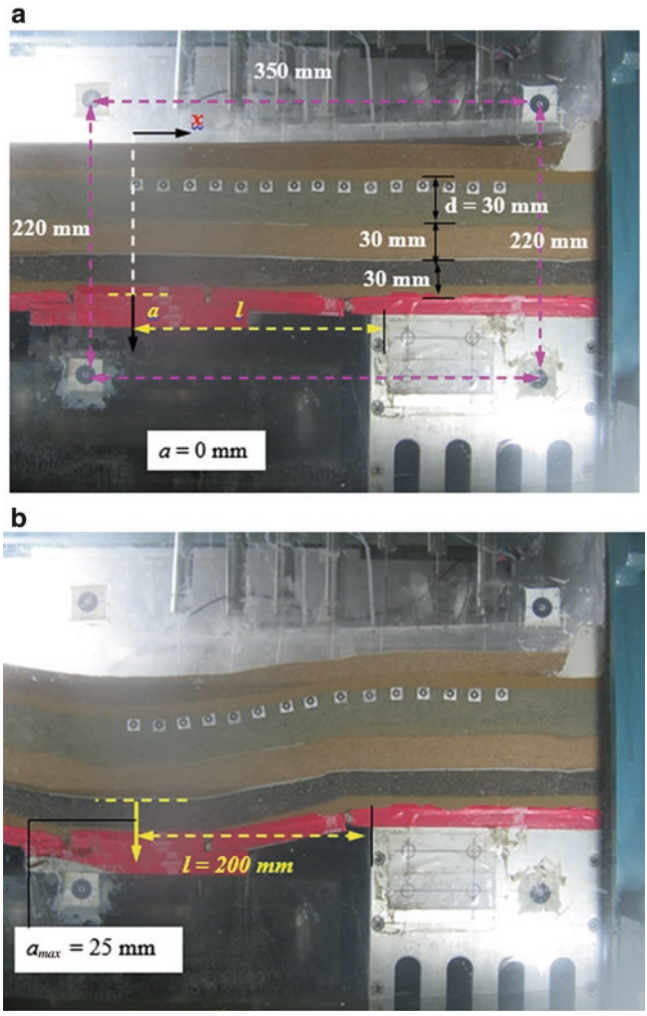

Fig. 20.3 Front elevation of model coal ash-based barrier at 40 gravities (**a**) Before inducing differential settlements, (**b**) After inducing differential settlements

20.2.2 Response of Coal Ash-Based Barriers to Induced Distortion

In this paper, an attempt had been made to evaluate the integrity and sealing efficiency of coal ash-based barriers subjected to differential settlements, by varying thickness of bentonite-based coal ash-based barriers (BCABs). In model CLG16a1, the thickness of a coal ash-based barrier is 15 mm (0.6 m at 40 g), and it is 40 mm (1.6 m at 40 g) for model CLG17. Figure 20.4a–b shows the variation of measured pore water pressure with time after attaining 40 g for models CLG16a1 and CLG17.

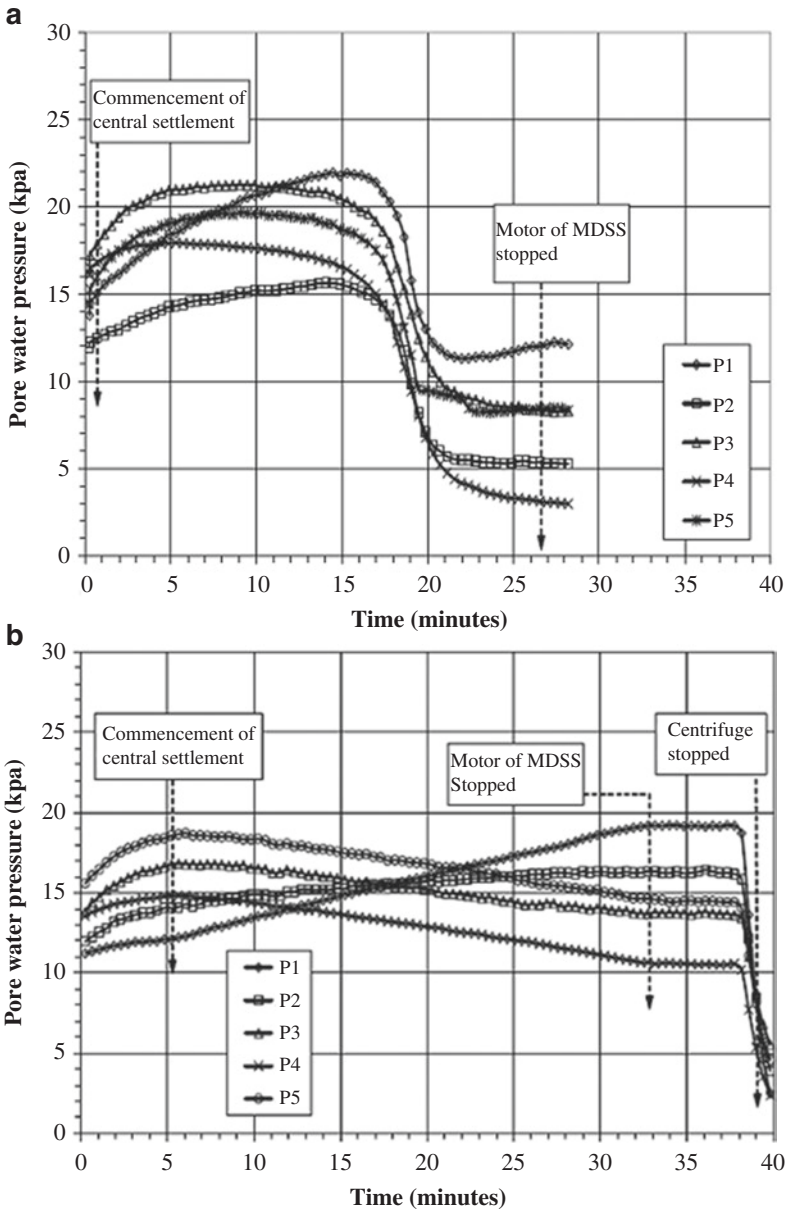

Fig. 20.4 Variation of pore water pressure with time in model dimensions for BCAB

With an increase in thickness from $d = 0.6$ to 1.6 m, a drastic change in variation of pore water pressure with time for model CLG17 can be noted. The presented variation in Fig. 20.4b indicates that 1.6 m-thick BCAB ensures sealing efficiency even after subjecting to distortion level of the order of 0.125 and is not subjected to any

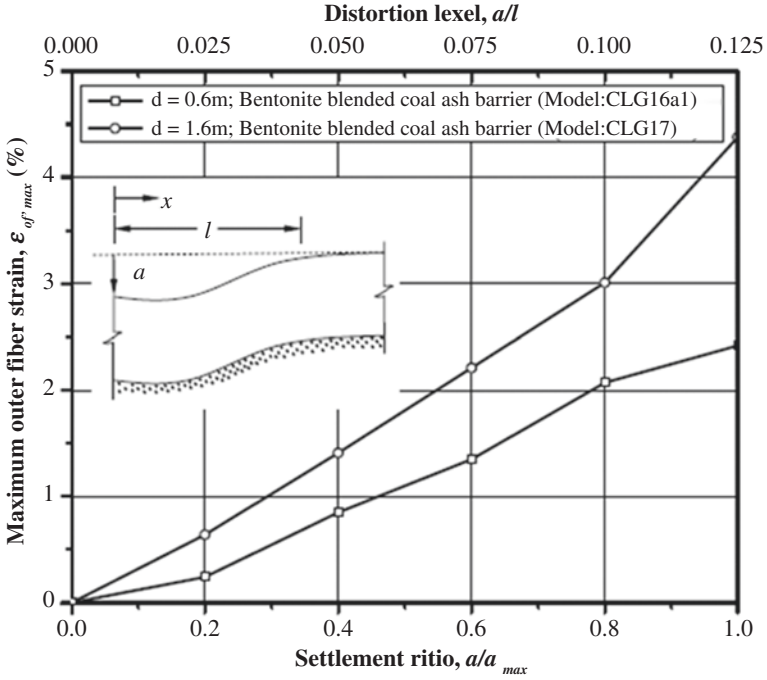

Fig. 20.5 Variation of $\varepsilon_{of,max}$ with a/l and a/a_{max}

leakage with the formation of full-penetration cracking at the zone of maximum curvature.

Figure 20.5 shows variation of maximum outer fibre strain, $\varepsilon_{of,max}$, along the top surface of coal ash barriers with a/l and a/a_{max}. As can be noted, with an increase in a/l and a/a_{max}, an increase in maximum outer fibre strain can be noted. During various stages of central settlements, photographs were captured at 40 gravities through an image-acquiring software and were later used for digital image cross-correlation (DIC) to establish deformation profiles of the coal ash-based barriers and for arriving at strain distribution along the top surface of coal ash barrier (Viswanadham 2012). The maximum value of strain at the zone of maximum curvature is referred herein as $\varepsilon_{of,max}$. Variation of infiltration ratio (IFR) with a/l and a/a_{max} is plotted in Fig. 20.6.

Infiltration ratio, *IFR*, is defined as the ratio of $(v_o - v_a)$ to v_o, where v_a is the volume of water at a particular central settlement and v_o is the volume of water above the BCAB surface $a = 0$ mm at 40 g.

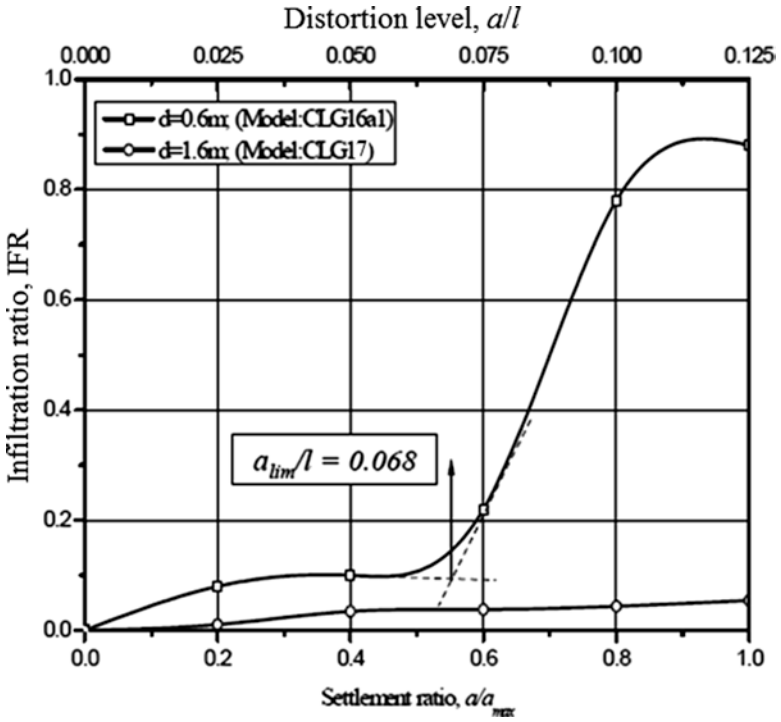

Fig. 20.6 Variation of IFR with a/l and a/a_{max}

20.3 Conclusions

In this paper, performance evaluation of coal ash-based barriers of landfill covers subject to differential settlements in a geocentrifuge is presented A 0.6 m-thick coal ash-based barrier with an overburden of 25 kN/m^2 was observed to experience a limiting distortion level of 0.068 and a strain at breakthrough of 0.98%. In comparison, a 1.6 m-thick coal ash-based barrier has not registered any water breakthrough and been noted to sustain large deformations. This centrifuge study demonstrates that coal ash-based barriers of adequate thickness can be used as impervious barriers of landfill cap covers.

Acknowledgements Thanks are to the Department of Science and Technology, Government of India, for sponsoring this project. The author would also like to thank laboratory staff at the National Geotechnical Centrifuge Facility, IIT Bombay, India, for their untiring support.

References

Bowders JJ, Usmen MA, Gidley JS (1987) Stabilized fly ash for use as low-permeability barriers. In: Woods RD (ed) Geotechnical practice for waste disposal 87. ASCE, New York, pp 320–333

Chand SK, Subbarao C (2007) Strength and slake durability of lime stabilized pond ash. J Mater Civil Eng ASCE 19(7):601–608

Cokca E, Yilmaz Z (2004) Use of rubber and bentonite added fly ash as a liner material. Waste Manag 24(2):153–164

Edil TB, Berthouex PM, Vesperman KD (1987) Fly ash as a potential waste liner. In: Woods RD (ed) Geotechnical practice for waste disposal 87. ASCE, New York, pp 447–461

Faber JH, Digioia AM Jr (1976) Use of fly ash in embankment construction. Transp Res Rec 593:13–19

Gourc JP, Camp S, Viswanadham BVS, Rajesh S (2009) Deformation behaviour of clay cap barriers of hazardous waste containment systems: full-scale and centrifuge tests. Geotext Geomembr 28(3):281–291

Kaya A, Durukan S (2004) Utilization of bentonite-embedded zeolites as clay liner. Appl Clay Sci 25(1–2):83–91

Miller CJ, Mi H, Yesiller N (1998) Experimental analysis of desiccation crack propagation in clay liners. J Am Water Resour Assoc 34(3):677–686

Morris HP, Graham J, Williams (1992) Cracking in drying soils. Can Geotech J 29(2):263–277

Prashanth JP, Sivapullaiah PV, Sridharan A (2000) Pozzolanic fly ash as a hydraulic barrier in landfills. Eng Geol 60(1–4):245–252

Rajesh S, Viswanadham BVS (2010) Development of a motor-based differential settlement simulator setup for a geotechnical centrifuge. Geotech Test J ASTM 33(6):507–514

Sridharan A, Pandian NS, Prasad PS (2000) Liquid limit determination of class F fly ash. J Test Eval ASTM 28(6):455–461

Toth PS, Chan HT, Cragg CB (1988) Coal ash as structural fill with reference to Ontario experience. Can Geotech J 25(4):694–704

Viswanadham, BVS (2012) Evaluation of coal ash as a potential liner for waste containment systems, Department of Science and Technology Report, Government of India

Chapter 21
Sustainability Analysis of the Vertical Barriers Based on Energy and Carbon Assessment for Leachate Containment

G.L. Sivakumar Babu and Mandeep Raj Pandey

Abstract Although there are well-established methods for economic (cost) estimation of any process, the estimation of the environmental and the social effects is relatively less understood and rarely incorporated in engineering calculations. In this paper, the effectiveness of different types of vertical barrier system for a present waste dump is compared in terms of the embodied energy (EE) and carbon emission in addition to the targeted service life. The model used for the assessment is streamlined energy and emission assessment model (SEEAM). The project involved constructing the vertical barrier around Bingipura fill in order to prevent the contamination of nearby water body due to the leachate from the waste dump. Different types of barriers are analyzed: sheet pile walls, concrete barriers, and the slurry-based cutoff walls (Na-bentonite). The performance analysis was carried out in the well-established software POLLUTEv7 which indicated the effectiveness of the sodium bentonite (Na-B) slurry wall and Soil-Bentonite backfill over other two for the leachate containment.

Keywords Barriers • Contaminant transport • Embodied energy • Carbon emission • Bentonite

21.1 Introduction

The environmental impacts of the waste dumps are adverse, and the effect they have can be directly seen on the environment and social aspects. Although measures are being carried out for the solution and though huge investments are being made, there still is problem of its effectiveness in long term. Sustainability has been a part of the first priority of ASCE codes since 1996 along with the following definition: "Sustainable development is the challenge of meeting human needs for natural resources, industrial products, energy, food, transportation, shelter, and effective waste management while conserving and protecting environmental

G.L. Sivakumar Babu (✉) • M.R. Pandey
Department of Civil Engineering, Indian Institute of Science, Bangalore 560012, India
e-mail: gls@civil.iisc.ernet.in; mandeeprp@yahoo.com

G.L. Sivakumar Babu et al. (eds.), *Geoenvironmental Practices and Sustainability*, Developments in Geotechnical Engineering,
DOI 10.1007/978-981-10-4077-1_21

quality and the natural resource base essential for future development." To come up with the construction processes and to comply with the principles of sustainable development are a challenge for the engineers. In this paper, we try to compare the three different containment systems: concrete barriers, slurry-based cutoff walls, and the sheet pile walls in terms of their efficiency and sustainability for their use in our present case study. Due to lack of any standard code, streamlined energy and emission assessment model (SEEAM) are used for the sustainability determination in terms of the energy consumption and CO_2 emission (Shillaber et al. 2015a).

21.2 Background

Achieving a goal of sustainability requires a balance between three interlinked dimensions: environment, society, and economy. In contrast to the previously defined model, in which the sustainability was defined as the intersection of the three components, economic, social, and environmental, the recent definition of sustainability emphasizes more on environment. When any project is majorly based on the environmental considerations, where society and economy depend on the environment and their growth is determined by the environmental carrying capacity, it is termed as the strong sustainability (Fig. 21.1a). When these three aspects are considered as separate overlapping realms, it is defined as the weak sustainability where compromise exists when fewer components are considered as shown in Fig. 21.1b.

In this study, the concept of sustainability has been applied to the vertical barrier system for the restriction of horizontal flow of the leachate from the waste dump toward the water bodies. In the current site, sustainability outline for the three main methods, concrete barriers, slurry-based cut off walls, and the sheet pile walls, is established. Firstly, the performance criteria of the walls are determined, and based on the material requirement, sustainability analysis is carried out later. The analysis can be simplified by using streamlined model or limiting it to specific impact factors (Todd and Curran 1999) such as energy consumption and carbon emission (Menzies et al. 2007). The simplified LCA methodology used herein focuses on embodied energy (EE) and the CO_2 emission (Shillaber et al. 2015a). EE is defined as the

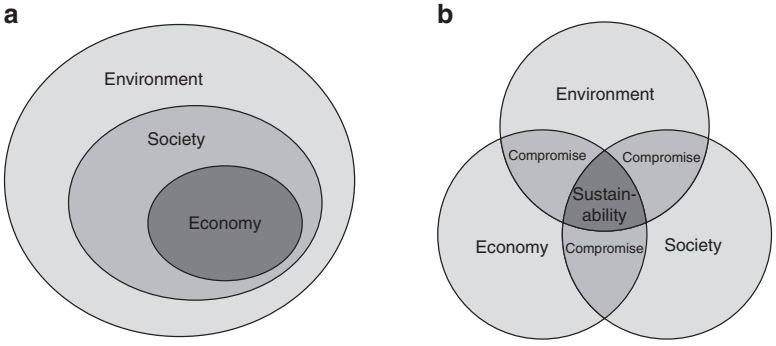

Fig. 21.1 Different definition of sustainability (Source: Shillaber et al. 2015a) (**a**) Strong sustainability, (**b**) Weak sustainability

energy required in bringing an item to its present state (Chau et al. 2008, 2012; Soga et al. 2011). The SEEAM can assess EE and CO_2 emission associated with the project design that meets project-specific performance requirement (Shilllaber et al. 2015b). The analysis relies on embodied energy coefficients (EECs) and CO_2 emission coefficients (CCs) for particular project. The values for EEC and CC obtained from different literature are represented in Table 21.1.

21.3 Site Condition

The existing waste dump site is an abandoned quarry site where dumping is done for more than 7 years. Due to the protest from the locals, dumping of waste is stopped from September 2015. Although at present the waste is not dumped, due to the previous waste and due to the lack of proper cover system, the leachate head at the dump was found to be very high. On site investigation, the leachate head was encountered at about two meters depth from the top of the fill. Table 21.2 gives the details of the site (Sivakumar Babu 2016), and Fig. 21.2 shows the plan view of the area.

To determine the potential contamination due to the leachate, the leachate characteristics were important to be determined. Thus, chemical tests were carried out

Table 21.1 Selected EEC and CC

Material	Unit	EEC (MJ/unit)	CC (kg CO_2/unit)	References
General steel	kg	35.4	2.71	Hammond and Jones (2011)
Cement concrete (nonstructural)	kg	0.77	0.096	Hammond and Jones (2011)
Bentonite	kg	1.65	0.101	Jiang et al. (2011) and Carnegie Mellon University (2008)
Water	L	0.01	0.001	Hammond and Jones (2011)
Diesel	L	43.0	3.25	Shillaber et al. (2014)
High-density polyethylene (HDPE)	kg	76.70	1.60	Hammond and Jones (2011)

Table 21.2 Details of landfill capacity, height, and area (based on site in charge)

Component	Details
Base	105,216 m^2
Average depth	25 m
Total quantity of waste dumped till now	750,000 tones
Area at the bottom	73,651 m^2

Fig. 21.2 Boundary of the Bingipura fill

Table 21.3 Details of landfill capacity, height, and area (based on site in charge)

Parameter	Values
pH	7.8
TDS mg/L	8416
BOD mg/L	405
TSS mg/L	216
COD mg/L	1950
Chloride mg/L	2468
Total nitrogen mg/L	412
Zinc mg/L	1.67
Nickel mg/L	0.1

in order to determine the leachate characteristics and the details of the same listed in Table 21.3.

The present condition of the waste dump and its potential for the contamination of the water body were simulated using finite element software CODE_BRIGHT. The

Table 21.4 Soil parameters considered for the simulation (silty soil)

Notations	Identification	Units	Values
γ	Unit weight	kN/m^3	17
n	Porosity	[−]	.3
S_{rl}	Residual saturation	[−]	0.2
S_{ls}	Maximum saturation	[−]	1
d_l	Longitudinal dispersivity of solute	m	0.1
d_t	Transverse dispersivity of solute	m	0.01
k	Hydraulic conductivity	m/s	10^{-6}
μ	Dynamic viscosity (at 20°C)	N s/m^2	1.002
K	Intrinsic Permeability (at 20°C)	m^2	1.02×10^{-14}
λ	Shape function for retention curve	–	0.4
σ_0	Surface tension (at 20°C)	N/m	0.072

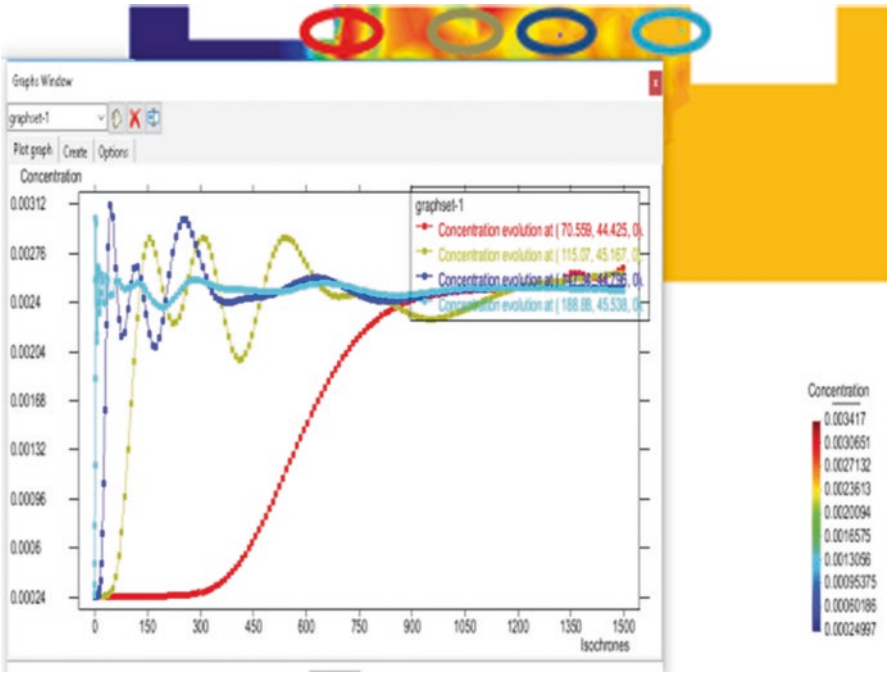

Fig. 21.3 Concentration vs. time plot between lake and fill

material inputs for the present (as it is) condition, i.e., without the vertical barriers, are listed in Table 21.4. After simulation, it was found that, with the present condition, the contamination occurred within 3 years of the operation which is shown in Fig. 21.3. Thus, it was environmentally unacceptable to leave the site as it is and thus the vertical barrier had to be constructed. Since the depth of the landfill is 25 m, it was proposed to have the depth of 35 m. The contaminant used for the

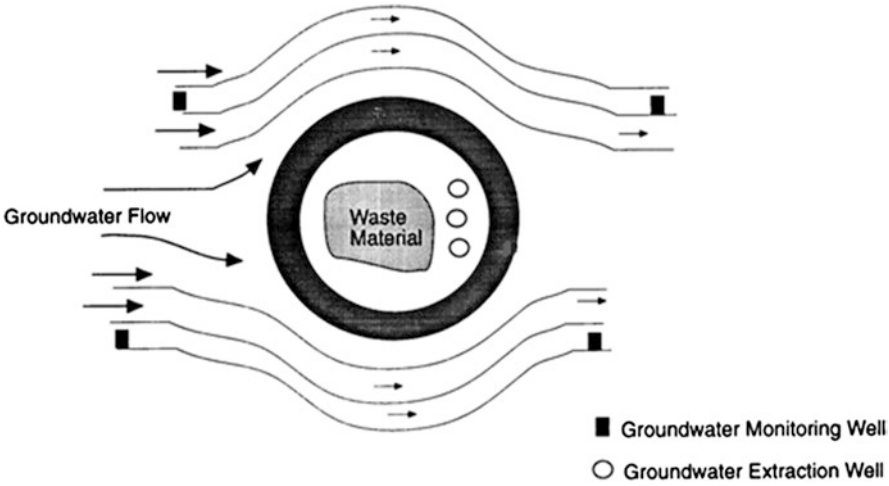

Fig. 21.4 Circumferential barrier

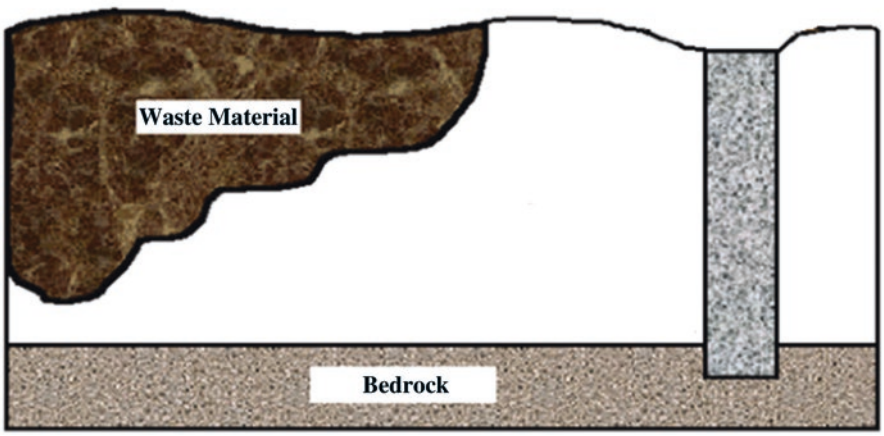

Fig. 21.5 Cross-sectional view

simulation was chloride (Cl^-) as it is nonreactive, and hence the migration front of the ion would be same as the seepage front of the carrier liquid.

The performance of the vertical barriers henceforth is analyzed using POLLUTEv7 model. For the containment to be most efficient, it was proposed to have circumferential walls over the entire contaminated area as shown in Fig. 21.4. The ideal construction of the vertical wall for maximum containment by ensuring the restriction of the flow below the wall is represented in Fig. 21.5.

21.4 Performance Analysis and Design Requirement

21.4.1 Soil Bentonite

At first, bentonite slurry is filled in the excavated trench. Soil-Bentonite (SB) backfill is then placed into the trench (displacing the slurry) to create the cutoff wall. Such wall provides low-permeability nonreactive barrier at low cost. Initial Cl^- concentration of 2400 mg/L was considered for the analysis. Thickness of the vertical barrier wall is considered as 600 mm which is the minimum requirement for soil-bentonite cutoff wall specified by State of California, i.e., 24 inches (California Code of Regulations 1990). Geomembrane was used to enhance the efficiency of the containment system. The source was considered as the constant concentration type, and the calculation method adopted for the leakage through geomembrane was based on Rowe et al. (2004). Over a period of 10 years, the barrier was able to contain the contaminant, and thus the concentration of the ion under consideration reduced from 2400 mg/L to 600 mg/L. Over a period of 15 years, the concentration was 800 mg/L (Fig. 21.8). The values used as the model parameter are described in Table 21.5.

In case of the absence of the alternate source, IS code for drinking water limits the required concentration of the Cl^- ions to be less than 1000 mg/L. Analysis by POLLUTEv7 software thus show that, with respect to the performance criterion, SB barrier system of thickness 600 mm (with 30 mil GM) is acceptable. The concentration profile along the width of the barrier is shown in Fig. 21.8.

21.4.2 Concrete Barriers

A case was taken to simulate the effect when the slurry wall was replaced with the concrete barrier. As concrete has very less permeability in the range of 10^{-10} cm/s, it is an effective mean of containment of the liquid waste (Fig. 21.6).

For concrete, the chloride diffusion coefficient is 3×10^{-8} cm^2/s (Andrade 1993; Truc et al. 2000). The modal parameters used for the simulation of this condition are represented in Table 21.6, and the concentration profile with time is represented in Fig. 21.8.

The result of the simulation indicated that for the similar performance as of the bentonite slurry wall over a period of 10 years, the thickness of the concrete barrier wall required would be 150 mm where the concentration over 10 years reduced from 2400 mg/L to 600 mg/L. But for the period of 15 years, the concrete barrier was not efficient where the concentration was at 1100 mg/L. On increasing the thickness to 200 mm the, concentration reduced to 800 mg/L over the period of 15 years. Hence, a thickness of 200 mm was recommended for the site.

Table 21.5 Modal parameters for the simulation

Parameter	Values
Source concentration, mg/L	2400
Waste width, m	122
Leachate head, m	23
Geomembrane thickness, mil	30
Diffusion coefficient for GM, m^2/a	3×10^{-5}
Slurry density, g/cc	1.2
Diffusion coefficient of slurry, m^2/a	0.018
Area at the bottom	**73,651 m^2**

Fig. 21.6 Concrete wall for leachate containment

21.4.3 Sheet Pile Walls

For the simulation of the case where sheet pile walls are used for the containment, steel sheet piling system with sealable joints was considered. The product was known as Waterloo Barrier developed by C3 Environmental Limited. There are many case studies of this system where it had been used for the waste containment like to prevent migration of coal tar contaminants into waster from decommissioned manufactured gas plant (MGP) site (January 2000) and to prevent contamination of pond with heavy metals from abandoned mine in Yukon Territory (September 1995). The types of sheet piling used for the sites were Waterloo Barrier WEZ95 and Waterloo Barrier WZ75, respectively. The grouting was done using a silica fume modified cementitious grout WBS-301 to seal the joint between the sheet piles as it is resistant to chemical attack (Source: Waterloo Barrier®). The properties of the steel sheet pile are listed in Table 21.7. Cutoff walls generally consist of the low

Table 21.6 Modal parameters for the simulation (concrete barrier)

Parameter	Values
Source concentration, mg/L	2400
Waste width, m	122
Leachate head, m	23
Concrete density, g/cc	2.4
Permeability of concrete, m/s	10^{-12}
Diffusion coefficient of concrete, cm^2/s	3×10^{-8}

Table 21.7 Properties of the barrier

Parameter	Values
Coefficient of water permeability for grouting material, m/s	3.19×10^{-15}
Coefficient of water permeability for steel material, m/s	10^{-25}
Bulk hydraulic conductivity, m/s	1.03×10^{-15}
Thickness, mm	
WZ75	*7.50*
WEZ95	*9.50*

hydraulic conductivity material, but typically they also have imperfections. A hypothetical cutoff wall consists of high and low hydraulic conductivity portion. Taking this consideration for sheet pile wall, the bulk hydraulic conductivity of the system is taken into account for simulation (Starr et al. 1992). The k_{nominal} for steel and $k_{\text{imperfection}}$ for grout were considered as 10^{-23} cm/s and 10^{-13} cm/s, respectively. The schematic of the Waterloo Barrier system is shown in Fig. 21.7.

The only problem that arises performance wise in the use of such piles is the presence of a number of corners and splicing needed for reaching greater depths (both reduce its efficiency due to leakage). Using the Waterloo Barrier WZ75, concentration of the contaminant over 10 years reduced from 2400 mg/L to 600 mg/L and to 700 mg/L for 15 years. Use of the WZ75 steel sheet pile with WBS-301 as sealant would satisfy the performance criteria of the barrier system (Fig. 21.8).

21.5 SEEAM Analysis of the Proposed Design

After comparing the performance criteria for all three alternatives, analysis was done to find out the best choice in terms of its sustainability based on the SEEAM (Shillaber et al. 2015a). SEEAM simplifies the analysis in terms of inputs and knowledge required without compromising environmental, economic, or social aspect. Quantification of EE and CO_2 emissions associated with different recommended design from previous section is done and compared to find out the design with least environmental effects.

Fig. 21.7 Internal cavity sealable joint sheet pile

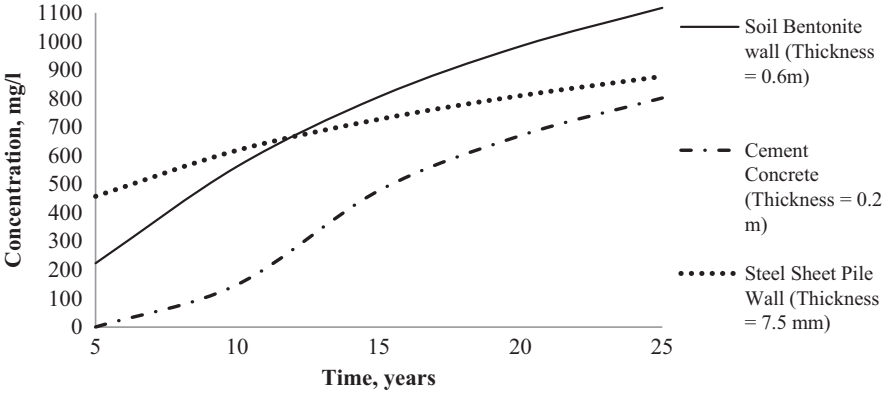

Fig. 21.8 A plot of concentration of contaminant coming out through a barrier system versus time

21.5.1 SEEAM Analysis Methodology

For the SEEAM analysis of the barrier system being discussed, the four major stages of the construction are the material and its production, transportation to the site, site operation, and transportation of the waste off the site. The analysis of the EE is done based on the total amount of energy required to bring the material to its present state (Shillaber et al. 2015b). The total EE associated with the input material is the total sum of the product of each material and its EEC (Chau et al. 2008, 2012; Soga et al. 2011):

$$EE_M = \sum_{i=1}^{n} (Q_i) * EEC_{i.}$$

where Q represents material and the total EE is the sum of EE of n materials used. EEC is considered as given in Table 21.1.

The total EE associated with the transportation is based on the quantity of the fuel required and the EEC of the type of the fuel required:

$$Q_F = \sum_{j=1}^{m} \frac{D_j}{FE_j} (N_j)$$

Table 21.8 Fuel economy of common construction vehicle

Vehicle	Payload capacity (kN)	Average fuel economy (km/L)
Light heavy-duty truck	82	2.72
Heavy-duty truck	240	2.42

Davis et al. (2012)

and

$$EE_F = \sum_{k=1}^{p} (Q_F)_k * EEC_k$$

where D is the one-way travel distance, FE is the fuel economy (Table 21.8), N is the total no. of one way trips, and Q_F is the total quantity of particular fuel.

21.5.2 Soil Bentonite

Based on the total length of the wall of 1.4 km and the thickness of the slurry wall, the volume of the soil-bentonite mixture required was 29,400 m^3. The amount of dry bentonite added is generally 3% (Owaidat and Day 1998). For the slurry during excavation, bentonite content used is 6%. The density of slurry should be at least 0.24 g/cc less (i.e., 15 lb/ft^3) than the density of SB backfill for easy replacement of slurry by the SB backfill. The slurry level should be maintained at least 0.9 m (i.e., 3 ft) above the ground water elevation and no more than 0.6 m (i.e., 2 ft) below the top of the working platform (Ref: Colorado Dept. of Natural Resources, Sept. 2000). While introducing the slurry into the trench, slurry shall be a mixture of not less than 18 pounds per barrel (i.e., 8 kg per 158 L).Based on all the requirements listed above, the total EE for the materials used was calculated to be 2380.69 GJ for slurry and 1309.77 GJ for SB. The respective CO_2 emissions were 146.81 tons of CO_2 and 80.17 tons of CO_2, respectively. Considering the nearest source of commercial Na-B as Gujarat which is approximately 1700 km from the site, the total number of trips required for a heavy-duty truck is approximately 90. Thus, the total EE and CO_2 emissions due to the transportation were calculated as 5263.2 GJ and 397.8 tons of CO_2, respectively. Since the excavated soil is mixed with bentonite and used as backfill, there is no requirement of transportation of excavated soil. For HDPE material of density 970 kg/m^3, the EE and CO_2 associated with the barrier are 2777.9 GJ and 579.5 tons of CO_2, respectively.

Thus, the total EE and CO_2 emissions associated with the SB slurry trench cutoff wall for the proposed design were 11,731.56 GJ and 1204.28 tons of CO_2.

21.5.3 Concrete Barriers

Considering that the barrier is for containment alone and does not require a very high strength, the concrete grade considered for the energy analysis was 1:3:6 mix (i.e., M10). The amount of EE associated with the concrete barrier for the particular volume of the concrete barrier wall was 18,110.4 GJ, and the CO_2 emission was 2257.92 tons of CO_2. Without considering the EE and CO_2 emission associated with the transportation, the concrete barrier was found out to be very much unacceptable design for the purpose of the waste containment of the particular site.

21.5.4 Sheet Pile Walls

From the performance analysis, the barrier of thickness 7.5 mm performed satisfactorily for the desired period of time in containing the contaminant. Thus, the total volume of the steel sheet pile wall required for the circumferential barrier system of the proposed site of 1.4 km circumference till the depth of 35 m was 367.5 m^3. It being steel sheet piling system with sealable joints, the EE associated with the material required was found out to be 102,124.5 GJ, and the CO_2 emission was 7818 tons. This proves that although a very good measure for the waste containment when flows in particular direction is to be restricted, the steel sheet pile actually is not sustainable for the site considered as the proposed design was circumferential barrier system.

21.6 Summary and Conclusion

The suitability of different barrier systems based on the performance criteria and the sustainability analysis was carried out. Firstly, the design was developed for the required performance of the barrier system. This analysis included the thickness of the barrier required. After the performance evaluation, the sustainability analysis was carried out for each method.

Based on the SEEAM analysis, the use of the Na-B slurry trench cutoff wall for the containment of the leachate proved to be the most preferable method. The total energy associated with the materials involved for the construction and the carbon emission was least for the slurry wall, whereas it was highest for the steel sheet pile wall. Although faster in construction, the steel sheet pile was not a sustainable design for this particular site where a circumferential design is proposed. The main aim behind providing the circumferential design of the slurry wall and not just at one particular side is in order to ensure maximum containment even in the rainy season when the rainfall is about 950 mm per year.

References

Andrade C (1993) Calculation of chloride diffusion coefficients in concrete from ionic migration measurements. Cem Concr Res 23(3):724–742

Carnegie Mellon University Green Design Institute (2008) Economic input-output life cycle assessment (EIO-LCA)

Chau C, Soga K, Nicholson D, O'Riordan N, Inui T (2008) Embodied energy as an environmental impact indicator for basement wall construction, Proceedings of Geo Congress 2008. ASCE, Reston, pp 867–874

Chau C, Soga K, O'Riordan N, Nicholson D (2012) Embodied energy evaluation for sections of the UK channel tunnel rail link. Proc Inst Civ Eng Geotech Eng 165(2):65–81

Colorado Department of Natural Resources (2000) Guide to specification preparation for slurry walls and clay liners as a component of a Colorado mines land reclamation permit

Davis SC, Diegel SW, Boundy RG (2012) Transportation energy data book: edition 31. Report No ORNL-6987, US Department of Energy

Hammond G, Jones C (2011) Inventory of Carbon and Energy (ICE), Sustainability Energy Research Team (SERT), University of Bath, UK

Jiang M, Griffin MW, Hendrickson C, Jaramillo P, VanBriesen J, Venkatesh A (2011) Life cycle greenhouse gas emission of Marcellus shale gas. Environ Res Lett 6(3):1–9

Menzies GF, Turan S, Banfill PFG (2007) Life-cycle assessment and embodied energy: a review. Proc Inst Civ Eng Constr Mater 160(4):135–143

Owaidat LM, Day SR (1998) Installation of a composite slurry wall to contain mine tailings. Tailings and Mine Waste '98

Rowe RK, Quigley RM, Brachman RWI, Booker JR (2004) Barrier systems for waste disposal facilities. Taylor & Francis Books Ltd (E & FN Spon), London, p 579

Shillaber CM, Mitchell JK, Dove JE (2014) Assessing environmental impact in geotechnical constructions: insight from the fuel cycle. Proceedings Geo Congress 2014, geo-characterization and modelling for sustainability, Geotechnical Special Publication No. 234, ASCE, VA, 3516–3525

Shillaber CM, Mitchell JK, Dove JE (2015a) Energy and carbon assessment of ground improvement works. I: definitions and background. J Geotech Geoenviron Eng. 10.1061/(ASCE)GT.1943-5606.0001410, 04015083

Shillaber CM, Mitchell JK, Dove JE (2015b) Energy and carbon assessment of ground improvement works. II: working model and example. J Geotech Geoenviron Eng. 10.1061/(ASCE)GT.1943-5606.0001411, 04015084

Sivakumar Babu GL (2016) Detailed project report for remediation of Bingipura landfill. Karnataka Urban Infrastructure Development and Financial Corporation

Soga K, Chau C, Nicholson D, Pentelidou H (2011) Embodied energy: soil retaining geosystems. ASCE J Civ Eng 15(4):739–749

Starr RC, Cherry JA, Vales ES (1992) A new type of steel sheet piling with sealed joints for groundwater pollution control. In: Proceedings of 45th Canadian geotechnical conference, October 26–28, 1992, Toronto, Ontario

Todd JA, Curran MA (1999) Streamlined life-cycle assessment: a final report from the SETAC North America streamlined LCA workgroup. Streamlined LCA workshop, Society of environmental Toxicology and Chemistry

Truc O, Ollivier JP, Carcassès M (2000) A new way for determining the chloride diffusion coefficient in concrete from steady state migration test. Cem Concr Res 30:217–226

Chapter 22
Geotechnical Characterization and Performance Assessment of Organo Clay Enhanced Bentonite Mixtures for Use in Sustainable Barriers

Vandana Sreedharan and P.V. Sivapullaiah

Abstract The widespread occurrence of organic contaminants demands the use of innovative barrier materials with improved organic sorption efficiency. In the present study, an attempt has been made to assess geotechnical and sorption characteristics of organo clay and its mixture with varying proportions of bentonite. A noticeable increase in plasticity and swelling characteristics and TOC sorption efficiency suggest that organo clay can effectively be used as a sorptive amendment in barrier materials against organic fluids of low polarity without compromising on the permeability.

Keywords Clay • Sorption • Organic contaminant • Swell • Bentonite • Barrier

22.1 Introduction

Decades of discharge of contaminants directly into air, water and land from a variety of sources have released a range of pollutants onto the planet. Of the different contaminants encountered day to day, the organic contaminants are a key group. They are often characterized by low water solubility and high lipid solubility, leading to their bioaccumulation, and may pose serious health risks and environmental hazard. With the number of organic chemicals in use on the increase, the potential for continued contamination of water and land resources exists and demands serious

V. Sreedharan (✉)
Government College of Engineering, Kannur 670563, Kerala, India
e-mail: vandanasreedharan@gcek.ac.in

P.V. Sivapullaiah
Indian Institute of Science, Bangalore 560012, India
e-mail: siva@civil.iisc.ernet.in

G.L. Sivakumar Babu et al. (eds.), *Geoenvironmental Practices and Sustainability*, Developments in Geotechnical Engineering,
DOI 10.1007/978-981-10-4077-1_22

attention. Hence, emphasis has been given to develop efficient barrier system, with high attenuating capacity so as to minimize the transport of organic contaminants.

Clays are for long often preferred as components in engineered waste containment systems and in many environmental applications. They have high cation exchange capacity and large surface area and hence are capable of sorbing a wide range of pollutants. However, studies have revealed that natural clays are found to be ineffective in sorbing nonpolar, nonionic organic compounds (NOCs) (Xu et al. 1997). The diffusion of organic contaminants through the conventional clay barriers is significant, and it may lead to an early breakthrough and large flux of contaminants. This inability of the clay barrier is often dealt with by enhancing the organic sorption capacity of the material.

22.1.1 Organic Modification of Clays

Even though several routes can be employed to modify clays, ion exchange with alkylammonium ions is a well-known and the preferential method to modify clays for enhancing the organic sorption (Bergaya et al. 2006). The clays are modified by introducing long- or short-chain organic compounds by simple cation exchange reactions. Jordan (1949) and Jordan et al. (1950) have presented important findings on the properties of organically modified clay. The organo clay used in the current study has been manufactured by intercalation of quaternary ammonium compounds from purified bentonite originated from Kutch. A long-chain alkylammonium compound, viz., dioctadecyl dimethyl ammonium chloride (DODMA-Cl) [$(CH_3(CH_2)_{17})_2(CH_3)_2\ N^+Cl^-$] (MW, 586.50), was used for the commercial organic modification of the clay. The commercially modified bentonite is also supposed to have been synthesized by replacing 100% of the inorganic cations with $DODMA^+$. A commercial bentonite from Kolar, India, was used in the study to prepare different mixtures of organo clay-enhanced bentonite.

Many researchers have concentrated their efforts on studying the hydraulic conductivity of organo clays synthesized with different modifiers on permeation with different organic fluids (Bartelt-Hunt et al. 2005; Smith and Jaffe 1994; Smith et al. 2003; Sarah 2003; Lorenzetti et al. 2005; Benson et al. 2015). However, only a very few systematic studies are reported on the basic geotechnical characteristics of organo clay. Moreover, very often, inorganic and organic contaminants can occur simultaneously; hence, admixtures of bentonite and organically modified clays are often suggested to be employed as a part of clay barrier system. Hence, studies are carried out on mixtures containing different proportions of organo clay and bentonite as well, to evaluate their geotechnical and sorption behavior.

22.2 Geotechnical Characterization

22.2.1 Organo Clay

Even if the correlations accomplished for unmodified clays are not fully applicable for the organically modified clays, they can still give a broad basis to estimate the swelling and hydraulic characteristics of clays which are of vital importance from the perspective of geoenvironmental applications. Attempts are made to correlate the changes in the geotechnical characteristics to the physicochemical characteristics of organo clay which were measured by different instrumental techniques. Table 22.1 gives the major index properties of clays used in the study.

A significant decrease in the specific surface area of organo clay has been noted since the organic cations exchanged onto the clay surface inhibit the penetration of the nitrogen gas used for the surface area determination. A lower specific gravity value is observed for the bentonite exchanged with organic cation as the large intercalated organic cations lead to a lower mass per volume (Burns et al. 2006; Bate 2010). An increased basal spacing (d_{001}) of 18 Å (Fig. 22.1) also brings out the shift in the d_{001} of the basic TOT structure of the smectite clay which can be associated to a bilayer arrangement of the intercalated alkylammonium chain in the interlayer.

The organic modification of the clay has brought in a noticeable reduction in the liquid limit value and an increase in the plastic limit value with water as the pore medium. This is due to exchange of the inherent hydrophilic inorganic cations of the clay surface with hydrophobic organic cations resulting in the reduction in the water holding capacity of the clay, and hence organic modification makes the clay less plastic. This observation is supported by the thermal analysis (TGA/DSC) and Fourier transform infra red spectro scopy (FTIR) studies (Fig. 22.2a, b). As observed from the TGA/DSC results, the unmodified bentonite showed a weight loss of nearly 10% in the temperature range of 20–100 °C, whereas it was only 3% in the case of the organo clay. Moreover, the endothermic peaks which can be assigned to the dehydration of the adsorbed water from the montmorillonite are also reduced on organic modification of the bentonite making it more hydrophobic in

Table 22.1 Index properties of clays

Property	Unmodified bentonite (BT_0)	Commercial organo clay (OC)	Commercial bentonite (BN_0)
Specific surface area (BET) (m^2/g)	26.19	3.0	23.81
Specific gravity	2.65	1.3	2.71
Clay content (%)	70.0	90.0	72.0
CEC (meq/100 g)	110.0	–	100
Liquid limit (%)	226.0	125.0	339.0
Plastic limit (%)	59.35	74.03	35.5
Free swell index (mL/g)	18.0	–	27.5

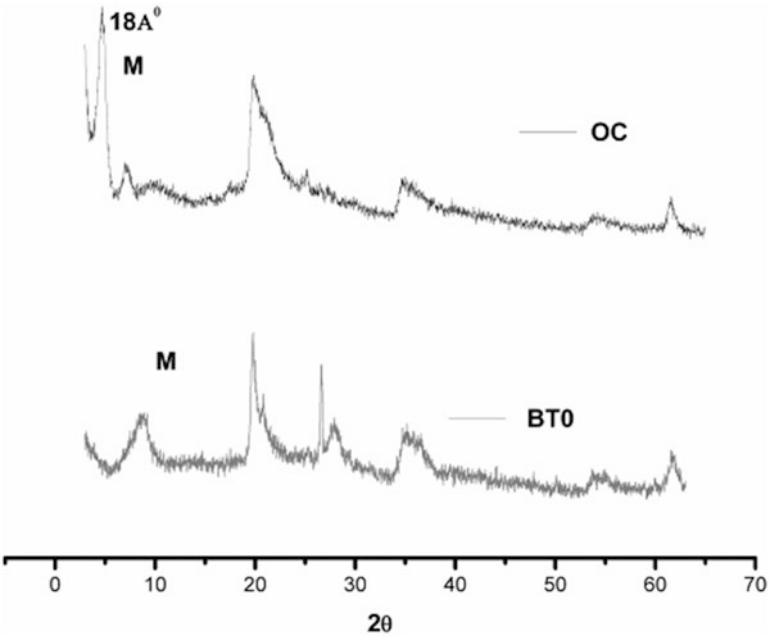

Fig. 22.1 XRD pattern for commercial organo clay and unmodified bentonite

nature. The FTIR spectra of the organo clay demonstrate sharp bands at 2919 cm^{-1} and 2852 cm^{-1} which can be assigned to the asymmetric and symmetric stretching of the CH_2 group of the exchanged alkylammonium compound. The bands pertaining to the scissoring and rocking vibrations of the methylene group are also observed in the FTIR spectrum at 1469 cm^{-1} and 720 cm^{-1}, respectively, and this is typical of the intercalated alkylammonium compound. All these point to the reduced water holding capacity of organically modified clays when compared to unmodified clays.

It is well understood that the swell potential of clays plays a critical role in deciding their role as engineered barrier and the swell potential of clay can often successfully be predicted with the aid of free swell measurements. However, attempts to study the changes in the swell behavior of the organically modified clays in different pore fluids are scarce. The variations of the free swell index of unmodified clay and organically modified clays with the dielectric constant of the pore medium are presented in Fig. 22.3. The sediment volume of modified clay decreases with increase in dielectric constant of the pore fluid, which is opposite to that of the unmodified clay. The bulky organic cations attached to the clay surface may tend to cover the clay surface rendering it more hydrophobic, and the nonpolar adsorbate molecules are attracted to the alkylammonium chain of the organic cations of the organo clay by van der Waals interactions leading to higher sediment volume. The long-chain organic cations of the organo clay can also agglomerate and facilitate the uptake of a low polar liquid. Further, the alkylammonium-treated montmorillonite facilitates

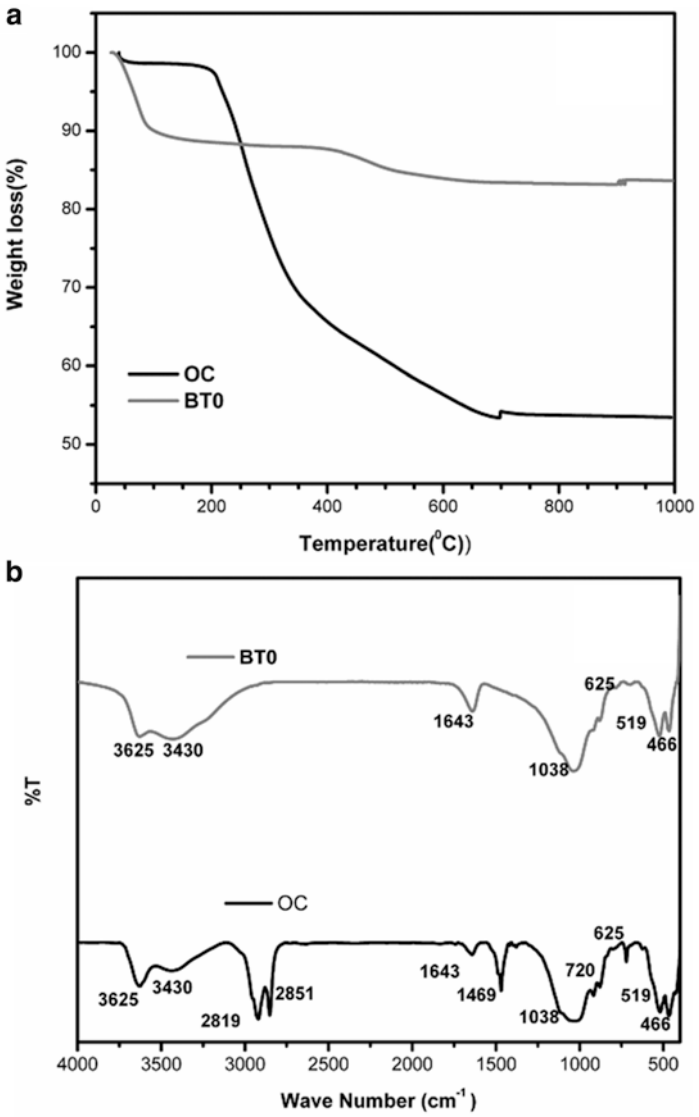

Fig. 22.2 (**a**, **b**) TGA curve and FTIR spectra for commercial organo clay and unmodified bentonite

an easy dispersal of the nonpolar organic molecules, thereby increasing the sediment volume. This shows that the swell volume of the modified clays was controlled more by surface solvation than by the development of the interparticle repulsive forces unlike in the case of unmodified clays.

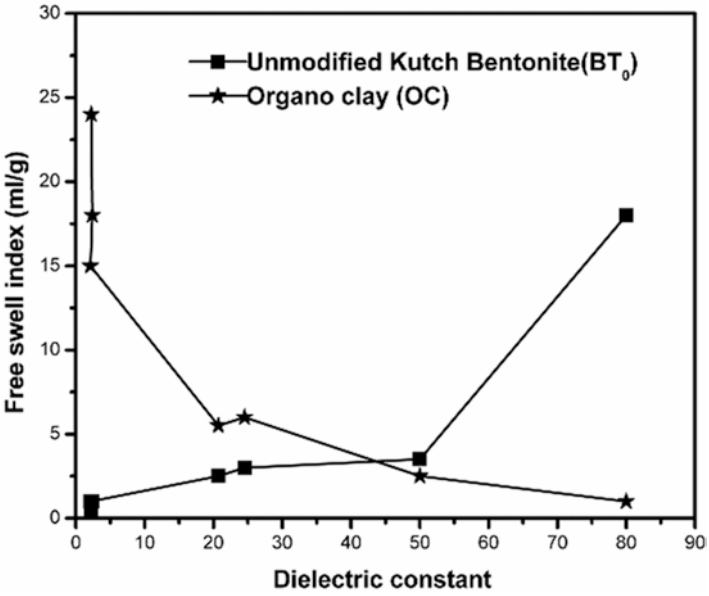

Fig. 22.3 Variation of free swell index of organo clay and unmodified bentonite

22.2.2 Organo Clay-Enhanced Bentonite Mixtures

Figure 22.4a compares the liquid limit values of different organo clay-bentonite mixtures in water and ethanol (plotted on volume basis). When the pore fluid was changed to ethanol, the liquid limit of the organo clay-bentonite mixture demonstrated an increasing trend with the increase in organo clay content. A sharp increase in liquid limit was noted up to an organo clay content of 50% in the mix, and thereafter, it remained more or less the same. The plasticity of the mixtures thus shows a conflicting trend of decrease and increase, respectively, in water and ethanol on increase in organo clay content.

The variation of free swell index of the mixture of the organo clay and bentonite is also found to be largely controlled by the organo clay content and the nature of the fluid (Fig. 22.4b). A distinctly opposite behavior between low and high polar fluids is brought out. The very strong interactions of organo clay with low polar fluids owing to its organophilicity lead to higher swell volumes at higher organo clay contents and at lower dielectric constants. As the percentage of organo clay in the mixture increases, this behavior is more pronounced. The free swell measurements observed are indicative of the self-healing capacity of the clay in mediums of different polarity. The increased swell with higher organo clay content in less polar fluids may also suggest a reduced permeability for these fluids.

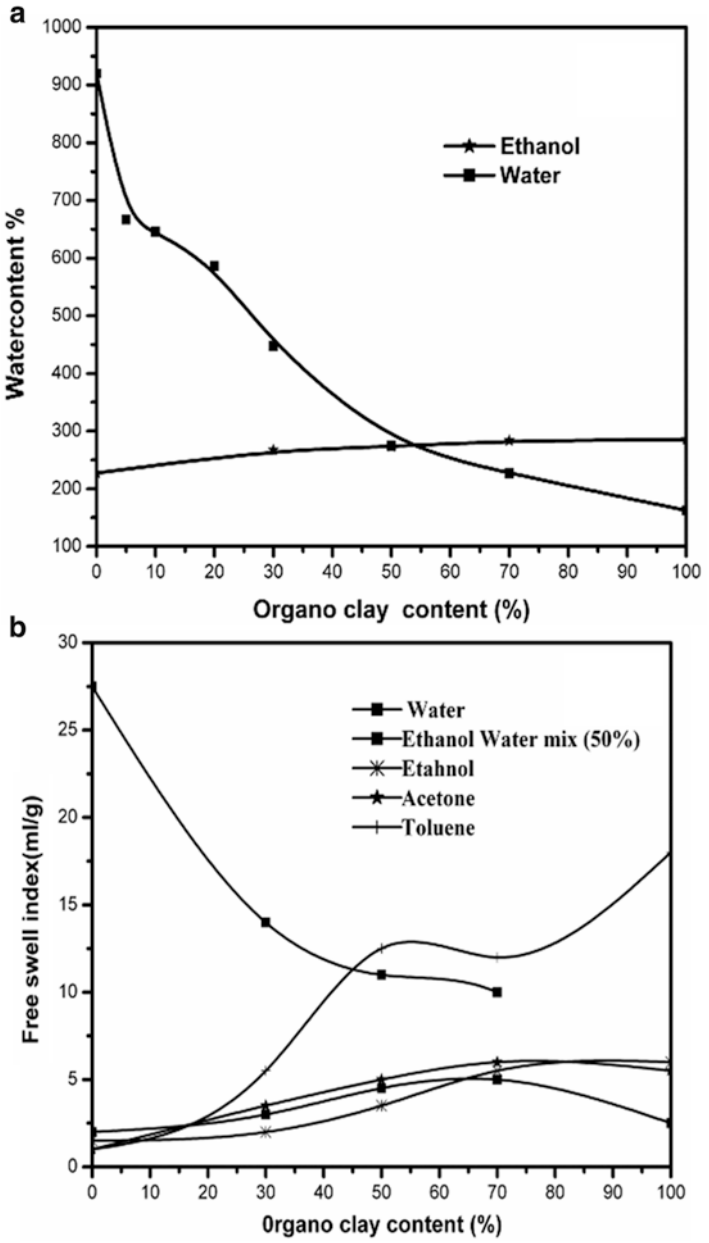

Fig. 22.4 (**a**,.**b**) Variation of liquid limit and free swell index of organo clay-enhanced bentonite mixtures

22.3 Sorption Characteristics

Elucidating the mechanistic function of organo clays as sorbents for different organic contaminant molecules present in leachates is very important for understanding, predicting, and designing various organo clay-enhanced mixtures which can find use as barriers. The sorption of organics from a synthetic solution and MSW leachate was studied by batch sorption tests. The efficiency of removal of the organics is assessed in terms of the reduction in the total organic carbon (TOC) of the leachate, as the individual measurement of the numerous organic compounds present was technically very challenging. The mixtures of commercial organo clay and commercial bentonite were used for evaluating their organic sorption efficiency. Based on the tests, an attempt was made to assess the mechanism of sorption of organics by the organo clays as it is very important in the design of the sorption barriers.

22.3.1 Batch Sorption Studies

Batch sorption tests for TOC removal were conducted with synthetic solution of varying TOC concentrations as well as with MSW leachate obtained from a landfill in Bangalore. The tests were conducted maintaining the optimum solid/liquid ratio as 1:20 and contact period as 2 h. The amount of clay used was fixed as 3 g. The equilibrium TOC concentrations were assessed after the prescribed period of contact. All the other parameters which affect the sorption capacity such as temperature and pH were maintained constant. The TOC concentration was measured using a TOC analyzer (Shimadzu made).

22.3.2 TOC Removal Efficiencies of Organo Clay-Enhanced Bentonite Mixtures

The effect of organo clay on the TOC removal efficiency of organo clay-enhanced bentonite mixtures from synthetic solution and MSW leachate is presented in Fig. 22.5a, b. The addition of commercial organo clay to the commercial bentonite is shown to improve the TOC removal capacity of bentonite irrespective of the initial TOC concentration.

TOC removal from MSW leachate was also found to increase on addition of organo clay to bentonite. In both the cases, the TOC removal efficiency was found to increase steeply till the organo clay content was almost 30%, and there was only a marginal increase in the TOC sorption on further increase in the organo clay content. The improved TOC removal efficiency of the mixture could be due to the strong affinity of organo clay to the organic compounds present in the leachate.

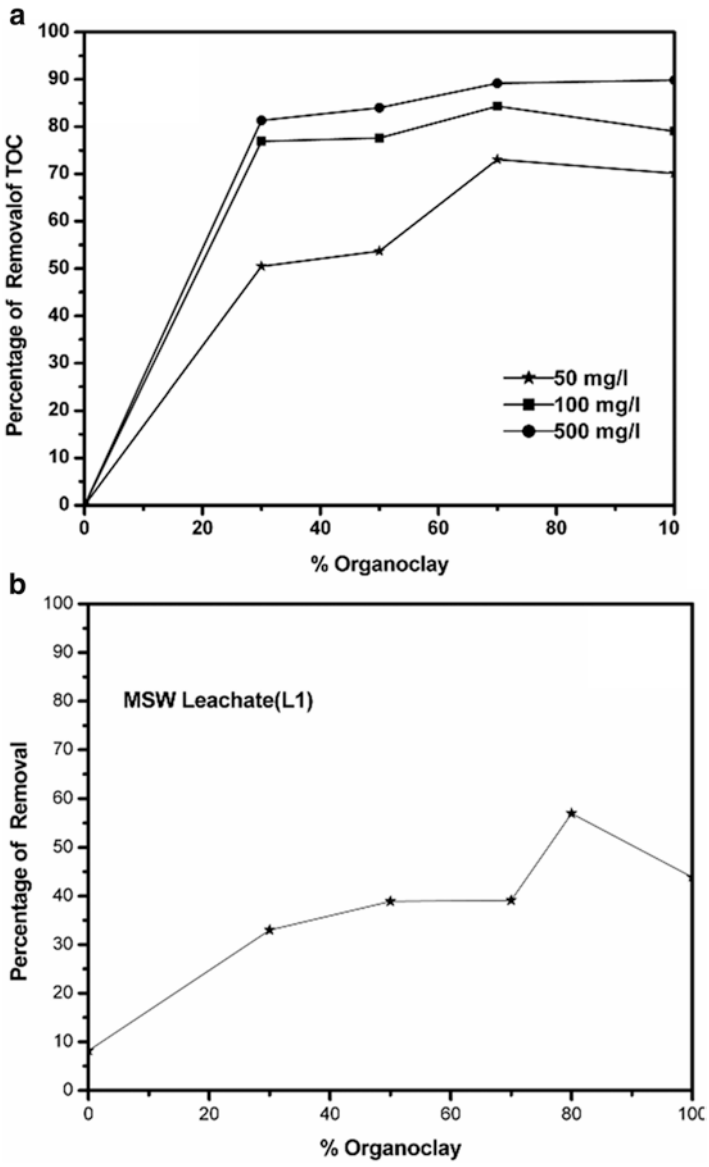

Fig. 22.5 (**a**, **b**) Sorption of TOC from synthetic leachate and MSW leachate by organo clay-enhanced bentonite mixture

However, the more aqueous nature of the leachate restrains the enhanced interactions of organo clay with the organic contaminants as organo clay is more hydrophobic in nature. The strong chemical interactions of organo clay with leachates are established FTIR studies.

22.3.3 FTIR Study

The characteristic peaks of organo clay at 2919 and 2850 cm^{-1} corresponding to the symmetric and asymmetric stretching of CH bond of the alkyl chain were observed to be broadened and reduced when interacted with leachate. The typical peak corresponding to the Al-OH and H-O-H vibration of montmorillonite clay at 3430 cm−1 and 1640 cm^{-1} was found to become broader on interacting with the aqueous-based leachates. The peak at 1463 cm^{-1} due to the intercalated alkyl chain of organo clay also showed more number of shoulders on interacting with leachates. All these observations support the fact that the organo clay chemically interacts with the leachates and facilitates the TOC removal unlike in the case of unmodified bentonite.

22.4 Conclusions

Manipulation of the changes in the mechanic properties of the organo clays with intercalation of organic cations enables to control the geotechnical performance of the organo clay-amended barrier systems. Apart from the dielectric constant of the pore fluid, chemical bonding also contributes to the behavior of organically modified clays. The addition of organo clay to bentonite results in the suppression of swelling of clays in water. The swelling of the mixture of organo clay and bentonite in different pore fluids is also largely controlled by polarity of the fluid and the chemical interactions. The impressive sorptive capabilities of organo clays brought out suggest their potential utility as components of containment barriers and clay slurry walls in hazardous waste disposal, landfills, etc. The major challenge on long-term sustainability of environment due to various organic contaminants can therefore to a large extent be dealt with, by suitably designed organo clay-enhanced barrier systems.

References

Bartelt-Hunt SL, Smith JA, Burns SE, Rabideau AJ (2005) Evaluation of granular activated carbon, shale and two organoclays for use as sorptive amendments in clay landfill liners. J Geotech Geoenviron Eng 131:848–856

Bate B (2010) Engineering behavior of fine-grained soils modified with a controlled organic phase. Ph.D thesis, Georgia Tech., USA

Benson C, Jo H, Musso T (2015) Hydraulic conductivity of organoclay and organoclay-sand mixtures to fuels and organic liquids. J Geotech Geoenviron Eng 141(2):0401–4094

Bergaya F, Theng BKG, Lagaly G (2006) Developments in clay science. Handbook of clay science, vol 1. Elsevier Ltd, Amsterdam

Burns SE, Bartelt-Hunt SL, Redding AZ, Smith JA (2006) Coupled mechanical and chemical behavior of bentonite engineered with a controlled organic phase. J Geotech Geoenviron Eng 132:1404–1412

Jordan JW (1949) Organophilic bentonites, I. Swelling in organic liquids. J Phys Colloid Chem 53:294–306

Jordan JW, Hook BJ, Finlayson CM (1950) Organophilic bentonites. II. Organic liquid gels. J Phys Colloid Chem 54:1196

Lorenzetti RJ, Bartelt-Hunt SL, Burns SE, Smith JA (2005) Hydraulic conductivities and effective diffusion coefficients of geosynthetic clay liners with organobentonite amendments. Geotext Geomembr 23(5):385–400

Sarah R (2003) Production and assessment of modified clay for organic containment, Ph.D thesis, Monash University, Australia

Smith JA, Jaffe PR (1994) Benzene transport through landfill liners containing organophilic bentonite. J Environ Eng 120:1559–1577

Smith JA, Bartelt-Hunt SL, Burns SE (2003) Sorption and permeability of gasoline hydrocarbons in organobentonite porous media. J Hazard Mater 96:91–97

Xu S, Sheng GY, Boyd SA (1997) Use of organoclays in pollution abatement. Adv Agron 59:25–62

Chapter 23
Observations of Field Condition of an Exposed Geosynthetic Liner System

J.L. Hanson and N. Yesiller

Abstract Preliminary field observations during the removal of a composite geosynthetic liner system that had been exposed for more than a decade are presented. The liner system was installed at a cell in a Subtitle D municipal solid waste landfill in San Luis Obispo, California (USA). The liner system consisted of (from top to bottom) a 1.5 mm-thick black HDPE geomembrane, a needle-punched geosynthetic clay liner (GCL), and a compacted subgrade. The liner system was not covered at any time since construction. The sides of the cell were relatively steep at 2H:1V slopes. Initially, the geomembrane was removed followed by removal of the geosynthetic clay liner. The geosynthetic clay liner panels were observed to be separated at multiple locations with gaps up to 220 mm wide and up to approximately 17 m long. The GCL also was relatively dry with granular consistency. In addition, a significant amount of bentonite that migrated from the GCL had accumulated between the GCL and the geomembrane at the toe of the slope.

Keywords Landfill • GCL • Exposed liner • Bentonite • Exhume

23.1 Introduction

Composite liner systems consisting of geomembranes placed over geosynthetic clay liners (GCLs) commonly are used for containment applications. Timely cover of the geosynthetics is critical for performance of the liner system. Multiple problems have been identified for exposed conditions including development of wrinkles in geomembranes due to cyclic temperature variations and ageing and degradation of the geomembranes due to UV exposure and oxidation (Rowe 2005;

J.L. Hanson (✉)
Civil and Environmental Engineering Department, California Polytechnic State University,
1 Grand Ave, San Luis Obispo, CA 93407-0353, USA
e-mail: jahanson@calpoly.edu

N. Yesiller
Global Waste Research Institute, California Polytechnic State University,
1 Grand Ave, San Luis Obispo, CA 93407-0353, USA
e-mail: nyesiller@gmail.com

G.L. Sivakumar Babu et al. (eds.), *Geoenvironmental Practices and Sustainability*, Developments in Geotechnical Engineering,
DOI 10.1007/978-981-10-4077-1_23

Koerner 2012). In addition, the service life of HDPE geomembranes was estimated to decrease significantly with temperature ranging from up to 900 years at 20 °C temperature to less than 20 years at 60 °C (Rowe 2005). For GCLs, separation of GCL panels underneath exposed geomembrane liners has been reported (Koerner and Koerner 2005a, b; Thiel and Rowe 2010). Panel separations of 50–1200 mm (5–28% strain) were reported for GCLs under geomembranes along slopes with 2–34° angles that were originally overlapped over a distance of 150–300 mm (Gassner 2009; Thiel and Rowe 2010). The composite barriers were left exposed without placement of overlying layers for durations between 2 and 60 months. Significant cation exchange (i.e., replacement of monovalent cations with divalent cations) and variations in field water content (between approximately 20 and 63%, depending on site) of GCLs exhumed from cover systems in landfill facilities were reported for GCLs in composite liners (Scalia and Benson 2011). In addition, migration of bentonite from locations near the top of slopes towards the toe of slopes was reported for GCLs in exposed liner systems (Take et al. 2015). Observations of the condition of a geomembrane-GCL composite liner system that was left exposed at a municipal solid waste landfill located in USA are presented herein. The liner system was constructed and then left exposed without placement of overlying materials for over a decade.

23.2 Observations During Field Exhumation

A geomembrane-GCL composite liner system was constructed in 2004 at a municipal solid waste landfill in San Luis Obispo, California (USA). The cell was constructed with 2H:1V slopes. The length of the slopes ranged from approximately 24 m for the north-facing slope to 30 m for the west-facing slope. The geomembrane consisted of a 1.5 mm-thick black HDPE geomembrane, which was textured on the bottom side against the underlying GCL and smooth on the top exposed side. The GCL consisted of a needle-punched nonwoven-nonwoven product. A view of the exposed liner system is presented in Fig. 23.1.

The composite liner system was removed in 2016. Initially, the geomembrane was removed at the site, followed by the removal of the underlying GCL. Photographs of the cell during the exhumation process are presented in Fig. 23.2. Expansion of the geomembrane and resulting wrinkles and space between the geomembrane and underlying GCL were observed throughout the cell. The height of the cavity between the geomembrane and the GCL was on the order of 150–200 mm along the base of the cell with less space present between the geosynthetic liners along the slopes. While the condition of the geomembrane appeared relatively uniform in the cell, the condition of the underlying GCL was observed to be variable. The GCL was dry near the top and relatively wet at the bottom of the west-facing slope. Less variation of the moisture content of the GCL was present along the north-facing slope. In all cases for upper portions of the slopes, the bentonite in the GCL was partially

Fig. 23.1 Exposed liner system

hydrated with granular consistency (Fig. 23.3). The bentonite core of the GCL had macrocracks in these cases. At some locations at lower elevations along the slopes where the GCLs were wetter, the bentonite had gel structure.

The GCL seams along the west- and north-facing slopes were investigated during exhumation. Of 43 panel seams, seam separation was observed at eight locations, along seven separate seams (i.e., one seam had two separate zones of separation). The minimum separation was on the order of 20 mm wide, whereas the maximum separation was 220 mm wide. The length of the zones with seam separation along the direction of the slopes ranged from 1.72 to 17 m. The zones of seam separation were generally in the upper half of the slope length, with distances from the crest of the slope to onset of seam separation ranging from 0.9 to 14.0 m. Photos of seam separation and measurement of gap width are presented in Fig. 23.4.

In addition, migration of bentonite and accumulation of bentonite between the geomembrane and the GCL were observed near the toe of the west-facing slope. The bentonite migration was particularly aligned with the locations with relatively high moisture at the toe locations. The bentonite accumulated in a wedge-shaped geometry with maximum thickness of accumulation at the toe of the slope. The length of the wedge (in alignment with length of slope) was 2.93 m. The thickness of accumulated bentonite was minimal at the top of the wedge and up to 90 mm at the bottom of the wedge (near the toe). Photographs of the accumulation of bentonite between the geomembrane and the GCL as well as of the thickness of the accumulated wedge of bentonite are presented in Figs. 23.5 and 23.6.

Fig. 23.2 Removal of liner system

23.3 Summary

Preliminary field observations during the removal of a geomembrane-GCL composite liner system that had been exposed for more than a decade are presented. The liner system was installed at a cell in a municipal solid waste landfill in San Luis Obispo, California (USA). Wrinkles and expansion of the geomembrane and space between the geomembrane and the underlying GCL were observed. The geosynthetic clay liner panel seams were separated at eight locations along 43 seams. The gaps were up to 220 mm wide and up to approximately 17 m long. The GCL was generally relatively dry with granular consistency with the exception of some wet conditions near the toe of the slope. At a region along the west-facing slope, a

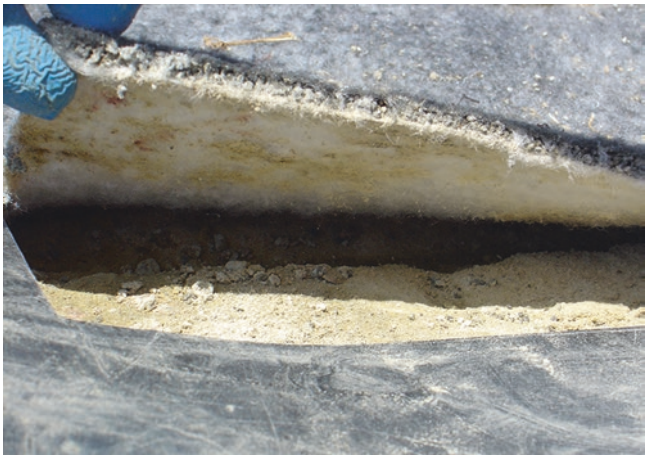

Fig. 23.3 Bentonite with granular consistency

Fig. 23.4 Zone of seam separation and seam gap

significant amount of bentonite that migrated from the GCL had accumulated at the toe of the slope. Specimens of geosynthetics and underlying soil were collected during the removal of the liner system. Quantitative evaluation of samples collected is currently underway to determine moisture contents of GCLs and subgrade soils, mass per unit area of GCLs, hydraulic conductivity of the GCLs, and properties of the bentonite component of the GCLs including Atterberg limits, swell index, bound

Fig. 23.5 Accumulation of bentonite between geomembrane and GCL

Fig. 23.6 Thickness of accumulated bentonite near toe of slope

cations in the exchange complex, and cation exchange capacity. Further analysis will be prepared as a separate publication.

Acknowledgments Waste Connections, Inc. and Cold Canyon Landfill are acknowledged for allowing site access and sampling of the liner system. Dr. Amro El Badawy, Mr. Kyle O'Hara, Mr. John Buringa, Mr. Sean Herman, and Mr. Spencer Jemes assisted with sampling.

References

Gassner F (2009) Field observation of GCL shrinkage at a site in Melbourne Australia. Geotext Geomembr 27(5):406–408. , Elsevier

Koerner RM (2012) Designing with geosynthetics (volumes 1 and 2), 6th edn. Xlibris, Bloomington

Koerner RM, Koerner GR (2005a) In-situ separation of GCL panels beneath exposed geomembranes. In: GRI White Paper #5. Geosynthetic Research Institute, Folsom

Koerner RM, Koerner GR (2005b) In-situ separation of GCL panels beneath exposed geomembranes. GFR Ind Fabr Assoc Int 23(5):34–39

Rowe RK (2005) Long-term performance of contaminant barrier systems. 45th Rankine Lecture, Geotechnique, ICE Publishing 55(9):631–678

Scalia J, Benson CH (2011) Hydraulic conductivity of geosynthetic clay liners exhumed from landfill final covers with composite barriers. J Geotech Geoenviron Eng ASCE 137(1):1–13

Take WA, Brachman RWI, Rowe RK (2015) Observations of bentonite erosion from solar-driven moisture migration in GCLs covered only by a black geomembrane. Geosynthetics Int, ICE Publishing 22(1):78–92

Thiel R, Rowe RK (2010) Technical developments related to the problem of GCL panel shrinkage when placed below an exposed geomembrane. In: Proceedings, GBR-C 2k10: 3rd international symposium on geosynthetic clay liners, CemOA Publications, pp 93–102

Chapter 24
Advances in Bentonite-Based Containment Barriers

Kristin M. Sample-Lord

Keywords Barriers • Bentonite • Containment • Diffusion • Modified clays

24.1 Introduction

The state of the art in geoenvironmental engineering has expanded in breadth to address a range of engineering challenges, including improvement of long-term performance of barriers for waste and chemical containment systems, remediation of contaminated sites, management of contaminated dredged sediments, and development of sustainable (green) infrastructure. Specifically, recent advancements in engineered barrier systems for waste and chemical containment include (1) improved understanding of contaminant transport mechanisms and coupled flows through engineered barriers and (2) development of innovative barriers and barrier materials. Such advancements may allow for enhanced performance of barrier systems as well as motivate future collaborative and interdisciplinary research in these areas, supporting development of more sustainable geoenvironmental practices.

24.2 State of the Art for Engineered Barriers

Sodium bentonites (Na-bentonites) commonly are used in engineered barriers for waste containment (e.g., compacted clay liners, geosynthetic clay liners (GCLs), highly compacted buffers for high-level radioactive waste (HLRW), vertical cutoff walls) due to the ability of Na-bentonite to provide low values of hydraulic conductivity, k (e.g., $k < 10^{-10}$ m/s for water). Thus, the standard practice of using

K.M. Sample-Lord (✉)
Department of Civil and Environmental Engineering, Villanova University, Villanova, PA 19085, USA
e-mail: kristin.sample-lord@villanova.edu

G.L. Sivakumar Babu et al. (eds.), *Geoenvironmental Practices and Sustainability*, Developments in Geotechnical Engineering,
DOI 10.1007/978-981-10-4077-1_24

Na-bentonite in engineered barriers is based on the goal of limiting advective transport of contaminants into the environment. However, significant research focused on bentonite-based barriers has illuminated the following potential issues:

- *Reduced barrier effectiveness due to chemical incompatibility*: Liquids with high ionic strength and/or containing high concentrations of multivalent cations (e.g., calcium, magnesium) may decrease the swelling behavior of Na-bentonite, resulting in significant increases in k and reduced effectiveness of the barrier (e.g., Jo et al. 2001; Meer and Benson 2004; Kolstad et al. 2004).
- *Underestimation of contaminant flux due to neglecting diffusion:* At values of k less than 10^{-9} m/s, diffusion (transport due to chemical gradients) has been shown to be a significant to dominant contaminant transport mechanism, rather than advective transport due to fluid flow (Rowe et al. 2004; Lange et al. 2009; Shackelford 2014). Therefore, diffusion may be the dominant mechanism for contaminant transport in some bentonite-based barriers, resulting in unconservative predictions of containment duration for analyses based solely on Darcy's law (Shackelford 2014).

The challenge of potential chemical incompatibility between bentonite-based barrier materials and leachate chemistry has prompted experimental research and commercial development of chemically modified bentonites (e.g., bentonites amended with organic modifiers, such as polymers) for enhanced chemical resistance. Examples of chemically modified bentonites include dense pre-hydrated GCLs, multiswellable bentonite, bentonite polymer nanocomposite, and HYPER clay. Research to date has shown that chemically modified bentonites may perform very well, maintaining values of k less than 10^{-9} m/s even when permeated with synthetic leachates with high ionic strength (e.g., Zimmel et al. 2013; Benson et al. 2014) and solutions with multivalent species (e.g., Mazzieri et al. 2010; Scalia et al. 2014; Di Emidio et al. 2015). Additional research is required to evaluate the long-term performance of chemically modified bentonites and chemical compatibility with waste liquids.

The importance of diffusion in the evaluation of contaminant transport across engineered barriers for waste containment started to gain attention in the late 1970s (Shackelford 2014). Significant research has been performed to measure diffusion coefficients of clays using traditional testing methods, such as the through-diffusion method, half-cell method, and column testing (Shackelford 1991). However, there is limited experimental data available regarding diffusion coefficients of (1) chemically modified bentonites (Di Emidio et al. 2015; Bohnhoff and Shackelford 2015; Malusis and Daniyarov 2016), (2) bentonite pastes (e.g., backfills, filter cakes), and (3) high-water content waste materials (e.g., slurried mine tailings). This may be due, in part, to the time-consuming and challenging nature of traditional diffusion testing techniques. However, the use of innovative test methods, such as the dialysis-leaching test (DLT) method described by Sample-Lord and Shackelford (2016), may allow for simpler and more efficient (e.g., test durations of 5 days to 2 weeks) collection of experimental data to evaluate and model diffusion in containment facilities and engineered barriers.

In addition to a low k, bentonite and soil mixtures containing bentonite also have been shown to exhibit semipermeable membrane behavior resulting in reduced liquid and contaminant flux across the barrier due to reduced liquid-phase diffusion and development of chemico-osmosis. Thus, bentonite-based barriers may exhibit improved containment performance, which has motivated the development of laboratory research programs to evaluate and quantify membrane behavior for a variety of barrier materials and chemical solutions. For example, membrane behavior has been shown to exist in GCLs with Na-bentonite (e.g., Malusis and Shackelford 2002), natural clay soils amended with low amounts of bentonite (~5% by dry mass) (e.g., Kang and Shackelford 2010), and soil-bentonite backfills used in vertical cutoff walls (e.g., Henning et al. 2006; Evans et al. 2008). However, partial or complete destruction of the membrane behavior in bentonite by invading salt cations has been observed (e.g., Shackelford and Lee 2003). Thus, the results of limited research regarding the persistence of semipermeable membrane behavior in barriers with traditional Na-bentonite suggest that membrane behavior may only play a significant role in contaminant transport for specific barrier applications, such as highly compacted buffers for HLRW (Shackelford 2014). Recent research has focused on evaluation of membrane behavior in novel barrier materials that are potentially more chemical resistant, leading to improved persistence of membrane behavior (e.g., Bohnhoff and Shackelford 2013; Malusis and Daniyarov 2014). In addition, recent advances have been made in laboratory testing capabilities, including simultaneous measurement of membrane behavior and diffusion under *unsaturated* conditions. Initial experimental results from Sample-Lord and Shackelford (2014) and Sample-Lord (2015) indicate that membrane behavior increases as the degree of water saturation decreases. These results are potentially significant for applications where clay barriers may be present at varying degrees of saturation (e.g., long-term disposal of HLRW), but further research focused on membrane behavior under unsaturated conditions is necessary.

24.3 Expertise and Facilities at Villanova University

Dr. Kristin Sample-Lord has been an assistant professor in the Department of Civil and Environmental Engineering at Villanova University since 2015. Her research and industry experience has focused on the geotechnical and geoenvironmental design and evaluation of containment facilities with soil and geosynthetic barriers. Some of her current and recent projects include experimental research in the following areas: (1) evaluation of semipermeable membrane behavior and diffusion in unsaturated clay, (2) evaluation of novel materials for enhanced performance of engineered barriers (e.g., chemically modified bentonites, clay mixtures), and (3) development of novel testing methods for efficient measurement of transport properties of soils (e.g., soil-bentonite backfills, high-water content geomaterials, Na- and modified bentonites).

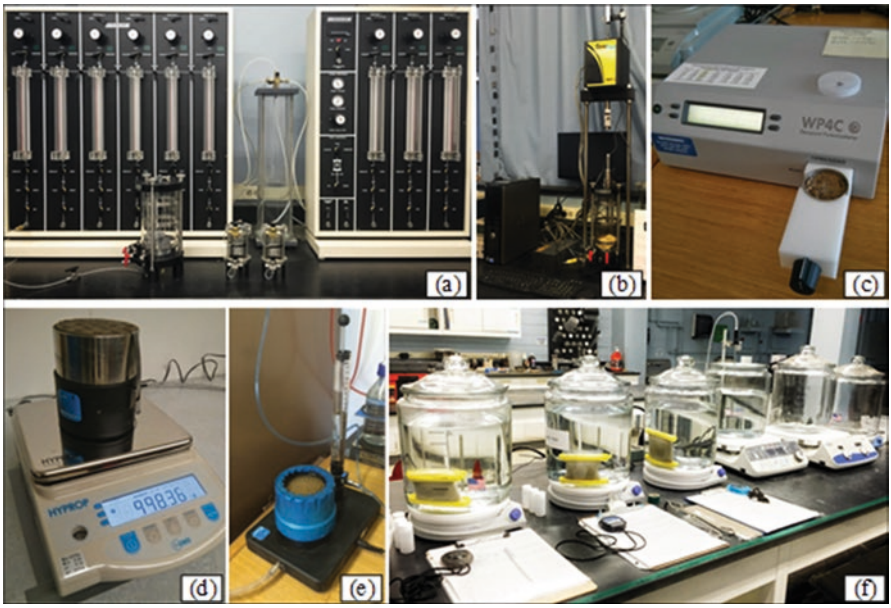

Fig. 24.1 Laboratory equipment for geoenvironmental and geotechnical research at Villanova University: (**a**) triaxial control panels and flexible-wall cells, (**b**) automated triaxial load frame, (**c**) WP4C dew-point potentiometer, (**d**) HYPROP system, (**e**) KSAT system, and (**f**) dialysis-leaching test setups

The Soils Laboratory, located on the ground floor of John Barry Hall, serves as a teaching laboratory for undergraduate Soil Mechanics courses as well as a research laboratory for geoenvironmental and geotechnical research. The laboratory is fully equipped with modern geotechnical testing equipment, including triaxial control panels and flexible-wall cells (Fig. 24.1a), rigid-wall permeameters, constant-head reservoirs, a fully automated triaxial load frame (GeoJac, Fig. 24.1b), a load frame for unconfined compression, direct shear machines, a consolidometer, deaerators, and a large standing soil mixer. Equipment for measuring physical properties of soils includes several sets of sieves and sieve shakers, hydrometers, tabletop mixers, liquid limit devices, modified and standard Proctor hammers, and compaction molds, ovens, triple beam balances, and digital scales with multiple capacities. Specialty laboratory equipment includes a VersaTester, Tinius Olsen (120 kip capacity), multiaxial geomembrane testing device, vibratory table, and 16-carrier braiding machine for composite material manufacturing. Additional equipment for measuring water characteristic curves and permeability include a WP4C dew-point potentiometer (Fig. 24.1c), HYPROP system (for retention curves and unsaturated hydraulic conductivity, Fig. 24.1d), KSAT system (for saturated soils, Fig. 24.1e), and double ring and modified Philip-Dunne infiltrometers. For soil purification and diffusion testing, there are five dialysis-leaching test (DLT) setups (Fig. 24.1f) and a VersaStar pH/conductivity meter with ion-selective electrodes for calcium, chloride, potassium, and sodium.

Geoenvironmental researchers at Villanova also have access to the following facilities and equipment in the Environmental Engineering and Water Resource Laboratories: Agilent gas chromatograph with mass spectrometer (GC/MS) detector, two Agilent gas chromatographs with flame ionization and thermal conductivity detectors, Dionex ion chromatography system, Shimadzu high-performance liquid chromatograph (HPLC), Dohrmann UV-persulfate total organic carbon analyzer system, HACH DR/4000 Spectrophotometer (total nitrogen and total phosphorous), atomic absorption spectrometer (AA 800), EasyChem Plus autoanalyzer, fume hoods, muffle furnace, centrifuges, and Milli-Q ultrapure water purification systems.

24.4 Future Research and Collaboration Opportunities

Some opportunities for future, collaborative research that could advance the state of the art and the state of the practice for engineered barriers are summarized below:

- There is limited data available regarding diffusion in chemically modified bentonites. Additional diffusion testing (e.g., dialysis-leaching test method (Sample-Lord and Shackelford 2016), through-diffusion method) needs to be performed to better compare the performance of traditional and modified bentonites and improve predictions of contaminant flux through barriers with modified bentonites.
- Based on the limited data available, the persistence of membrane behavior for chemically modified bentonites (for enhanced barrier performance) is promising. However, additional research is required to evaluate (1) the limiting concentrations at which the effects of membrane behavior remain relevant and (2) the long-term integrity of modified bentonites.
- Recent research indicates membrane behavior increases as the degree of saturation (S) decreases (Sample-Lord 2015), which is an important consideration for applications such as barriers for HLRW. However, additional testing needs to be performed at lower values of S ($S < 0.79$) and for multivalent solutions to better understand unsaturated membrane behavior.
- Additional experimental research using solutions more representative of chemical wastes in practical applications (e.g., real or synthetic leachates) is essential to evaluate transport properties of the barrier materials for field conditions. For example, transport properties of GCLs need to be evaluated for containment of coal combustion products, which were classified as Subtitle D waste under the Resource Conservation and Recovery Act in 2015.

References

Benson C, Chen J, Edil T (2014) Engineering properties of geosynthetic clay liners permeated with coil combustion product leachates: Final report. Sustainability Report No. OS-14-11, Office of Sustainability, University of Wisconsin-Madison, Madison

Bohnhoff G, Shackelford C (2013) Improving membrane performance via bentonite polymer nanocomposites. Appl Clay Sci 86:83–98

Bohnhoff G, Shackelford C (2015) Salt diffusion through a bentonite-polymer composite. Clay Clay Miner 63(3):145–162

Di Emidio G, Mazzieri F, Verastegui-Flores R-D, Van Impe W, Bezuijen A (2015) Polymer-treated bentonite clay for chemical-resistant geosynthetic clay liners. Geosynth Int 22(1):1–13

Evans J, Shackelford C, Yeo S-S, Henning J (2008) Membrane behavior of soil-bentonite slurry-trench cutoff walls. Soil Sediment Contam Int J 17(4):316–322

Henning J, Evans J, Shackelford C (2006) Membrane behavior of two backfills from field-constructed soil-bentonite cutoff walls. J Geotech Geoenviron 132(10):243–249

Jo H, Katsumi T, Benson C, Edil T (2001) Hydraulic conductivity and swelling of non-prehydrated GCLs permeated with single species salt solutions. J Geotech Geoenviron 127(7):557–567

Kang J-B, Shackelford C (2010) Membrane behavior of compacted clay liners. J Geotech Geoenviron 136(10):1368–1382

Kolstad D, Benson C, Edil T (2004) Hydraulic conductivity and swell of nonprehydrated GCLs permeated with multi-species inorganic solutions. J Geotech Geoenviron 130(12):1236–1249

Lange K, Rowe R, Jamieson H (2009) Diffusion of metals in geosynthetic clay liners. Geosynth Int 16(1):11–27

Malusis M, Daniyarov A (2014) Membrane efficiency of a Dense, Prehydrated GCL. 7th international congress on environmental geotechnics, ISSMGE, Engineers Australia, pp 1166–1173

Malusis M, Daniyarov A (2016) Membrane efficiency and diffusive tortuosity of a dense prehydrated geosynthetic clay liner. Geotext Geomembr 44:719–730

Malusis M, Shackelford C (2002) Chemico-osmotic efficiency of a geosynthetic clay liner. J Geotech Geoenviron 128(2):97–106

Mazzieri F, Di Emidio G, Van Impe P (2010) Diffusion of calcium chloride in a modified bentonite: impact of osmotic efficiency and hydraulic conductivity. Clay Clay Miner 58(3):351–363

Meer S, Benson C (2004) In-service hydraulic conductivity of GCLs used in landfill covers – laboratory and field studies. Geo Engineering Report No. 04–17, University of Wisconsin at Madison

Rowe R, Quigley R, Brachman R, Booker J (2004) Barrier systems for waste disposal facilities. Spon Press, London

Sample-Lord K (2015) Membrane behavior and diffusion in unsaturated sodium bentonite. Ph.D. dissertation, Colorado State University, Fort Collins

Sample-Lord K, Shackelford C (2014) Membrane behavior of unsaturated bentonite barriers. In: Abu-Farsakh M, Yu X, Hoyos L (eds) Proceedings of geo-congress 2014: geo-characterization and modeling for sustainability, Geotechnical Special Publication 234, ASCE, Reston, pp 1900–1909

Sample-Lord K, Shackelford C (2016) Solute diffusion in bentonite pastes. J Geotech Geoenviron. doi:10.1061/(ASCE)GT.1943-5606.0001494, 04016033

Scalia J, Benson C, Bohnhoff G, Edil T, Shackelford C (2014) Long-term hydraulic conductivity of a bentonite-polymer composite permeated with aggressive inorganic solutions. J Geotech Geoenviron 140(3):04013025

Shackelford C (1991) Laboratory diffusion testing for waste disposal – a review. J Contam Hydrol 7(3):177–217

Shackelford C (2014) The ISSMGE Kerry Rowe lecture: the role of diffusion in environmental geotechnics. Can Geotech J 51(11):1219–1242

Shackelford C, Lee J-M (2003) The destructive role of diffusion on clay membrane behavior. Clay Clay Miner 51(2):187–197

Zimmel E, Narejo D, Youngblood J (2013) An innovative composite liner system for coal combustion residual containment projects. World of coal ash (WOCA) conference, April 22–25, Lexington

Chapter 25
Feasibility Study of Retaining Walls Backfilled with Sand-Tire Chip Mixtures

S. Bali Reddy, A. Murali Krishna, and Arun Ch. Borsaikia

Abstract Proper management of waste tires is a major problem in many regions of the world. Scrapped tires in different forms are being used in various civil engineering applications. This paper presents the feasibility study on the use of recycled tire chips mixed with sand as lightweight backfill material for retaining wall applications. Properties of sand and sand-tire chip (STC) mixtures and model tests conducted on retaining wall models with these materials are briefly summarized. Investigations on use of different STC mixtures (different proportions) indicated that STC30 mixture (30% of tire chips by weight) is most efficient in improving wall behavior in terms of displacements and pressures. To evaluate the financial benefits in the construction of cantilever retaining wall for three different sizes (3, 6, and 9 m height) with STC0 (sand alone) and STC30 mixture as the backfill material, wall designs including the structural designs and cost analyses are presented. Based on the feasibility studies, it is indicated that STC30 mixtures have lower bending moment and shear force on stem, heel, and toe. Thus, the STC30 shows the better sustainable backfill material for retaining wall structures providing a financial benefit of about 30%.

Keywords Feasibility study • Sand-tire chip mixtures • Retaining walls • Lateral earth pressure • Cost saving

25.1 Introduction

Scrap tires are the undesired urban waste and are increasing every year. In the future, the volume of waste tires is going to increase significantly in many developing countries. Recycling of waste is practiced nowadays to manage industrial wastes.

S. Bali Reddy (✉) • A. Murali Krishna • A.C. Borsaikia
Department of Civil Engineering, Indian Institute of Technology Guwahati, Guwahati, Assam 781039, India
e-mail: sodom@iitg.ernet.in; amurali@iitg.ernet.in; arubors@iitg.ernet.in

G.L. Sivakumar Babu et al. (eds.), *Geoenvironmental Practices and Sustainability*, Developments in Geotechnical Engineering,
DOI 10.1007/978-981-10-4077-1_25

This happens to be very efficient approach in the management of scraped tires and path breaking in the sustainability of natural resources. Reuse of scrap tires in civil engineering applications is an essential step in creating a sustainable future. In some situations, the use of tire-derived materials may provide greater economy than those traditionally used materials. Bosscher et al. (1997) designed highway embankment using tire chips. In addition to other applications, shredded tires, with or without conventional granular material, have been used as retaining wall backfills in the past (Cecich et al. 1996; Humphrey et al. 1992; Tweedie et al. 1998; Hazarika and Yasuhara 2007).

This paper presents the use of tire chips (scrap tire-derived material) in sand-tire chip (STC) mixtures as an alternative backfill material for retaining structures. Properties of sand and STC mixtures and tests conducted on retaining wall models with these materials are briefly presented from the authors' recent publications (Reddy and Krishna 2015; Reddy et al. 2015, 2016). Cantilever retaining walls with STC mixtures as backfill have been considered for study, and behavior has been compared to the retaining wall using natural sand backfill. Considering properties of optimum STC mixture, which yielded better performance from the results of physical model tests, three retaining walls (3, 6, and 9 m heights) have been designed. Cost analyses have been performed to determine the financial feasibility of the retaining walls with sand alone and STC30 mixture backfill materials.

25.2 Properties of STC Mixtures

Reddy et al. (2016) reported the characterization of different STC mixtures. Different STC mixtures (0–100% of tire chips by weight) were considered to find the index and engineering properties. Tire chips of 10 × 10 mm size and about 20 mm length, obtained from scraped tires, and locally available poorly graded sand were used for the study. Figure 25.1 shows the pictorial view of tire chips. Specific gravities of the sand and tire chips were reported to be 2.62 and 1.08, respectively. Properties of STC mixtures, i.e., void ratio, dry unit weight, and angle of friction value of STC mixtures, are shown in Fig. 25.2. From the figure, it can be inferred that the optimum mixing ratio of STC mixture is in 30–40% range, where higher friction angle value and lower void ratio are observed. Further, it can also be seen from the figure that at the optimum mixing ratio of the STC mixture, the dry unit weight was reduced by nearly 20%. These observations show that STC mixtures can effectively work as lightweight material as well as provide better compressibility characteristics (due to lesser void ratio) and high load-carrying behavior (due to high shear strength) for geoengineering applications.

Fig. 25.1 Picture of tire chips

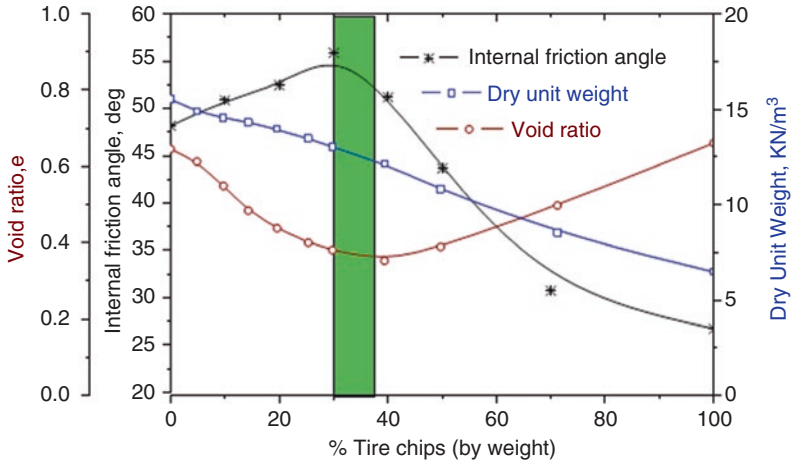

Fig. 25.2 Properties of STC mixtures (After Reddy et al. 2016)

25.3 Model Studies on Retaining Walls with STC Mixtures

Reddy and Krishna (2015) and Reddy et al. (2015) studied the behavior of retaining wall models backfilled with different STC mixtures, loaded with different surcharge pressures under static loading and without surcharge pressures under seismic loading. The retaining wall models of 600 mm height were constructed in a Perspex container of 1200 mm × 600 mm in plan and 1000 mm height (Fig. 25.3). The wall of 600 mm high and 580 mm wide was made with eight hollow rectangular (2 mm

Fig. 25.3 Model container with typical model wall on shaking table

thick) steel sections, each 580 mm length 25 mm wide and 75 mm height, which were joined using steel rods of 12 mm diameter. These steel rods were further connected to a bottom plywood board base of 12 mm thickness, forming a rigid connection. STC mixtures were prepared by manual mixing to maintain the selected TC percentage levels (10, 20, 30, 40, and 50% that were represented as STC10, STC20, STC30, STC40, and STC50, respectively). The STC mixtures were filled in stages using free-falling technique in the backfill area and then compacting manually to achieve the target density. The model wall, after complete construction, tested at static loading conditions with different surcharge pressures. Similar configuration model walls, after complete construction, were placed on a 1 g shaking table for seismic testing. The single-axis shaking table of 2.5 × 2.5 m in size was used to simulate horizontal shaking action associated with sinusoidal and different earthquake motions. During shaking table tests, wall displacements and accelerations at different elevations were recorded using LVDT and accelerometers, respectively, as shown in Fig. 25.4 (Reddy et al. 2015). The earth pressures were determined for various STC percentages. Percentage (%) reduction of measured maximum earth pressures with percentage of tire chips, under static loading of 10 kPa surcharge, is shown in Fig. 25.5 (Reddy and Krishna 2015). It is seen that % reduction of earth pressure was increased with increasing %TC up to STC30. The displacement profiles and incremental earth pressures, for the model walls with different backfill materials (STC0–STC50), observed during South Napa (SN) earthquake motion are shown in Fig. 25.6 (Reddy et al. 2015). From Figs. 25.5 and 25.6, it can be noted that by using STC30 backfill, about 50–60% reduction in earth pressures and displacements is achieved.

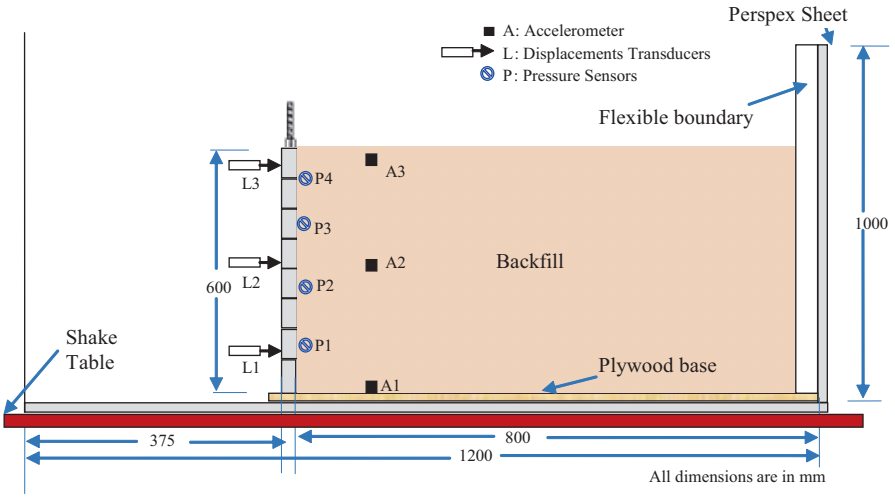

Fig. 25.4 Schematic diagram of model wall (After Reddy et al. 2015)

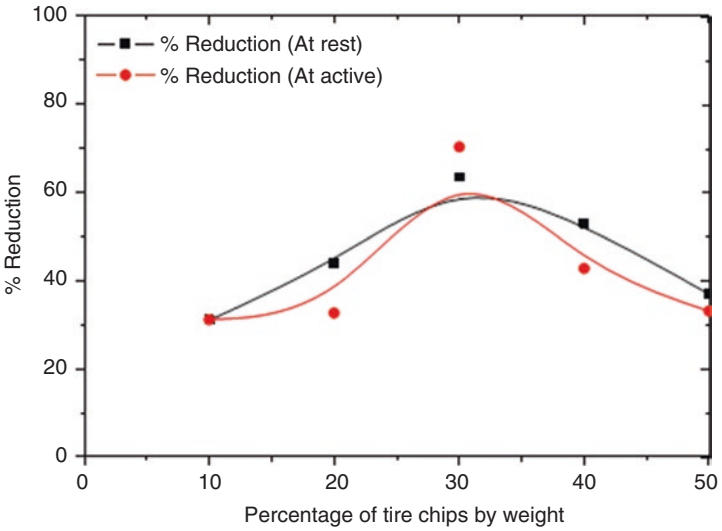

Fig. 25.5 Percentage reduction of maximum earth pressures (After Reddy and Krishna 2015)

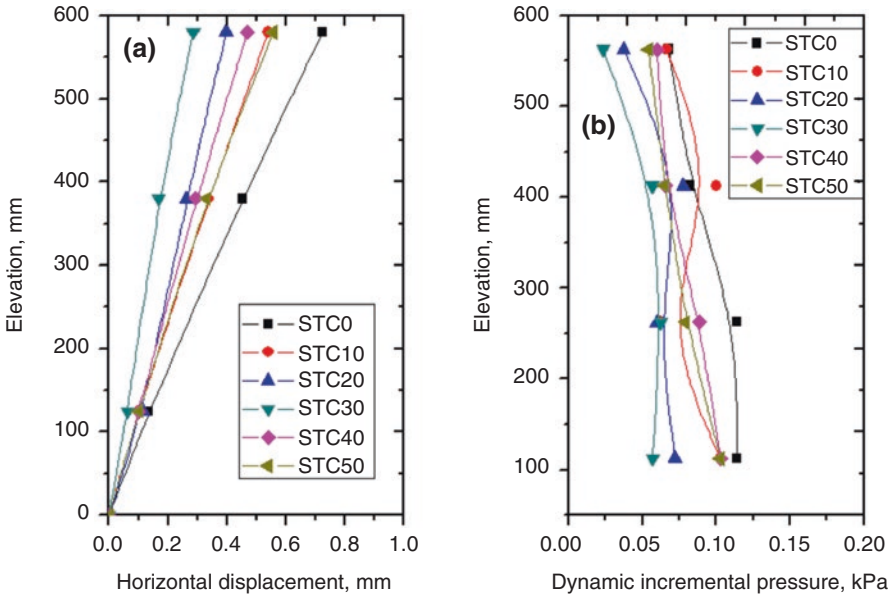

Fig. 25.6 Response of model wall for SN earthquake motion: (**a**) displacement profile and (**b**) incremental earth pressures (After Reddy et al. 2015)

25.4 Design of Retaining Walls

Based on the observed material properties as well as static and dynamic behaviors of model retaining wall with different backfills, STC30 backfill depicted the better performance hence considered to be the optimum mix material. To evaluate the financial benefits in the construction of cantilever retaining wall for three different sizes (3, 6, and 9 m height) with STC0 (sand) and STC30 mixture as the backfill material, wall design including the structural designs is presented. The design of this wall consists of two parts: (1) the geotechnical design and (2) the structural design. Cost analysis of both the wall systems has been carried out after arriving final designs of two retaining wall systems. The purpose of cost analysis is to assess the economic feasibility of the proposed retaining wall system with the STC30 mixture as backfill. In the design of both the wall systems, the wall friction has been assumed as two-thirds of friction angle.

A typical cantilever retaining wall shown in Fig. 25.7 indicates various wall parameters that are to be designed for a given wall height, *H*. The retaining wall dimensions have been initially assumed (as per Bowles 1996) as shown in Fig. 25.8. Stability analyses against sliding and overturning have been done by determining the active earth pressures on the wall using Coulomb's method. The factor of safety against sliding is the ratio of horizontal resisting forces divided by the horizontal driving forces. The factor of safety against overturning is the ratio of the resisting

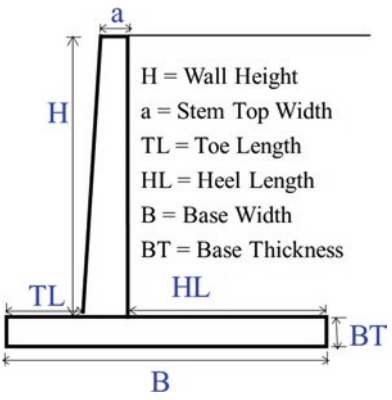

Fig. 25.7 Typical cantilever retaining wall with notations

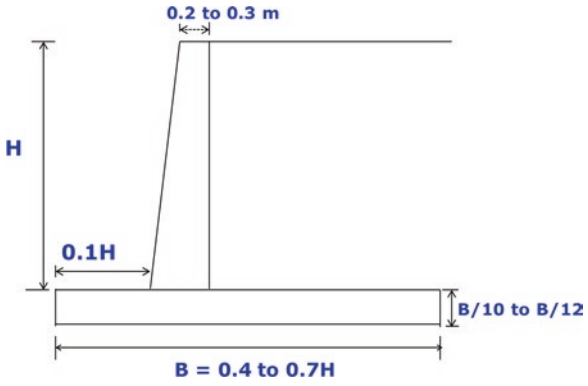

Fig. 25.8 Typical dimensions of cantilever retaining wall (After Bowles 1996)

Table 25.1 Comparison of factors of safety

	Sliding factor of safety		Overturning factor of safety	
Height of wall (m)	Sand	STC30	Sand	STC30
3	3.77	4.64	4.22	2.69
6	3.63	4.00	4.00	2.32
9	3.54	4.09	4.08	2.30

moment and overturning moment. The factors of safety for the cases of both the backfill materials are reported in Table 25.1. The final dimensions of three retaining walls using sand and STC30 as backfills are shown in Table 25.2. The final dimensions of retaining walls lower than after Bowles (1996) are not considered even if it is safe when STC30 mixture is used as backfill material. Both the wall systems with the assumed base widths are found to be safe against both the stability criteria. Once the dimensions of the retaining wall are satisfactory with respect to geotechnical stability, the structural designs of stem, toe slab, and heel slab have been carried out.

Various related stipulations and clauses of IS 456 (2000) and SP 16 (1980) have been followed while doing structural design of both the wall systems. M25 grade

Table 25.2 Final dimensions of retaining walls

Notations	3 m height		6 m height		9 m height	
	Sand	STC30	Sand	STC30	Sand	STC30
a	0.2	0.2	0.2	0.2	0.2	0.2
TL	0.3	0.3	0.6	0.6	0.9	0.9
HL	0.9	0.4	2.0	1.1	3.0	1.6
B	1.5	1.0	3.0	2.0	4.5	3.0
BT	0.2	0.2	0.3	0.3	0.7	0.5

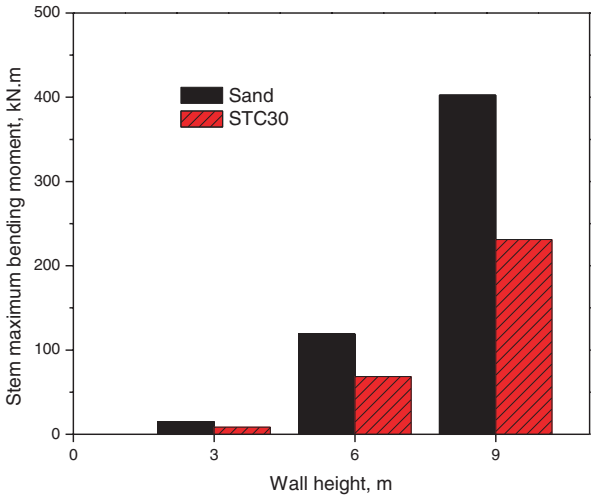

Fig. 25.9 Comparison of maximum bending moment for stem

concrete and Fe500 grade steel have been considered in the structural designs. The retaining wall stem and heel were designed as cantilever members. Shear and moment acting on the wall have been used for flexural analysis of the wall systems. Once the maximum ultimate moment has been determined, the type, spacing, lengths, and quantity of reinforcing bars required have been determined. The calculated maximum bending moments and shear forces at stem, toe, and heel for wall with both the backfill soils are shown in Figs. 25.9, 25.10, 25.11, and 25.12. It is seen from Figs. 25.9 to 25.12 that the maximum bending moment and shear force are lower in the case of STC30 backfill compared to sand backfill. It means the retaining wall with STC30 backfill will be more safe than sand alone as backfill material. The percentages of reinforcement for various heights of retaining walls for stem, heel, and toe for STC0 backfill and STC30 backfill have been reported in Table 25.3. Based on Table 25.3, it may be concluded that percentage of reinforcement is decreased by using STC30 mixture as backfill material of retaining wall, and the difference is clearly shown in higher height of retaining wall.

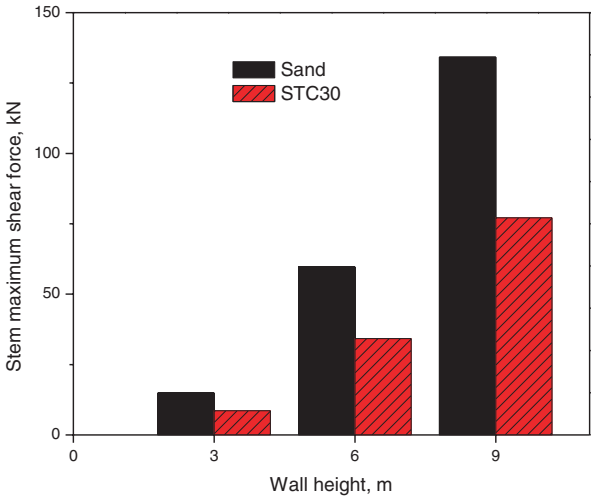

Fig. 25.10 Comparison of maximum shear force for stem

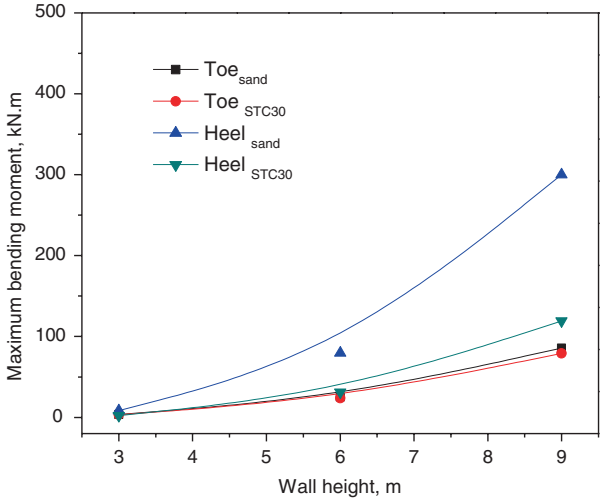

Fig. 25.11 Comparison of maximum bending moment for toe and heel

25.5 Cost Analysis

Cost analysis is performed for retaining wall systems with only sand and STC30 as backfill materials. The cost estimation is based on rate of various materials: steel, sand, aggregate, cement, and others. Based on survey in local market, material rates are adopted as presented in Table 25.4. Cecich et al. (1996) considered that tire chip cost is less than that of the sand (sand, $12; tire chips, $10 per ton). In this study, tire chip cost is double the sand cost (sand price is 1.5 INR per kg and tire chip price 3 INR per kg) considered for cost estimation.

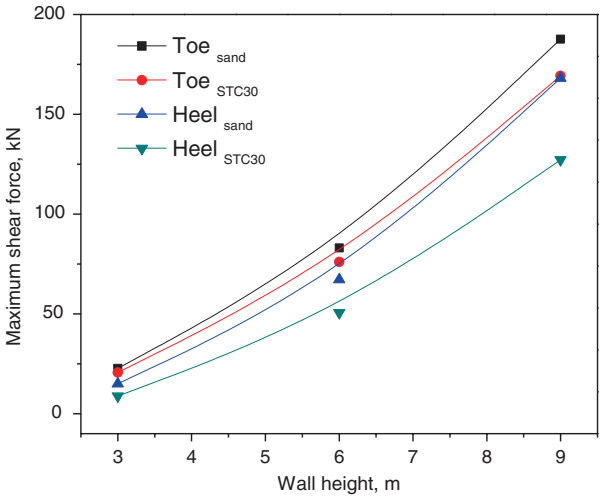

Fig. 25.12 Comparison of maximum shear force for toe and heel

Table 25.3 Percentage of reinforcement

	Percentages of reinforcement					
	Stem		Heel		Toe	
Height of wall (m)	Sand	STC30	Sand	STC30	Sand	STC30
3	0.07	0.07	0.29	0.07	0.07	0.07
6	0.229	0.167	0.29	0.11	0.09	0.08
9	0.32	0.267	0.17	0.09	0.07	0.07

Table 25.4 Material rates range from local builders

Material	Rate range per kg (INR)	Rates considered per kg (INR)
Sand	1.0–1.5	1.5
Steel	40–50	50
Cement	4–7	7
Aggregate	1.0–1.5	1.5

For estimating the cost of retaining wall of a specific height, 30 m-long wall is considered. Volumes of different materials are calculated as per the designs obtained in the previous section. To quantify the backfill volume, as per Cecich et al. (1996), theoretical volume evaluated from Rankine's wedge (depends on friction angle of the backfill material chosen) is considered. Based on this, for a 30 m-long wall, the required volume of backfill of two (sand alone and STC30) retaining wall systems with different heights of wall is shown in Fig. 25.13. The backfill materials and total costs for both the sand and STC30 backfill walls were calculated, for 3, 6, and 9 m height of retaining walls, and are reported in Table 25.5. For comparison, total cost

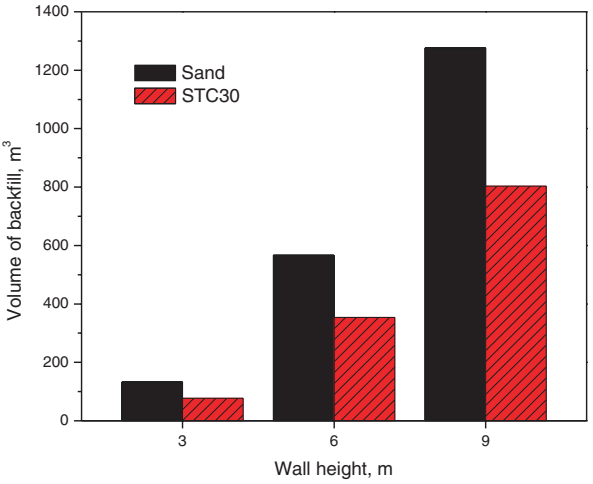

Fig. 25.13 Comparison of backfill volumes for retaining walls

Table 25.5 Comparison of costs for retaining walls (30 m long)

Wall height (m)	Estimated backfill material cost (INR)		% saving	Estimated total cost (INR)		% saving
	Sand	STC30		Sand	STC30	
3	3,16,315	2,02,360	36.02	4,98,240	3,63,635	27.01
6	13,51,000	9,27,300	31.36	18,66,435	13,33,350	28.56
9	30,39,745	21,04,100	30.78	43,67,340	30,50,000	30.16

of three retaining walls is shown in Fig. 25.14 for sand and STC30 backfills. Based on total cost of walls with both the backfill materials, about 30% saving is seen for the wall with STC30 backfill. This cost saving and utilization of waste materials show the sustainability of retaining wall systems with the STC30 mixture backfill. It is to be noted that the amount of savings projected is based on the material rates adopted in the study. The same may vary place to place depending on availability of various materials.

25.6 Conclusions

This paper presented the feasibility study for STC mixtures as backfill material in retaining wall applications. Characterization of various STC mixtures and model tests conducted on retaining walls with different STC backfills indicated that STC30 is the optimum mixture, depicting beneficial performance. The design of three different retaining walls with heights of 3, 6, and 9 m using sand and STC30 mixture as backfill materials and their cost implications has been presented for comparison purpose. Wall sizes and the corresponding reinforcement requirement have been

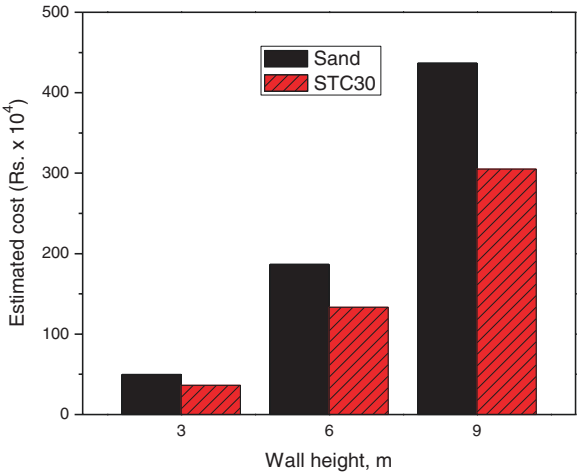

Fig. 25.14 Comparison of total cost for retaining walls

significantly reduced for STC30 backfill wall in comparison to sand backfill wall. From these cost analyses, it has been found that the use of STC30 mixture as backfill generates a saving of about 30% in cost. This cost saving may vary from place to place. Based on the study, it can be concluded that using STC30 mixture can be an alternative backfill material, which is not only economically feasible but also environmentally advantageous with the use of scrap-derived materials in retaining wall applications.

References

Bosscher J, Edill TB, Kuraoka S (1997) Design of highway embankments using tire chips. J Geotech Geoenviron Eng 123(4):297–304

Bowles JE (1996) Foundation analysis and design, 5th edn. McGraw-Hill International Editions, New York

Cecich V, Gonzales L, Hoisaeter A, Williams J, Reddy K (1996) Use of shredded tires as lightweight backfill material for retaining structures. Waste Manag Res 14:433–451

Hazarika H, Yasuhara K (2007) Scrap tire derived geo materials-opportunities, challenges. Taylor, and Francis, London

Humphrey DN, Sandford TC, Cribbs MM, Gharegrat H, Manion WP (1992) Tire chips as lightweight backfill for retaining walls – phase I. Department of Civil Engineering, University of Maine, Orono

IS 456 (2000) Code of practice for plain and reinforced concrete. Bureau of Indian Standards, New Delhi

Reddy SB, Krishna AM (2015) Recycled tire chips mixed with sand as lightweight backfill material in retaining wall applications: an experimental investigation. Int J Geosyn Ground Eng. doi:10.1007/s40891-015-0036-0

Reddy SB, Krishna AM, Dasaka SM (2015) Seismic resilience of retaining walls backfilled with sand–tire chips mixtures. Proceedings of Second Japan-India Workshop in Geotechnical Engineering, Fukuoka

Reddy SB, Kumar DP, Krishna AM (2016) Evaluation of optimum mixing ratio of sand- tire chips mixture for geo-engineering applications. J Mat Civil Eng ASCE 28(2) doi:10.1061/(ASCE)MT.1943-5533.0001335

SP 16 (1980) Design aids for reinforced concrete to IS 456:1978. Bureau of Indian Standards, New Delhi

Tweedie JJ, Humphrey DN, Sanford TC (1998) Tire-shreds as lightweight retaining wall backfill. J Geotech Geoenviron Eng 124(11):1061–1070

Chapter 26
Shredded Waste Tires as a Geomaterial

Umashankar Balunaini and Monica Prezzi

Abstract Recycling and reuse of waste materials for various civil engineering applications will not only ease problems associated with their disposal but also help preserve dwindling granular materials. In this study, a composite material made up of shredded waste tires and sand is proposed as a fill material in the construction of reinforced retaining walls and reinforced embankments. Accordingly, the pullout resistance of different reinforcements (ribbed metal strip, geogrid, and ladder-type metal) embedded in sand is obtained. In addition, the shear strength characteristics of the mixtures are obtained. Three sizes of tire shreds equal to 9.5 mm in nominal size, and 50–100 mm and 100–200 mm in length are considered. Different mixing ratios of tire shreds in the mixtures are evaluated in the study. For test conditions considered in the study, the pullout resistance factors of metal strips, ladder-type metal, and geogrid reinforcements are proposed. The shear strength of tire shred-sand mixtures in terms of friction angle is found to be in the range 30°–33° in comparison to the end-of-test friction angle for clean Ottawa sand equal to 32°.

26.1 Introduction

Scrap tires are nonbiodegradable waste registering a steady increase in their production across the world. As per Rubber Manufacturers Association (2013), nearly 300 million scrap tires were produced per year in the USA in the year 2013. Statistics also indicate large volumes of waste tires generated in other parts of the world (Shulman 2004; Rao and Dutta 2006; Japan Automobile Tyre Manufacturers Association 2007). Waste tires possess properties that are suited of a fill material used in various geotechnical applications – lightweight, thermally resistive, and free- draining characteristics. Typically, whole scrap tires are shredded to

U. Balunaini (✉)
Department of Civil Engineering, Indian Institute of Technology Hyderabad, Kandi, Telangana 502285, India
e-mail: buma@iith.ac.in

M. Prezzi
School of Civil Engineering, Purdue University, West Lafayette, Indiana 47907-1284, USA
e-mail: mprezzi@ecn.purdue.edu

G.L. Sivakumar Babu et al. (eds.), *Geoenvironmental Practices and Sustainability*, Developments in Geotechnical Engineering,
DOI 10.1007/978-981-10-4077-1_26

smaller-size tire shreds (with sizes ranging from 10 to 300 mm) and mixed with sand to improve the properties of the composite material. Many field studies on the use of tire shreds and sand mixtures for various civil engineering applications can be found in the literature (Ahmed and Lovell 1993; Eldin and Senouci 1993; Bosscher et al. 1997; Humphrey et al. 1997; Poh and Broms 1995; O'Shaughnessy and Garga 2000).

In this study, the use of tire sheds mixed with sand as a backfill material in reinforced retaining walls or reinforced embankments is highlighted. Accordingly, the relevant properties, viz., shear strength of mixtures and pullout resistance of different reinforcement types placed in tire shred-sand mixtures, are provided.

26.2 Materials Used

26.2.1 Tire Shreds

Tire chips and tire shreds used in this study were produced and supplied by Entech Inc., which is located in White Pigeon, Michigan, USA (Fig. 26.1). Tire chips were 9.5 mm in nominal size and were nearly equidimensional in shape, whereas the tire shreds were found to be elongated and flat. The larger-size tire shreds were grouped into two size ranges: 50–100 mm in length and 100–200 mm in length. Owing to irregular shapes of tire shreds, the length of tire shred was defined as the largest distance between any two points on periphery of tire shred, and the width of tire shred was taken as the largest distance between two points on its periphery measured in a direction perpendicular to the length direction. Average values of length, width, thickness, and the aspect ratio (defined as the ratio of length to width) of 50- to 100-mm and 100- to 200-mm tire shreds were equal to 76 mm, 49 mm, 10 mm, and 1.6 and 137 mm, 65 mm, 11 mm, and 2.2 mm, respectively. The specific gravity, G_{TS}, was determined as per ASTM C127, and G_{TS} of 9.5-mm tire chips and 50- to 100-mm and 100- to 200-mm tire shred sizes was found to be 1.16, 1.26, and 1.24.

26.2.2 Sand

The sand used in the study was supplied by US Silica Company, Ottawa, IL, and is commercially known as Ottawa sand. Figure 26.2 shows its gradation curve, and the specific gravity of Ottawa sand was equal to 2.65.

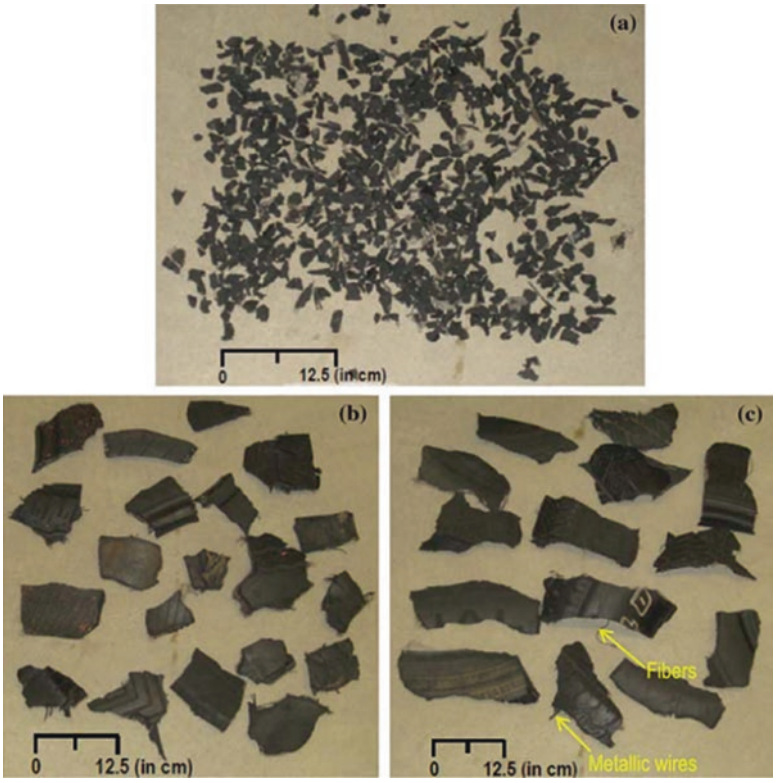

Fig. 26.1 Different sizes of tire shreds considered in this study: (**a**) 9.5-mm tire chips, (**b**) 50- to 100-mm-long tire shreds, and (**c**) 100- to 200-mm-long tire shreds

26.2.3 Ribbed-Metal-Strip Reinforcement

The ribbed metal strips used in this study were galvanized with a zinc coating manufactured. They were supplied by the *Reinforced Earth* Company. The strips were 1000-mm long, 50-mm wide, and 4-mm thick. In order to mobilize passive resistance during pullout, the top and bottom surfaces of the metal strip had pairs of 3-mm-high ribs equally spaced along its length (Fig. 26.3a).

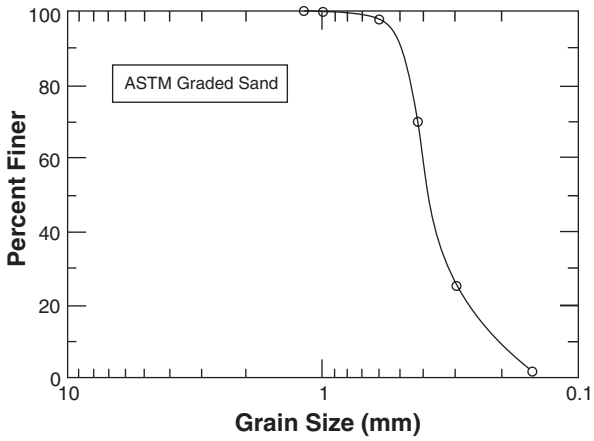

Fig. 26.2 Gradation of Ottawa sand

26.2.4 Geogrid Reinforcement

A commercially available uniaxial geogrid made of high-density polyethylene (HDPE) with a tensile strength of 52 kN/m at 5% strain was used in the pullout tests (geogrid type, UX 1500 MSE manufactured by Tensar). Figure 26.3b shows the UX 1500 MSE geogrid with a relatively large aperture size (17 mm × 445 mm in size).

26.2.5 Ladder-Type Metal Reinforcement

The ladder-type metal reinforcements used in this study were manufactured by the *Reinforced Earth* Company (http://www.reinforcedearth.com/). This reinforcement type consists of two parallel, cylindrical steel bars welded to a series of cross bars (Fig. 26.3c). The total length of the reinforcement used for pullout testing was equal to 1 m. The center-to-center distance between the two longitudinal bars was equal to 0.05 m, and the length of the cross bars was 0.1 m. The diameter of the circular steel bars (longitudinal and transverse) was equal to 0.01 m. At one end, a flat connection plate is welded between the longitudinal bars. This connection plate has a hole, through which a bolted connection can be established to the facing panels of mechanically stabilized earth (MSE) walls.

26.3 Pullout Testing

Figure 26.4 shows pullout test setup used in the study. The dimensions of the tire shred-sand mixture chamber were equal to 1.0 m × 0.38 m × 0.47 m (length × width × height). Two stepper motors were used to apply the pullout load.

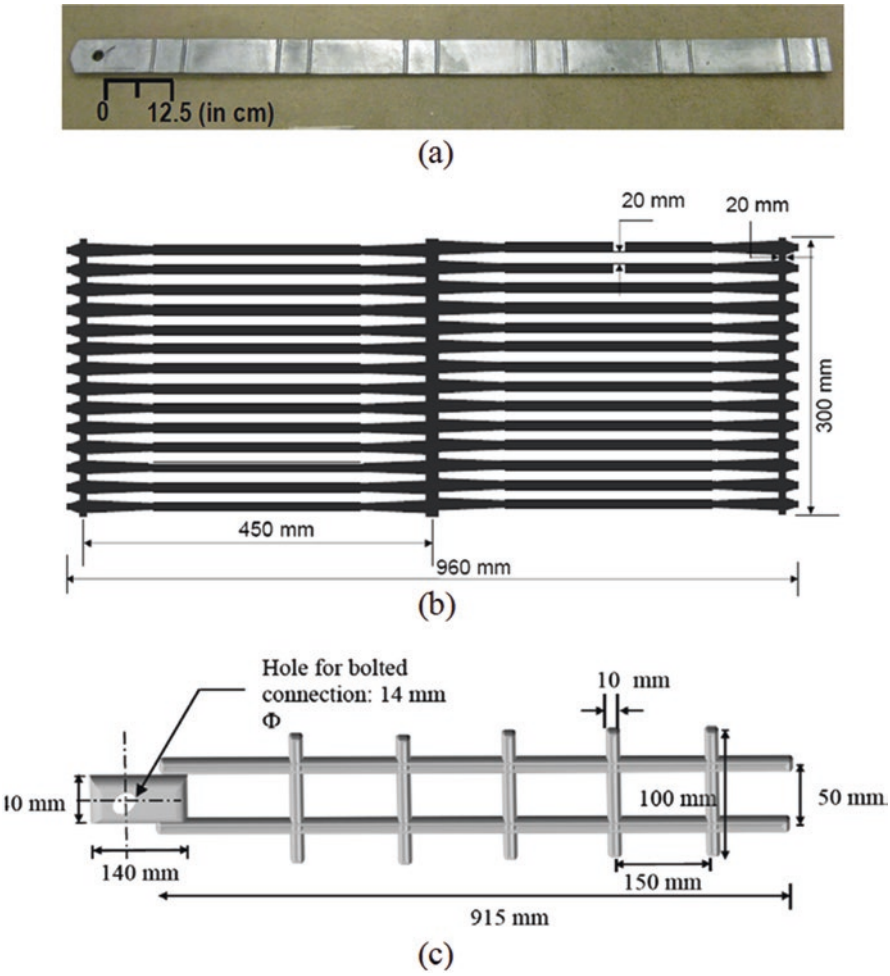

Fig. 26.3 Different reinforcement types used in the study: (**a**) ribbed metal strip, (**b**) geogrid, and (**c**) ladder type

The rate of pullout was maintained at 1 mm/min. Smooth-vinyl sheets were attached to the greased sidewalls of the pullout box to minimize friction between the inner sidewalls and the sample during the application of the normal pressure. An L-shaped sleeve was used to transfer the point of application of the pullout load beyond the rigid front wall. More details on this pullout test set-up can be found in Balunaini and Prezzi (2010). Figure 26.4 shows one reinforcement type, viz., ribbed metal strip, embedded in tire shred and sand mixture and subjected to pullout.

A pneumatically operated piston compactor was used to compact the samples. The desired quantities of tire shreds and Ottawa sand were thoroughly mixed in a container and placed inside the pullout box and compacted in four layers of 10-cm

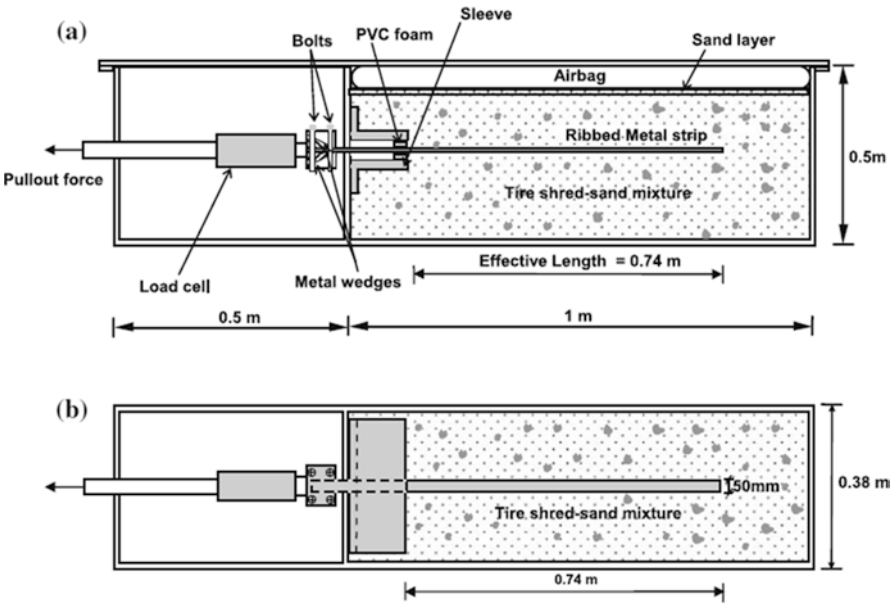

Fig. 26.4 Schematic of pullout testing of ribbed-metal-strip reinforcement with metal strip clamped at mid-height of the pullout box: (**a**) longitudinal cross section of the pullout box and (**b**) plan view of test chamber (Balunaini and Prezzi 2010)

thickness. After compaction of the second lift of the mixture, the reinforcement was placed through the gap between the sleeves and tightly fixed to the clamping system. The remaining two lifts were then placed and compacted. A thin sand layer was then placed on top of the final compacted lift of the tire shred-sand mixture to prevent the pressurized airbag from being punctured by the exposed steel wires present in the tire shreds. The airbag was inflated to the desired confining pressure against the steel plate bolted on top of the pullout box.

The metal strip was pulled at a rate of 1 mm/min. The pullout force, the frontal displacement, and the confining pressure were monitored until the test was completed. The pullout capacity of the metal reinforcements (ribbed metal strip and ladder type) was taken as pullout load corresponding to 20-mm front-end displacement of the reinforcement (Balunaini and Prezzi 2010; Mohan et al. 2016), whereas the pullout capacity was taken as the pullout load corresponding to front-end displacement equal to 50 mm for geogrid reinforcement (Balunaini et al. 2014b).

26.3.1 Pullout Resistance Factors

In the design of MSE structures, it is essential to estimate the pullout resistance factor, F^*, between the reinforcement and the backfill material. For a known value of F^*, the pullout resistance of the reinforcement can be estimated using (Elias et al. 2001)

$$P_{ult} = F^* . \alpha . \sigma_v^{'} . L_e . B . C \tag{26.1}$$

where P_{ult} is the pullout capacity of the reinforcement, F^* is the pullout resistance factor, α is a correction factor to account for nonlinear shear stress distribution along the embedded length of the reinforcement, $\sigma_v^{'}$ is the vertical effective stress at the reinforcement-soil interface, L_e is the embedment length of the reinforcement in the resisting zone, B is the width of the metal strip, and C is the effective unit perimeter of the reinforcement. The total surface area per unit width of the reinforcement is given by $L_e.C$. $C = 2.0$ for reinforcement in the form of strips, grids, and sheets. Elias et al. (2001) recommend using $\alpha = 1.0$ and 0.8 in the case of a metal (inextensible) and geogrid (extensible) reinforcements. Tables 26.1, 26.2, and 26.3 give the pullout resistance factors for the three reinforcement types embedded in tire shred-sand mixtures.

26.4 Direct Shear Testing

A large-scale direct shear box with inner dimensions of the lower box equal to 1.2 m long × 1.0 m wide × 0.47 m high, and dimensions of the upper box equal to 1.0-m long × 1.0-m wide × 0.5-m high, was used to obtain the shear strength properties of the mixtures (Balunaini et al. 2014a). Results of large-scale direct shear testing performed on mixtures prepared using tire shreds 50- to 100-mm long are provided. Table 26.4 shows the shear strength parameters of mixtures prepared at different mixing ratios.

26.5 Conclusions

Based on the pullout test and direct shear testing on tire shred-sand mixtures, the following conclusions were drawn:

1. The proposed pullout resistances of various reinforcements embedded in tire shred-sand mixtures are useful in the internal stability check of reinforced earth structures constructed with tire shred-sand mixtures as the fill material.

Table 26.1 Summary of pullout test results of ribbed-metal-strip reinforcement

Size of shredded tires	Tire shred-sand ratio (by weight)	Confining pressure (kPa)	Maximum unit weight of the mixture (kN/m^3) (Yoon 2006)	Average dry unit weight achieved in the pullout box (kN/m^3)	Relative compaction (%)	Average sand-matrix unit weight (kN/m^3)	Pullout resistance factor, F*
Ottawa sand		40					1.49
	0/100	65	18.0	17.2	95.5	17.2	1.08
		90					0.87
9.5 mm in nominal size		40					1.25
	12/88	65	17.2	15.9	92.5	17.2	0.89
		90					0.75
		40					1.08
	25/75	65	15.2	14.3	94.3	16.6	0.83
		90					0.74
		40					0.41
	100/0	65	5.3	5.3	99.7	–	0.35
		90					0.32
50–100 mm in length		40					1.15
	12/88	65	17.6	15.9	90.5	16.7	0.77
		90					0.75
		40					1.05
	25/75	65	16.6	14.7	88.5	15.8	0.77
		90					0.66
		40					0.44
	100/0	65	6.2	4.9	78.7	–	0.35
		90					0.38
100–200 mm in length		40					1.11
	12/88	65	17.5	16.2	92.4	17.1	0.77
		90					0.66
		40					1.01
	25/75	65	16.5	14.2	86.2	15.4	0.71
		90					0.57
		40					0.54
	100/0	65	6.3	4.6	73.9	–	0.52
		90					*

*Pullout test for reinforcement placed in only tires (100–200 mm in length) and at confining pressure of 100 kPa was not performed due to significant compression of the sample which could damage the rubber air bag during its inflation

Table 26.2 Summary of pullout test results of geogrid reinforcement

Size of shredded tires	Tire shred: sand ratio (by weight)	Confining pressure (kPa)	Maximum unit weight of mixture (kN/m^3)	Average unit weight achieved in pullout box (kN/m^3)	Relative compact on (%)	Pullout resistance (kN/m)	Pullout resistance factor, F^*
Ottawa Sand	0/100	40	18.0	17.2	95.5	23.6	0.49
		70				31.7	0.38
		100				36.1	0.30
9.5 mm nominal size	12/88	40	17.2	15.9	925	22.2	0.46
		70				26.8	0.32
		100				32.8	0.27
	25/75	40	15.2	14.3	94.3	20.3	0.42
		70				26.6	0.32
		100				30.4	0.25
	100/0	40	5.3	5.3	99.7	6.3	0.13
		70				11.0	0.13
		100				14.9	0.12
50–100 mm in length	12/88	40	17.6	15.9	90.5	20.9	0.44
		70				28.4	0.34
		100				31.2	0.26
	25/75	40	16.6	14.7	88.5	18.0	0.38
		70				23.7	0.28
		100				28.4	0.24
	100/0	40	6.2	4.9	78.7	8.4	0.18
		70				12 2	0.15
		100				17.1	0.14
100–200 mm in length	12/88	40	17.5	16.2	914	20.7	0.43
		70				27.9	0.33
		100				34.6	0129
	25/75	40	16.5	14.2	86.2	14.2	0.30
		70				21.1	0.25
		100				27.4	0.23
	100/0	40	6.3	4.6	73.9	8.3	0.17
		70				12.1	0.14
		100				*	*

*Pullout test for reinforcement placed in only tires (100–200 mm in length) and at confining pressure of 100 kPa was not performed due to significant compression of the sample which could damage the rubber air bag during its inflation

Table 26.3 Summary of pullout test results of ladder-type metal reinforcement

Size of shredded tires	Tire shred: sand ratio (by weight)	Confining pressure (kPa)	Maximum unit weight of mixture (kN/m^3)	Aveage unit weight achieved in pullout box (kN/m^3)	Relative compaction (%)	Pullout resistance (kN/m)	Pullout resistance factor, F^*
Ottawa Sand	0/100	40	18.0	17.2	95.5	4.2	1.31
		65				4.9	0.97
		90				6.6	0.95
50–100 mm in length	20/80	40	17.2	15.6	90.1	6.1	1.91
		65				7.2	1.43
		90				8.3	1.20
	25/75	40	15.2	14.8	97.3	5.5	1.73
		65				8.0	1.59
		90				9.5	1.38
	35/65	40	14.2	12.3	86.7	6.4	2.04
		65				9.4	1.88
		90				9.7	1.42

Table 26.4 Summary of pullout test results of ladder-type metal reinforcement

Tire shred: sand ratio (by weight)	Average dry unit weight of mixture (kN/m^3)	End-of-test shear strength parameters in terms of friction angle ϕ (in degrees)
20:80	15.5	30
25:75	14.9	33
35:65	13.5	32

2. The pullout capacity of ladder-type metal reinforcements embedded in tire shred-sand mixtures is much higher than that of ribbed-metal-strip reinforcement. This can be attributed to the contribution of the passive resistance resulting from the tire shreds interlocking in the grids of the ladder-type metal reinforcement, in addition to the resistance due to interface friction.
3. The pullout capacity of ladder-type metal reinforcements embedded in tire shred-sand mixtures is higher than that of ladder-type metal reinforcement embedded in sand alone. This can again be attributed to interlocking of tire shred pieces against the grids.
4. The present study provides values of shear strength parameters that can be used for stability checks of fill structures constructed with mixtures of sand and tire shreds. The end-of-test friction angle of tire shred-sand mixtures considered in the study was found to be in the range 30°–33°. In comparison, the end-of-test friction angle for clean Ottawa sand was found to be 32°. This indicates that tire shred-sand mixtures can be viable alternative to conventional fill material.

References

Ahmed I, Lovell C (1993) Use of rubber tires in highway construction. Utilization of Waste Materials in Civil Engineering Construction, ASCE, New York, pp 166–181

ASTM C127 (2004) Standard test method for density, relative density (specific gravity), and absorption of coarse aggregate. ASTM International, Philadelphia

Balunaini U, Prezzi M (2010) Interaction of ribbed-metal strip reinforcement with tire shred-sand mixtures. Geotech Geol Eng 28(2):147–163

Balunaini U, Mohan VD, Prezzi M, Salgado R (2014a) Shear strength of tyre chip–sand and tyre shred–sand mixtures. J Geotech Eng 167:GE1

Balunaini U, Yoon S, Prezzi M, Salgado R (2014b) Pullout response of uniaxial geogrid in tire shred- sand mixtures. Geotech Geol Eng 32(2):505–523

Bosscher PJ, Edil TB, Kuraoka S (1997) Design of highway embankments using tire chips. J Geotech Geoenviron Eng ASCE 123(4):295–304

Eldin NN, Senouci AB (1993) Rubber-tire particles as concrete aggregate. J Mater Civ Eng 5(4):478–496

Elias V, Christopher BR, Berg RR (2001) Mechanically stabilized earth walls and reinforced soil slopes, design, and construction guidelines. Federal Highway Administration Report

Humphrey DN, Katz LE, Blumenthal M (1997) Water quality effects of tire chip placed above the groundwater table. Testing soil mixed with waste or recycled materials, ASTM STP 1275, ASTM, West Conshohocken, pp 299–313

Japan Automobile Tyre Manufacturers Association (2007) Tire recycling handbook. Japan Automobile Tyre Manufacturers Association, Tokyo, p 25

Mohan VKD, Kim H, Balunaini U, Prezzi M (2016) Pullout capacity of ladder-type metal reinforcements in tire shred-sand mixtures. Constr Build Mater 113:544–552

O'Shaughnessy V, Garga VK (2000) Tire-reinforced earth fill. Part 3: Environmental assessment. Can Geotech J 37(1):117–131

Poh PSH, Broms BB (1995) Slope stabilization using old rubber tires and geotextiles. J Perform Constr Facil 9(1):76–80

Rao GV, Dutta RK (2006) Compressibility and strength behavior of sand-Tyre chip mixtures. J Geotech Geol Eng 24:711–724

Rubber Manufacturers Association (2013) U.S. Scrap Tire Management summary 2005–2009. Rubber Manufacturers Association, Washington, DC

Shulman VL (2004) Tyre recycling. European Tyre Recycling Association (ETRA), Brussels, Belgium, Rapra Review Reports, 15(7)

Yoon S (2006) Mechanical response of tire shred-sand mixtures and applications to geotechnical structures. Ph.D. thesis, Purdue University

Chapter 27
Strength Characteristics of Geopolymer Fly Ash-Stabilized Reclaimed Asphalt Pavement Base Courses

Sireesh Saride and Deepti Avirneni

Abstract Safe disposal of recycled construction materials and industrial by-products has become a real environmental concern. Reclaimed asphalt pavements (RAP) and fly ash are such materials, among many other recycled materials, highly produced and stockpiled across the world. The reuse of these secondary materials in civil engineering applications in large quantities is always a challenge due to their inferior properties. RAP materials in pavement base courses have proven to be a viable alternative not only to conserve the natural resources but also to reduce the environmental pollution and landfilling. Since RAP is inefficient to be used as a pavement material, they are blended with virgin aggregates (VA) or stabilized with cementitious materials.

This study characterizes RAP/VA mixes stabilized with alkali-activated fly ash. The presence of the aged bitumen coat over the RAP aggregates may affect the long-term strength and durability of the design mixes; the mixes meet the strength requirements. Hence, the present study verifies the durability of the mixes by subjecting the specimens to aggressive wet–dry cycles to verify the weight loss. The permanency of the stabilizer/activator is also verified through leachate studies. The comprehensive experimental test results indicated that the RAP/VA mixes are durable and found suitable for the base course applications.

Keywords Reclaimed asphalt pavements • Fly ash • Stabilization • Geopolymer • Shear strength

S. Saride (✉)
Civil Engineering Department, Indian Institute of Technology Hyderabad, Hyderabad, India
e-mail: sireesh@iith.ac.in

D. Avirneni
Civil Engineering Department, VNRVJIET, Hyderabad, India
e-mail: deepti_a@vnrvjiet.co.in

G.L. Sivakumar Babu et al. (eds.), *Geoenvironmental Practices and Sustainability*, Developments in Geotechnical Engineering,
DOI 10.1007/978-981-10-4077-1_27

27.1 Introduction and Background

Safe disposal of recycled construction materials and industrial by-products such as reclaimed asphalt pavements (RAP), fly ash, waste tires, quarry waste, construction and demolition waste, etc. has become a real environmental challenge. RAP is a reclaimed material obtained when a portion of distressed asphalt pavement is milled. RAP has been a resource material, when properly stabilized, for a new surface or a base course layer of a flexible pavement. The strength and stiffness properties of RAP can be enhanced by stabilizing them with cement/lime/fly ash. Fly ash being another industrial by-product, if adopted as a stabilizer, can address the landfilling concerns. However, the strength, stiffness, and durability of these mixes are questionable due to the presence of the thin asphalt coat present over the RAP aggregates. To enhance the strength and stiffness properties of fly ash-stabilized RAP bases, alkali activators are adopted.

Durability in this context may be defined as the ability of the mix to resist severe moisture and temperature fluctuations, chemical attack, and abrasion while sustaining its desired engineering properties. The durability of cement-treated RAP/VA mixes was studied by Ganne (2009) by subjecting the mixes to alternate wet–dry cycles to measure the resistance to weight loss after 14 cycles. Ganne (2009) found that the percentage strength loss was around 10–15% on an average for all the mixes studied. It is also important to study the permanency of the design mixes as few researchers have reported the loss of stabilizers from the base layers after certain service period. These problems are due to the detrimental secondary chemical changes in the stabilization process.

In the current study, initially the influence of alkali-activated fly ash stabilization on the strength development of the RAP/VA mixes is evaluated in terms of UC strength. The strength of the design mixes after the durability and permanency studies conducted on 28-day cured specimens is evaluated. The interaction of activated fly ash with RAP/VA mixes in strength gain is presented through Fourier transform infrared spectroscopic analysis.

27.2 Materials Used

The RAP was collected from an ongoing cold-milling operation at the National Highway No. 5 at Nellore, Andhra Pradesh. The grain size distribution of the RAP was determined according to American Society for Materials and Testing, ASTM C 136 (ASTM 2014) and the gradation curve is presented in Fig. 27.1. As the present gradation of RAP is deviating from the cement-stabilized base course material according to the Ministry of Road Transportation and Highways (MoRTH 2000), the material was segregated and maintained an average grade proposed by the agency. The average grade was also chosen for the selected virgin aggregates (VA) collected from nearby quarry. The specific gravity of the RAP and VA is found to be 2.7 and 2.6, respectively.

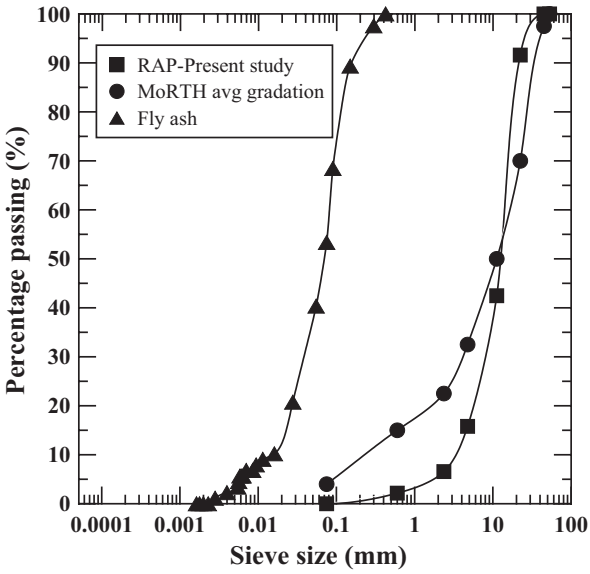

Fig. 27.1 Grain size distribution of RAP and FA

Fly ash was collected from Neyveli Lignite Corporation Limited (NLC), Tamil Nadu. Chemical composition of the fly ash was obtained from X-ray florescence (XRF) method. The calcium oxide (CaO) content is about 12%, and according to ASTM C 618 (ASTM 2012a), the fly ash can be classified as class "F" as CaO is less than 20%. The gradation curve of the fly ash is presented in Fig. 27.1. The specific gravity of the fly ash was determined in accordance with ASTM C 311 (ASTM 2016) and was found to be 2.21.

The laboratory grade sodium hydroxide pellets with 98.9% purity were used as an activator. Since the reaction between NaOH and water is exothermic, utmost care should be taken during the preparation of the solution. The solution shall be prepared at least 6–8 h prior to the mixing.

27.3 Methodology

According to Indian Roads Congress (IRC)(IRC 2012), cement-stabilized bases after 28-day curing period should exhibit a minimum unconfined compressive strength (UCS) of 4.5 MPa to qualify as base/subbase material. To meet this requirement, UCS tests were conducted on the specimens prepared and cured in moist chamber at a constant temperature (25 °C) and humidity (75% relative humidity) for 28 days. A RAP/VA mix proportion of 80:20 stabilized with 20 and 30% fly ash was considered in the present study with and without 2% and 4% NaOH activation. The fly ash dosages were adopted based on the prior performance of the fly ash-stabilized RAP/VA mixes reported by the authors (Saride et al. 2015). The mix proportions

Table 27.1 Mix proportions and their nomenclature

RAP	VA	Fly ash	NaOH	Nomenclature	OMC (%)	MDD (g/cc)
80	20	20	0	80R:20VA+20F+0N	7.05	2.16
80	20	30	0	80R:20VA+30F+0N	7.25	2.14
80	20	20	2	80R:20VA+20F+2N	7.00	2.17
80	20	30	2	80R:20VA+30F+2N	7.20	2.15
80	20	20	4	80R:20VA+20F+4N	6.90	2.17
80	20	30	4	80R:20VA+30F+4N	7.15	2.18

and their nomenclature followed throughout the paper are shown in Table 27.1. Prior to the UC strength tests, modified proctor compaction tests were carried out in accordance with ASTM D 1557-12 (ASTM 2012b) for different mixes to determine optimum moisture content (OMC) and maximum dry density (MDD). Table 27.1 also presents the compaction characteristics of the mixes. With the increase in dosage of fly ash, as expected, the compaction curves have shifted toward the right-hand side reflecting the increase in OMC.

The UC strength tests were also conducted after a repeated wet–dry cycles on compacted specimens of size 100 × 200 mm. The procedure outlined in ASTM D 559 (ASTM 1996) was followed to simulate the moisture fluctuations due to seasonal variation in the field. According to ASTM D 559, at the end of 28-day curing, the specimens were immersed in potable water for a duration of 5 h at room temperature. The samples were then removed and oven-dried at 70 °C for 42 h. This exposure of specimens for 47 h to both wetting and drying activities constitutes a single cycle. Then, the specimens were weighed. The procedure is repeated for 12 such cycles and each specimen is weighed after each cycle to calculate the weight loss. The UC strength is then determined at the end of 12 cycles to assess the retained strength of each specimen.

Apart from the seasonal variations, water infiltration during rainfall may also alter the performance of these mixes. Hence, leachate or permanency studies were performed to verify the loss of stabilizer due to the rain water infiltration and its impact on the UC strength. Any loss in the reactants can be observed by testing the leachate for the respective ion concentrations and pH variation. In these tests, 28-day cured specimens were subjected to water percolation under a controlled pressure of 50 kPa, such that, the packing of the sample is not disturbed. The pore volume of the compacted specimens was calculated, and the collection of in-filtered water equivalent to each pore volume constitutes one cycles. Leachate tests were continued until such 14 pore volumes of in-filtered water are collected. The strength of the specimens after 14 such cycles was determined for all the mixes considered.

27.4 Results and Discussion

The results from UCS tests conducted on fly ash-treated 80R:20VA mixes with and without 2% and 4% NaOH activation before and after the performance of durability and permanency operations are presented in Figs. 27.2 and 27.3. The results proved that, at all fly ash dosages, the mixes without alkali activation (series 1 and 2) do not satisfy the minimum UCS requirement of 4.5 MPa as per the IRC: 37-2012 at 28-day curing. At 2% and 4% NaOH, except 80R:20V+20F+2N specimens (series 3), all the other mixes (series 4–6) have satisfied the specified strength requirement. The increase in UC strength is observed to be about 1.7–1.8 times when activated with 2% NaOH. This increase in strength clearly indicates the enhanced reactivity of the fly ash due to alkali activation. In addition, with the increase in NaOH dosage from 2 to 4%, all the mixes have gained 8–10% of additional UC strength.

It is also of interest to determine the retained strength of the mixes after the durability and permanency studies, where the specimens were subjected to aggressive wet–dry cycles and perfused with pore fluids, respectively. The weight loss of all the mixes is observed to be well within the permissible limit of 14% as specified in the IRC: 37-2012 (IRC 2012) for a cemented base material. It can be observed that for a given RAP proportion (80%), the weight loss is higher for low fly ash (20%) and NaOH (2%) contents. This may be attributed to the hindered pozzolanic activity due to the presence of high amount of aged bitumen in the mix and relatively low cementation. In addition, during permanency or leachate studies, the leaching out of

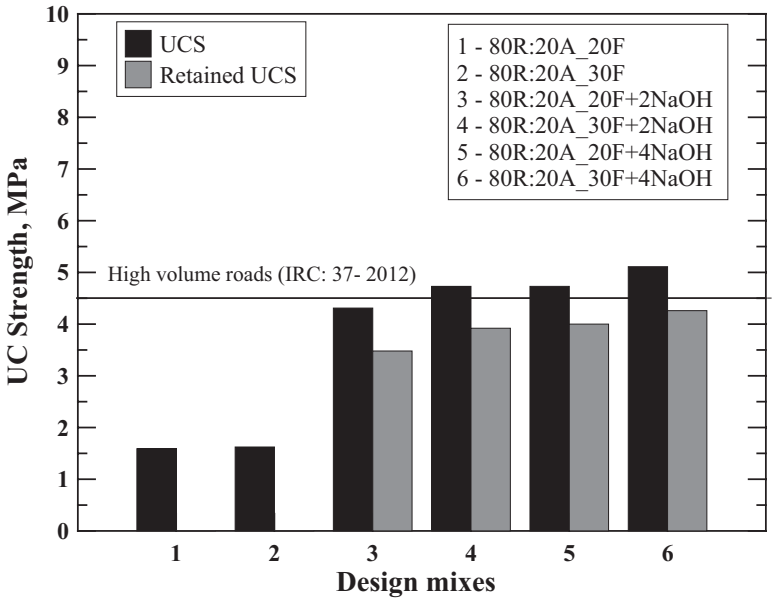

Fig. 27.2 Variation of UCS and retained strength after 12 wet–dry cycles for different mixes

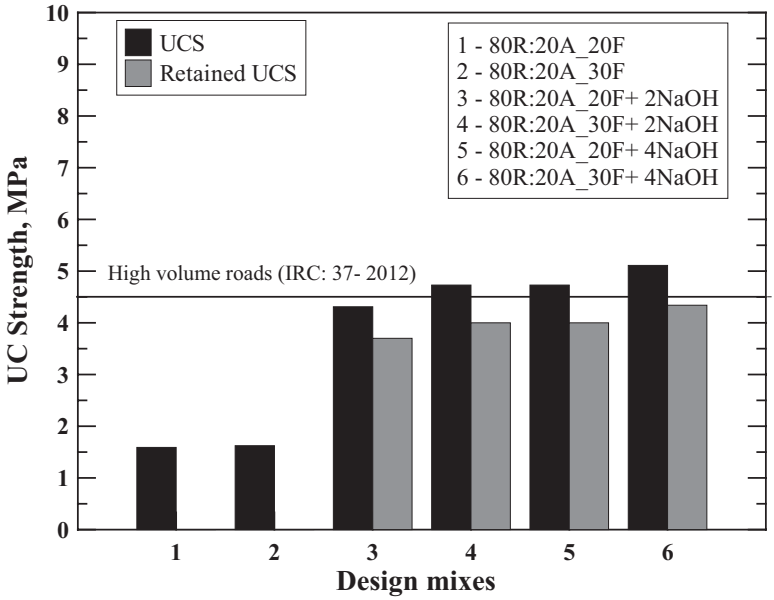

Fig. 27.3 Strength retained after 14 leachate cycles for different mixes

the stabilizer and activator was recorded. It is found that about 50 ppm of CaO leached out of the specimens during the first cycle, thought in the permissible limits, becomes less than 15 ppm in fourth cycle, indicating that the excess lime present in the mix has leached out. On an average, the pH concentration of the leachate was observed to be reduced from 12.5 to 9.5 in 14 cycles. The initial high pH concentration of the leachate can be attributed to the amount of free CaO liberated from the mixes.

It is interesting to note that after the durability and permanency studies on the UC specimens cured for 28 days, the specimens have retained about 80–85% of the original strength. This observation indicates that the pozzolanic reactions between the activated fly ash and RAP/VA mix are considerably high and the designed base course mixes can be adopted for the pavement construction. In addition, the strength of the geopolymer fly ash-stabilized RAP/VA mixes exhibited continuous improvement in the strength of the mixes even at 224 days after cast and cured under controlled humidity conditions (Fig. 27.4). However, the strength improvement after 56 days of curing is marginal. Further, to understand and quantify the interaction between the activated fly ash and RAP base course mixes, Fourier transform infrared (FTIR) spectroscopic studies were performed.

The FTIR transmission spectra of 80R:20V+30F mix with 0, 2, and 4% NaOH activation at a curing period of 28 days is presented in the Fig. 27.5. The significant broad bands observed in the range of 3200–3500 cm^{-1} correspond to the stretching vibrations of −OH groups ($\nu 3$) of $Ca(OH)_2$ formed during the hydration process and/or due to the free −OH groups ($\nu 1$) of water molecules present in the matrix.

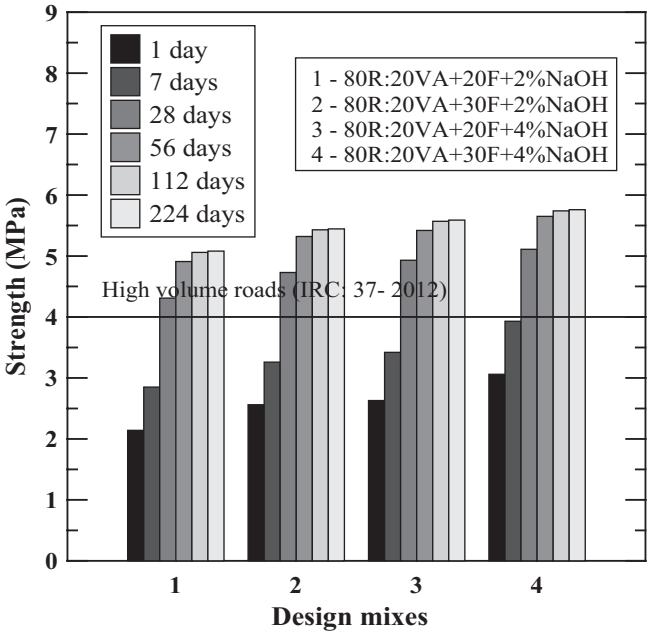

Fig. 27.4 Variation of UCS with curing period for different 80R:20VA mixes

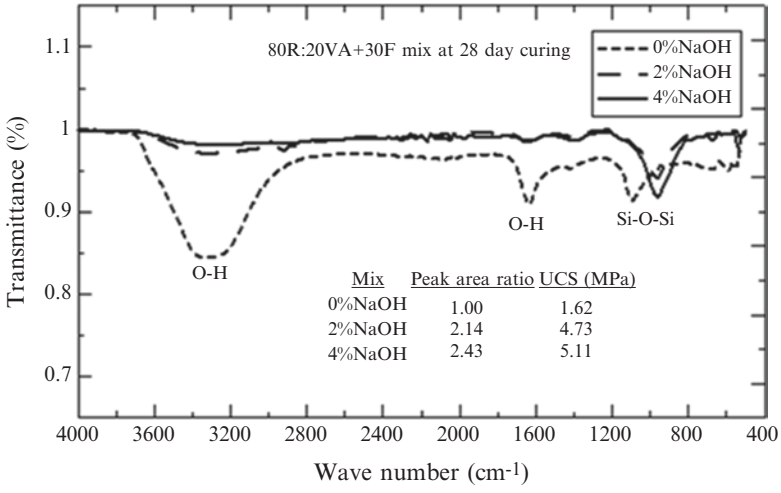

Fig. 27.5 Typical FTIR spectra of 80R:20VA+30F with and without activation at 28-day curing

The bands appearing between 1100 and 900 cm^{-1} are due to the asymmetric stretching vibrations of Si–O–Si or Al–O–Si. This is referred to the formation of amorphous to semicrystalline aluminosilicate materials. Interesting observation is that this band shifted from 1050 to 950 with the addition of NaOH, which can be

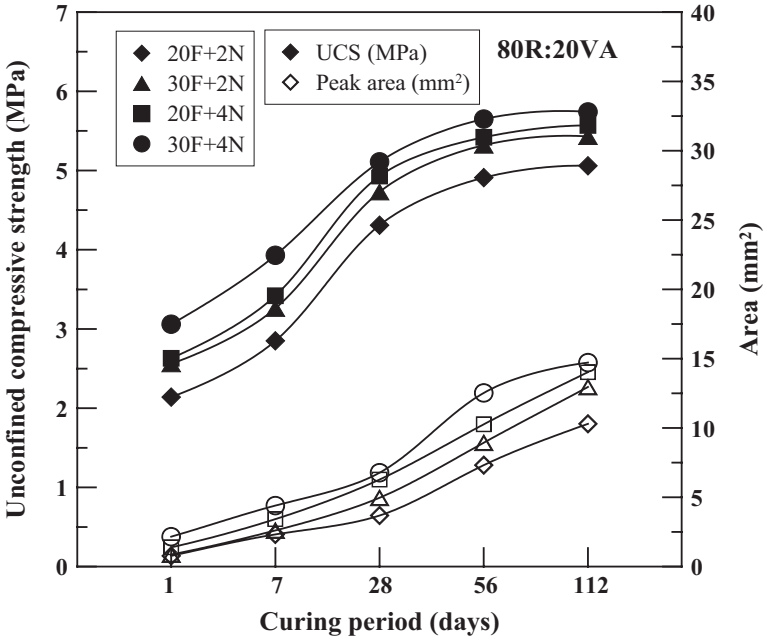

Fig. 27.6 Variation of UCS and peak areas with curing periods for 80R:20VA mixes

attributed to the formation of hydration products. It is reported that the peak areas and peak heights at Si–O–Si stretching vibrations can be used for the quantitative assessment of the reactions (Chindaprasirt et al. 2009). The peak areas are calculated using SCION, an image processing software which gives area of the selected boundary in pixels. The ratios of peak area of Si–O–Si stretching vibration of 80R:20VA+30F mix are also presented in Fig. 27.5. The values correspond to the normalization with respect to the mix without activation. For the mix without activation, peak area ratio is relatively low. The peak area ratio of the mix increases with increase in the activator content from 0 to 4% suggesting that a relatively high degree of hydration has occurred. These results are also in accordance with the trends observed in UC strengths which are presented in Fig. 27.6.

27.5 Conclusions

The following conclusions can be drawn from this paper:

- In spite of the presence of excess calcium, fly ash stabilization could not impart sufficient UC strength to the RAP/VA mixes.
- Around threefold increase in strength for all the mixes was observed with NaOH activation. Mixes activated with 4% NaOH showed 15% higher improvement in strength than the mixes with 2% NaOH activation.

- The fly ash was successfully activated with 2 and 4% NaOH to further the strength gain to meet the design strength 4.5 MPa.
- The durability and permanency studies in terms of aggressive wet–dry cycles indicated that the activated fly ash-stabilized RAP/VA mixes performed satisfactorily. The weight loss after the durability cycles was found to be less than 14% as specified by IRC: 37-2012. The retained strength of the mixed after the durability and permanency studies is about 85%.
- Reduction in intensity of bands formed due to free −OH groups ($\nu 1$) of water molecules with curing period indicates that the hydration is proceeding. The asymmetric stretching vibrations of Si–O–Si increased with activator content and curing period, thereby implying the formation of hydration products which is also confirmed by the increased UC strength.
- Overall, it is observed that the geopolymer fly ash-treated RAP/VA base course mixes can be successfully employed in new pavement construction.

Acknowledgments Authors would like to thank the Technology Systems Development program of the Department of Science and Technology, government of India, for providing financial assistance to carry out this project (Project Sanction No. DST/TSG/STS/2013/40-G). Authors would like to thank M/s. Neyveli Lignite Corporation Limited for their support by supplying fly ash for this research study.

References

ASTM (1996) Standard test methods for wetting and drying compacted soil-cement mixtures, ASTM D559-96. ASTM International, West Conshohocken, PA. www.astm.org

ASTM (2012a) Standard specification for coal fly ash and raw or calcined natural pozzolan for use in concrete. ASTM C 618-12a, West Conshohocken, PA

ASTM (2012b) Standard test methods for laboratory compaction characteristics of soil using modified effort (56,000 ft-lbf/ft3 (2,700 kN-m/m3)). ASTM D1557-12e1 ASTM International, West Conshohocken, PA. www.astm.org

ASTM (2014) Standard test method for sieve analysis of fine and coarse aggregates. ASTM C 136. West Conshohocken

ASTM (2016) Standard test methods for sampling and testing fly ash or natural pozzolans for use in portland-cement concrete ASTM C311/C311M-16, ASTM International, West Conshohocken

Chindaprasirt P, Jaturapitakkul C, Chalee W, Rattanasak U (2009) Comparative study on the characteristics of fly ash and bottom ash geopolymers. Waste Manag 29, 539–543

Ganne VK (2009) Long-term durability studies on chemically treated reclaimed asphalt pavement materials. Master thesis report. University of Texas, Arlington

Indian Roads Congress (2012) Guidelines for the design of flexible pavements. IRC-37, New Delhi

MoRTH (2000) Specifications for road and bridge works. Published by the Indian Roads Congress on behalf of the Govt. of India, Ministry of Road Transport and Highways, Government of India

Saride S, Avirneni D, Javvadi S (2015) Utilization of reclaimed asphalt pavements in indian low-volume roads. J Mater Civ Eng. doi:10.1061/(ASCE)MT.1943-5533.0001374, 04015107

Chapter 28
Sustainable Waste Management Using MSE Berms at Disposal Sites

Ranjiv Gupta, Jeremy W.F. Morris, and R. David Espinoza

Abstract Operators of existing waste facilities try to optimize the airspace above already permitted facility boundaries because of the difficulty of permitting greenfield sites for waste disposal. One technique used successfully to maximize the airspace at active disposal sites involves vertical expansion gained by constructing a mechanically stabilized earth (MSE) berm around the perimeter of the landfill footprint. MSE berms utilize reinforcing geosynthetics in combination with soil to create a safe and cost-effective system that increases the usable airspace within a given permitted landfill footprint. This paper presents two case histories where MSE berms were used to increase waste disposal capacity within the permitted facility boundary. The first case study presents an innovative technique used in the construction of a MSE berm over soft dredge material, thereby using the berm for the dual purpose of ground improvement and the provision of additional waste disposal capacity at the landfill site. The second case study details the use of a MSE berm to optimize the footprint of spoil stockpile at a gold mine, thereby eliminating the need for transportation of spoils at the end of operations and reducing capping costs incurred during mine closure.

Keywords Sustainable • Waste management • MSE Berms • Mines • Landfills

R. Gupta (✉)
Geosyntec Consultants, Phoenix, AZ, USA
e-mail: rgupta@geosyntec.com

J.W.F. Morris
Geosyntec Consultants, Columbia, MD, USA
e-mail: jmorris@geosyntec.com

R. David Espinoza
Geosyntec CAT Advisory, Washington, DC, USA
e-mail: despinoza@geosyntec-cat.com

G.L. Sivakumar Babu et al. (eds.), *Geoenvironmental Practices and Sustainability*, Developments in Geotechnical Engineering,
DOI 10.1007/978-981-10-4077-1_28

28.1 Introduction

MSE berms have been successfully designed and constructed at dozens of landfills across the United States since the mid-1990s (Luettich and Quiroz 2012). Utilizing MSE berms around a landfill perimeter helps increase landfill capacity while accommodating restrictive boundary conditions. In general, a landfill facility can be categorized broadly into three areas: off-limit, inactive, and active. The off-limit area consists of land that cannot be developed for landfill disposal capacity and includes a buffer zone to meet setback requirements, ponds for stormwater management, and areas required for operation and administration of the facility. The inactive area comprises portions of the landfill that have achieved final grades and thus can no longer be used for waste disposal. The active area is used for waste placement. By constructing a MSE berm for vertical expansion of the landfill, the active waste disposal volume is increased without increasing the area of the facility.

Figure 28.1 shows a hypothetical landfill property divided into four groups (G) consistent with the land area categories outlined above but also reflecting expansion of disposal volume offered by an MSE berm. Group G1 indicates the various off-limit areas of the landfill property that are outside the current and proposed limits of the waste disposal. Group G2 indicates the total waste volume that is in place prior to MSE berm construction to expand the landfill (the surface of G2 comprises both inactive and currently active areas). Group G3 indicates the volume of additional waste that can be placed in the future after the MSE Berm construction (G3 therefore represents only future active areas). Finally, Group G4 indicates the external inactive surface of the landfill and MSE berm when the expanded landfill is filled to capacity and closed. The G4 surface represents the area available for redevelopment of the site following closure; as such, proactive consideration of final grades and the orientation of surfaces can increase the range of beneficial reuse options such as solar projects (Gupta and Morris 2013).

In this paper, two case studies are presented in which the existing volume of waste (G2) was nearing capacity under the existing facility design. Rather than closing the site or attempting lateral expansion into G1 areas, the design engineers recommended an MSE berm to expand vertically (i.e., create G3 disposal volume).

28.2 Case Study 1: Cherry Island Landfill, Delaware, USA

The Cherry Island Landfill, located in Wilmington, Delaware, is owned and operated by Delaware Solid Waste Authority (DSWA). DSWA has utilized the landfill to provide safe disposal of waste since 1985. This 100-hectare facility is hemmed in by Interstate 495, the city's wastewater treatment plant (WWTP), and the confluence of the Delaware and Christina Rivers, which are two of the eastern seaboard's most navigable rivers (Fig. 28.2).

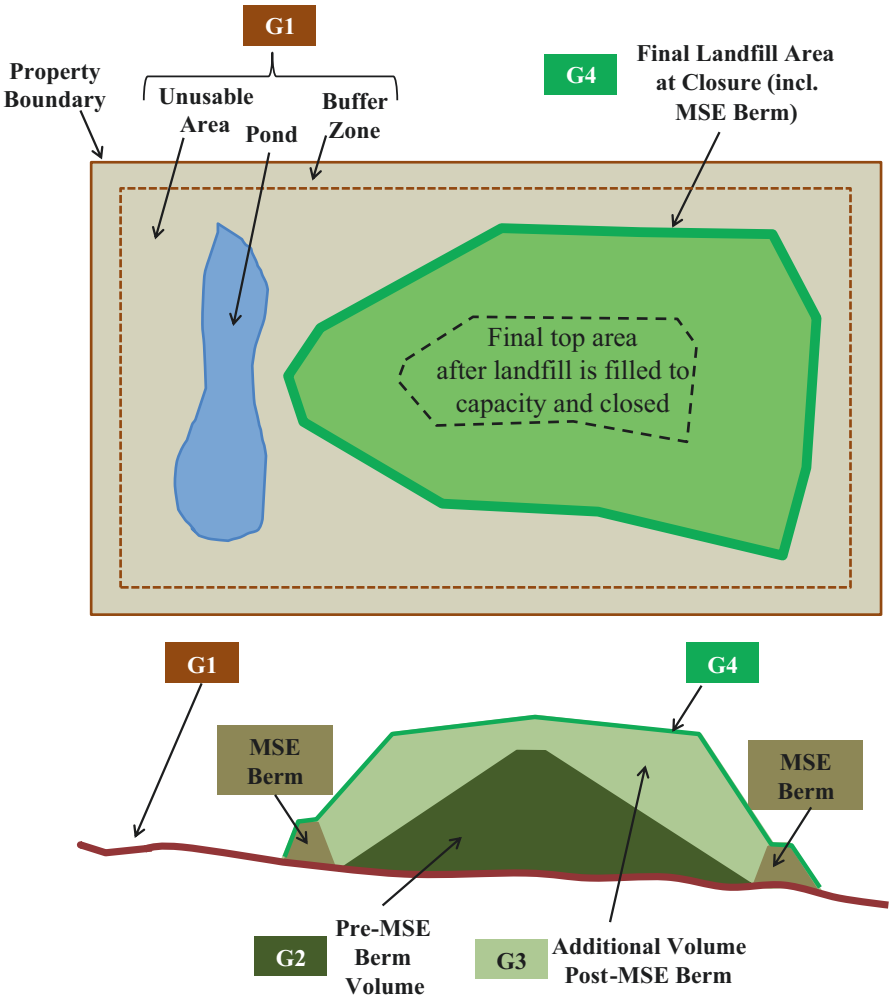

Fig. 28.1 Plan view and cross section showing airspace gained from MSE berm construction at a hypothetical landfill property (Gupta and Morris 2013)

The subsurface conditions at the site consisted of about 12 m thick dredged materials, overlying 14 m thick alluvial deposit, underlain by a medium dense to dense sand layer. The soft and compressible characteristics of the dredge/alluvium material constrained the landfill capacity within the permitted footprint as waste disposal was limited to the relatively flat slope of 8H:1V on average, rather than the typical configuration with 3H:1V slopes. As a result, after only 15 years of operation, disposal capacity was nearing exhaustion. To meet the waste disposal needs of the community for the next 20 years, DSWA estimated that an additional 16,000,000 m^3 of disposal capacity would be required. Following an investigation of several candidate sites for a replacement landfill, DSWA concluded that the most

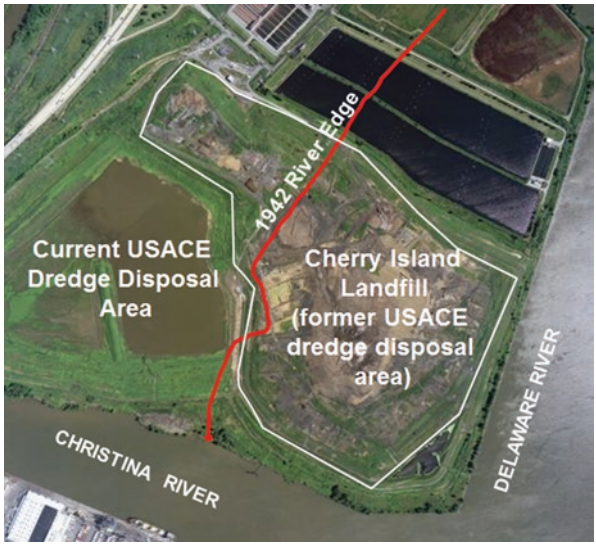

Fig. 28.2 Aerial view of the Cherry Island Landfill

cost-effective and sustainable path forward was to pursue an expansion of the existing landfill. As the landfill was constrained from expanding laterally, a vertical expansion was proposed using a perimeter MSE berm of length 2400 m and height up to 20 m.

A preliminary feasibility study for the project indicated that in order to build the berm, the foundation strength would need to be improved from 10 to 150 kPa. The initial conceptual solution proposed for foundation improvement was the use of deep soil mixing (DSM), a technique that consists of mixing soil with cement. Using the DSM method, approximately 2,000,000 m^3 of soil would need treating at an estimated cost of $170 million. Due to the high cost of DSM, several alternatives were evaluated from which it was concluded that using prefabricated vertical drains (PVDs) to take advantage of the massive weight of the MSE berm to improve the foundation strength would be far more economical. PVDs help dissipate the excess pore pressures generated in the foundation soil during the construction of the MSE berm, thereby allowing the foundation soil to consolidate and gain strength.

Figure 28.3 shows the schematic of the MSE berm design with PVDs (top) and the picture of the constructed berm at the site (bottom). This innovative design resulted in a savings of over $159 million (i.e., $170 million with DSM vs. $11 million with PVDs).

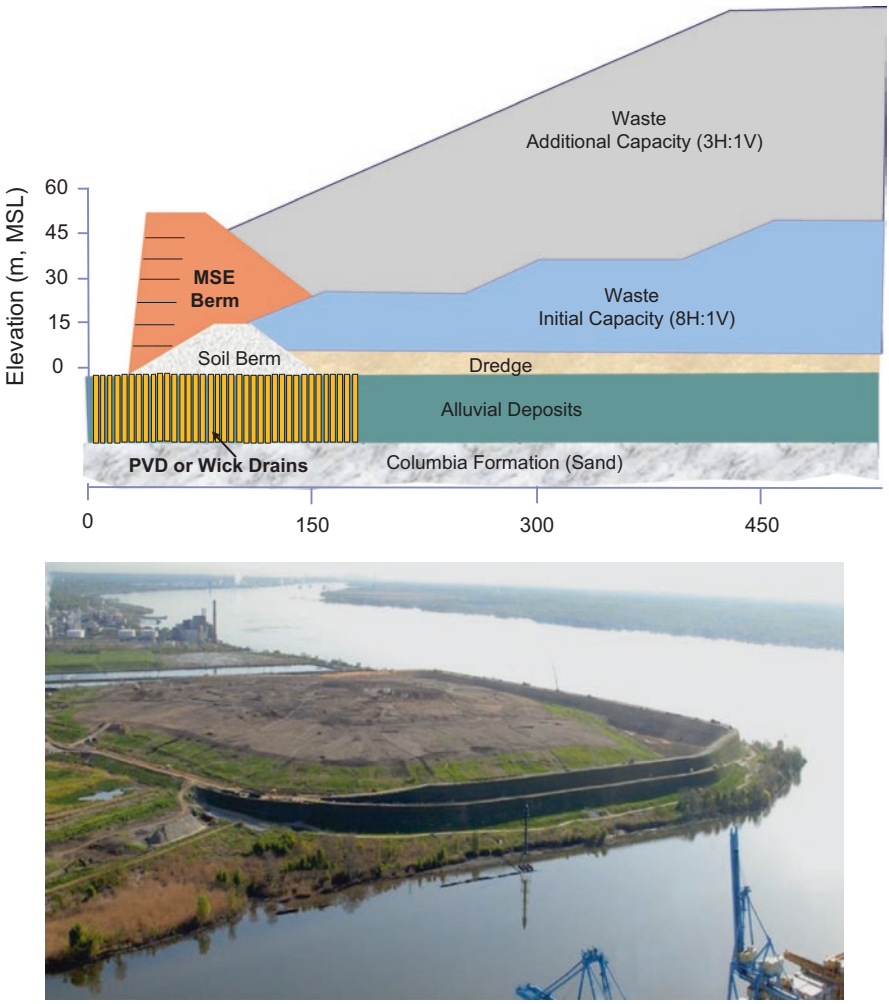

Fig. 28.3 MSE berm at Cherry Island Landfill (Espinoza 2012)

28.3 Case Study 2: Yanacocha Gold Mine, Peru

Yanacocha is the largest gold mine in South America, located in Cajamarca region of Peru and operated by Newmont Corporation. The mine covers 25,000 hectares and started operations in 1993, producing over 970,000 ounces of gold in 2014. During mining operations, spoils or waste rocks (i.e., material overlying the area of economic interest) were removed and stockpiled at the site. However, the spoil stockpile had slopes steeper than typically accepted for closure of the site and post-closure maintenance, thus requiring significant regrading and transportation of spoils at end of operations. In the initial phase of the project, regrading of the spoil

stockpile using either 4H:1V or 3H:1V slopes was assessed assuming the stockpile footprint would be unchanged so that the existing leachate collection system could be utilized. The cut and fill volumes, net volume (the difference between the cut and fill), and total volume (the sum of cut and fill) are summarized in Table 28.1.

Both the total and net earth moving volumes were considered because the total volume indicated the amount of material which needed to be moved (irrespective of whether it was placed as cut or fill during the stockpile closure), while the net volume indicated the amount of material available elsewhere or the amount of material that would need to be transported to the site to achieve the required closure grades. These amounts greatly influence the quantity of earthwork required and, therefore, the final closure costs. The net volume of material requiring relocation (and, by association, alternative disposal) under the 3H:1V option was 35,500,000 m^3. This would increase significantly to 86,600,000 m^3 under the 4H:1V option. Therefore, a conventional closure design would result in significant regrading and relocation of spoils, resulting in high final costs. Based on this, alternative closure design options were considered.

Expanding the stockpile footprint either horizontally or vertically was considered an effective way to reduce construction costs by reducing the net volume of material that would need transporting off-site for disposal. However, a horizontal expansion would require an increase in the stockpile footprint and installation of a new leachate collection system, both expensive undertakings resulting in significant additional site disturbance. Therefore, vertically expanding the site with the use of a MSE berm was preferred as a more cost-effective and sustainable option given the geometric constraints at the site (steeply sloping natural terrain). To evaluate vertical expansion of the stockpile using a MSE berm, vertical cut and fill volumes were calculated for various berm heights assuming the stockpile footprint remained unchanged with side slopes of either 3H:1V or 4H:1V, as summarized in Table 28.2.

The optimal solution is a MSE berm height such that the net volume is zero (i.e., corresponding to the point where the cut and fill volumes balance out, leading to no spoils needing off-site transportation). As expected, the shallower the side slope, the higher the berm required to store the same amount of material in the stockpile.

Table 28.1 Summary of earthwork quantities for closure alternatives

	Earthwork moving volumes (million m^3)			
Options	Cut	Fill	Net	Total
3H:1V	41.8	6.3	35.5	48.1
4H:1V	88.5	1.9	86.6	90.4

Table 28.2 Summary of earthwork quantities for closure alternatives with MSE berm

		Earthwork moving volumes (million m^3)			
Options	MSE wall height (m)	Cut	Fill	Net	Total
3H:1V	12	17.2	19.4	−2.2	36.6
4H:1V	28	26.9	28.9	2.0	55.8

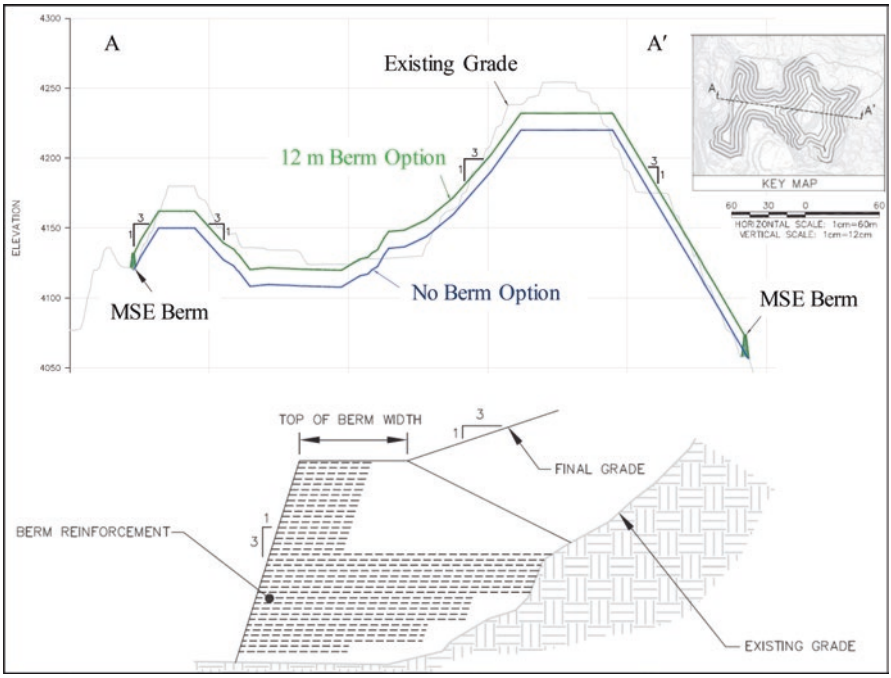

Fig. 28.4 Cross section of MSE berm for spoil stockpile (DeMelo et al. 2014)

The average berm height calculated was about 12 m for a slope of 3H:1V and approximately 28 m for a slope of 4H:1V. The selected design alternative based on the above optimization scheme thus involved a 12 m high perimeter wall with 3H:1V slopes (Fig. 28.4).

28.4 Conclusion

The paper presents two case studies where a MSE berm was used to extend the operational life of an existing landfill facility and minimize the closure cost of existing spoil stockpile at a mine site. By developing an ingenuous, site-specific, cost-effective solution, the construction of MSE berms contributed to more sustainable waste management at both sites by reducing the amount of material required to be transported off-site and by eliminating the need to permit and construct a new facility.

References

DeMelo L, Gupta R, Espinoza RD (2014) Mining closure strategies to optimize capping of spoils and tailing lagoons, Mine Closure Solutions, Ouro Preto, Minas Gerais, Brazil, 27–30 April

Espinoza RD (2012) Innovative design and application of a mechanically stabilized earth wall to compress highly unstable foundation soils at the Cherry Island Landfill, Wilmington, DE, 2012 ASCE OCEA Award Submission

Gupta R, Morris JWF (2013) Converting waste disposal sites to renewable energy sites using MSE berms. ASCE Geo-Congress, San Diego

Luettich SM, Quiroz JD (2012) Landfill stability analyses for the application of mechanically stabilized earth (MSE) perimeter berms. Global waste management symposium, Phoenix, AZ, 30 September–3 October 2012

Chapter 29
Heavy Metal Removal by Aquatic Plants and Its Disposal by Using as a Concrete Ingredient

D. Chaudhuri, Kaushik Bandyopadhyay, A. Majumder, and A.K. Misra

Abstract Cadmium is a very toxic heavy metal which serves no beneficial effect to living organism. Industrial discharge can contain cadmium and contaminate surface water. Phytoremediation, a new cost-effective energy-efficient removal technology, deserves special attention. In the present study, phytoremediation efficiency of *Eichornia crassipes* from cadmium-contaminated water has been demonstrated. Cadmium removal from solution was dependent upon residual cadmium concentration and treatment period. In this process, macrophytes absorb and accumulate cadmium mainly within its root system. After saturation of cadmium-accumulating sites, harvested plant biomass was dried completely to reduce its volume and then solidified after rendering it as a concrete ingredient for use in concrete industry. This process was intended to restrict mobility of cadmium by compacting it inside some inert material like concrete. Findings of TCLP test ensured this process as eco-safe disposal technique of phtytoremediated plant.

Keywords Phytoremediation • Cadmium • Disposal • TCLP

D. Chaudhuri
Central Pollution Control Board, Delhi 110032, India
e-mail: piu.7021@gmail.com

K. Bandyopadhyay (✉)
Department of Construction Engineering, Jadavpur University,
Kolkata, West Bengal, India
e-mail: drkaushik99@gmail.com; kb@const.jusl.ac.in

A. Majumder
School of Water Resources Engineering, Jadavpur University, Kolkata, West Bengal, India
e-mail: arunabhamajumder@hotmail.com

A.K. Misra
Department of Civil Engineering, Jadavpur University, Kolkata, West Bengal, India

G.L. Sivakumar Babu et al. (eds.), *Geoenvironmental Practices and Sustainability*, Developments in Geotechnical Engineering,
DOI 10.1007/978-981-10-4077-1_29

29.1 Introduction

Mobilization of heavy metals in the environment due to industrial activities is of serious concern especially due to toxicity of these metals in human and other living organisms. Most of the heavy metals are nonbiodegradable, and they are characterized by the risk of biomagnifications through food chain. Discharge of heavy metals into the environment in the form of industrial wastewater is one of the major causes of water pollution (Zhang et al. 2011).

Cadmium is a highly toxic heavy metal and has been recognized as potential human carcinogen (Nawrot et al. 2006). Existing conventional methods which include precipitation, electrocoagulation, ion exchange, reverse osmosis, etc. remove cadmium from wastewater (Rahman and Hasegawa 2011). But sometimes, this primary treated water may contain trace amount of cadmium. This can cause toxicity to aquatic organisms through bioaccumulation and finally reach human body through biomagnifications. Therefore, there is a need to develop some cost-effective, eco-friendly technology for toxic metal removal from aqueous solution which contains cadmium at lower concentration in comparison to raw wastewater. In this context, phytoremediation of toxic metal from contaminated site has emerged as a suitable alternative.

Phytoremediation is the process that cleans up toxic contaminants like organic and inorganic pollutants, pesticides, etc. from contaminated sites by utilization of plants. Thus, phytoremediation takes the advantage of natural water and mineral uptake processes of plants. Effectiveness of phytoremediation process depends upon selection of appropriate plant species.

The aim of the present study is to phytoremediate cadmium from contaminated water using aquatic macrophyte *Eichornia crassipes* (EC). Suitability of the selected macrophyte was evaluated through analysis of cadmium removal percentage and cadmium content in plant tissue. After phytoremediation, a cost-effective eco-friendly measure was proposed to dispose these exhausted cadmium-rich phytoremediated plant by incorporating it as a concrete ingredient.

29.2 Material and Method

Experimental Setup *Eichornia crassipes* was collected from a local pond. First, the plants were thoroughly washed to eliminate remains of pond sediments and acclimatized in acid-cleaned plastic tubs with corresponding pond water for 7 days. Thereafter, required amount of fresh plant was transferred to experimental tub containing cadmium-spiked pond water. Culture media was prepared by adding cadmium stock solution to pond water to achieve desired cadmium concentration. Cadmium chloride ($CdCl_2.H_2O$) salt of GR grade was used for preparation of cadmium stock solution.

Each experimental unit contained 50 L of cadmium-spiked pond water as working solution and 2016.13 g/m^2 *Eichornia crassipes*. The experimental setup was kept on roof under cover of plastic sheet for 30 days. On a daily basis, evaporative water loss was compensated by adding pond water collected from same pond. Initial cadmium concentration considered for the present study was 0.5, 1.0, 1.5, 2.0, 2.5, and 3.0 mg/L. A control setup was also used where same amount of plant was cultured in pond water under similar experimental condition but without addition of any cadmium. Each experiment was conducted in three replicates. Periodically water sample was collected for estimation of residual Cd content using the process specified by APHA (1998). After completion of experiment, plants were harvested from the tubs, and cadmium content in plant shoot and root was estimated separately by using atomic absorption spectrophotometer (AAS).

After having harvested cadmium-rich plants, they were dried completely to reduce their volume and then mixed with ingredients of concrete. Principal constituents of concrete mix, i.e., water, cement, fine aggregate (sand), and coarse aggregate (stone chips), were mixed to prepare M25 grade of concrete. Dry plant biomass was added at the rate of 0.2%, 0.4%, and 0.6% by weight of cement (marked as 0.2%EC, 0.4%EC and 0.6%EC, respectively). Compressive strength of concrete was measured after 7 days and 28 days of curing. A control set of concrete cubes devoid of cadmium-containing plant biomass was also prepared. The possibility of leaching of cadmium from concrete after disposal was evaluated by performing toxicity characteristic leaching procedure (TCLP) test following the standard procedure mentioned by EPA.

Metal Removal Percentage Removal of cadmium was calculated on percentage basis using the following equation (Chaudhuri et al. 2014):

$$R(\%) = \frac{C_0 - C_t}{C_0} \times 100$$

C_0 and C_t were used for denoting residual cadmium concentration at initial time and at time t, respectively.

Data Analysis Average value of three replicates with standard deviation in each set of experiment is presented in result section. Statistical comparison of the mean was done by two-way analysis of variance (ANOVA). The difference was considered to be significant at 95% confidence level, i.e., at value of probability (p) ≤ 0.05.

29.3 Result and Discussion

Cadmium Removal Cadmium removal by *Eichornia crassipes* exposed to six different initial cadmium concentrations against treatment period has been graphically presented in Fig. 29.1. Cadmium removal percentage was found to increase with

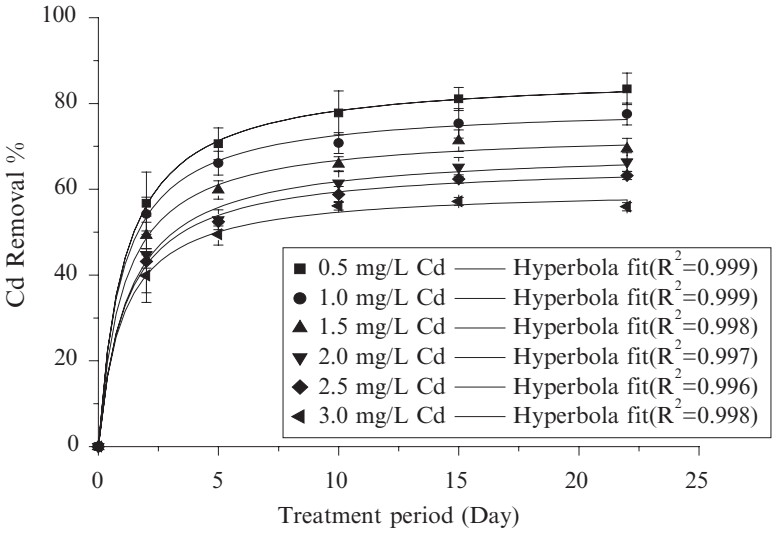

Fig. 29.1 Variation of cadmium removal with treatment period

progress of treatment period, though rate of removal decreased with time. Within first 2 days of treatment period 45.80 ± 1.2 to 17.00 ± 2.17%, cadmium was removed, depending upon initial cadmium concentration in solution. Sharma and Gaur (1995) explained that initially passive uptake was the main driving force for rapid metal accumulation and subsequent removal. But with progress of time, this removal process was gradually shifted under metabolic control. It was further noted that after 27 days of treatment period, residual cadmium concentration did not change considerably. This finding suggested that metal accumulation sites of plant reached saturation level. Uysal and Taner (2010) described this state as dynamic equilibrium treatment period of macrophyte. Again, cadmium removal percentage was gradually found to decrease with increase in initial cadmium concentration.

Cadmium Accumulation in Plant Tissue Accumulated cadmium concentration in shoot and root tissue of *Eichornia crassipes* after 30 days of treatment has been graphically presented in Fig. 29.2. It was observed that cadmium concentration in plant tissue was correlated with initial cadmium concentration in solution. Cadmium concentration in root tissue increased from 1260.25 ± 271.08 to 6130.47 ± 76.56 mg/kg of plant dry weight with increase in initial cadmium concentration from 0.5 to 3.0 mg/L, respectively. In case of shoot tissue, cadmium concentration ranged from 387.25 ± 15.53 to 1037.35 ± 55.22 mg/kg plant dry weight corresponding to the same range of initial cadmium concentration, respectively. This indicated that cadmium concentration in shoot was much less than that of root.

Disposal of Phytoremediated Plants It was observed that cadmium concentration in plant tissue increased with increase in available cadmium in the solution which induced toxic effect of cadmium within the macrophyte. This higher cadmium

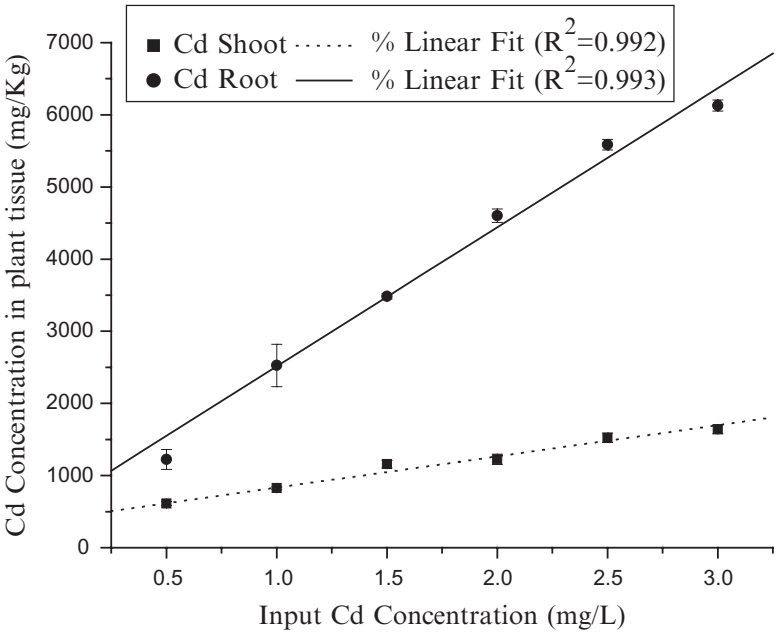

Fig. 29.2 Change in cadmium concentration in plant tissue with change in initial cadmium concentration in solution

toxicity inhibited physiological activity of cadmium accumulation efficiency of *Eichornia crassipes*.

Effect of Cadmium-Rich Dry Plant Biomass on Physical Property of Concrete In order to study the change in physical property of concrete on addition of dry plant biomass, compressive crushing strength of concrete was measured after 7 days and 28 days of curing (Fig. 29.3).

Compressive crushing strength of 7 days cured control concrete cube was 22.42 ± 1.14 N/mm^2. It was slightly higher in case of test cubes. Compressive crushing strengths of concrete cubes containing 0.2%, 0.4%, and 0.6% *Eichornia crassipes* were 24.67 ± 1.05, 24.95 ± 1.54, and 23.51 ± 1.26 N/mm^2, respectively. Again, after 28 days of curing, it was observed that after addition of cadmium-rich plant biomass, compressive crushing strength of concrete did not change significantly in comparison with control set of concrete cube. In all the sets, crushing strength varied within the range of 35–36 N/mm^2. Thus, it can be inferred that the presence of cadmium-containing plant biomass did not influence compressive strength of concrete significantly.

Workability of concrete was also measured by means of slump test. It was found to vary within the range of 75–110 indicating that the concrete was characterized by medium degree of workability (IS 456: 2000). This concrete can be used in heavily reinforced section of slabs, beam, walls, and columns.

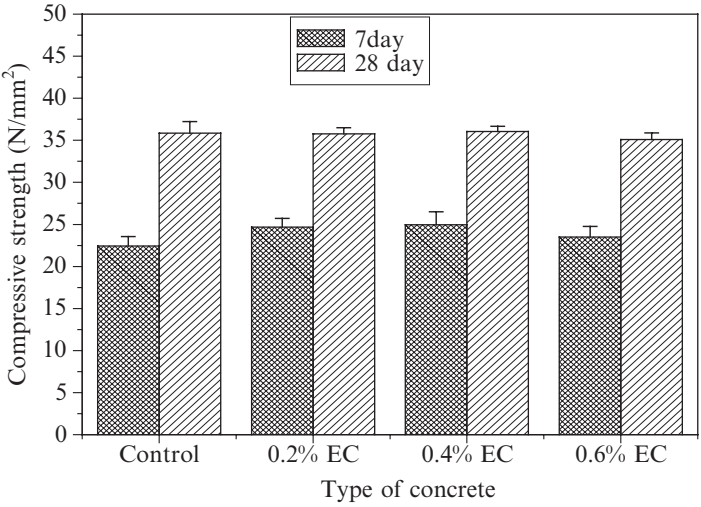

Fig. 29.3 Compressive strength of concrete cubes containing Cd-rich *Eichornia crassipes*

Thus, based on the finding of compressive crushing strength and workability, it can be opined that the addition of cadmium-rich dry plant biomass did not alter physical characteristics of concrete notably and was found to comply well with the standard code of practice.

Results of TCLP Test Three replicates of each set were passed through TCLP test. A set of non-solidified dried plant biomass was also conducted to compare risk of disposing phytoremediated plant without stabilizing inside concrete matrix.

EPA recommended maximum cadmium concentration in TCLP-filtered solution for toxicity characteristics as 1.0 mg/L (Liu et al. 2011). Results of TCLP test showed that cadmium concentration in TCLP filtered solution was considerably below this limit which claimed that cadmium-rich plant containing concrete cannot be classified as "hazardous." Again, it was also demonstrated that disposal of unsolidified dry plant biomass can cause further cadmium contamination in disposal ground. Therefore, suggested disposal measure of cadmium-phytoremediated plant would not create additional environmental nuisance with regard to cadmium contamination. It also indicated that different ingredients, especially cement of concrete mix, effectively immobilized and fixed cadmium inside concrete matrix. Cement which is a particulate inorganic material containing calcareous, siliceous, and argillaceous components formed a plastic mass upon mixing with appropriate proportion of water. The plastic mass was subsequently solidified by a complex mechanism of chemical combination, gelation, and crystallization with time (Chen and Majewski 1978). Portland Pozzolana cement is mainly made up of lime, and hence in contact with water, it creates a strong alkaline environment. Heavy metals are usually made immobile at pH above 8. Therefore, cementitious plastic mass cover along with alkaline environment rendered cadmium immobile inside concrete matrix and thus

reduced its leachability to outer environment. Cement-based matrices produced strong buffering capacity, which neutralized the extraction solution and limited cadmium leaching process (Singh and Pant 2005).

29.4 Conclusion

In this study it was observed that *Eichornia crassipes* could effectively remove cadmium from contaminated water. Its rate of removal was found to be dependent on residual cadmium concentration, and thus removal rate gradually decreased with progress of treatment period. After removal, this cadmium was found to be accumulated in plant tissue. Experimental data indicated that plant root plays a major role in cadmium accumulation than its aerial parts. It was also established that after phytoremediation, Cd-rich plant could be disposed of by using it as an ingredient of concrete in the construction industry. Thus, it can be concluded that the present study highlighted a suitable low-cost Cd removal process from contaminated water and finally demonstrated a measure to restrict further contamination during disposal of exhausted removing media.

References

APHA American Public Health Association (1998) Standard methods for the examination of water and wastewater, 20th ed. APHA American Public Health Association

Chaudhuri D, Majumder A, Misra AK, Bandyopadhyay K (2014) Cadmium removal by *Lemna minor* and *Spirodela polyrhiza*. Int J Phytorem 16(11):1119–1132

Chen KS, Majewski HW (1978) United States Patent, 4113507

Indian Standard 456 (2000) Plain and reinforced concrete – code of practice

Liu R, Durham SA, Rens KL (2011) Effects of post-mercury-control fly ash on fresh and hardened concrete properties. Constr Build Mater 25:3283–3290

Nawrot T, Plusquin M, Hogervorst J, Roels HA, Celis H, Thijs L, Vangronsveld J, Hecke EV, Staessen JA (2006) Environmental exposure to cadmium and risk of cancer: a prospective population-based study. Lancet Oncol 7:119–126. doi:10.1016/51470-2045(06)70545-9

Rahman MA, Hasegawa H (2011) Review on aquatic arsenic: phytoremediation using floating macrophytes. Chemosphere 83(5):6333–6646

Sharma SS, Gaur JP (1995) Potential of *Lemna polyrrhiza* for removal of heavy metals. Ecol Eng 4:37–43

Singh TS, Pant KK (2005) Solidification/stabilization of arsenic containing solid wastes using Portland cement, fly ash and polymeric materials. J Hazard Mater 131(1–3):29–36

United States Environmental Protection Agency (USEPA) SW-846 1311.1992.Toxicity characteristic leaching procedure (TCLP)

Uysal Y, Taner F (2010) Bioremoval of cadmium by *Lemna minor* in different aquatic conditions. Clean Soil Air Water, 38(4):370–377, Wiley Inter Science; www.clean-journal.com

Zhang D, Wang J, Zeng X, Fallandysz J (2011) Competitive sorption efficiency studies of Cd(II), Cu(II) and Pb(II) by powered mycelium of Cloud Ear Fungus *Auricularia polytricha*. J Environ Sci Health A 46:1776–1782

Chapter 30
Human Health Risk-Based Sustainable Management for a Contaminated Site: A Case Study

V.P. Singh and R.K. Srivastva

Abstract This study is carried out to prepare a sustainable management model for the cleanup of contaminated agricultural land at Jajmau, Kanpur, India, contaminated with heavy metals due to frequent irrigation by partially treated tannery effluents. The proposed model includes three steps: in the first step, the characterization of hot spot (frequently irrigated, low lying, and near the source and village) of area approx. 105 hectares has been carried out by qualitative and quantitative analysis of 336 samples, which were collected from 112 sampling points from the surface and 15 cm and 30 cm depth from the center line of 100 meter square grid to evaluate the characteristics of soil and contaminants. The data evince that the soil in the area is significantly contaminated with heavy metals: Cr (III) 71–773 mg/kg, Cr(VI) 23–32 mg/kg, Pb 27–61 mg/kg, Cu 21–55 mg/kg, Mn 363–901 mg/kg, Fe 25,812–32,201 mg/kg, Zr 280–449 mg/kg, Zn 51–185 mg/kg, and V 113–228 mg/kg. In the second step, potential human health risk has been evaluated based on conservative approach considering potential pathways, the most sensitive receptors, and long-term exposure of the highest contaminant levels on-site. The third step is focused on ranking a set of suitable sustainable remediation techniques for the site using analytical hierarchy process (AHP) method of multicriteria decision analysis (MCDA).

30.1 Introduction

Jajmau cluster is located on the right bank of river Ganga on the northeastern border of Kanpur City, India. There are 400 tanneries in the cluster (NGT 2015). Most tanneries are chrome tanning with varying scale of operations. The partially treated effluent from overloaded common effluent treatment plant contains high concentration of heavy metals and has been used to irrigate nearly 2100 acres of agricultural land for more than two decades (Sinha et al. 2006).

V.P. Singh (✉) • R.K. Srivastva
Civil Engineering Department, MNNIT Allahabad, Allahabad, Uttar Pradesh, India
e-mail: vps15783@mnnit.ac.in; rksciv@yahoo.co.in

G.L. Sivakumar Babu et al. (eds.), *Geoenvironmental Practices and Sustainability*, Developments in Geotechnical Engineering,
DOI 10.1007/978-981-10-4077-1_30

Several studies have addressed various aspects of contamination of the above agricultural land (Rawat et al. 2009; Gowd et al. 2010; Singh et al. 2006), contamination of surface and groundwater (Singh et al. 2009), crops and edible vegetables (Sinha et al. 2006; Gupta and Sinha 2006), genotoxic and mutagenic potential of soil (Alam et al. 2009), and assessment, characterization, and spatial distribution of heavy metal pollution using enrichment factor (EF), geo-accumulation index (I_{geo}), and pollution load index (PLI) (Paul et al. 2015).

This study describes the site characterization based on risk to human health and the development of a sustainable strategy for selection of the best suitable sustainable and greener remediation option(s) for the site.

30.2 Methodology

30.2.1 Site Characterization

The study area measures approximately 105 hectare hot spot of contaminated agriculture farm located near the source at a distance of 2.2 km from common effluent treatment plant (CETP) of Jajmau and 0.6 km from the receptor point, Village Motipur. The villagers derive their livelihood mainly from agriculture practice and animal husbandry.

The site geology consists of more than 325 meter thick alluvial-layered deposit of loamy soil consisting of a mixture of sand, silt, and clay. The bore log data at the site shows that 0–20 m is clay deposit, 20–100 m is fine sand with clay kankar, and 100–130 m is medium sand and clay kankar.

A total of 336 soil samples was collected from 112 sampling point from the center of approx. 100 meter square grid in 3 days. Three samples were collected from each sampling point: the surface, 15 cm, and 30 cm depth. The samples were collected in self-locking polythene bags and analyzed for metal contaminants, soil texture, moisture content, total organic content, cation exchange capacity, pH, and leaching behavior. The soil metal concentrations were analyzed by well-calibrated handheld portable X-ray fluorescence (PXRF) analyzer (Olympus DELTA Premium, which is equipped with a 4 W Rh anode X-ray tube and large-area silicon drift detector). All the soil samples were oven-dried by keeping in a hot-air oven at 60–700°C for 24 hrs. This temperature was used to remove the moisture without thermal decomposition. The dried samples were finely powdered and then sieved through the 2 mm opening size and then placed in thin polyethylene ziplock bags. To ensure a good contact with the probe aperture, the soil samples in the bag were smoothened by the spade and then measured by the PXRF equipment in a vertical position. Three measurements were performed, and a brief description was recorded for each soil sampling site. The count time of analysis was fixed at 120 s. Chromium is separately analyzed by SW846 method 3050B of USEPA. The statistics of determined metals in soil samples is shown in Table 30.1.

Table 30.1 Statistics of observed metals in soil samples

Heavy metal	Depth (cm)	Minimum concentration (mg/kg)	Maximum concentration (mg/kg)	Reference concentration (mg/kg)	
				USEPA (residential) (2016)	Canada (agricultural) (2013)
Cr(III)	Surface	71	773	120,000	64
	15	58	695		
	30	55	658		
Cr(VI)	Surface	23	32	0.30	0.40
	15	12	27		
	30	5	18		
Cu	Surface	21	55	31,000	63
	15	18	52		
	30	14	32		
Ni	Surface	17	51	15,000	45
	15	13	41		
	30	13	28		
Pb	Surface	27	61	400	70
	15	13	43		
	30	15	31		
Mn	Surface	363	901	2000	–
	15	239	702		
	30	201	687		
Fe	Surface	25,812	32,201	55,000	–
	15	21,201	28,100		
	30	19,032	23,223		
Zn	Surface	51	185	23,000	200
	15	40	148		
	30	42	103		
Zr	Surface	280	449	6.3	–
	15	211	422		
	30	306	430		
V	Surface	113	228	39	130
	15	176	279		
	30	201	303		

Table 30.2 Equations for exposure of contaminant to human via ingestion, inhalation, and dermal contact pathways

Chronic Average Daily Dose (CADD/LADD)			
Ingestion	Inhalation	Dermal contact	References
$\frac{\mathrm{C} \times \mathrm{IingR} \times EF \times ED \times CF}{BW \times AT}$	$\frac{\mathrm{C} \times \mathrm{InhR} \times EF \times ED}{PEF \times BW \times AT}$	$\frac{\mathrm{C} \times SA \times ABS \times AF \times EF \times ED \times CF}{BW \times AT}$	USEPA (1989)

30.2.2 Human Health Risk Assessment

Table 30.1 shows that concentrations of several contaminants are below the threshold levels, individually not hazardous, but they may add to risk with contaminants which have concentration levels above the threshold. Hence, the detailed human health risk assessment was carried out to confirm the overall site contamination.

Human health risk assessment (HHRA) is an analysis of probability of the occurrence of adverse effect and magnitude of the consequences of unwanted adverse effect to a receptor exposed to detected contaminant at a contaminated site. It is all about linking exposure to the effect (Swartjes 2011). The requirement of extensive site investigation and uncertainties in consideration of exposure factors and toxicological data make its evaluation complex and require comprehensive methodology and guidelines. Different risk assessment methodologies and tools have been developed by different countries, but overall approach of all is similar in nature. The differences are only in conceptual site modeling, consideration of exposure factors, and toxicological data, which are dependent upon the present and past site profile, behavior, and physiological factors and may vary from site to site.

In this study potential, carcinogenic or noncarcinogenic risks to human health were estimated using equations given in Table 30.2 (USEPA 1989) and evaluated using site-specific and standard exposure parameters given in Table 30.3. The chemical-specific toxicity parameters were taken from USEPS (2002). A simple, deterministic, and conservative approach was taken, i.e., the most sensitive receptors, i.e., children and farmer, maximum and average contaminant levels in soil media, and potential pathways, i.e., ingestion of surface soil, dermal contact and inhalation of soil dust, and the most likely exposure frequency and length of exposure.

The evaluated risks (noncarcinogenic and carcinogenic) to different receptors for different concentrations and all pathways are summarized in the following tables, and detailed observations have been presented in Appendix. Table 30.4 shows that the hazard index (HI) is greater than one for the child for all exposure routs for both concentrations (maximum and mean concentrations) at the site; hence, the site is unacceptable for the child receptor (USEPA).

Table 30.5 shows the carcinogenic risk for both child and adult receptors at the site and higher than acceptable value 1×10^{-6}(USEPA).

The HHRA indicates that the site is contaminated and hazardous to human receptor; the risk may increase due to the presence of PAHs and pesticide that are not considered here and also after consideration of exposure to other media (water, vegetable plants, and animal products). Therefore remediation is required.

Table 30.3 Factors used for estimation of CADD for cancer and noncancer risk

Factors	Symbol	Unit	Value				References
			Adult	Children	Worker		
					Outdoor	Indoor	
Soil ingestion rate	IngR	mg/day	100	200	100	50	USEPA (2002)
Exposure duration	ED	Year	24	6	25	25	USEPA (2002)
Exposure frequency	EF	Day/year	350	350	305	305	USEPA (2002)
Average body weight	BW	kg	63	14	63	63	
Average time for noncancer risk	AT[a]	Days	8760	2190	25,550	25,550	USEPA (2002)
Average time for cancer risk	AT[a]	Days	24,258	24,258	24,258	24,258	USEPA (2002)
Conversion factor	CF	kg/mg	1×10^{-6}	1×10^{-6}	1×10^{-6}	1×10^{-6}	USEPA (2002)
Surface area of the skin that contact the soil	SA	cm^2/event	5700	2800	3300	3300	USEPA (2002)
Skin adherence factor	AF_{soil}	mg/cm^2	0.07	0.2	0.2	NA	USEPA (2002)
Dermal absorption factor for NCR	ABS	mg/cm^2	0.001	0.001	0.001	0.001	USEPA (2011)
Dermal absorption factor for CR	ABS	mg/cm^2	0.03	0.03	0.03	0.03	USEPA (2011)
Inhalation factor	InhR	m^3/day	20	20	20	20	USEPA (2002)
Particle emission factor	PEF	m^3/day	1.36×10^9	1.36×10^9	1.36×10^9	1.36×10^9	USEPA (2002)
Life time (ED for cancer risk)	LT	Year	66.46				World Bank

[a]AT = 365 × E

Table 30.4 Hazard index for child and adult receptors exposed to both mean and maximum contaminant concentration

Site	Receptors	Hazard index (HI)	
		Mean concentration	Maximum concentration
Jajmau	Child	1.74	2.1379
	Adult	0.195	0.241

Table 30.5 Cancer risk for three receptors based on mean and maximum contaminant concentration

Site	Receptors	Cancer Risk	
		Mean concentration	Maximum concentration
Jajmau	Child	148×10^{-6}	226.54×10^{-6}
	Adult	16.45×10^{-6}	25.24×10^{-6}

30.2.3 Sustainable Remediation Option Selection

Based on published literatures, five in situ potential remediation technologies have been identified for the cleanup of soil based on basic screening parameters like contaminant type, soil and site characteristics, applicability, and commercial availability. Excavation and disposal, solidification/stabilization, phytoremediation, vitrification, and soil flushing have been selected as potential remediation methods. The selected remediation options are compared to each other with respect to selected sustainability criteria qualitatively and quantitatively. The qualitative comparisons are converted by using Saaty's nine-point numerical scales (Table 30.6). After pairwise comparisons, remediation options are systematically ranked using analytical hierarchy process (AHP) method of multicriteria decision analysis (MCDA).

30.2.4 Evaluation of Comparisons Matrices

In order to compare selected remediation technologies, a set of four criteria (three sustainability criteria and one technological criterion) and thirteen corresponding sub-criteria (evaluation criteria) have been considered (Table 30.7) for the defined goal. The indicators required for action description and scaling of criteria have been taken and derived from guidelines of different agencies, literatures, and technical reports (FRTR-2002, ITRC 2011, ASTM 2014a, b, Reddy and Adams 2015). All the matrix input data (qualitative or quantitative) are most conservative, i.e., worst case of criterion for corresponding option, for example, the average of the highest costs, most reliable, and the lowest performance (Table 30.8).

The analytical hierarchy process (AHP) method of structured multicriteria decision analysis (MCDA) has been used for systematically comparing decision elements and outcomes and ranking of decision outcomes. The AHP process used

Table 30.6 Saaty's (1980) fundamental nine-point numerical scale in the matrix of pairwise comparison

Intensity of importance	Definition	Explanation
1	Equal importance	Criteria *A* and *B* are of equal importance
3	Moderate importance	Criterion *A* is moderately more important than criterion *B*
5	Strong importance	Criterion *A* is strongly more important than criterion *B*
7	Very strong importance	Criterion *A* is very strongly more important than criterion *B*
9	Extreme importance	Criterion *A* is extremely more important than criterion *B*
2,4,6,8	For comparison between the above values	Intermediate values between defined ranking

Table 30.7 The criteria, sub-criteria, and cleanup alternatives (in situ techniques suitable for heavy metals contaminated large site)

Goal	Criteria	Sub-criteria	Alternatives
Sustainable management	Technological criteria	Cleanup time (TC1)	Vitrification (A1)
		Performance (TC2)	Soil flushing (A2)
		Reliability (TC3)	
	Economic criteria	Indirect cost (EC1)	Phytoremediation (A3)
		Direct cost (EC2)	
	Environmental criteria	Impact on air (EN1)	Solidification/stabilization (A4)
		Impact on water (EN2)	
		Impact on land (EN3)	
		Residual production (EN4)	
		Energy/resource use (EN5)	Excavation and disposal (A5)
	Social criteria	Human health and safety (SC1)	
		Impact on neighborhood land (SC2)	
		Uncertainty, evidence, and policy (SC3)	

Table 30.8 Local priority matrix or weight (Eigen values) matrix after pairwise comparisons of selected options

Alternatives	A1	A2	A3	A4	A5
TC1	0.128753	0.128753	0.024574	0.128753	0.128753
TC2	0.040208	0.107292	0.238542	0.107292	0.040208
TC3	0.04934	0.138021	0.023854	0.138021	0.04934
EC1	0.176586	0.077351	0.176586	0.057595	0.029787
EC2	0.044112	0.044112	0.282098	0.124336	0.124336
EN1	0.040208	0.107292	0.238542	0.040208	0.040208
EN2	0.034286	0.034286	0.201429	0.086190	0.201429
EN3	0.032315	0.077434	0.178968	0.032315	0.178968
EN4	0.107292	0.040208	0.238542	0.107292	0.040208
EN5	0.034286	0.201429	0.201429	0.086190	0.086190
SC1	0.097577	0.036827	0.231193	0.231193	0.036827
SC2	0.178968	0.032315	0.178968	0.032315	0.032315
SC3	0.089435	0.033978	0.089435	0.033978	0.225446

Table 30.9 The normalized priority (weight) of criteria

Criteria	Weight
TC1	0.027387
TC2	0.054186
TC3	0.046177
EC1	0.020333
EC2	0.02507
EN1	0.113763
EN2	0.113763
EN3	0.113763
EN4	0.058121
EN5	0.058121
SC1	0.242503
SC2	0.099713
SC3	0.027099

consists of four stages: (1) structuring the problem, (2) evaluating weight, (3) weight aggregation and ranking of alternatives, and (4) sensitivity analysis.

The problem is structured in four levels of hierarchy: final goal, criteria, sub-criteria, and selected remediation options from top to bottom. After structuring the problem, the pairwise comparison matrices have been evaluated for each hierarchy level, where the inputs of matrix are relative importance (priority) of elements to every other element in the same level of hierarchy w. r. t. a common parent element of the next hierarchy level. Thus, the total 12 pairwise comparison matrices (5 for alternatives of order 10×10; 4 for sub-criteria of orders 3×3, 4×4, 3×3, and 3×3; and 3 for criteria of order 4×4) consisting of 258 pairwise comparisons. The overall pairwise comparisons of criteria and corresponding sub-criteria are given in Table 30.9.

After evaluation and filling of comparison matrices, weights have been calculated using traditional AHP method known as the Eigen value method. In this method the normalized principle Eigen vector (priority vector or weight vector) of each matrix is equal to the priority or weight of elements of that matrix.

30.2.4.1 Weight Aggregation and Ranking

After evaluation of all the comparison matrices and their consistency check, the overall priority of alternatives has been determined by using linear additive weight aggregation of local priorities across all criteria using (Ishizaka and Labib 2009)

$$p_i = \sum_{j=1}^{j=13} w_j * l_{ij} \tag{30.1}$$

where p_i is the overall (global) priority of the alternatives (Table 30.10); l_{ij}, the local priority (Table 30.11); and w_j, the weight of the criteria j (Table 30.12).

It estimates the final score for each selected remediation technology.

$P_i = [\text{Matrix9}]^T_{10\times 13} * [\text{Matrix11}]_{13\times 1} = [\text{Matrix12}]_{10\times 1}$

30.3 Conclusion

Soil of the study area is contaminated. On a detailed human health risk assessment, it is found that heavy metal contamination is at levels that pose risk to human health; hence, remediation action is required. The sustainability evaluation of possible remediation technologies is carried out using AHP method of MCDA to select the best sustainable remediation option after comparisons of options with respect to different social, environment, and economic aspects for maximum social benefits at minimum impact on the environment, and a score is evaluated for each option. The phytoremediation option has scored the highest and is the recommended method for remediation of a contaminated site of the study area.

Table 30.10 Evaluation matrix

Alternatives	C1	C2	C3	C4	C5	C6	C7	C8								C9	C10	C11	C12	C13
								As	Cr	Cu	Cd	Hg	Ni	Pb	Zn					
A1	No	Yes	Yes	Low	Very high	Avg.	Better	NA	NA	NA	NA	NA	NA	NA	NA	Low	Yes	Yes	Very High	Avg.
A2	No	Yes	No	Low	Avg.	Better	Better	NA	NA	NA	NA	NA	NA	NA	NA	Avg.	Yes	No	Avg.	Low
A3	No	No	No	Very low	Low	Worse	Worse	NV	38	NV	NV	42	NV	90	98	Very Low	No	No	Low	Very Low
A4	Yes	No	No	Low	Avg.	Better	Better	NV	NV	NV	60	NV	NV	74	60	Low	No	No	Avg.	Low
A5	Yes	No	Yes	Low	Low	Avg.	Better	NA	NA	NA	NA	NA	NA	NA	NA	High	No	Yes	Low	Avg.

Where:

Symbol	Name (criteria)	Symbol	Name (alternatives)	Symbol	Name
C1	Effect on environment (air)	A1	Vitrification	NA	Not applicable
C2	Effect on environment (surface and groundwater)	A2	Soil flushing	NV	Not available
C3	Effect on environment (land)	A3	Phytoremediation	As	Arsenic
C4	Human health and safety	A4	Solidification/stabilization	Cr	Chromium
C5	Comparative cost	A5	Excavation and disposal	Cu	Copper
C6	Reliability/maintenance			Cd	Cadmium
C7	Cleanup time			Hg	Mercury
C8	Performance (removal rate)			Ni	Nickel
C9	Impact on neighborhood land			Pb	Lead
C10	Residual production			Zn	Zinc
C11	Hazardous reagent use				
C12	Energy/resource use				
C13	Uncertainty, evidence, and policy				

Table 30.11 Pairwise comparisons matrix of evaluation criteria

		Technological criteria			Economic criteria		Environmental criteria					Social criteria		
		TC1	TC2	TC3	EC1	EC2	EN1	EN2	EN3	EN4	EN5	SC1	SC2	SC3
Technological criteria	TC1	1	1/3	1/3	2	2	1/5	1/5	1/5	1/3	1/3	1/5	1/3	1
	TC2	3	1	3	3	3	1/3	1/3	1/3	1/2	½	1/5	1/3	3
	TC3	3	1/3	1	3	3	1/3	1/3	1/3	1/2	½	1/5	1/3	3
Economic criteria	EC1	1/2	1/3	1/3	1	1/3	1/5	1/5	1/5	1/3	1/3	1/7	1/3	1
	EC2	1/2	1/3	1/3	3	1	1/5	1/5	1/5	1/3	1/3	1/7	1/3	1
Environmental criteria	EN1	5	3	3	5	5	1	1	1	3	3	1/3	1	3
	EN2	5	3	3	5	5	1	1	1	3	3	1/3	1	3
	EN3	5	3	3	5	5	1	1	1	3	3	1/3	1	3
	EN4	3	2	2	3	3	1/3	1/3	1/3	1	1	1/5	1/3	3
	EN5	3	2	2	3	3	1/3	1/3	1/3	1	1	1/5	1/3	3
Social criteria	SC1	5	5	5	7	7	3	3	3	5	5	1	5	5
	SC2	3	3	3	3	3	1	1	1	3	3	1/5	1	3

Table 30.12 Ranking of remediation technologies

Alternatives	Scoring	Normalized score
Vitrification(A1)	0.076991	17
Soil flushing (A2)	0.070425	17
Phytoremediation (A3)	0.197681	30
Solidification/stabilization (A4)	0.109511	21
Excavation and disposal (A5)	0.085164	19

Appendix

Site: Jajmau (Tables 30.13, 30.14, 30.15)

Table 30.13 Noncarcinogenic hazard index (HI) for adult and child for different exposure pathways

Metal	Conc. (mg/kg)		Oral				Dermal				Inhalation				HI	
			Adult		Child		Adult		Child		Adult		Child			
			CADD	HQ	CADD	HQ	CADD	HQ	CADD	HQ	CADD	HQ	CADD	HQ	Adult	Child
Cr(III)	Min	71	1.08E-04	7.20E-05	9.73E-04	6.48E-04	4.31E-07	–	9.51E-07	–	1.59E-08	–	7.17E-08	–	7.20E-05	6.48E-04
	Max	773	1.18E-03	7.84E-04	1.06E-02	7.06E-03	4.69E-06	–	1.04E-05	–	1.73E-07	–	7.81E-07	–	7.84E-04	7.06E-03
	Mean	277	4.22E-04	2.81E-04	3.79E-03	2.53E-03	1.68E-06	–	3.71E-06	–	6.20E-08	–	2.80E-07	–	2.81E-04	2.53E-03
Cr(VI)	Min	23	3.50E-05	1.17E-02	3.15E-04	1.05E-01	1.40E-07	2.33E-03	3.08E-07	5.14E-03	5.15E-09	5.15E-05	2.32E-08	2.32E-04	1.40E-02	1.10E-01
	Max	32	4.87E-05	1.62E-02	4.38E-04	1.46E-01	1.94E-07	3.24E-03	4.29E-07	7.15E-03	7.17E-09	7.17E-05	3.23E-08	3.23E-04	1.95E-02	1.54E-01
	Mean	21	3.20E-05	1.07E-02	2.88E-04	9.59E-02	1.27E-07	2.12E-03	2.81E-07	4.69E-03	4.70E-09	4.70E-05	2.12E-08	2.12E-04	1.28E-02	1.01E-01
Cu	Min	21	3.20E-05	8.62E-04	2.88E-04	7.75E-03	1.27E-07	6.71E-05	2.81E-07	1.48E-04	4.70E-09	1.17E-07	2.12E-08	1.12E-05	9.29E-04	7.91E-03
	Max	55	8.37E-05	2.26E-03	7.54E-04	2.03E-02	3.34E-07	1.76E-04	7.37E-07	3.88E-04	1.23E-08	3.06E-07	5.56E-08	2.92E-05	2.43E-03	2.07E-02
	Mean	35	5.33E-05	1.44E-03	4.80E-04	1.29E-02	2.12E-07	1.12E-04	4.69E-07	2.47E-04	7.84E-09	1.95E-07	3.54E-08	1.86E-05	1.55E-03	1.32E-02
Ni	Min	17	2.59E-05	1.29E-03	2.33E-04	1.16E-02	1.03E-07	1.03E-04	2.28E-07	2.28E-04	3.81E-09	1.85E-07	1.72E-08	8.33E-07	1.40E-03	1.19E-02
	Max	51	7.76E-05	3.88E-03	6.99E-04	3.49E-02	3.10E-07	3.10E-04	6.83E-07	6.83E-04	1.14E-08	5.55E-07	5.15E-08	2.50E-06	4.19E-03	3.56E-02
	Mean	30	4.57E-05	2.28E-03	4.11E-04	2.06E-02	1.82E-07	1.82E-04	4.02E-07	4.02E-04	6.72E-09	3.26E-07	3.03E-08	1.47E-06	2.47E-03	2.10E-02

(continued)

Table 30.13 (continued)

Metal	Conc. (mg/kg)		Oral				Dermal				Inhalation				HI	
			Adult		Child		Adult		Child		Adult		Child			
			CADD	HQ	CADD	HQ	CADD	HQ	CADD	HQ	CADD	HQ	CADD	HQ	Adult	Child
Pb	Min	27	4.11E-05	1.17E-02	3.70E-04	1.06E-01	1.64E-07	3.12E-04	3.62E-07	6.89E-04	6.05E-09	1.72E-06	2.73E-08	7.75E-06	1.21E-02	1.06E-01
	Max	61	9.28E-05	2.65E-02	8.36E-04	2.39E-01	3.70E-07	7.05E-04	8.17E-07	1.56E-03	1.37E-08	3.88E-06	6.16E-08	1.75E-05	2.72E-02	2.40E-01
	Mean	31	4.72E-05	1.35E-02	4.25E-04	1.21E-01	1.88E-07	3.58E-04	4.15E-07	7.91E-04	6.94E-09	1.97E-06	3.13E-08	8.89E-06	1.38E-02	1.22E-01
Zn	Min	51	7.76E-05	2.59E-04	6.99E-04	2.33E-03	3.10E-07	5.16E-06	6.83E-07	1.14E-05	1.14E-08	1.90E-07	5.15E-08	8.59E-07	2.64E-04	2.34E-03
	Max	185	2.82E-04	9.39E-04	2.53E-03	8.45E-03	1.12E-06	1.87E-05	2.48E-06	4.13E-05	4.14E-08	6.91E-07	1.87E-07	3.11E-06	9.58E-04	8.49E-03
	Mean	103	1.57E-04	5.23E-04	1.41E-03	4.70E-03	6.25E-07	1.04E-05	1.38E-06	2.30E-05	2.31E-08	3.85E-07	1.04E-07	1.73E-06	5.33E-04	4.73E-03
Fe	Min	25,812	3.93E-02	5.61E-02	3.54E-01	5.05E-01	1.57E-04	2.24E-04	3.46E-04	4.94E-04	5.78E-06	–	2.61E-05	–	5.63E-02	5.06E-01
	Max	32,201	4.90E-02	7.00E-02	4.41E-01	6.30E-01	1.95E-04	2.79E-04	4.31E-04	6.16E-04	7.21E-06	–	3.25E-05	–	7.03E-02	6.31E-01
	Mean	26,432	4.02E-02	5.75E-02	3.62E-01	5.17E-01	1.60E-04	2.29E-04	3.54E-04	5.06E-04	5.92E-06	–	2.67E-05	–	5.77E-02	5.18E-01
Mn	Min	363	5.52E-04	–	4.97E-03	–	2.20E-06	–	4.86E-06	–	8.13E-08	–	3.67E-07	–	–	–
	Max	901	1.37E-03	–	1.23E-02	–	5.47E-06	–	1.21E-05	–	2.02E-07	–	9.10E-07	–	–	–
	Mean	301	4.58E-04	–	4.12E-03	–	1.83E-06	–	4.03E-06	–	6.74E-08	–	3.04E-07	–	–	–

Zr	Min	280	4.26E-04	–	3.84E-03	–	1.70E-06	–	3.75E-06	–	6.27E-08	–	2.83E-07	–	–	–
	Max	449	6.83E-04	–	6.15E-03	–	2.73E-06	–	6.02E-06	–	1.01E-07	–	4.53E-07	–	–	–
	Mean	363	5.52E-04	–	4.97E-03	–	2.20E-06	–	4.86E-06	–	8.13E-08	–	3.67E-07	–	–	–
V	Min	113	1.72E-04	5.73E-02	1.55E-03	5.16E-01	6.86E-07	–	1.51E-06	–	2.53E-08	8.73E-07	1.14E-07	3.94E-06	5.73E-02	5.16E-01
	Max	228	3.47E-04	1.16E-01	3.12E-03	1.04E + 00	1.38E-06	–	3.06E-06	–	5.11E-08	1.76E-06	2.30E-07	7.94E-06	1.16E-01	1.04E + 00
	Mean	209	3.18E-04	1.06E-01	2.86E-03	9.54E-01	1.27E-06	–	2.80E-06	–	4.68E-08	1.61E-06	2.11E-07	7.28E-06	1.06E-01	9.54E-01

Table 30.14 Noncarcinogenic hazard index (HI) for industrial worker for different exposure pathways

Metal	Metal conc. (mg/kg)		Industrial Worker						HI
			Oral		Dermal		Inhalation		
			ADD	HQ	ADD	HQ	ADD	HQ	
Cr(III)	Min	71	1.13E-04	7.53E-05	2.17E-07	–	1.38E-08	–	7.53E-05
	Max	773	1.23E-03	8.19E-04	2.37E-06	–	1.51E-07	–	8.19E-04
	Mean	277	4.40E-04	2.94E-04	8.48E-07	–	5.40E-08	–	2.94E-04
Cr(VI)	Min	23	3.66E-05	1.22E-02	7.04E-08	1.17E-03	4.49E-09	4.49E-05	1.34E-02
	Max	32	5.09E-05	1.70E-02	9.79E-08	1.63E-03	6.24E-09	6.24E-05	1.87E-02
	Mean	21	3.34E-05	1.11E-02	6.43E-08	1.07E-03	4.10E-09	4.10E-05	1.22E-02
Cu	Min	21	3.34E-05	4.77E-05	6.43E-08	3.38E-05	4.10E-09	1.02E-07	8.16E-05
	Max	55	8.75E-05	1.25E-04	1.68E-07	8.86E-05	1.07E-08	2.67E-07	2.14E-04
	Mean	35	5.57E-05	7.95E-05	1.07E-07	5.64E-05	6.83E-09	1.70E-07	1.36E-04
Ni	Min	17	2.70E-05	1.35E-03	5.20E-08	5.20E-05	3.32E-09	1.61E-07	1.40E-03
	Max	51	8.11E-05	4.05E-03	1.56E-07	1.56E-04	9.95E-09	4.83E-07	4.21E-03
	Mean	30	4.77E-05	2.39E-03	9.18E-08	9.18E-05	5.85E-09	2.84E-07	2.48E-03
Pb	Min	27	4.29E-05	1.23E-02	8.26E-08	1.57E-04	5.27E-09	1.00E-05	1.24E-02
	Max	61	9.70E-05	2.77E-02	1.87E-07	3.56E-04	1.19E-08	2.27E-05	2.81E-02
	Mean	31	4.93E-05	1.41E-02	9.49E-08	1.81E-04	6.05E-09	1.15E-05	1.43E-02
Zn	Min	51	8.11E-05	2.70E-04	1.56E-07	2.60E-06	9.95E-09	3.32E-08	2.73E-04
	Max	185	2.94E-04	9.81E-04	5.66E-07	9.44E-06	3.61E-08	1.20E-07	9.90E-04
	Mean	103	1.64E-04	5.46E-04	3.15E-07	5.25E-06	2.01E-08	6.70E-08	5.51E-04
Fe	Min	25,812	4.10E-02	5.86E-02	7.90E-05	1.13E-04	5.03E-06	–	5.87E-02
	Max	32,201	5.12E-02	7.31E-02	9.85E-05	1.41E-04	6.28E-06	–	7.33E-02
	Mean	26,432	4.20E-02	6.00E-02	8.09E-05	1.16E-04	5.15E-06	–	6.02E-02

(continued)

Table 30.14 (continued)

Metal	Metal conc. (mg/kg)		Industrial Worker						
			Oral		Dermal		Inhalation		
			ADD	HQ	ADD	HQ	ADD	HQ	HI
Mn	Min	363	5.77E-04	–	1.11E-06	–	7.08E-08	–	0.00E + 00
	Max	901	1.43E-03	–	2.76E-06	–	1.76E-07	–	0.00E + 00
	Mean	301	4.79E-04	–	9.21E-07	–	5.87E-08	–	0.00E + 00
Zr	Min	280	4.45E-04	–	8.57E-07	–	5.46E-08	–	0.00E + 00
	Max	449	7.14E-04	–	1.37E-06	–	8.76E-08	–	0.00E + 00
	Mean	363	5.77E-04	–	1.11E-06	–	7.08E-08	–	0.00E + 00
V	Min	113	1.80E-04	5.99E-02	3.46E-07	–	2.20E-08	7.60E-07	5.99E-02
	Max	228	3.63E-04	1.21E-01	6.98E-07	–	4.45E-08	1.53E-06	1.21E-01

Table 30.15 Carcinogenic risk for adult and child for different exposure pathways

Metal	Conc. (mg/kg)		CSF	Adult						Child						Risk	
				Ingestion		Dermal		Inhalation		Ingestion		Dermal		Inhalation			
				LADD	Risk	LADD	Risk	LADD	Risk	LADD	Risk	LADD	Risk	LADD	Risk	Adult	Child
Cr(VI)	Min	23	0.5	3.50E-05	1.75E-05	1.40E-07	6.98E-08	5.15E-09	2.58E-09	3.15E-04	1.58E-04	3.08E-07	1.54E-07	2.32E-08	1.16E-08	1.76E-05	1.58E-04
	Max	32	0.5	4.87E-05	2.44E-05	1.94E-07	9.71E-08	7.17E-09	3.58E-09	4.38E-04	2.19E-04	4.29E-07	2.14E-07	3.23E-08	1.62E-08	2.45E-05	2.19E-04
	Mean	21	0.5	3.20E-05	1.60E-05	1.27E-07	6.37E-08	4.70E-09	2.35E-09	2.88E-04	1.44E-04	2.81E-07	1.41E-07	2.12E-08	1.06E-08	1.60E-05	1.44E-04
Pb	Min	27	0.0085	4.11E-05	3.49E-07	1.64E-07	1.39E-09	6.05E-09	5.14E-11	3.70E-04	3.14E-06	3.62E-07	3.08E-09	2.73E-08	2.32E-10	3.51E-07	3.15E-06
	Max	61	0.0085	9.28E-05	7.89E-07	3.70E-07	3.15E-09	1.37E-08	1.16E-10	8.36E-04	7.10E-06	8.17E-07	6.95E-09	6.16E-08	5.24E-10	7.92E-07	7.11E-06
	Mean	31	0.0085	4.72E-05	4.01E-07	1.88E-07	1.60E-09	6.94E-09	5.90E-11	4.25E-04	3.61E-06	4.15E-07	3.53E-09	3.13E-08	2.66E-10	4.03E-07	3.61E-06

References

Alam MZ, Ahmad S, Malik A (2009) Genotoxic and mutagenic potential of agricultural soil irrigated with tannery effluents at Jajmau (Kanpur), India. Arch Environ Contam Toxicol 57:463–476

ASTM (2014a) Standard guide for greener cleanups. E2893-13e1. ASTM International, West Conshohocken. www.astm.org

ASTM (2014b) Standard Guide for Integrating Sustainable Objectives into Cleanup. E2876–13. ASTM International. West Conshohocken, ASTM International. www.astm.org

Gowd SS, Reddy MR, Govil PK (2010) Assessment of heavy metal contamination in soils at Jajmau (Kanpur) and Unnao industrial areas of the Ganga Plain, Uttar Pradesh, India. J Hazard Mater 174(1–3):113–121. Elsevier

Gupta AK, Sinha S (2006) Chromium levels in vegetables and grains grown on tannery effluent irrigated area of Jajmau, Kanpur, India: influence on dietary intake. Bull Environ Contam Toxicol 77(5):658–664. Springer

Ishizaka A, Labib A (2009) Analytic hierarchy process and expert choice: benefits and limitations. ORInsight 22(4):201–220

ITRC, Interstate Technology & Regulatory Council (2011) Green and sustainable remediation: a practical framework, GSR-2. Washington, DC

NGT Principal Bench (2015) Report on inspection carried out by the team in compliance of NGT order. CPCB New Delhi, India

Paul D, Chaudhary B, Gupta T, Jose MT (2015) Spatial distribution and the extent of heavy metal and hexavalent chromium pollution in agricultural soils from Jajmau, India. Environ Earth Sci 73(7):3565–3577

Rawat M, Ramanathan AL, Subramanian V (2009) Quantification and distribution of heavy metals from small scale industrial areas of Kanpur city, India. J Hazard Mater 172(2–3):1145–1149

Redddy KR, Adams JA (2015) Sustainable remediation of contaminated sites. Momentum Press LLC, New York

Saaty TL (1980) The analytic hierarchy process. McGraw Hill, New York

Singh KP, Malik A, Singh VK, Sinha S (2006) Multi-way data analysis of soils irrigated with wastewater: a case study. Chemom Intell Lab Syst 83(1):1–12. Elsevier

Singh RK, Sengupta B, Bali R, Shukla BP, Gurunadharao VVS, Srivatstava R (2009) Identification and mapping of chromium (VI) plume in groundwater for remediation: a case study at Kanpur, Uttar Pradesh. J Geol Soc India 74(1):49–57. Springer

Sinha S, Gupta AK, Bhatt K, Pandey K, Rai UN, Singh KP (2006) Distribution of metal in the edible plant grow at Jajmau, Kanpur (India) receiving treated tannery wastewater: relation with physico-chemical properties of the soil. Environ Monit Assess 115(1):1–22. Springer

Swartjes FA (2011) Dealing with contaminated sites: from theory towards practical application. Springer Science, New York

USEPA (1989) Risk assessment guidance for Superfund Volume I Human health evaluation manual (Part A) interim final. Office of Emergency and Remedial Response U.S. Environmental Protection Agency, Washington, DC

USEPA (2002) Risk assessment guidance for Superfund (RAGS), vol I – Human health evaluation manual, Part D. Standardized planning, reporting and review of Superfund risk assessments. (OSWER9285747)

USEPA (2011) Exposure factors handbook

USEPA US Environmental Protection Agency (2016) Regional screening levels. http://www.epa.gov/reg3hwmd/risk/human/rb-concentration_table/usersguide.htm

Chapter 31
Coupled Hydro-Biomechanical Modeling of Bioreactor Landfills: New Modeling Framework and Research Challenges

Krishna R. Reddy and Girish Kumar

Abstract Bioreactor landfills are emerging as a sustainable option in place of traditional landfills because of their inherent benefits such as waste to energy conversion, early waste stabilization, landfill space recovery, and its beneficial reuse with no long-term risks of leachate treatment and disposal. However, the performance of a bioreactor landfill is dictated by the coupled processes within the landfill. Understanding the individual system processes and their interdependencies is crucial in order to numerically model this system. Till date, there is no single model which can account for coupled processes to assess the performance of bioreactor landfills holistically. In this paper, a new mathematical modeling approach is presented that incorporates coupled hydraulic, mechanical, and biological processes in bioreactor landfills. Few results obtained from numerical simulations using this mathematical framework are briefly discussed, and major research challenges associated with the numerical modeling are highlighted.

Keywords Bioreactor landfills • Coupled processes • Numerical modeling • MSW settlement • MSW stabilization

31.1 Introduction

Engineered MSW landfills are often visualized to represent a closed system consisting of a relatively impermeable bottom liner system, a leachate collection and removal system (LCRS), and a relatively impermeable final cover system, all designed to prevent infiltration of precipitation and any seepage of groundwater into the landfill and also to prevent accumulation of leachate over the LCRS. However, this system eventually becomes a long-term liability with regard to land use,

K.R. Reddy (✉) • G. Kumar
Department of Civil and Materials Engineering, University of Illinois at Chicago, 842 West Taylor Street, 60607 Chicago, IL, USA
e-mail: kreddy@uic.edu; gkumar6@uic.edu

G.L. Sivakumar Babu et al. (eds.), *Geoenvironmental Practices and Sustainability*, Developments in Geotechnical Engineering,
DOI 10.1007/978-981-10-4077-1_31

leachate treatment, safe disposal, and odor problems, because of slow degradation of MSW. In this regard, bioreactor landfill technology is emerging as an interesting alternative wherein the leachate generated is recirculated back into the waste mass, thereby accelerating MSW degradation and causing high rates of methane gas generation and eventually leading to early waste stabilization. This transforms a traditional landfill into a resource for production of energy and recyclable and reusable materials with recovery of landfill space for fresh waste. In addition, the carbon footprint and the long-term risks associated with leachate treatment and its disposal are greatly reduced. But, the performance of bioreactor landfill results from the coupled processes in landfills. As MSW is heterogeneous and anisotropic in nature, the coupled processes vary spatially. Leachate injection into the landfill causes increased moisture levels and fluid pore pressures distributed nonuniformly within MSW. The increased moisture levels enhance the biodegradation of MSW causing rapid changes in engineering properties of MSW. This affects the slope stability and mechanical compression of the MSW and the landfill slopes and settlement both spatially and temporally. Therefore, all these processes have to be given due consideration and should be solved simultaneously in order to understand the interdependency among the individual system processes. Such temporal coupled effects are recognized but have not been addressed adequately till date, in the analysis and design of bioreactor landfills. A numerical modeling framework that incorporates coupled hydro-biomechanical processes is being formulated. A brief overview of our previous studies on numerical modeling of bioreactor landfills, the current modeling approach, and the associated research challenges are discussed.

31.2 Previous Research at UIC

Over the years, a focused progressive research has been performed in order to emphasize the benefits and environmental sustainability associated with bioreactor landfill technology at UIC. A comprehensive study on the engineering properties of MSW was performed on field waste and synthetic waste. Laboratory testing on field samples of different ages was carried out to understand the geotechnical properties of MSW. The changes in the major geotechnical properties of field MSW samples with biodegradation under leachate recirculation were assessed. Correlations between the MSW properties and degradation indicators were developed to evaluate the variation in major engineering properties of MSW with time (Reddy et al. 2009a, b, c, 2011).

To understand the evolution and distribution of the injected leachate by different LRS and the developed fluid and gas pore pressures, two-phase flow modeling was performed (Kulkarni and Reddy 2012, Reddy et al. 2013a, b, 2014, 2015a). Several scenarios were assumed, and numerical simulations were performed to study the response of HTs, VWs, and DBs when used as LRS on moisture distribution and the pore water and gas pressures while accounting for the effects of saturated and

unsaturated hydraulic properties of MSW, inhomogeneity and anisotropic property of waste, LRS system geometric configurations, leachate injection rates, and mode of leachate injection. Results from this study indicated that unsaturated hydraulic properties, heterogeneity and anisotropy of MSW, geometric configuration of LRS, and mode of leachate injection (continuous and intermittent) greatly influence the moisture distribution. High pore pressures developed during leachate injection may jeopardize the stability of landfill slopes by decreasing the shear strength of MSW. In this regard, a detailed study on the influence of leachate recirculation on the stability of bioreactor landfill slopes was carried out (Giri et al. 2014a, b, 2015a; Reddy et al. 2015b). A numerical two-phase flow model was used to study the effects of heterogeneity and anisotropy of MSW, unsaturated hydraulic properties of MSW, geometric configurations of LRS, and mode of leachate injection on the slope stability of bioreactor landfills. Despite these studies, there is a pressing need for research on coupled processes and optimal leachate recirculation systems for the effective design and operation of bioreactor landfills.

Several researchers have investigated the influence of coupled processes and tried to model the changes in fluid flow, mechanical compression, biochemical reactions, gas generation, temperature evolution, and leachate characteristics on the response of MSW in bioreactor landfills (Reddy et al. 2017a). However, there is no single mathematical model which can account all the above changes simultaneously in assessing the performance of bioreactor landfills. Moreover, the majority of these models are highly parameter intense, and operators are very unlikely to use such complex models. Hence, there is a need for mathematical model with a rational and holistic approach while accounting for coupled processes and at the same time predict the performance of bioreactor landfill with reasonable accuracy with limited number of parameters. Therefore, a new mathematical modeling framework is being formulated using Fast Lagrangian Analysis of Continua (FLAC), a finite difference code, to account for coupled hydro-biomechanical processes in bioreactor landfills.

31.3 New Modeling Framework

A schematic of the formulation of a new mechanical modeling framework that integrates mechanical, hydraulic, and biodegradation behavior of MSW is shown in Fig. 31.1.

The numerical modeling framework consists of a two-phase flow model, large strain mechanical model, and a first-order decay biodegradation model. The hydraulic two-phase flow model is based on the two-dimensional unsaturated Richards's equation and considers that fluid and gas exist simultaneously as two immiscible entities in MSW pores (Itasca 2011). The mechanical model is a large-strain formulation of Mohr-Coulomb yield criteria. The biodegradation model is formulated as a first-order decay model similar to USEPA's LandGEM model. However, there is an improvisation in the biodegradation model by accounting the influence of water

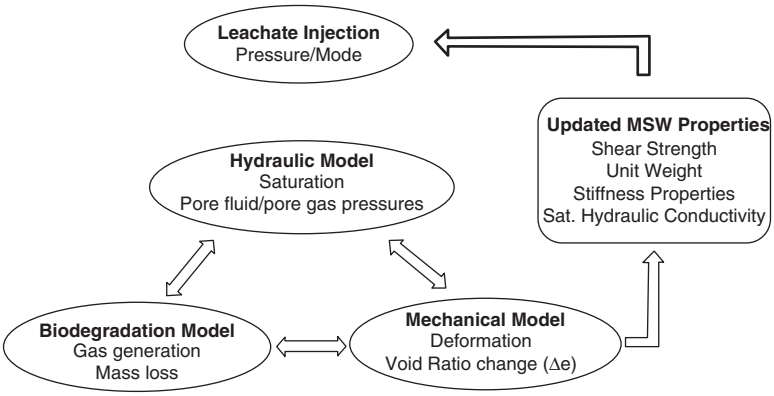

Fig. 31.1 Coupled processes in MSW bioreactor landfills

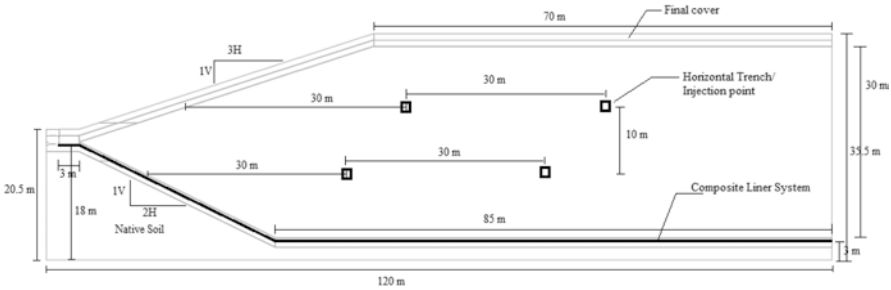

Fig. 31.2 Landfill configuration considered for numerical simulations

content on the rate of biodegradation of MSW. A brief overview of the framework that provides a new approach for coupled hydro-biomechanical processes in bioreactor landfills is discussed here. To demonstrate model application, a landfill configuration as shown in Fig. 31.2 is created, and the MSW is assumed to be placed in lifts to represent layered waste placement in landfills. The MSW properties and constitutive model are defined based on mechanical model.

The initial and boundary conditions are specified, and the initial mechanical response of the landfill is evaluated by bringing the landfill to elastic equilibrium. Thereafter, the leachate is injected into the landfill, and the hydraulic behavior (saturation, pore fluid, and gas pressures) of the MSW is modeled as per the two-phase flow formulation. The injection of leachate causes simultaneous volumetric deformation due to changes in pore fluid pressures and effective stress, and, at the same time, changes in mechanical properties (e.g., void ratio, volumetric deformation) influence hydraulic behavior, representing the coupled hydro-mechanical process. Moreover, the leachate injection enhances the moisture levels in MSW, and this influences the rate of biodegradation of MSW, with mass loss and dynamic changes

in engineering properties of MSW. The first-order decay biodegradation model influences both hydraulic and mechanical processes thereby representing a transient and dynamic coupled hydro-biomechanical processes in bioreactor landfills.

Few important results obtained from numerical simulations of conventional and bioreactor landfills under the proposed framework are presented here. It is clear from Fig. 31.3 that the rate of biodegradation is enhanced with leachate injection in case of bioreactor landfill, and this results in high surface settlement rates, high rates of methane gas production, and early MSW stabilization (within 15–16 years). However, the conventional landfill requires around 50 years to stabilize due to low biodegradation rates. In addition, the variation of degree of degradation (DOD) along the landfill depth for both the landfill cases is shown in Fig. 31.4. As it can be seen, the DOD values for bioreactor landfill reach almost 98% in 16 years of leachate injection, while the DOD values reach around 95% only after 50 years of post-closure in conventional landfill. Similarly, in Fig. 31.5, the variation of MSW settlement along the landfill depth for both the landfill cases is shown. A high rate of biodegradation in bioreactor landfill induces high settlement rates and thereby achieving the maximum settlement within 16 years of leachate injection, while the total settlement of conventional landfill takes place after around 50 years of post-closure. Several other detailed results of the numerical simulations performed, including the shear stress-displacement behavior of composite liner systems as MSW degrades, can be found elsewhere (Reddy et al. 2017b).

31.4 Research Challenges

A new mathematical modeling framework for numerical modeling of coupled hydro-biomechanical processes in bioreactor landfills is presented. The results obtained from numerical simulations performed on an assumed landfill configuration for conventional and bioreactor landfills are plotted. The results clearly demonstrate the ability of the modeling framework to account for coupled hydraulic, mechanical, and biodegradation processes holistically and thereby effectively predict the performance of bioreactor landfills. However, numerical modeling of bioreactor landfills is posed with several research challenges, some of which are listed below, which are being addressed in our research:

- In order to accurately model the coupled processes in MSW landfills, it is essential to have a thorough understanding of the unsaturated hydraulic properties of MSW, shear strength properties of MSW, unit weight, saturated hydraulic conductivity, stiffness, and their variability with waste composition and with biodegradation.
- Evolution and distribution of temperature in full-scale landfills have to be studied, and its effect on biodegradation of MSW should be evaluated and incorporated in the modeling.

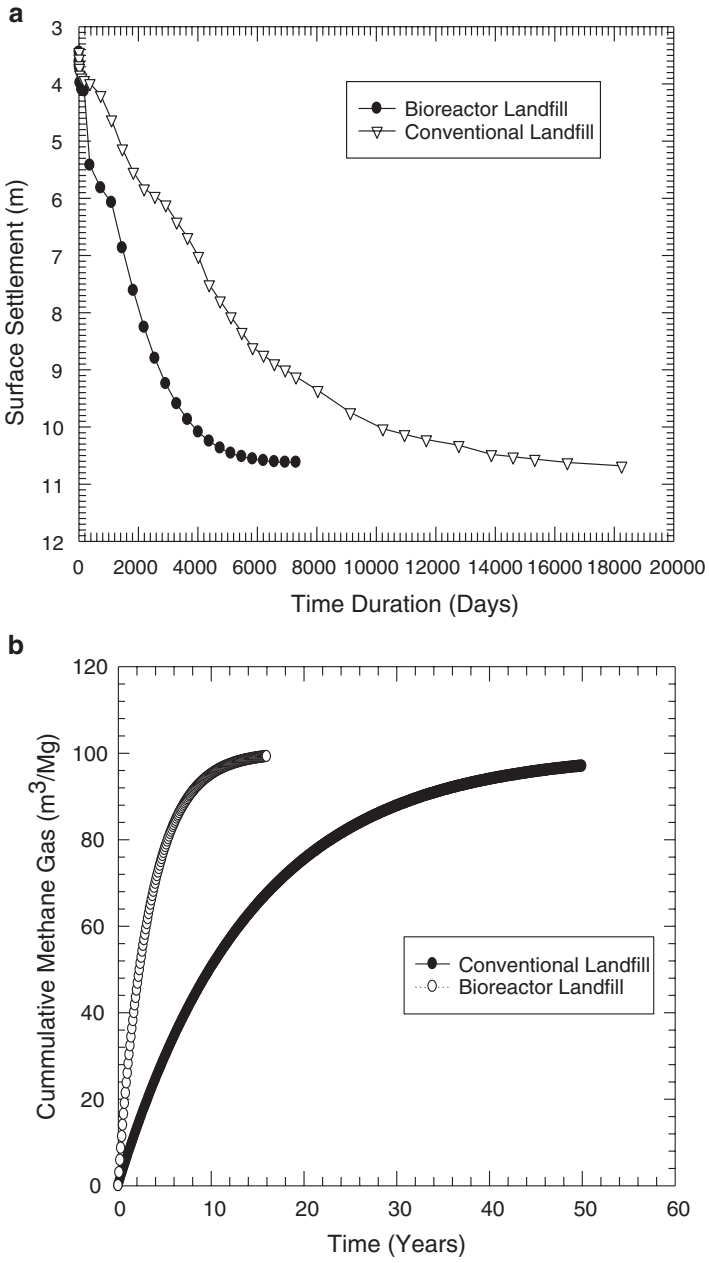

Fig. 31.3 (**a**) Surface settlement of landfill with time. (**b**) Cumulative methane gas production with time

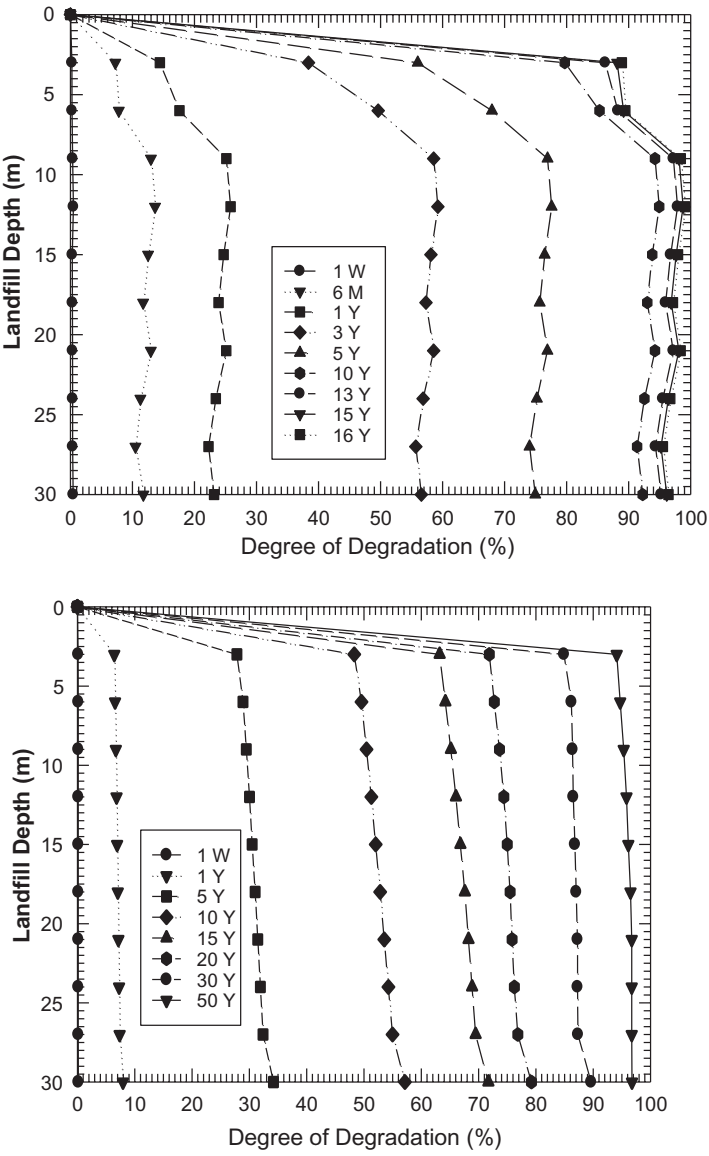

Fig. 31.4 Variation of degree of decomposition along landfill depth. (**a**) bioreactor landfill and (**b**) conventional landfill

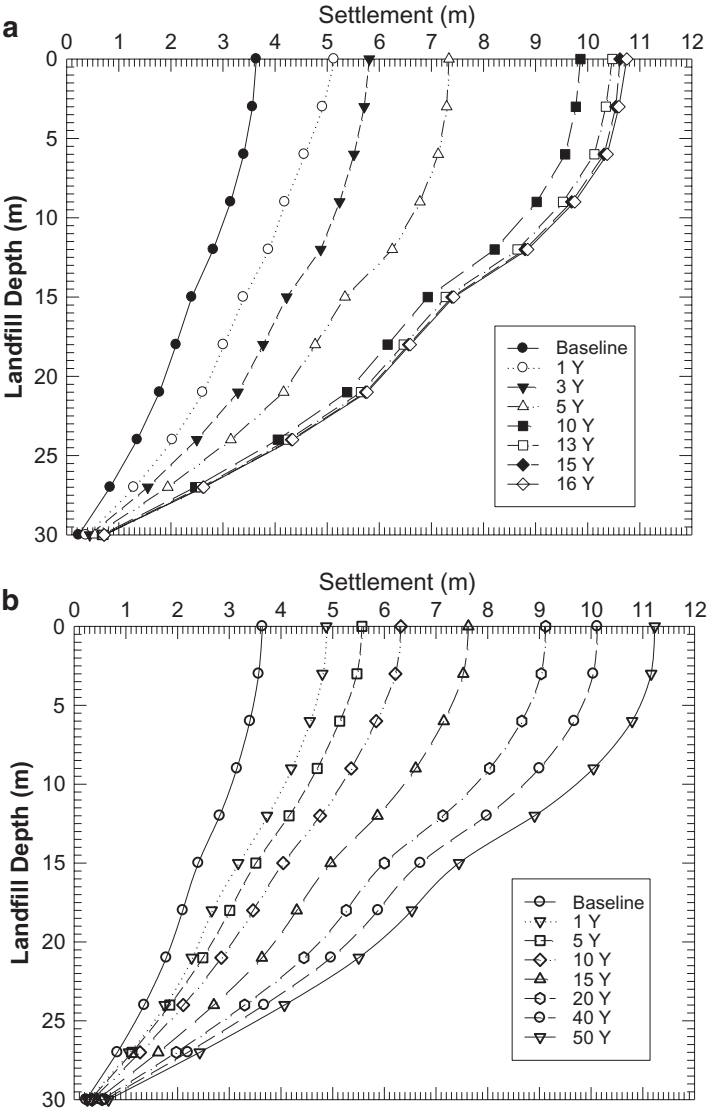

Fig. 31.5 Variation of settlement along landfill depth. (**a**) bioreactor landfill and (**b**) conventional landfill

- There is a need for development of a constitutive model that can accurately predict the MSW behavior in landfills. In addition, the biodegradation model should incorporate the biochemical reaction kinetics that occurs in the waste mass in landfill.
- Influence of engineering properties of MSW on the shear response of liner systems is not very well understood.

Acknowledgments This project is funded by the US National Science Foundation (grant CMMI #1537514), which is gratefully acknowledged.

References

Giri RK, Reddy KR (2014a) Slope stability of bioreactor landfills during leachate injection: effects of unsaturated hydraulic properties of municipal solid waste. Int J Geotech Eng 8(2):144–156. doi:10.1179/1939787913Y.0000000013

Giri RK, Reddy KR (2014b) Slope stability of bioreactor landfills during leachate injection: effects of heterogeneous and anisotropic municipal solid waste. Waste Manag Res 32(3):186–197. doi :10.1177/0734242X14522492

Giri RK, Reddy KR (2015) Slope stability of bioreactor landfills during leachate injection: effects of geometric configurations of horizontal trench systems. Geomech Geoeng Int J 10(2):126–138. doi:10.1080/17486025.2014.921335

ITASCA Consulting Group Inc (2011) FLAC-Fast Lagrangian Analysis of Continua. ITASCA Consulting Group Manuals, Minneapolis

Kulkarni HS, Reddy KR (2012) Moisture distribution in bioreactor landfills: a review. Indian Geotech J 42(3):125–149

Reddy KR, Hettiarachchi H, Parakalla NS, Gangathulasi J, Bogner JE (2009a) Geotechnical properties of fresh municipal solid waste at Orchard Hills landfill, USA. Waste Manag 29(2):952–959

Reddy KR, Hettiarachchi H, Parakalla N, Gangathulasi J, Bogner JE, Lagier T (2009b) Hydraulic conductivity of MSW in landfills. J Environ Eng 135(8):677–683

Reddy KR, Hettiarachchi H, Gangathulasi J, Parakalla N, Bogner JE, Lagier T (2009c) Compressibility and shear strength of municipal solid waste under short-term leachate recirculation operations. Waste Manag Res 27(6):578–587

Reddy KR, Hettiarachchi H, Gangathulasi J, Bogner JE (2011) Geotechnical properties of municipal solid waste at different phases of degradation. Waste Manag 31(11):2275–2286

Reddy KR, Kulkarni HS, Khire MV (2013a) Two-phase modeling of leachate recirculation using vertical wells in bioreactor landfills. J Hazard Toxic Radioact Waste 17(4):272–284

Reddy KR, Kulkarni HS, Srivastava A, Sivakumar Babu GL (2013b) Influence of spatial variation of hydraulic conductivity of municipal solid waste on performance of bioreactor landfills. J Geotech Geoenviron 139(11):1968–1972

Reddy KR, Kulkarni HS, Giri RK (2014) Validation of two-phase flow modeling of leachate recirculation in bioreactor landfills. J Waste Manag, 2014, Article ID 308603, 24 pages doi:10.1155/2014/308603

Reddy KR, Kulkarni HS, Giri RK (2015a) Design of horizontal trenches for leachate recirculation in bioreactor landfills using two-phase modeling. Int J Environ Waste Manag 15(4):347–376. doi:10.1504/IJEWM.2015.069962

Reddy KR, Kulkarni HS, Giri RK (2015b) Modeling coupled hydro-mechanical behavior of landfilled waste in bioreactor landfills: numerical formulation and validation. J Hazard Toxic Radioact Waste ASCE. doi:10.1061/(ASCE)HZ.2153-5515.0000289

Reddy KR, Kumar G, Giri RK (2017a) Modeling coupled processes in municipal solid waste landfills: An overview with key engineering challenges. Int J Geosynth Ground Eng 3(1):1–21. doi: 10.1007/s40891-016-0082-2

Reddy KR, Kumar G, Giri RK (2017b) Influence of dynamic coupled hydro-bio-mechanical processes on response of municipal solid waste and liner system in bioreactor landfills. Waste Manag. doi:10.1016/j.wasman.2016.12.040

Chapter 32
Electromagnetic Enhancement of Microbially Induced Calcite Precipitation

Jon Bender, Arvin Farid, Ken Cornel, Jim Browning, and Elisa Barney Smith

Abstract Uniform distribution of soluble and insoluble materials into saturated porous soil is often challenging for geotechnical applications, due to the random formation of fingers, i.e., a form of instability at the interface of materials with contrasting density and viscosity. A mechanism by which, one could control this random fingering tendency would support a broad array of applications where it is desirable to uniformly penetrate soil with a substance. In our previous research, the use of electromagnetic (EM) waves has been demonstrated to be effective to induce multiphase flow of dense ($\rho > 1$ g/cm3) materials in aqueous media, as well as to control air-channel formation in air sparging. EM waves with carefully predesigned radiation pattern were shown to induce a directed two-phase flow in aqueous and saturated porous media with relatively low energy input and minimal heat generation. A homogeneous medium of saturated Ottawa sand within a dimensionally scaled cavity (a Plexiglas tank with its walls covered with transparent, electrically conductive films), designed with a reservoir at the bottom plumbed to maintain constant head, was used to simulate the soil medium. Then, a nonaqueous liquid was supplied, an even distribution of which (throughout the soil volume) was desired. In current practice, such an application would have limited success, owing to the aforementioned fingering effects, as well as the relatively slow process of natural dispersion. Such a case is used as the control. In the study case, EM waves were then launched into the cavity using a loop antenna sharing the ground as the cavity at the best impedance-matched frequency. The EM filed was also numerically

J. Bender (✉) • A. Farid
Civil Engineering, Boise State University, MS 2060, 1910 University Drive, Boise, ID, USA
e-mail: jonbender@u.boisestate.edu; arvinfarid@boisestate.edu

K. Cornel
Chemistry and Biochemistry, Boise State University,
MS 1520, 1910 University Drive, Boise, ID, USA
e-mail: kencornell@boisestate.edu

J. Browning • E.B. Smith
Electrical and Computer Engineering, Boise State University,
MS 2075, 1910 University Drive, Boise, ID, USA
e-mail: jimbrowning@boisestate.edu; ebarneysmith@boisestate.edu

G.L. Sivakumar Babu et al. (eds.), *Geoenvironmental Practices and Sustainability*, Developments in Geotechnical Engineering,
DOI 10.1007/978-981-10-4077-1_32

simulated using COMSOL Multiphysics finite-element analysis software. The model was also experimentally validated using experimental measurement. Observations and measurements of the induced flow are then made to assess the effectiveness of the distribution. Infiltrating materials to be studied include ionic, soluble nonionic, and biological samples, selected based on their value for various geotechnical applications. Subsequent pilot- or field-scale testing is necessary to determine ultimate applicability of the system.

Keywords Microbial • Electromagnetic • Stabilization • Calcite precipitation • Stimulation

32.1 Introduction

Historically, civil engineers have regarded soil with little consideration of the biological activity therein, beyond the observation that a particular soil sample may contain "organics." This has been changing rapidly in recent decades, as researchers have begun to recognize the importance of complex biological and biochemical dynamics within nearly any subsurface system. The consequences of microbial metabolism, including changes in the chemical composition of soils, biofilm development, and precipitation of solids, have begun to affect significant changes in how issues are addressed in the field. Working with the natural biological processes inherent within soils potentially holds tremendous promise for the future of geotechnical engineering. The scientific understanding that allows for the manipulation of electromagnetism has been one of the most significant developments of the past centuries. Aside from the obvious advancements in telecommunication, the increasingly precise control of EM fields has made many exciting engineering practices possible, in particular, regarding the science of materials.

Capitalizing on the forces inherently applied to particles within different regions of an electromagnetic field, it is possible to manipulate the orientation, positions, and movement of individual particles (Farid et al. 2013). Applications of this ability include many breakthroughs in the development of new materials, particularly with respect to nanomaterials, but there is untapped potential that could revolutionize more macroscopic processes within the field of civil engineering (Tsurumi et al. 2010).

In the area of geoenvironmental engineering, the potential of EM fields to aid in groundwater contaminant remediation has recently been proposed and investigated by Farid et al. (2013), with promising results. Through control of the dielectrophoretic forces, induced at a distance, multiphase fluid flow has been successfully demonstrated, which could offer a huge advantage in previously intractable mitigation projects. This EM-induced multiphase flow has many potential applications. In the case of the geotechnical techniques, invoking natural processes enacted by in situ microorganisms, the ability to move desired nutrients into zones

where specific microorganisms might activate certain biochemical pathways could cause preferential modifications to soil properties. This could dramatically increase the range of applications of such processes.

32.2 Background and Literature Review

Microbially induced calcite precipitation (MICP) is a process by which natural biochemical pathways are utilized to induce the precipitation of calcium carbonate ($CaCO_3$) by a range of bacterial species. This method has shown great promise for aiding in a variety of geotechnical applications (Jong et al. 2006; Paassen et al. 2010; Ferris 1997). While there are a large number of species that are capable of precipitating calcite under proper conditions (some of which are indigenous in most soils, Fujita et al. 2000; Burbank et al. 2013), the species that has shown the greatest capacity to serve civil engineering goals is *Sporosarcina pasteurii* (Hammes et al. 2002). *S. pasteurii* is easily and safely cultured and can hydrolyze urea in the presence of Ca2+ ions to form $CaCO_3$ precipitate (Stocks-Fischer et al. 1999). Bacterial metabolism of urea via hydrolysis produces the conditions (i.e., elevated pH (see Fig. 32.1)) conducive to calcite precipitation. These reactions include (Whiffin 2004; Jahns 1999) the following.

Reaction 1: Urea diffuses into the cell according to the concentration gradient. Reaction 2: Urea is hydrolyzed by urease, which results in alkalinization of the cytoplasm to pH 8.4 and a decrease in ΔpH (i.e., difference in p^H between inside and outside of the cell).

Reaction 3: Ammonium ions are removed from the cell according to the ammonium concentration gradient, which results in an increase in Δψ (membrane potential—difference in charge between inside and outside of the cell).

Reaction 4: The increased membrane potential is reversed by driving in protons against the concentration gradient into the cell, which results in the generation of ATP.

Under these conditions, in the presence of calcium ions, $CaCO_3$ can form via the following reactions (Ramakrishnan et al. 2001).

$$Ca^{2+} + 2HCO^{3-} \leftrightarrow \mathrm{CaCO}^{3-} \downarrow + CO_2 + \mathrm{H_2O}$$

$$Ca^{2+} + HCO^{3-} + OH^{-} \leftrightarrow \mathrm{CaCO}^{3-} \downarrow + 2\mathrm{H_2O}$$

Further deposition of Ca^{2+} ions occurs subsequently due to the anionic condition along the cell wall that results from the preceding reactions. This deposition takes place along the membrane of the bacterial cells, and as calcium ions attach to the membrane, they bind with free ambient carbonate ions, forming additional calcite (Jong et al. 2006).

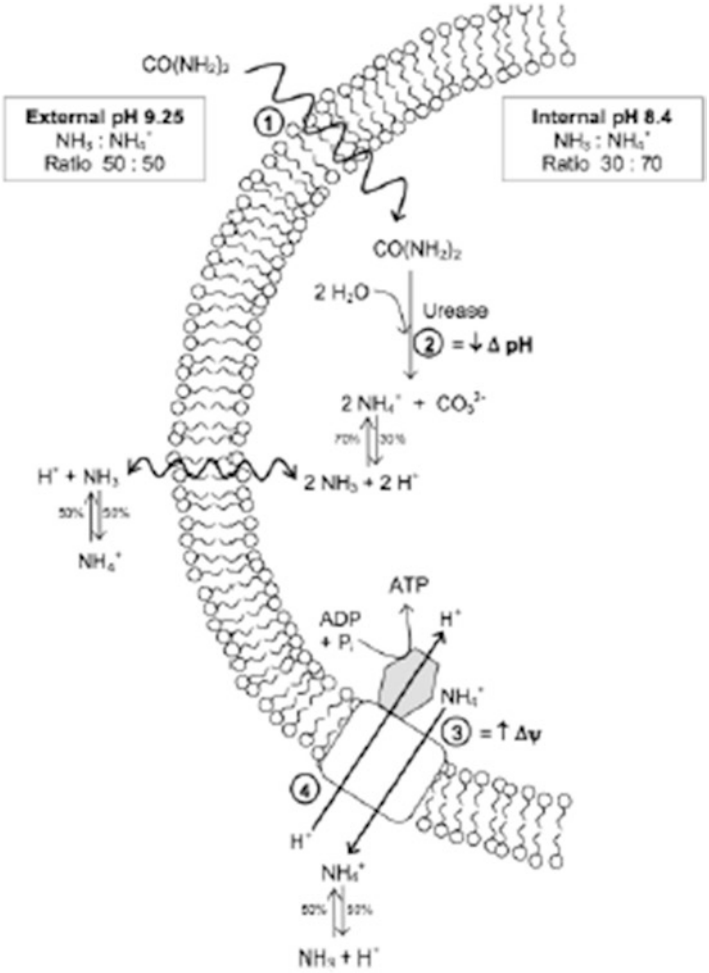

Fig. 32.1 Coupling of urea hydrolysis and ATP (adenosine triphosphate) generation in *S. pasteurii* reactions (Whiffin 2004; Jahns 1999)

$$Ca^{2+} + \text{Cell} \rightarrow \text{Cell} \cdot Ca^{2+}$$

$$\text{Cell} \cdot Ca^{2+} + CO_3^{2-} \rightarrow \text{Cell} \cdot \text{CaCO}_3 \downarrow$$

A final source of calcite is from the natural conversion of atmospheric CO_2 to carbonate ions under the basic conditions produced by urea hydrolysis. As elsewhere, these carbonate ions bond with calcium. Optimization of calcite production has been achieved by controlling water saturation, availability of Ca^{2+} ions, and availability of other nutrients (Al Qabany et al. 2012). Experiments have also shown that such ureolytic activity is affected positively by the presence of certain other

nonureolytic bacteria species, possibly due to predation facilitated by the high pH environment created and favored by *S. pasteurii* (Gat et al. 2014). All of this supports the selection of *S. pasteurii* for geotechnical projects in the field. MICP has been proven effective for a wide variety of geotechnical applications from erosion control (Jiang et al. 2014) and soil/rock porosity reduction (Ferris 1997; Cuthbert et al. 2013; Stocks-Fisher et al. 1999) to increasing soil elastic and shear moduli (Jong et al. 2006; Burbank et al. 2013) and sequestering heavy metal ions (Fujita et al. 2000). For a number of these applications, proven techniques, while often still in the process of technical refinement, can be used with relatively predictable results. However, there are many situations where further research is needed. In particular, it has often proven difficult to uniformly affect a region of soil. Specifically, calcite production from the MICP process tends to be concentrated around the site of nutrient and/or microbe injection.

While some flow and distribution are possible, MICP is always limited to some extent by the mechanism of application/injection (Paassen et al. 2010). Predesigned electromagnetic (EM) field patterns at the low microwave range (~130 MHz +/− 100 MHz) have been shown to dielectrophoretically mobilize nonaqueous molecules in water with insignificant heating and a relatively low energy input requirement (Farid et al. 2013). The potential, beneficial mechanism of flow induction in the case of MICP is either a dielectrophoretic or ponderomotive force, though the latter has not been tested for civil engineering applications and, instead, has been mostly applied to plasma physics (Sawley 1984). It has been shown that ponderomotive forces can have a significant effect on charged particles at low frequencies (Boot and Harive 1957). Both of these mobilization mechanisms can be controlled to produce a multiphase flow in a direction specified by the gradient of the square of the amplitude of the electric field (Jones 2003; Boot et al. 1957). Thus, a well-designed electric-field pattern could be used to deliver a specific material through an aqueous or water-saturated porous medium in a selected direction. Prior research has focused on groundwater remediation applications of this technology and has shown great promise at the bench scale using dielectrophoretic forces (Farid et al. 2013). This study attempts to determine whether controlled, low-frequency electromagnetic field can be used to aid in the distribution of all nutrients required for calcite formation by *S. pasteurii*, as well as increasing the metabolic activity of *S. pasteurii*, leading to improvement of the quality of resulting cementation by MICP throughout a volume of soil.

32.3 Methodology

The goal of the experimental sequence is to determine whether EM fields can be used to enhance the efficacy of MICP treatment in porous sand. Of interest are both the capacity of the fields to both distribute the precipitated calcite thoroughly throughout a region of soil and to enhance the growth and metabolism of the organisms.

All experiments will involve a loop-coupled resonant cavity (Fig. 32.2). The loop antenna is made from an RG8 coaxial cable, with its electrically conductive shield stripped, with its center conductor and dielectric curved into a loop within the cavity, and the center conductor then soldered to the shied, sharing the same ground with the cavity. The cavity walls are covered with transparent, electrically conductive films, allowing the capture of video and still photos of the multiphase flow within the cavity. A signal of specified frequency and power can then be directed into the cavity via the loop antenna. Using a signal generator and amplifier (Fig. 32.3), specific EM frequencies will be directed into the cavity through an impedance-matched network (minimizing reflection back into the amplifier). Impedance matching is accomplished with the aid of a network analyzer made of two two-gang variable capacitors (Fig. 32.3). Reflections are monitored through the use of a spectrum analyzer attached to a reflection monitoring coupler placed in the network (Fig. 32.3). Information from the spectrum analyzer is fed through a LabVIEW program designed to shut down the system in the event of excessive reflection, which could be dangerous for the amplifier. The project will have two main experimental sequences: Sequence 3.1 will test the efficacy of selected electromagnetic-field patterns for mobilizing relevant nutrients (urea and ionic calcium) and Sequence 3.2 will test the effect of evenly distributed nutrients, as well as the EM field itself, on the growth, distribution, and metabolism of *S. pasteurii* in support of calcite production.

Using SDS PAGE glass plates (Fig. 32.4), a relevant indicator/tracer dye (Coomassie and FURA-2 for urea and Ca^{2+}, respectively) is placed into a water-filled resonant cavity. EM waves will be launched at a preselected frequency. Each concentrated test chemical (urea or Ca^{2+}) is subsequently injected into the bottom corner of the chamber (due to their relative densities being >1 g/mL), and both the rate and extent of distribution of each chemical are observed over time. Observations will also be made with the aid of the indicator dyes and compared with the final concentration of a control, placed outside the cavity. Digital images and videos of the distribution and associated dye color changes will be captured. As mentioned, tests will be conducted on (1) urea (Coomassie dye) and (2) calcium (FURA-2 dye).

The electromagnetic fields within the cavity for each experimental scenario will first be modeled using COMSOL Multiphysics software (Fig. 32.5). This finite-element analysis software will aid in the selection of the appropriate frequencies, in consideration of all materials with which the EM fields will interact.

As mentioned, the selection of experimental EM frequencies will be made based on either the dielectric (where dielectrophoretic forces are of interest) or ionic (where ponderomotive forces are at play) properties of the test particles and best impedance match achieved using the impedance-matching network (shown in Fig. 32.3).

It is, therefore, possible to select frequencies that produce a desirable electric-field gradient. Identified frequencies, which result in an electric-field pattern that supports the optimal movement of the test substance will be selected, if the impedance of the cavity can be matched to that of the amplifier (50 Ω) using the aforementioned impedance-matching network.

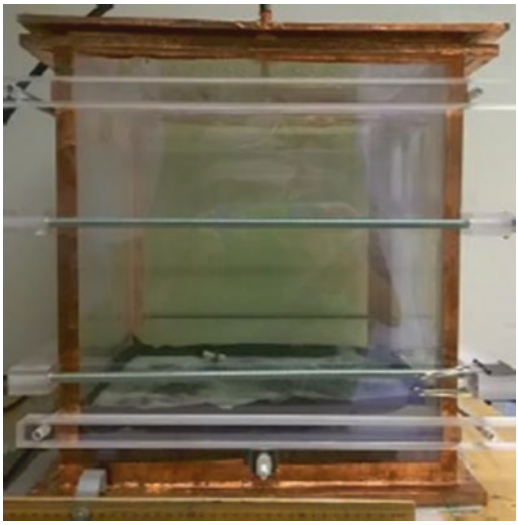

Fig. 32.2 YZ and XZ views of the resonant cavity covered with transparent reflective (i.e., electrically conductive) walls and coaxial cable (outside, *upper left*) terminating in a loop antenna (inside the cavity, *upper left corner*, XZ view)

$$F_{DEP} = 2pr^3 \text{Real}\left\{\left(e_p^* - e_m^*\right) / \text{e}_m^*\right\} \nabla \left|E\right|^2 \tag{32.1}$$

where F_{DEP} is the dielectrophoretic force, r is the radius of an approximately spherical particle of interest, e_p^* is the complex dielectric permittivity of the moving particles, e_m^* is the complex dielectric permittivity of the background medium, and $|E|$ is the amplitude of the electric field. Note that larger particles will experience a much larger force magnitude (Jones 2003). Since the dielectric constant of urea is much less than that of water, the dielectrophoretic force on them is oriented against the electric-field gradient.

$$F_P = -\left(e^2 / 4mw^2\right) V \left|E\right|^2 \tag{32.2}$$

where F_P is the ponderomotive force, e is the electrical charge of the particle of interest, V is the alternating electric field's frequency, m is the particle mass, and ω is the angular frequency. Note that the force and, in turn, acceleration of the particle are thus inversely proportional to the square of its mass and directly proportional to the square of its charge. Since calcium ions are positively charged, the direction of their force is against the electric-field gradient, as is also the case with urea.

Experiment 3.1.1 will then be repeated using water-saturated glass beads (sand simulant), placed between the glass plates, in place of the deionized deaerated water. This will help to show that the technique is viable within saturated soil.

Fig. 32.3 Experimental setup: signal generator, amplifier, network analyzer used for impedance matching at specified resonant frequencies, two two-gang variable capacitors used to build an impedance-matching network, dual-directional coupler used to monitor reflected and forward power out of the amplifier, and spectrum analyzer, used to monitor forward and reflected power at the matched frequency

32.4 Results and Conclusion

Though we have successfully mobilized test substances (green dye, Figs. 32.6, 32.7, and 32.8) in accordance with modeled field patterns, we have as yet been unable to mobilize our test nutrients (urea and Ca^{2+}) using either of two different sets of materials (SDS PAGE plates, polyurethane cylinder). Thus far, we have not determined the cause of this, though there are several hypotheses which we have been pursuing.

Directional mobilization of the test dye has been consistent with mapped field patterns generated using COMSOL and confirmed with physical measurements of the field in the cavity. Replicating these experiments using unconfined urea is not possible due to the volume of water, a corresponding requisite quantity of Coomassie dye, and the difficulty with which observations could be made of the subsequent reaction with urea. Work on resolving the aforementioned issues (e.g., determining the precise cause of the problem and modifying the experimental setup) is still in progress.

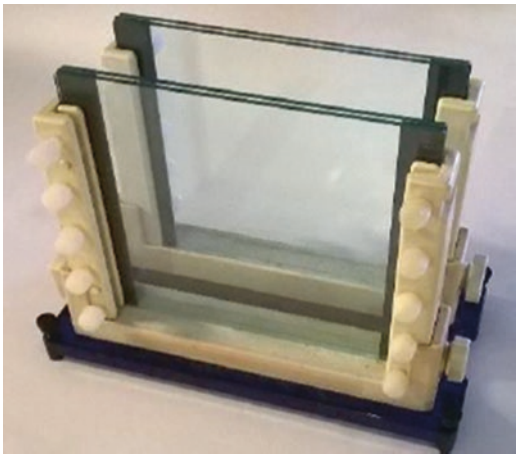

Fig. 32.4 SDS PAGE plates into which the test substances will be injected. Nutrient distribution: mobilizing urea and Ca^{2+} particles in water

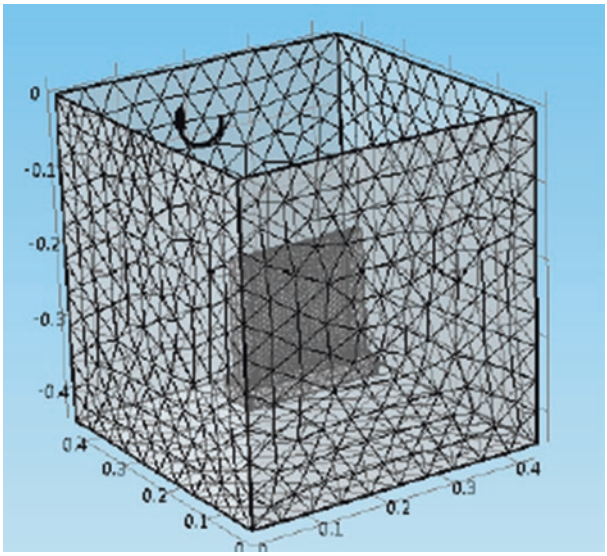

Fig. 32.5 Discretized cavity and test plates using finite-element mesh, showing the loop antenna at the top (box lid has been removed for this image). Image generated by COMSOL Multiphysics software

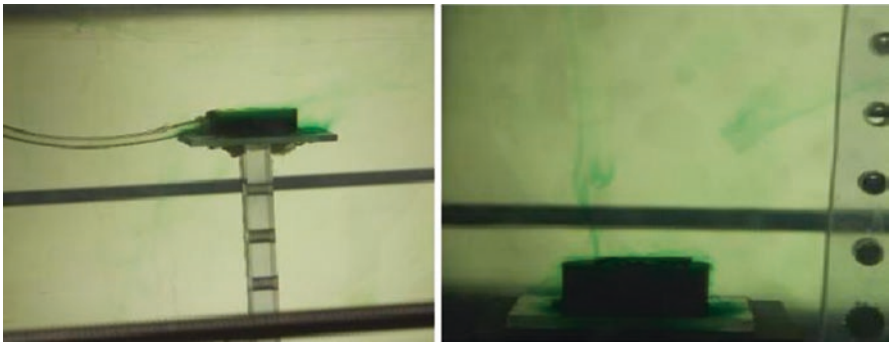

Fig. 32.6 Results of EM-induced dye flow out of open cup

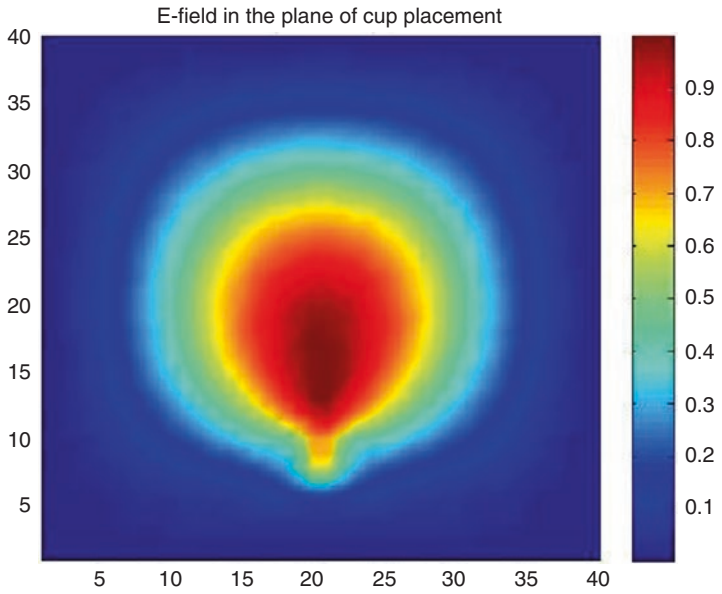

Fig. 32.7 E-field magnitude (not to scale), predicted according to experimentally validated, numerically simulated electric fields

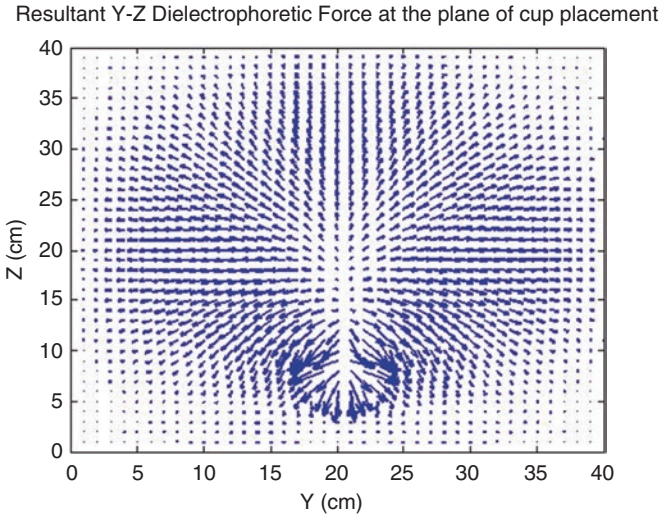

Fig. 32.8 Dielectrophoretic forces, predicted according to experimentally validated, numerically simulated electric fields. Placement of cups from Fig. 32.6 indicated by *circles*

Acknowledgments Many thanks to all of the contributors at Boise State University, the wonderful researchers whose work preceded us, and to the professional organizations that form the foundation of so many research initiatives.

References

Boot H, Harvie R (1957) Charged particles in a nonuniform radio-frequency field. Nature 4596:1187

Burbank et al (2013) Geotechnical tests of sands following bioinduced calcite precipitation catalyzed by indigenous bacteria. J Geotech Geoenviron 139:928–936

Cuthbert et al (2013) A field and modeling study of fractured rock permeability reduction using microbially induced calcite precipitation. Am Chem Soc Publ Environ Sci Tech 47:13637–13643

Farid et al (2013) Electromagnetically induced transport for soil/groundwater remediation. J Geotech Geoenviron 141(3):04014115. (10 pp)

Ferris FG (1997) Bacteriogenic mineral plugging. J Can Pet Technol 35(8):56–59

Fujita et al (2000) Subscribed content calcium carbonate precipitation by ureolytic subsurface bacteria. Geomicrobiol J 17(4):305–318

Gat et al (2014) Ureolysis and MICP with model and native bacteria: implications for treatment strategies. Geo-Congress 2014 Technical Papers, GSP 234:1713–1720

Hammes F et al (2002) Strain-specific ureolytic microbial calcium carbonate precipitation. Appl Environ Microbiol 69(8):4901–4909

Jahns T (1999) Ammonium/urea-dependent generation of a proton electrochemical potential and synthesis of ATP in Bacillus Pasteurii. J Biotechnol 178:403–409

Jiang et al (2014) Experimental study of mitigation of soil internal erosion by microbially induced calcite precipitation. Geo-Congress 2014 Technical Papers, 234:1586–1595

Jones TB (2003) Basic theory of dielectrophoresis and electrorotation. J IEEE Eng Med Biol 22(6):33–42
Jong D et al (2006) Microbially induced cementation to control sand response to undrained shear. J Geotech Geoenviron 132:1381–1392
Paassen V et al (2010) Quantifying biomediated ground improvement by ureolysis: large-scale biogrout experiment. J Geotech Geoenviron 136:1721–1728
Qabany A et al (2012) Factors affecting efficiency of microbially induced calcite precipitation. J Geotech Geoenviron 138:992–1001
Ramakrishnan V, Ramesh KP, Bang SS (2001) Bacterial concrete. In: Proceedings SPIE 4234, Smart materials, 168
Sawley ML (1984) The pondermotive force of an electromagnetic wave in a collisional Plasma. J Plant Physiol 32(3):487–493
Stocks-Fischer et al (1999) Microbial precipitation of CaCO3. Soil Biol Biochem 31:1563–1571
Tsurumi T, Hirayama H, Vacha M, Taniyama T (2010) Nanoscale physics for materials science. Taylor and Francis Group, Boca Raton
Whiffin VS (2004) Microbial CaCO3 precipitation for the production of biocement. Doctoral thesis, School of Biological Sciences and Biotechnology, Murdoch University, Western Australia

Author Index

G.L. Sivakumar Babu et al. (eds.), *Geoenvironmental Practices and Sustainability*, Developments in Geotechnical Engineering,
DOI 10.1007/978-981-10-4077-1

Subject Index

G.L. Sivakumar Babu et al. (eds.), *Geoenvironmental Practices and Sustainability*, Developments in Geotechnical Engineering,
DOI 10.1007/978-981-10-4077-1